UNIVERSITÄT
DUISBURG
ESSEN

From Small Molecules Towards Supramolecular Dendrimers

Dissertation

zur Erlangung des akademischen Grades eines Doktors der Naturwissenschaften

– Dr. rer. nat. –

vorgelegt von Diplom Chemiker

Michael Merschky

geboren in Mellrichstadt

Institut für Organische Chemie der Universität Duisburg-Essen

Essen 2010

From Small Molecules towards Supramolecular Dendrimers

Gutachter:	Prof. Dr. Carsten Schmuck
	Prof. Dr. Christian Mayer
Prüfungsvorsitzender:	Prof. Dr. Hans-Curt Flemming
Tag der Disputation:	03.12.2010

Die vorliegende Arbeit wurde von April 2006 bis Oktober 2010 in den Instituten für Organische Chemie der Universitäten Würzburg und Duisburg–Essen unter der Anleitung von Herrn Prof. Dr. Carsten Schmuck angefertigt.

Ich erkläre hiermit des Eides statt, dass ich die vorliegende Arbeit selbst verfasst und mich dabei keiner anderen als der von mir bezeichneten Quellen und Hilfen bedient habe.

Ich erkläre hiermit, dass ich an keiner anderen Stelle ein Prüfungsverfahren beantragt beziehungsweise die Dissertation in dieser oder anderer Form bereits anderweitig als Prüfungsarbeit verwendet oder einer anderen Fakultät als Dissertation vorgelegt habe.

Essen, im September 2010

……..

Michael Merschky

Curriculum Vitae

Der Lebenslauf ist in der Online-Version aus Gründen des Datenschutzes nicht enthalten.

DANKSAGUNG

Als erstes möchte ich meinen Eltern, Christina und August, danken, die mich mein ganzes Leben lang unterstützt haben und mir die Möglichkeit gaben meine Wünsche zu verwirklichen.

Einen besonderen Dank möchte ich natürlich meinem Doktorvater Prof. Dr. Carsten Schmuck aussprechen, der mir die Gelegenheit gegeben hat mich auf verschiedenen Gebieten der Supramolekularen Chemie zu verwirklichen. Auch danke ich für sein stetes Interesse, die erhaltene Unterstützung und das in mich gelegte Vertrauen, mit sehr viel Freiraum gestaltend im Arbeitskreis mitzuwirken.

Weiterer Dank gilt unserem Kooperationspartner der FU Berlin, Prof. Dr. Rainer Haag, für die Mitgestaltung dieses interessanten Themas und seiner früheren Mitarbeiterin Dr. Monika Wyszogrodzka für die sehr angenehme Zusammenarbeit.

Meinen jetzigen wie auch ehemaligen Arbeitskollegen möchte ich hier für ihre Unterstützung und die sehr schönen Jahre im Arbeitskreis danken. Besonders danke ich meinen Kollegen Dr. Michael Schwegmann, Dr. Christian Urban, Dr. Peter Wich, Barbara Geibel, Sebastian Langolf und Ute Michels für die schönen und lustigen Momente in unserem Labor.

Diese Arbeit hätte nicht ohne die Mithilfe vieler Personen aus der eigenen wie auch aus anderen Abteilungen fertiggestellt werden können. Ich möchte mich daher bei allen Angestellten in der Verwaltung, den analytischen Abteilungen, Kollegen aus anderen Arbeitskreisen und allen, die irgendwann mit mir hier im Arbeitskreis gearbeitet haben, bedanken. Jeden einzelnen von zwei Universitäten aufzuführen würde wohl den Rahmen sprengen, daher bedanke ich mich im Besonderen bei: Dr. Rolf Janiak für die Vermittlung seines umfangreichen HPLC Wissens, Markus Braun für den kurzen bürokratischen Weg und Michael Ramold für die schnell erledigten Aufträge aus der Werkstatt. Bei Dieter Jacobi, Manfred Zähres und Dr. Christoph Böttcher bedanke ich mich für die SEC, DOSY und cryo-EM Messungen. Nicht weniger möchte ich mich auch bei Dr. Hans-Gert Korth für die Vermittlung seiner langjährigen Erfahrung, Wilhelm Sicking für seine Rechenpower und bei

Klaus Kowski, dem Mann für alle Fälle, bedanken. Weiterer Dank gilt Christine Cangemi, die uns vom Zentrum der Macht aus unterstützt, es war eine sehr gute Entscheidung, dass du bei uns bist. Ebenso danke ich Ursula Nüchter, Werner Karow und allen meinen Auszubildenden, Bachelorstudenten und Vertiefungspraktikanten. Ich hoffe auch, dass Pia bald wieder in den Arbeitskreis zurückkommen kann.

Einen besonderen Dank für das kritische Lesen dieser Arbeit möchte ich an Barbara Geibel, Sebastian Langolf, Dr. Volker Bickert, Dr. Thomas Rehm und Dr. Hans-Gert Korth. Bei Prof. Dr. Christian Mayer bedanke ich mich für die Übernahme des zweiten Gutachtens.

Als letztes möchte ich natürlich meiner Freundin Barbara, meiner ganzen Familie, die während meiner Promotion Zuwachs bekommen hat, und meinen Freunden für die Zeit neben der Arbeit danken.

CONTENT

1. INTRODUCTION

1.1 Supramolecular Chemistry

"Beyond molecular chemistry based on the covalent bond there lies the field of supramolecular chemistry, whose goal it is to gain control over the intermolecular bond".[1] This definition of supramolecular chemistry by JEAN-MARIE LEHN – one of the leading proponents of supramolecular chemistry – is only one of many for this exciting topic.[2] The field of supramolecular chemistry is multidisciplinary and contains elements of organic and inorganic synthesis, biochemistry, physical and computational chemistry to understand, predict, and control the behaviour of the *"chemistry beyond the molecule"*.[2c] Supramolecular interactions between molecules are a sum of generally weak, non-covalent interactions, such as hydrogen bonds, electrostatic interactions, π–π interactions, and van der Waals forces.[3] JEAN-MARIE LEHN, DONALD J. CRAM and CHARLES J. PEDERSEN were awarded with the NOBEL Prize *"for their development and use of molecules with structure-specific interactions of high selectivity"* in 1987.[4]

Figure 1-1: One of the Nobel Prize winners in Chemistry 1987: JEAN-MARIE LEHN.[5]

Supramolecular chemistry is inspired by nature, creating extraordinarily complex systems from rather simple building blocks by self-assembly or host-guest-chemistry, like, for instance, catalytically active enzyme substrate complexes. In principle, self-assembly and host-guest-chemistry are the two main parts of supramolecular chemistry. The difference between these two fields depends on the size and shape of the involved molecules. Host-guest-chemistry in general deals with the study of a larger host molecule enclosing a smaller guest molecule *via* non-covalent bonds (see **Figure 1-2** top).[i, 6] On the other hand, in the self-assembly process no significant size difference exists between the interacting molecules. Neither of them is acting as host or guest. Two or more molecules self-assemble *via* non-covalent interactions spontaneous to larger aggregates of specific structure, due to the structural information that is encoded in the molecular building blocks (see **Figure 1-2** bottom).[7, 8, 9]

[i] *"The host component is defined as an organic molecule or ion whose binding sites converge in the complex* […] *The guest component is any molecule or ion whose binding sites diverge in the complex"*: by Donald J. Cram, "Preorganisation – from solvents to spherands", *Angew. Chem. Int. Ed.*, **1986**, *25*, 1039–1134.

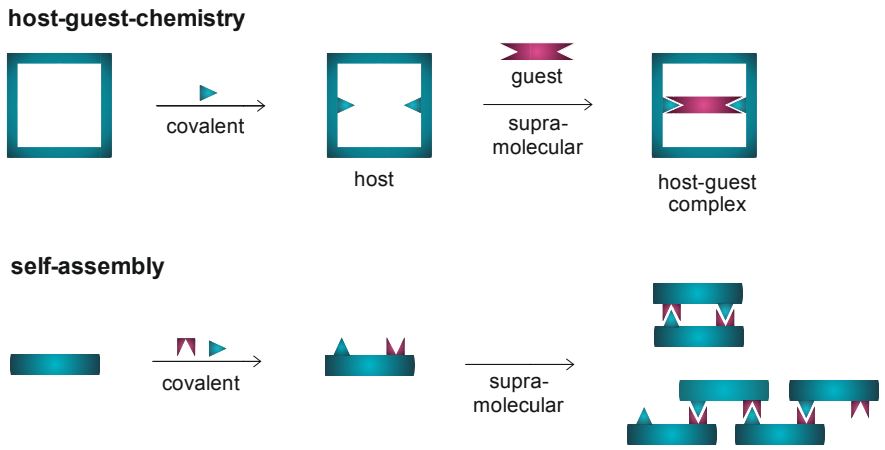

Figure 1-2: Top: Host-guest-chemistry; **Bottom**: Self-assembly

1.2 Self-Assembly

One of the most prominent examples for a self-assembled structure in nature is the DNA double helix containing the genetic information of all known living organisms (**Figure 1-3**). Two complementary strands recognise each other and self-assemble to a thermodynamically stable double-strand helix *via* hydrogen bonds and mainly π–π base pair interactions.[10] Another example is the light-harvesting antenna system in green bacteria. This molecular arrangement is the largest antenna system found in nature and consists of hundreds of self-assembled π–π-stacked bacteriochlorophyls. These rod-like aggregates enable the green bacteria to grow by photosynthesis under conditions of extremely low light intensities due to an efficient energy transfer.[11] These examples indicate the potential of self-assembly processes for medicinal, biological, and technical applications.

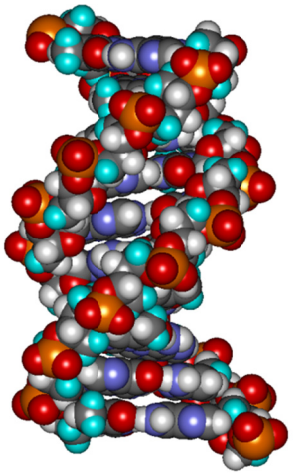

Figure 1-3: DNA helix

The thermodynamically controlled self-assembly process is a timesaving strategy to create nanoscale architectures. However, tailor-made building blocks are necessary to amplify the relatively weak interactions like intermolecular hydrogen bonds, electrostatic interactions, van der Waals forces, coordination interactions, and solvophobic effects. As the self-assembly process cannot be controlled in itself, the self-complementary building blocks have to be carefully designed and synthesised to accomplish the desired self-assembled aggregates.[7, 9]

The concept of self-assembly is not only of interest for the formation of nanoscale structures, but also because the process is reversible. The assembly and disassembly process is a consequence of the non-covalent nature of these aggregates and provides the possibility to use such supramolecular systems as stimulus-responsive nanotransporters for biomedical applications. An important aspect in using such systems is to gain control over the supramolecular assembly and disassembly process, which is triggered by external stimuli. One possible external trigger is the pH of the environment. Especially in cancer therapy self-assembly systems might be beneficial because tumour cells are more acidic compared to healthy cells. As tumour cells also exhibit a higher permeability for macromolecules, such as dendrimers, it would be interesting to use a pH-triggered self-assembly approach in forming dendrimer macromolecules in order to encapsulate drugs and to release the enclosed cytostatica by the pH change after endocytosis of the tumour tissue.[12, 13]

The self-assembly processes of dendritic molecules has become a dynamic field of research over the last 15 years. Before, dendrimer chemistry was predominantly concerned with covalent synthesis of dendrimers *via* the divergent and convergent method. The present thesis deals with the topic of supramolecular chemistry, especially the area of self-assembled supramolecular dendrimers in water.[i] The aim is to prepare supramolecular dendrimers using small, individual dendrons which self-assemble *via* non-covalent interactions and to get a better understanding of the self-assembly process in water as well as the possibility to trigger the assembly and disassembly process by an external pH-stimulus.

[i] During the doctoral work time was spend on both areas of supramolecular chemistry. The host-guest-chemistry topic is not included in this thesis. The results have been published as a full paper – reference 14: Merschky M., Schmuck C., "Synthesis and kinetic studies of a low-molecular weight organocatalyst for phosphate hydrolysis in water", *Org. Biomol. Chem.,* **2009***, 7,* 4895–4903, DOI: 10.1039/b914974k.

2. BACKGROUND INFORMATION

2.1 Covalent Dendrimers

2.1.1 Introduction

The characteristics of supramolecular dendrimers can only be properly explained based on a background knowledge on covalent dendrimers. Therefore, a short overview is given here. The following examples are only a few selected from the great variety found in the literature. No attempt is made to provide a complete historical overview in respect to type of dendrimers, concepts for synthetic approaches, or the various working groups involved in this scientific area. The examples were chosen because of either historical or conceptual reasons. A a lot of excellent books[15, 16, 17] and review articles[18, 19, 20] exist, which are recommended to the reader for more detailed information.

Before the development of dendrimer chemistry will be discussed, a few explanatory notes concerning this topic should be given. It should be noted that FLORY has theoretically discussed infinite polymeric networks already in 1941, i.e. long before the first dendrimer syntheses were carried out.[21] It should also be mentioned that a lot of different names were, and are still used, for this class of molecules. In this thesis, the notation "dendrimers" will be used because it is today the most commonly used name. The word originates from the greek words *dendron* (tree) and *meros* (part).[22] These multi branched architectures are wide-spread in nature, for example, in trees and root ramifications (**Figure 2-1**), in snow crystals, blood vessels, or the branching of neurons.[i]

Figure 2-1: The term dendrimer originates from the greek words *dendron* (tree) and *meros* (part). Photography of a tree taken in Franconia by Volker Merschky.

[i] The branched projections of the neurons are called dendrites, so this term should not be used for dendrimer structures.

Ideal dendrimers are monodisperse macromolecules with a regular branched, three-dimensional structure and a defined number of end groups.[i] Dendrimers are nano-architectures of defined size and, as shown in **Figure 2-2**, consist of a multifunctional core to which branching units are attached in different "generations" (G1–GX). The periphery of the dendrimer is formed by the end-groups. One branching segment with the end groups attached to the core is called a "dendron".[16]

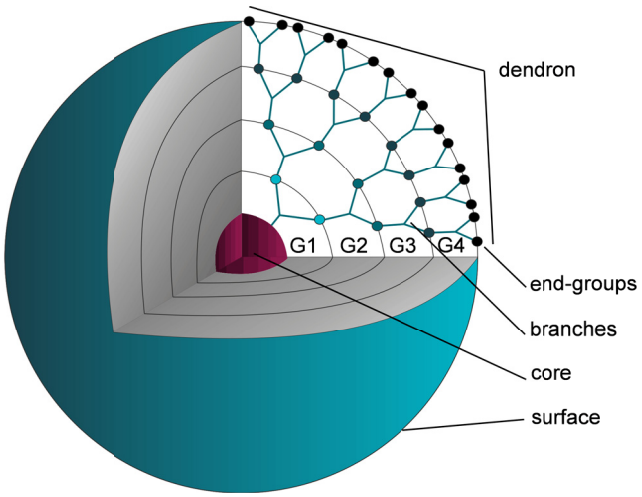

Figure 2-2: A three-dimensional schematic illustration of a dendrimer. Showing a 4th generation dendron attached to the interior core.

2.1.2 Divergent Synthesis

The first dendrimers were synthesised iteratively by connecting two or more monomers to a multi-functionalised core, so that the end-groups of the dendrimer grow exponentially by each generation as depicted in **Figure 2-3**.

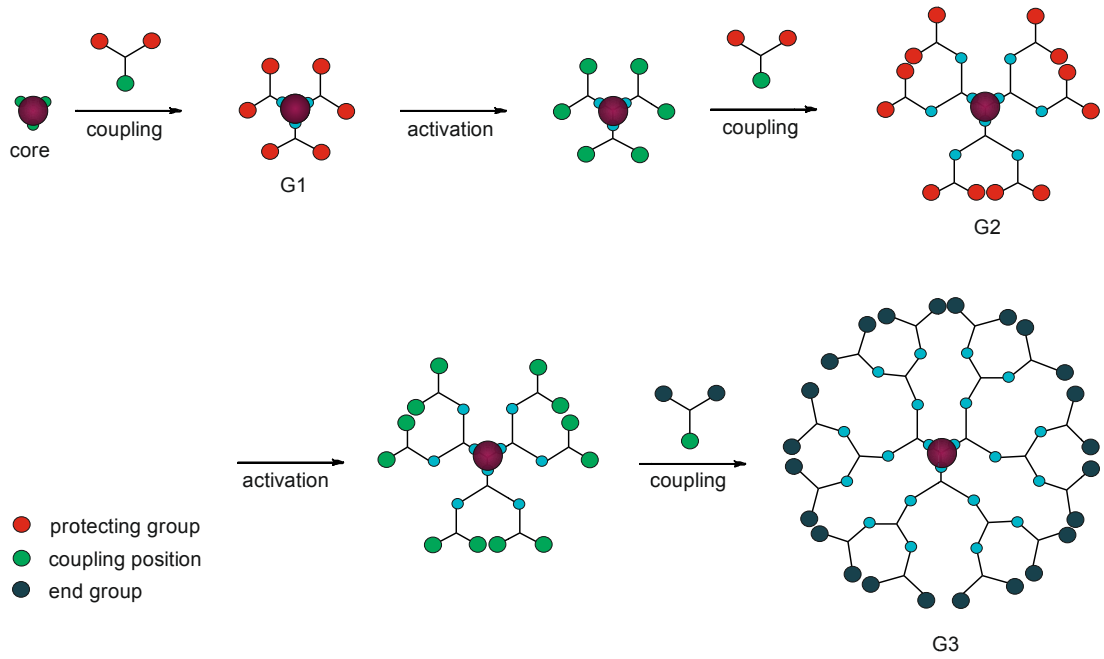

Figure 2-3: Divergent synthetic route to dendrimers. The activation and coupling steps are a pair of repetitive steps to build up the next generation dendrimer. Schematic overview depicted according to reference 16.

[i] Dendrimers are, in principle, like starburst polymers, but the latter ones are composed of only a branched core with linear polymers, while dendrimers are also branched in the side chains. Therefore, the terms "starburst polymers" and "dendrimers" should not be used synonymously.[22]

The first example of such an iterative synthesis was published by VÖGTLE *et al.* in 1978.[23] The molecules were called "cascade" molecules according to the repetitive synthesis. Various molecules starting from primary mono- and di-amines were synthesised. The number of end-groups rose exponentially with every repetition step, leading mostly to a tree-like spherical structure (**Figure 2-4**).

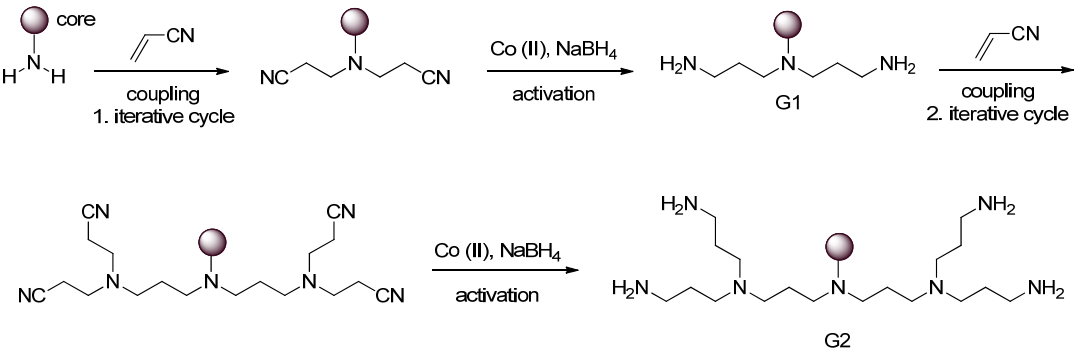

Figure 2-4: First dendrimer "cascade" molecules by VÖGTLE *et al.*.[23]

Among the most prominent and commercially available dendrimers are the polyamidoamine (PAMAM) dendrimers (**Figure 2-5**). These were invented by TOMALIA who brought up the name "dendrimer" in 1985.[24] TOMALIA also was the first who wrote a detailed review article on dendrimers and popularised the topic of this interesting class of macromolecules.[20]

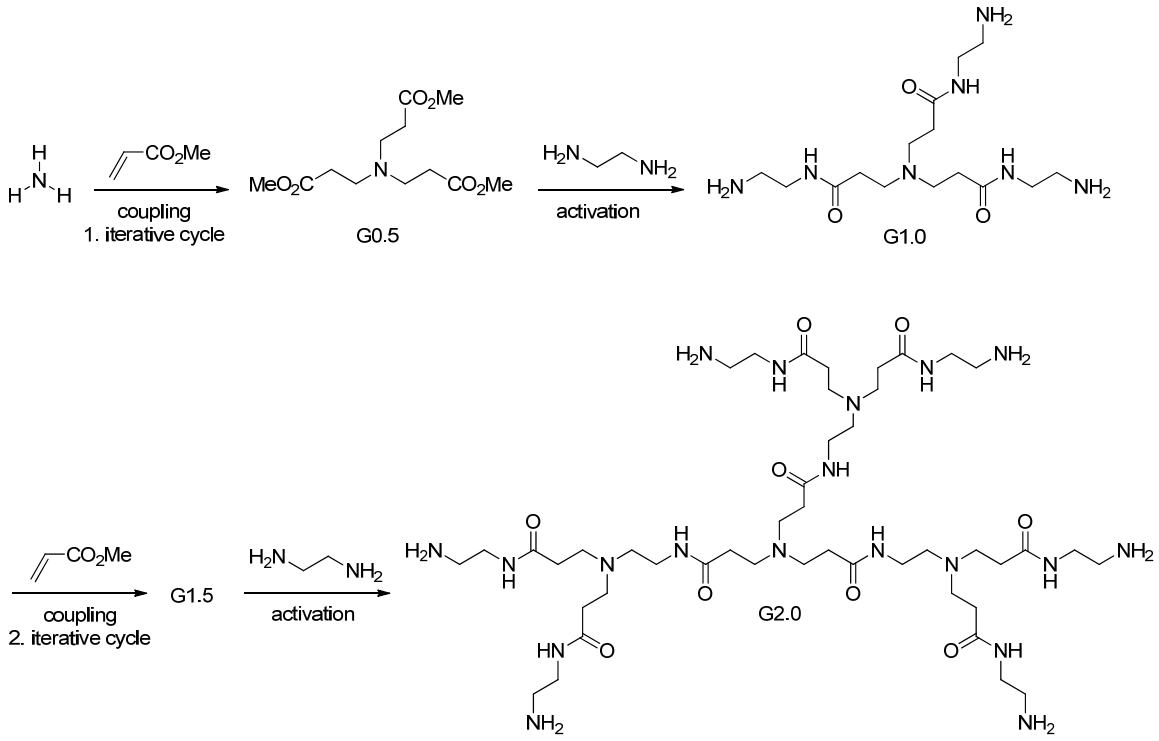

Figure 2-5: Synthesis of polyamidoamine dendrimers by TOMALIA *et al.*.[24]

Another example for the divergent approach to dendrimers are NEWKOMES "arborols" from 1985 (**Figure 2-6**).[25, 26] The term arborol is deduced from the latin word *arbor,* which means tree, and is sometimes used for water-soluble dendrimers with hydroxyl end-groups.[22]

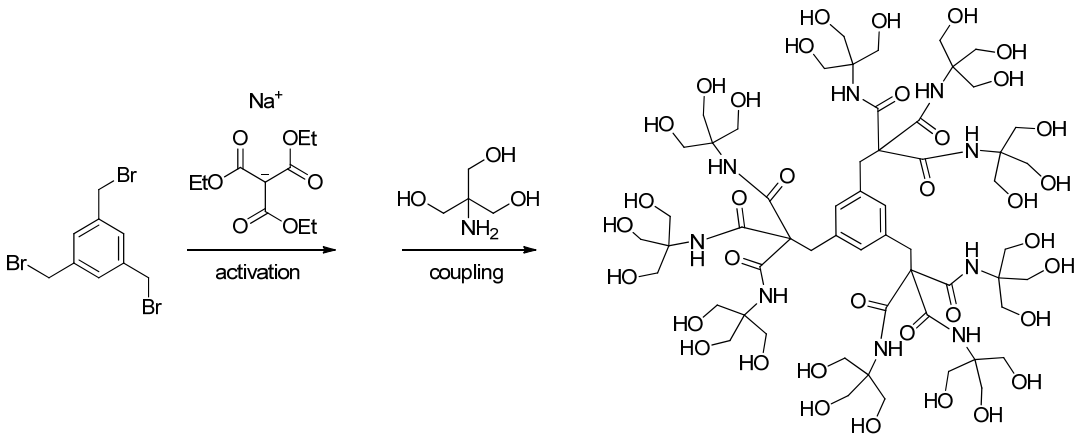

Figure 2-6: Arborol of NEWKOME *et al.*[26]

Besides PAMAM dendrimers, the polypropyleneimine (PPI) dendrimers reported by MÜLHAUPT[27] and DE BRABBANDER[28] are one of the most prominent examples for divergently synthesised dendrimers on the basis of VÖGTLE's[23] original work (**Figure 2-7**). The name polypropyleneimine is widely spread and often used, but, strictly speaking, implies the presence of imine functions. Another term for this type of dendrimers is polypropyleneamine (POPAM). This name is used to emphasise the exclusive amine character of the dendrimer. POPAM belongs to the most widely used kind of dendrimers in literature because it is commercially available like the above discussed PAMAMs.[16]

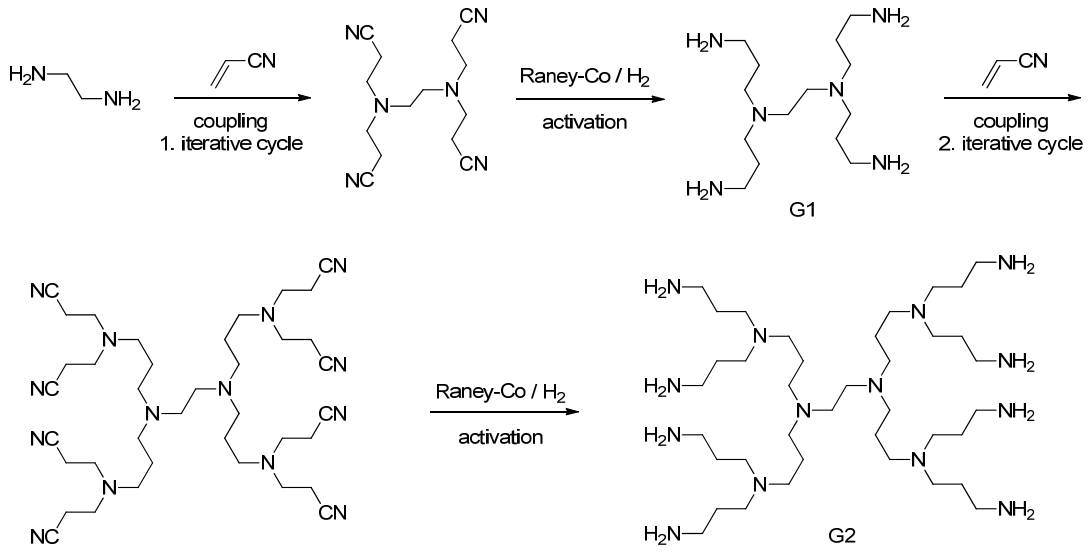

Figure 2-7: Synthesis of POPAM Dendrimers by DE BRABANDER.[28]

All of the examples shown above have been prepared by the divergent approach. A disadvantage of this method is that the evolution of the end-groups grows exponentially, therefore, the problem of non-quantitative transformations increases leading to uprising structural defects. A simple calculation will demonstrate the problem of such kind of synthesis. Similar to solid-phase MERRYFIELD synthesis of peptides the divergent method for automated dendrimer synthesis depends heavily on the yield of the individual reaction steps to achieve the desired, defect-free dendrimer. For example, the synthesis of a POPAM dendrimer of 5th generation with 64 amine end groups involves 248 reaction steps. Thus, only a yield of 29 % of defect-free dendrimer can be expected if an average of 99.5 % yield for each reaction step is assumed. Due to the fact that higher generation dendrimers with defects have very similar properties, like solubility or polarity, compared to defect-free target molecules, the separation of the various products will be very difficult. On the other hand, an advantage of the divergent approach is the possibility for automation of the repetitive synthetic steps. This is the reason why dendrimers like POPAM or PAMAM are commercially available.[16] However, as mentioned above, the purity is governed by statistics, thus, the resulting higher generation dendrimers are hyper-branched polymers rather than monodisperse dendrimers. Another approach to dendrimers is the convergent synthesis strategy first invented by FRÉCHET *et al.*.[29a]

2.1.3 Convergent Synthesis

The convergent synthesis route is, generally speaking, inverse to the divergent approach. Here, the dendrimer is synthesised going from the periphery to the core. Thus, a dendron with a functional group is synthesised that can be attached to the multivalent core. The advantage of the convergent path is the decreased number of coupling steps required for each generation of the dendron compared to the formation of the same generation of a divergently prepared dendrimer. For instance, the last step as described in **Figure 2-8** in the synthesis of the convergent 3rd generation dendron involves 4 coupling steps, while in the last step of the divergent 3rd generation dendrimer (**Figure 2-3**) 12 coupling steps are necessary. This is due to the fact that on the convergent route the dendrons are attached to the multivalent core only in the final step of the synthesis. The convergent 3rd generation dendron can be prepared with less defects due to the lower number of coupling reactions and, additionally, can be better purified because of a higher diversity of the starting material compared to the products of the divergent pathway. The final reaction to the convergent 3rd generation dendrimer consist of only 3 coupling reactions of the three 3rd generation dendrons to the trivalent core, in which the product again differs substantially from the starting material. The disadvantage of the convergent method, however, is the last reaction step, in which the dendrons are coupled to the

multivalent core. The problem is that with dendrons of higher generations the core is sterically overcrowded. Hence, the method is more widely used for preparing dendrimers of lower generations.[16]

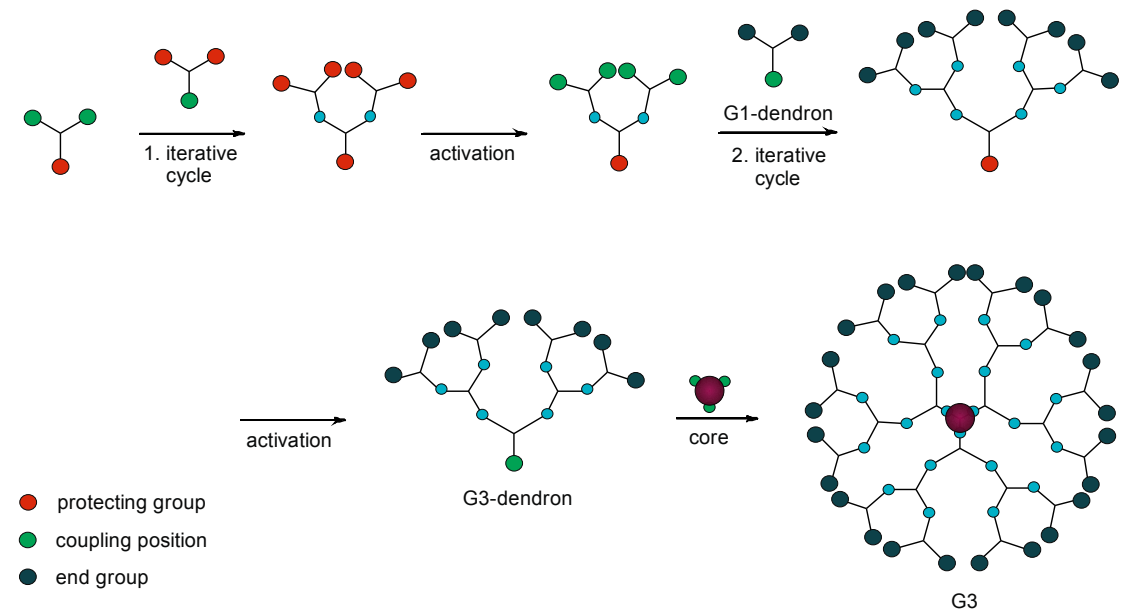

Figure 2-8: Schematic overview of the convergent synthetic route of dendrimers. Schematic overview depicted according to reference 16.

FRÉCHET *et al.* described the first convergent synthesis of a polyarylether dendrimer in 1990, as shown in **Figure 2-9**.[29]

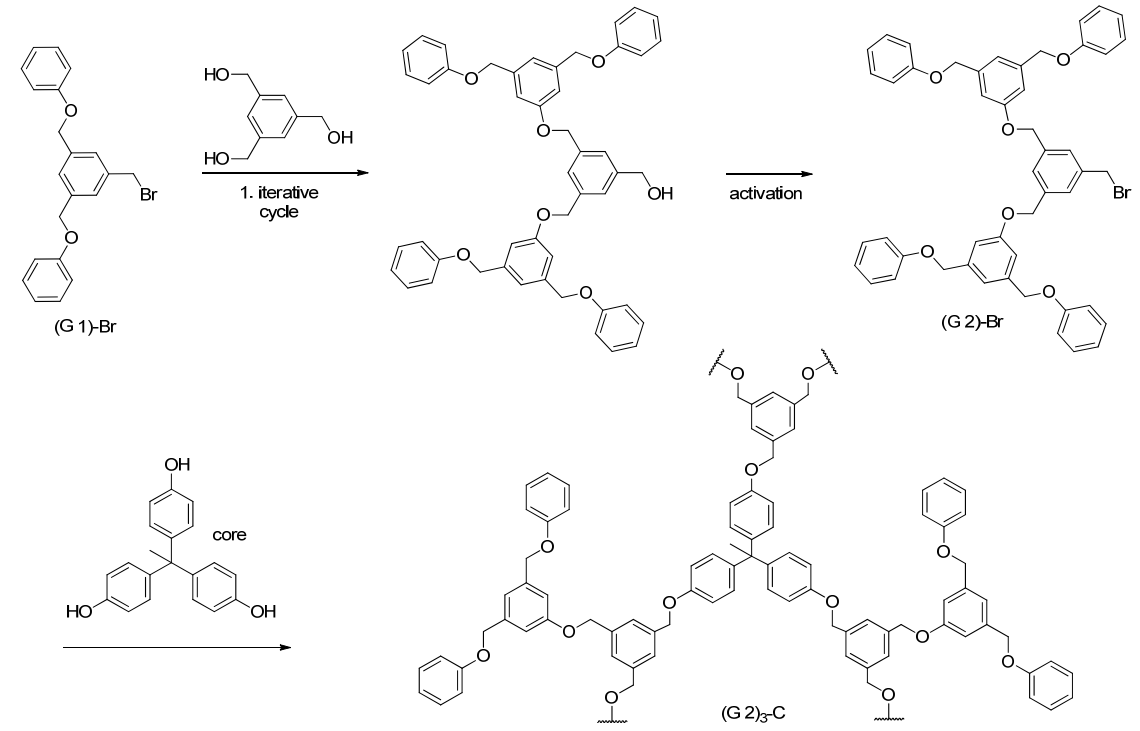

Figure 2-9: Convergent dendrimer synthesis invented by FRÉCHET.[29]

In addition to the two "historical" methods described above, there are newer synthetic strategies like the double stage convergent method, a combination of convergent and divergent approaches, in which a convergently synthesised dendron is attached to a divergently synthesised hyper-core.[30] Further methods are the orthogonal synthesis, the double exponential method, the hyper-monomer method, solid phase synthesis, coordination chemistry methods, and the main topic of this thesis, the supramolecular method as discussed in **Section 2.2**.[16] In supramolecular dendrimer syntheses the dendron is often prepared by covalent synthesis like in the convergent way, followed by supramolecular self-assembly of the covalent dendrons to form the desired supramolecular dendrimer.

Not only the synthesis of perfect dendrimers is a challenge but also the characterisation of such macromolecules can be problematic.[31] Recent progress in analytical methods like mass spectrometry allows an analytical insight and reveals the defects of POPAM[32] and PAMAM[33] dendrimers. But also false negative results due to inappropriate methods are clarified by newer analytical methods. For example, MALDI-MS was often used to characterise dendrimers and their defects. However, SCHALLEY *et al.* could show in a combined ESI and MALDI-MS study that some of the observed defects are in fact fragmentation patterns of the MALDI process.[34]

While in the early days of dendrimer chemistry efforts were concentrated on the development of synthetic methods to generate defect-free dendrimers of varying sizes, more recently the properties of dendrimers are explored to evaluate their potential for interesting applications.

2.1.4 Properties and Applications

In contrast to often shown pictorial representations, dendrimer structures are not highly ordered with outstretched end-groups. In reality, dendrimers have no homogenous periphery, and the end-groups can be back-folded to the core due to their flexibility and external influences like solvent polarity. Depending on the functional moiety of the end-groups, dendrimers can vary in their characteristics like shape, stability, solubility, or viscosity. Not only do the end-groups affect such characteristics and are important for the bulk properties of the macromolecule, but also the functional groups in the branches like esters, ethers, and amides are important for the inner density and shape of the dendrimer. The various components of the dendrimer affecting the properties of the macromolecule are summarised in **Table 2–1**.[16]

Table 2–1: The influence of the dendrimer components on the properties of the macromolecule according to reference 16.

dendrimer part	core	branching	surface	end-group
influenced property	shape	shape	shape	shape
	size	size	size	stability
	multiplicity	density	flexibility	solubility
	function	guest uptake	properties	viscosity

The layered architecture of dendrimers with the resulting properties like globular shape, multivalent periphery, and variable inner volume endow dendrimers with unique features. These general properties and the specific influence of the different parts can be used to synthesise macromolecules for diverse applications. The concepts of dendrimers and supramolecular chemistry can not only be combined for the construction of dendrimers by supramolecular chemistry. Covalently bound dendrimers themselves already possess supramolecular properties since dendrimers encapsulate guest molecules in their interior by supramolecular interactions. The dendrimer branches can act like a dendrimeric box selectively enclosing molecules by non-covalent interactions. This property was already observed in the very beginning of dendrimer chemistry when NEWKOME coined the term "unimolecular micelle".[25, 35] Another example is the so called "dendritic box" from MEIJER, encapsulating Bengal Rose.[36, 37] A special feature of dendrimers in contrast to classical micelles is that they do not show any critical micelle concentration as they are macromolecules themselves. Thanks to that characteristic a dendrimer with an apolar interior and polar periphery is not only capable to include guests, but may also solubilise low concentrations of apolar molecules in water. These aspects make dendrimers interesting vehicles for drug delivery, especially in cancer therapy.[38, 39, 40] The enclosed cytostatica can be transported into a cell by endocytosis, which especially in case of tumour blood vessel systems is favourable because of their higher permeability for macromolecules. This is called the "enhanced permeability and retention effect".[41] The tumour tissue is passively targeted by the dendrimer and toxicity for healthy cells is reduced. Beside the fact that dendrimers can enclose drugs and transport them into the tumour tissue, another fact is at least of the same importance, that is, the release of the drug in the interior of the tumour tissue. Here, another characteristic of tumour in contrast to healthy tissue has to be considered for the design of a dendrimer that can selectively release the drug inside the tumour: tumours have a pH of about 5.5, while a healthy tissue has a pH of circa 7.4. Covalent dendrimers carrying acid labile periphery groups have been used for such an application, as shown in **Figure 2-10**.[16, 17, 42]

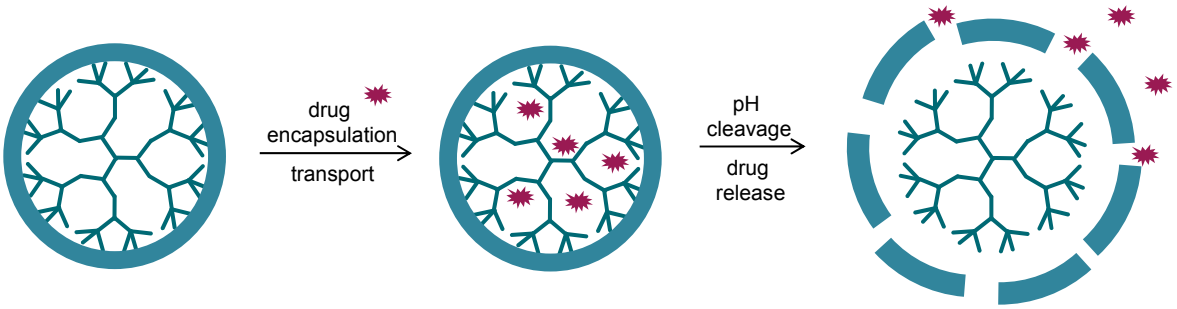

Figure 2-10: Dendritic nano-carrier of biological active compounds with drug release in acidic media. Schematic overview depicted according to reference 42.

The alternative release of active molecules by covalent fragmentation of the dendrimer has led to the concept of cleavable dendrimers.[43] In case of supramolecular dendrimers, such a fragmentation is paralleled by the reversal of the self-assembly process. For instance, a binding site showing acid base dependency may be used to induce the assembly and disassembly of the supramolecule by pH changes.

2.2 Supramolecular Dendrimers

2.2.1 Introduction

The area of dendrimer chemistry is expanding rapidly since the development of TOMALIA's divergent polyamidoamine and the convergent FRÉCHET dendrimers. As already noted above, in the beginning, the efforts were concentrated on developing and adapting synthetic methods needed for this area of "soft materials". More recently, dendrimers are coming into focus as an interesting class of new nanomaterials and are currently extensively explored for applications in chemistry,[44, 45]material sciences,[46] biology,[47, 48, 49] or medicine[17, 50]. Despite the great advances made in the preparation of dendrimers, a significant measure of synthetic effort is still required. An alternative route to dendrimers, going beyond the classical convergent and divergent covalent synthesis, is the non-covalent supramolecular approach. Combining the principles of supramolecular chemistry and dendrimer chemistry is not only of importance for the preparation of supramolecular dendrimers, but there are also many examples of covalent dendrimers which have been used as scaffolds for functionalised end-groups or cores in supramolecular recognition processes.[51, 52, 53]

As mentioned in **Chapter 1.2**, self-assembly is a powerful concept to build up complex nanostructures by various complementary non-covalent interactions. If the building blocks are well selected there exists the possibility to obtain nanoscale dendrimer architectures with significantly less synthetic effort than in covalent synthesis. As discussed in **Chapter 2.1**, the chemical synthesis of larger dendrimers is difficult and often hampered by defects in the structure along with problems of analytical characterisation and/or purification. An alternative is the self-assembly of smaller dendrons into larger supramolecular dendrimer nanostructures. The self-assembling building blocks can be relatively small and therefore are likely to be synthetically more easily accessible. The fact that the interactions used for the self-assembly process are non-covalent offers the opportunity to connect the building blocks reversibly. However, carefully designed molecules are necessary to achieve such a specific controllable self-assembly especially in water.

As depicted in **Figure 2-11**, there are different approaches to self-assemble dendritic building blocks to supramolecular architectures. This work will focus on the untemplated and templated self-assembly in solution.[54, 55, 56]

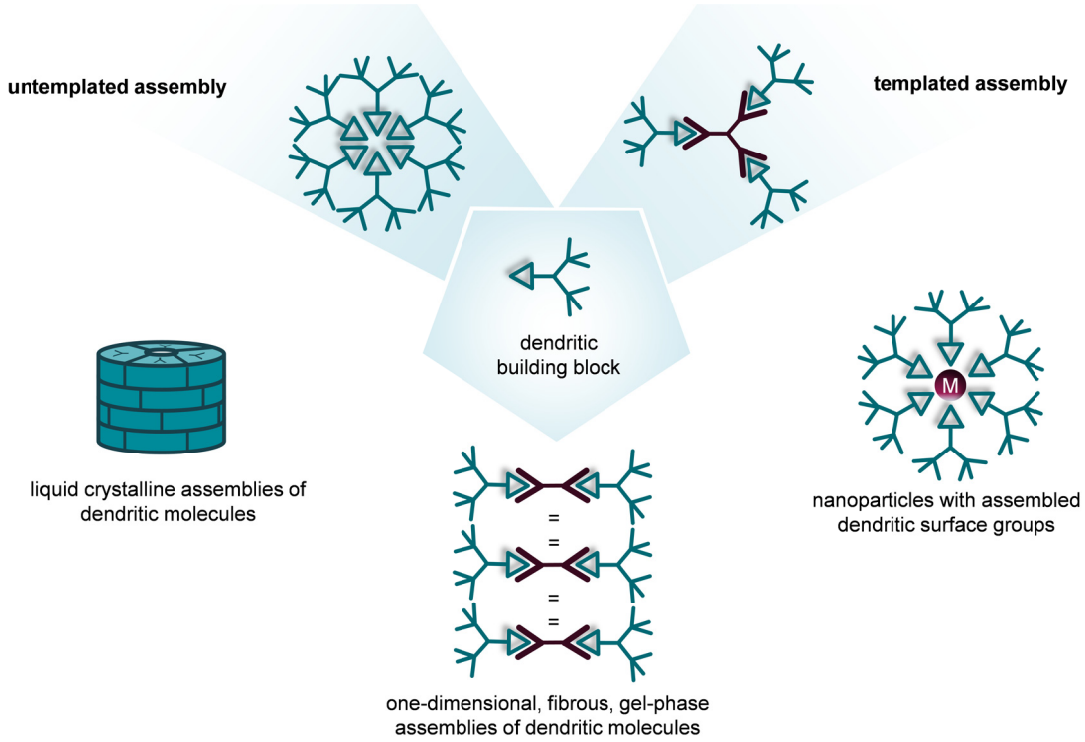

Figure 2-11: Schematic illustration of self-assembled dendritic building blocks according to SMITH *et al.*.[57] The discussion mainly focuses on the untemplated and templated assembly.

However, in most cases often polymeric aggregates such as columnar stacks, fibres, or hollow spheres result from the assembly of a large, often unpredictable, number of dendrons.[58] There exists a comprehensive review on this topic by SMITH *et al.,* and the reader is referred to this review because only selected examples are discussed here.[57]

2.2.2 Untemplated Self-Assembled Dendrimers

Direct and untemplated self-assembly of dendrons into well-defined, specific aggregates is difficult and only a few examples exist so far. The control of the exact size and sometimes even the shape of the supramolecular aggregates is less explored than in case of templated systems.

The first example of a self-assembled supramolecular dendrimer by forming discrete hydrogen bond interactions was published in 1996 by ZIMMERMAN *et al.*.[59] As shown in **Figure 2-12** these authors used isophthalic acid residues as binding site. Two isophthalic acid units were attached in a *syn* arrangement *via* a rigid aromatic spacer to increase the strength of hydrogen bonding. The tetracarboxylic acid hydrogen binding site was attached to the focal point of the 1st to 4th generation of FRÉCHET dendrons. ZIMMERMAN *et al.* observed that 1st generation dendrons self-assemble in chloroform to linear aggregates, but for higher

generations the linear aggregation of the dendrons was hampered because of steric reasons, and association preferentially led to a cyclic hexamer.[59, 60, 61]

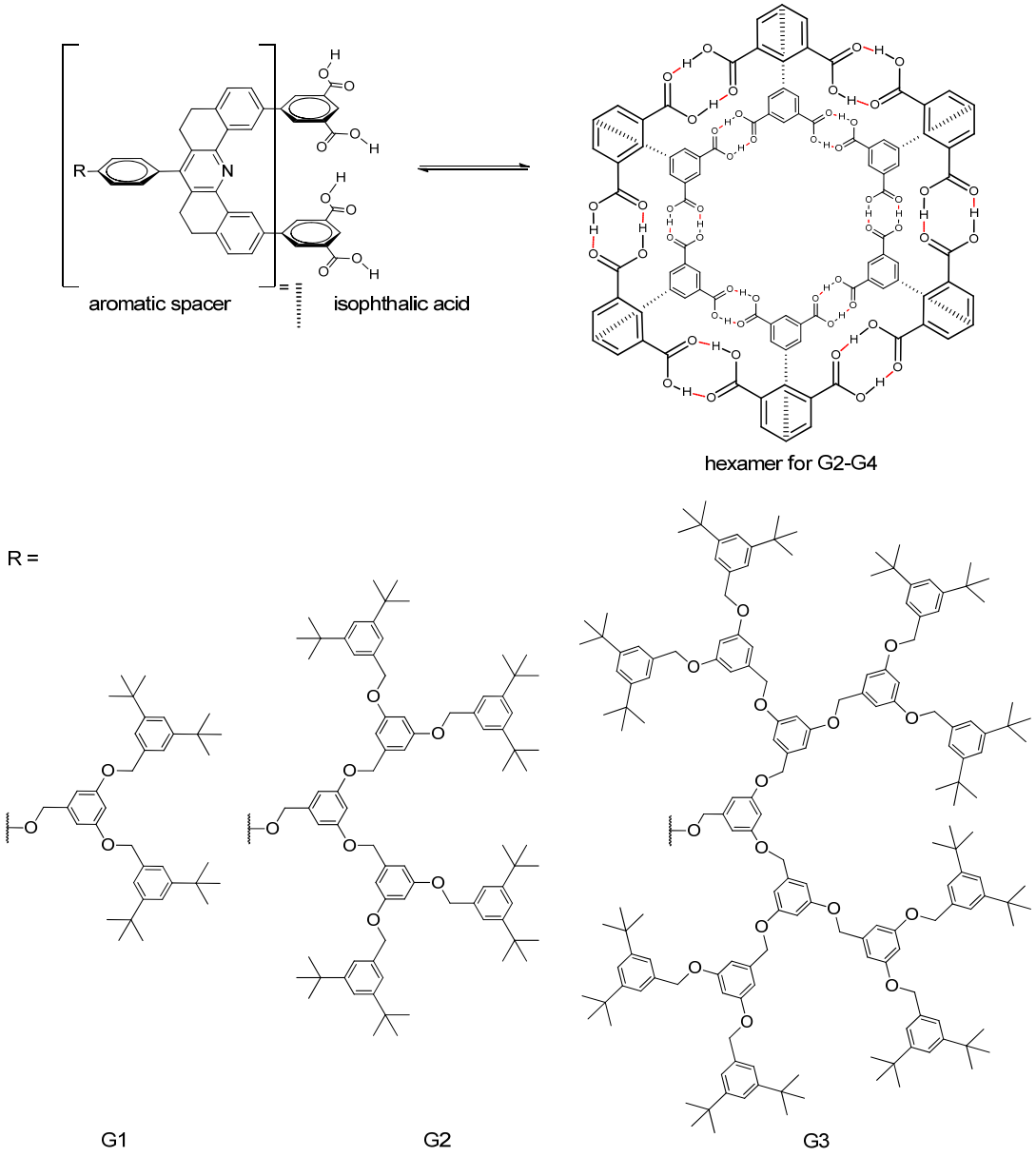

Figure 2-12: Self-assembling monomer of ZIMMERMAN *et al.* and its corresponding hexameric aggregate.

Due to the fact that more polar solvents like dimethylsulfoxide (DMSO) or tetrahydrofuran (THF) are competitive to the carboxylic acid binding site, only monomeric structures were observed in the presence of such solvents. The stability of the self-assembled aggregates was established by titrating dimethylsulfoxide or tetrahydrofuran to a chloroform solution of 3rd generation hexamer at 50 °C. The aggregate disassembled at a content of 23 % DMSO or 64 % THF, respectively. In order to overcome these stability limitations in moderately competitive solvents, ZIMMERMAN *et al.* developed a binding motif whose hydrogen donor (D) and acceptor

(A) bonding arrays DDA and AAD are fixed at a 60 ° angle, thereby being capable to form more stable hexameric aggregates (**Figure 2-13**).

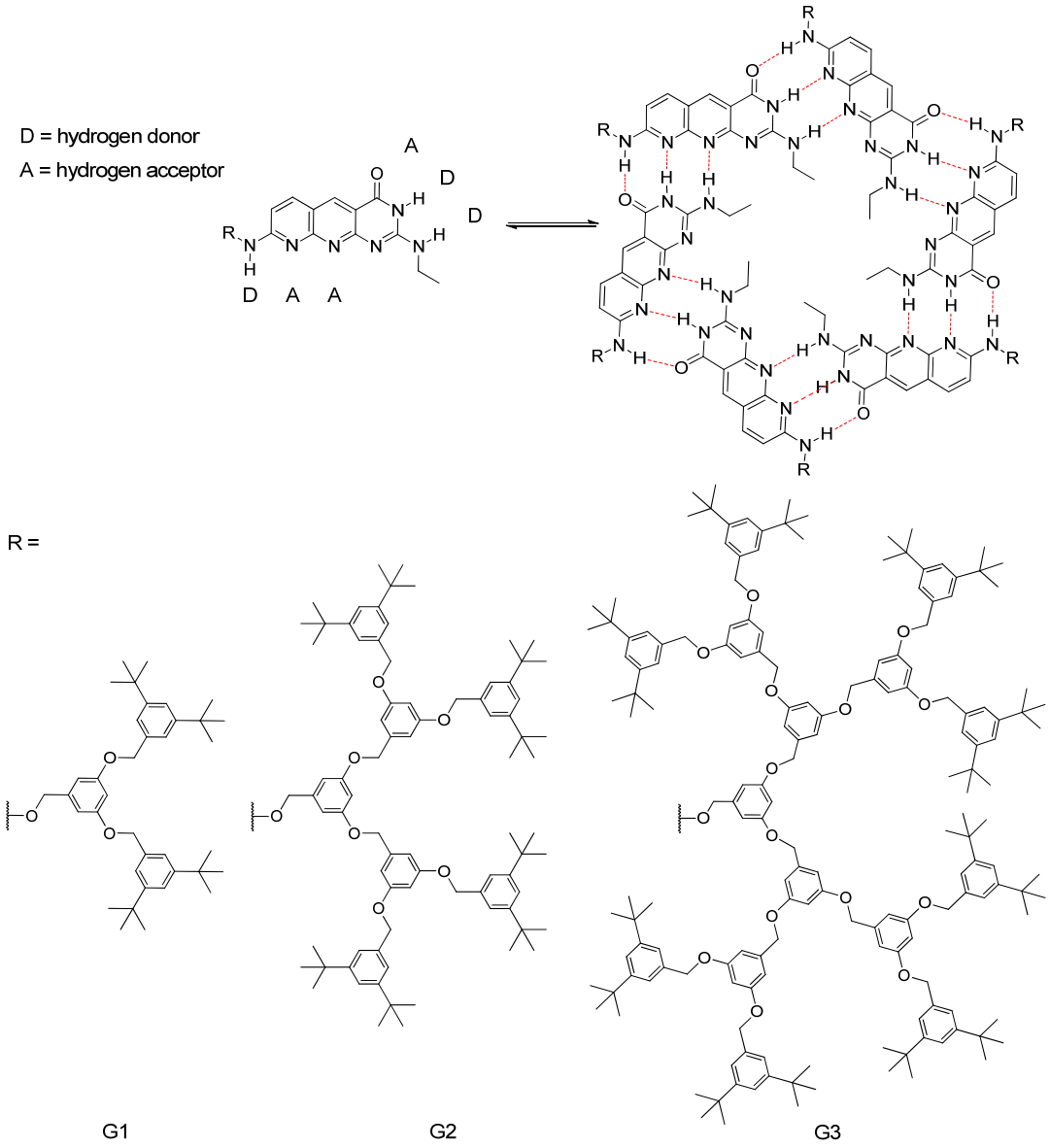

Figure 2-13: Self-assembling monomer and corresponding hexameric aggregate.

The untemplated self-assembly in solution was characterised by NMR and size exclusion chromatography (SEC). All related data were consistent with a cooperative self-aggregation process forming a hexamer *via* hydrogen bonding. In fact, even in 15 % aqueous tetrahydrofuran stable hexamers were formed *via* the DDA·AAD binding motif. The reversibility of hexamer formation was established by decreasing the concentration, increasing the temperature, or adding competitive solvents, e.g. dimethylsulfoxide, to shift the equilibrium toward the monomers. In contrast to the isophthalic hexamer (**Figure 2-13**), the 1st generation dendrimer forms the most stable aggregates while for higher generation

dendrimers the stability decreases. Most interesting was the observation that through the dynamic nature of these supramolecular hexamers an alternating aggregate of 1st and 3rd generation dendrons was formed in a 1:1 mixture of 1st and 3rd generation building blocks, as shown in **Figure 2-14**. This alternating hexameric aggregate was more stable than the pure 1st or 3rd generation hexamers. Out of the 13 possible hexameric assemblies, only the one with alternating 1st and 3rd generation dendrons was observed.[62, 63]

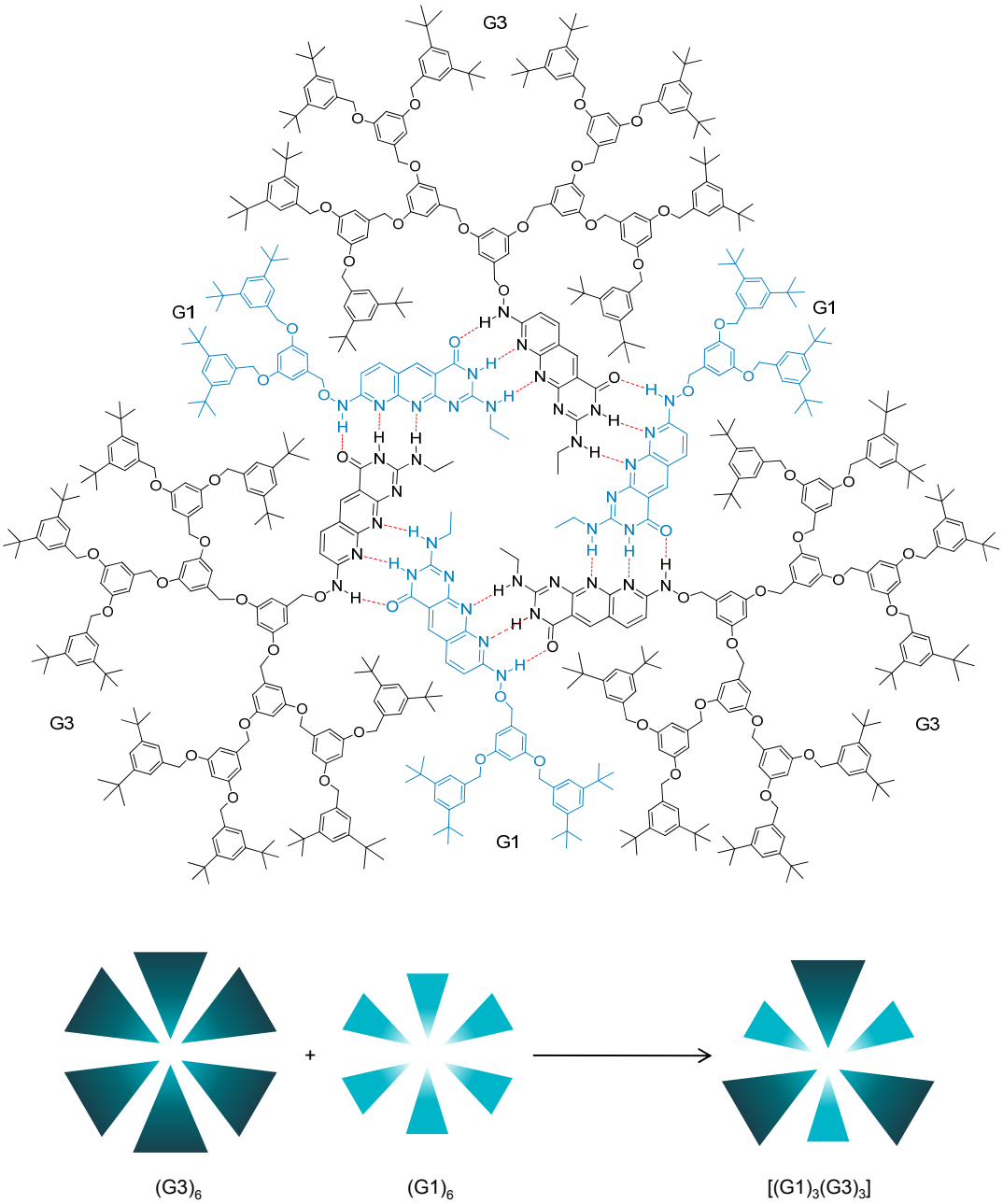

Figure 2-14: Schematic illustration of alternating 1st and 3rd generation dendrons forming a hexamer, according to ZIMMERMAN *et al.*.[62]

Another example for untemplated self-assembly *via* discrete hydrogen bonds to form rosettes was reported by REINHOUDT *et al.* in 1997.[64] Differently to the approach of ZIMMERMAN *et al.*, here two different types of compatible non-covalent interactions were used for the self-assembly process. The parent melamine/barbituric acid hydrogen-bonding array had been intensively studied by WHITESIDES *et al.* in non-dendritic systems.[65] The metallo-dendron wedges were functionalised at the focal point with the barbituric acid subunit. The combination of three barbituric acid dendrons and three melamine units through six hydrogen bonds each forms a 3:3 self-assembled hexameric rosette. As shown by NMR spectrometry in deuterated methylenechloride, self-assembly to hexameric aggregates was restricted to low temperatures. The characteristic signals of the hexameric rosette dendrimer disappeared above -20 °C.[64]

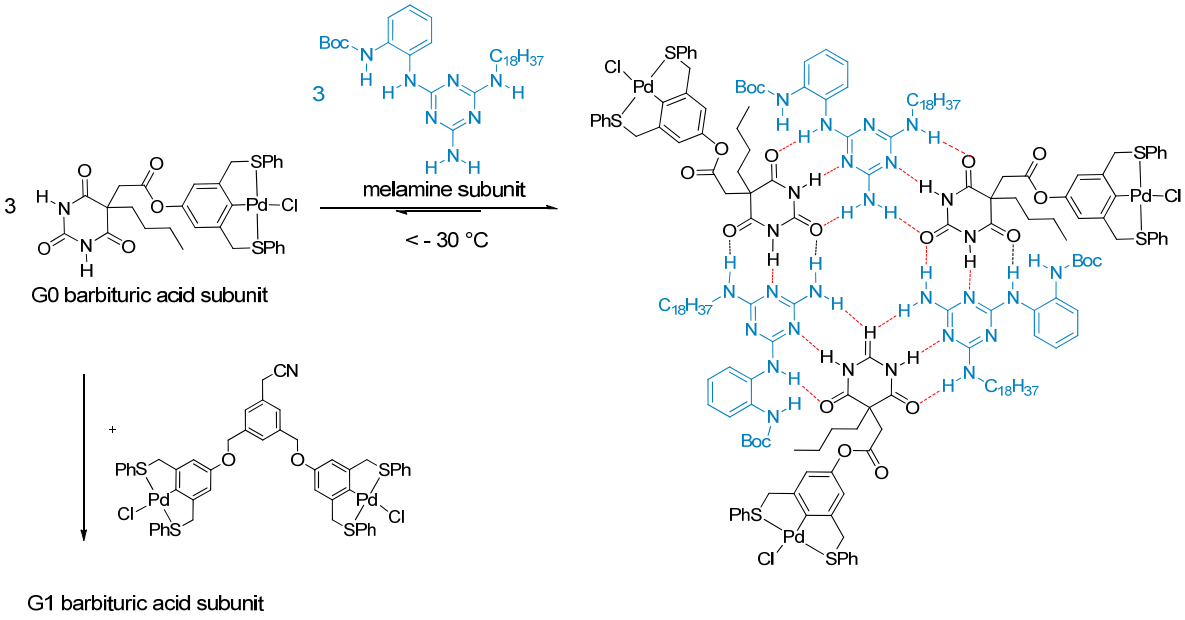

Figure 2-15: Hexameric rosette formation by melamine and barbituric acid interactions according to REINHOUDT *et al.*.[64]

A similar approach was taken by FRÉCHET *et al.,* who used a melamine derivative in combination with a cyanuric acid derivative. These authors observed that the higher generation dendrons do not form stable hexamers while the lower generations do, which was related to steric effects.[66] Generally speaking, the influence of the dendron generation size on the self-assembly process is still difficult to predict. An apolar branching around a hydrogen binding site can, in principle, shield the surrounding solvent, resulting in stronger hydrogen bonding especially in more polar solvents, but steric hindrance in higher generation dendrimers can be counterproductive. However, there are also examples in the literature which show that the dendron generation has almost no effect on the binding strength neither in a positive nor negative sense, as described in the following section on templated supramolecular dendrimers.

2.2.3 Templated Self-Assembled Dendrimers

Discrete self-assembled dendrimers of specific size and shape have been obtained with the help of structurally well-defined templates, which organise and assemble a given number of dendrons with complementary binding sites around themselves, thereby forming well-defined supramolecular aggregates. However, this templated assembly requires the synthesis of at least two different molecules, the dendron and the template, and the aggregation mode critically depends on their relative ratio.

The research group of ZIMMERMAN reported on a templated self-assembly based on an anthyridine-benzamidinium interaction as shown in **Figure 2-16**.[67]

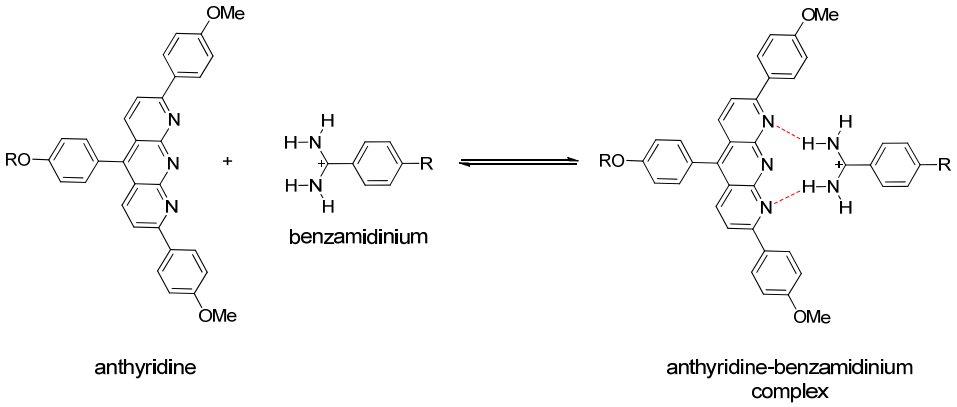

Figure 2-16: Anthyridine and benzamidinium forming a binary complex *via* two hydrogen bonds.

In this approach, FRÉCHET dendrons of 1st to 4th generation were linked covalently to an anthyridine moiety as depicted in **Figure 2-17**. Binding constants for interaction of the different generation dendrons and a benzamidinium ion were determined in 10 % acetonitrile/chloroform mixtures. Interestingly no significant difference in the binding constants were found, with values all in the range of $K = 2–3 \cdot 10^5$ M^{-1}, essentially independent on dendron generation size. This fact had been expected by the authors because of the fact that the geometry of the dendron is orientated "away" from the binding site. This example clearly shows that the binding strength cannot always be influenced by increasing or decreasing the generation size of the dendron.

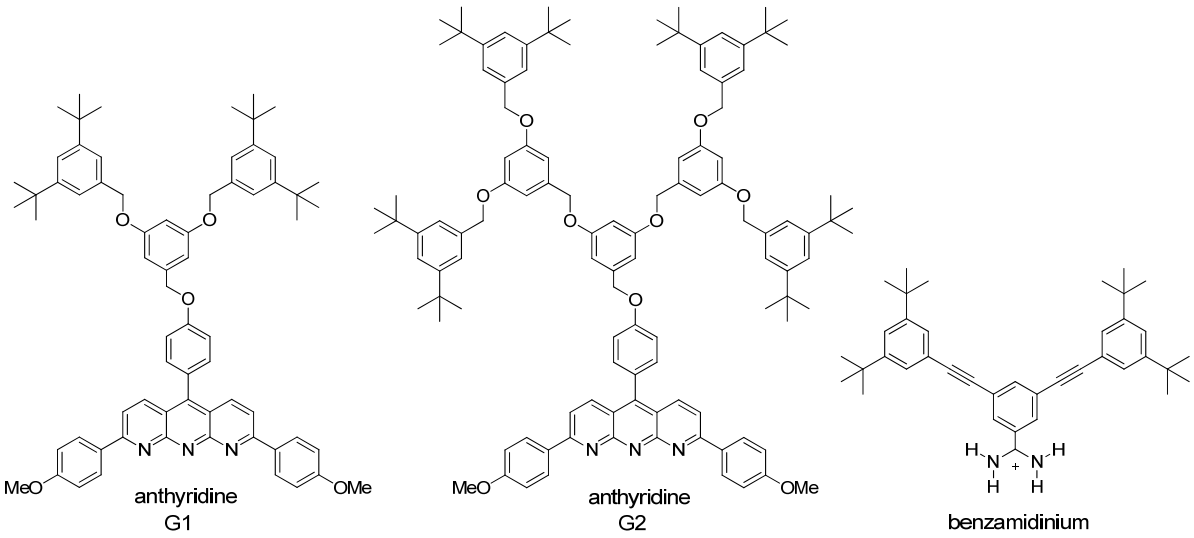

Figure 2-17: FRÉCHET dendrons of different generations coupled to an anthyridine moiety at the focal point for complexation of the benzamidinium substrate according to ZIMMERMAN *et al.*.[67]

ZIMMERMAN *et al.* then used the same dendrons and a bis-benzamidinium salt to assemble two dendrons around the core, thus producing the first supramolecular dendrimer in such a templated approach (**Figure 2-18**). The pentamidine core is active against the *Pneumocystis carinii* pathogen and therefore applied in the treatment of *Pneumocystis carinii pneumonia.* Thus, a potential medicinal application of such supramolecular dendrimeric system noted by the authors is the use as molecular carrier.

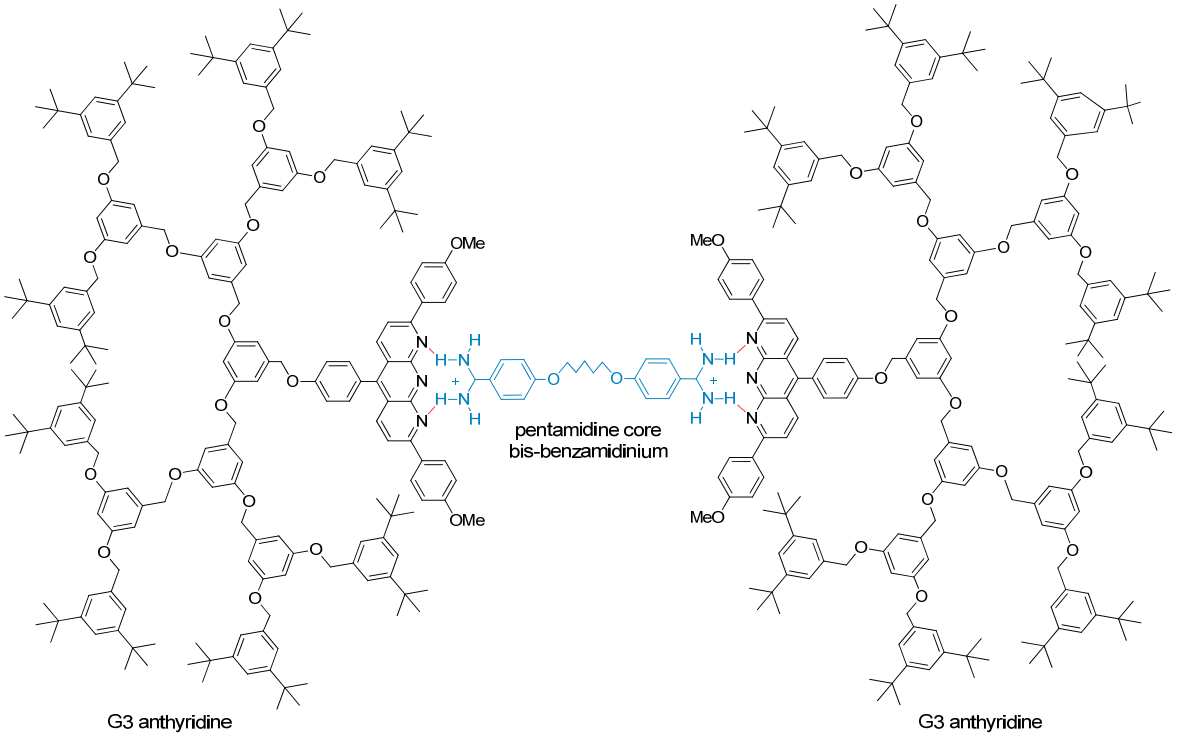

Figure 2-18: Templated self-assembly around an organic bis-benzamidinium core according to reference 67.

The first example of a complete self-assembly process not based on "dendritic subunits" was reported by the group of HIRSCH.[68, 69] They used the "Hamilton-Receptor" which is capable to form six hydrogen bonds to cyanuric acid as depicted in **Figure 2-19**.[70]

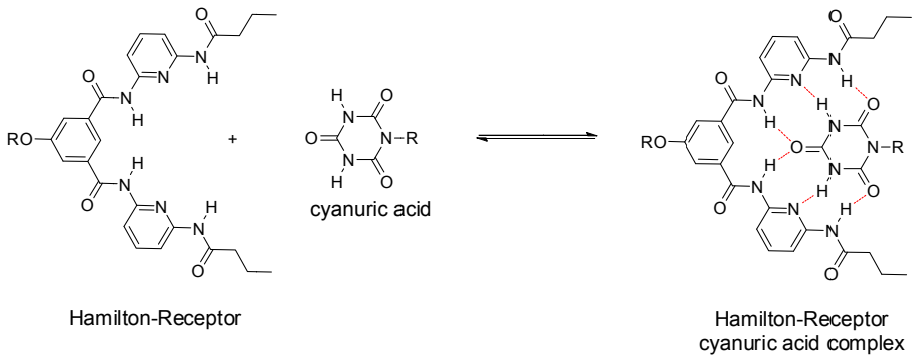

Figure 2-19: Hamilton-Receptor/cyanuric acid complex formed by 6 hydrogen bonds.

One homo-tritopic templating core and a hetero-tritopic branching element based on one cyanuric acid unit and two Hamilton-Receptor moieties were developed.[i] The principle of the shell-by-shell self-assembly is to mix the homo-tritopic Hamilton-Receptor core (H_3) and the hetero-tritopic branching units (C–H_2) in the related stoichiometric ratios for the desired generations of the dendrimers. The self-assembly is stopped by addition of end-capping units (C–GX) based on 1st to 3rd generation FRÉCHET type dendrons with a cyanuric acid moiety at the focal point. For example, one core H_3 assembles three branching units C–H_2, and six end-capping units C–GX will finish the self-assembly process, as illustrated in **Figure 2-20**.

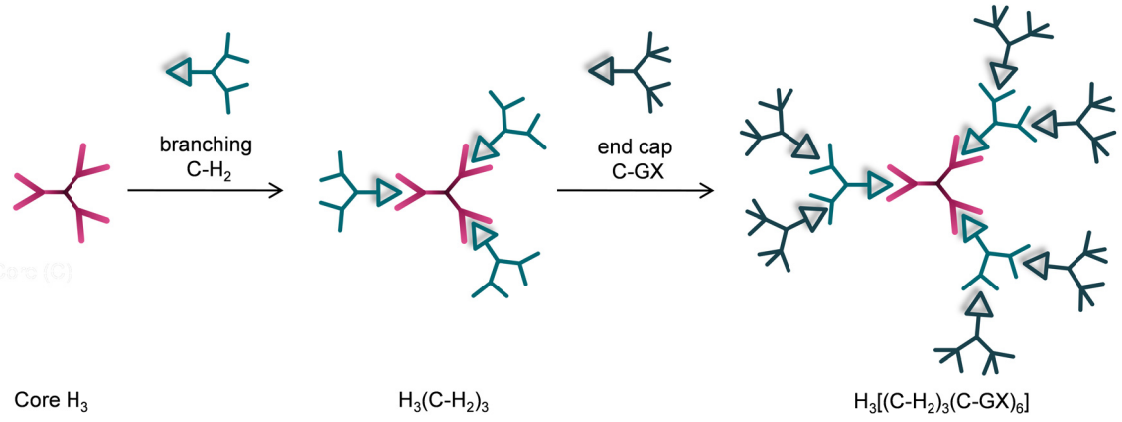

Figure 2-20: Schematic illustration of self-assembled supramolecular dendrimer according to HIRSCH *et al.*.[68]

[i] The groups of VÖGTLE and DE COLA already published in 2004 a poly-(propyleneamine) dendrimer functionalised at the periphery with the Hamilton-Receptor for multivalent recognition processes of barbiturate guests.[70]

The actual molecules prepared by this templated shell-by-shell self-assembly approach are shown in **Figure 2-21**.

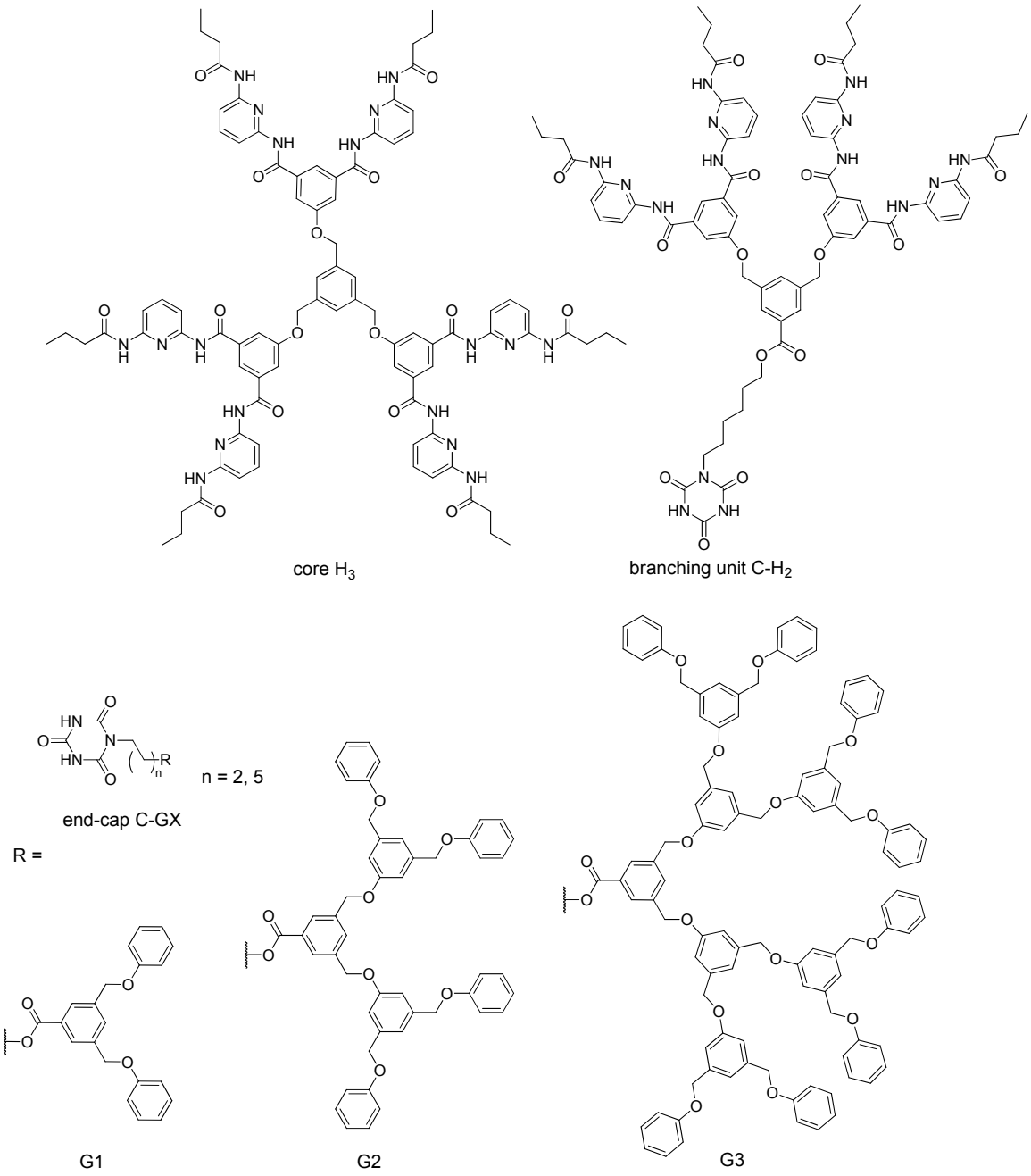

Figure 2-21: Tritopic Hamilton-Receptor functionalised core H_3, branching unit C–H_2 with two Hamilton-Receptor moieties and one cyanuric acid residue, and the cyanuric acid end-capping C–GX with different generations of FRÉCHET type dendrons.

Such a shell-by-shell self-assembly is a very promising approach because the self-assembled dendrimer can be increased by the generation size of the branching unit as well as by the generation size of the end-capping unit, thus forming more than one shell around the core. However, an inherent disadvantage of the system is that it cannot be guaranteed that the

tritopic core H_3 is only self-assembling with branching unit C–H_2 and the latter one only with the end-cap C–GX. There is the general possibility of formation of various mixtures in which the core is interacting with the end-capping and also the branching units with themselves. The only distinct systems are the combination of the core H_3 with three molecules of the end-capping unit C–GX forming the self-assembled H_3(C–GX)$_3$ dendrimer. In this case the system is based on two orthogonal interacting subunits, since the subunits alone are not capable to self-assemble.

Recently, HIRSCH *et al.* reported on the optimisation of the shell-by-shell assembly principle with the goal to obtain an orthogonal interaction of the core and the branching units and the branching with the end-capping units, respectively.[71] The core consists of a ruthenium metal centre forming a self-assembled metallo-dendrimer with three bipyridine branching units incorporating the Hamilton-Receptor. The end-capping units are derivatised cyanuric acid units, self-assembling with the Hamilton-Receptor to form the supramolecular dendrimer as discussed before (**Figure 2-22**).[i] The self-assembly around the core is thus a supramolecular self-assembly around a metallo-dendrimer forming a templated supramolecular dendrimer. HIRSCH *et al.* showed that the supramolecular dendrimer is formed in a one-pot-reaction by mixing core, branching-, and end-capping unit in the correct stoichiometric amounts.

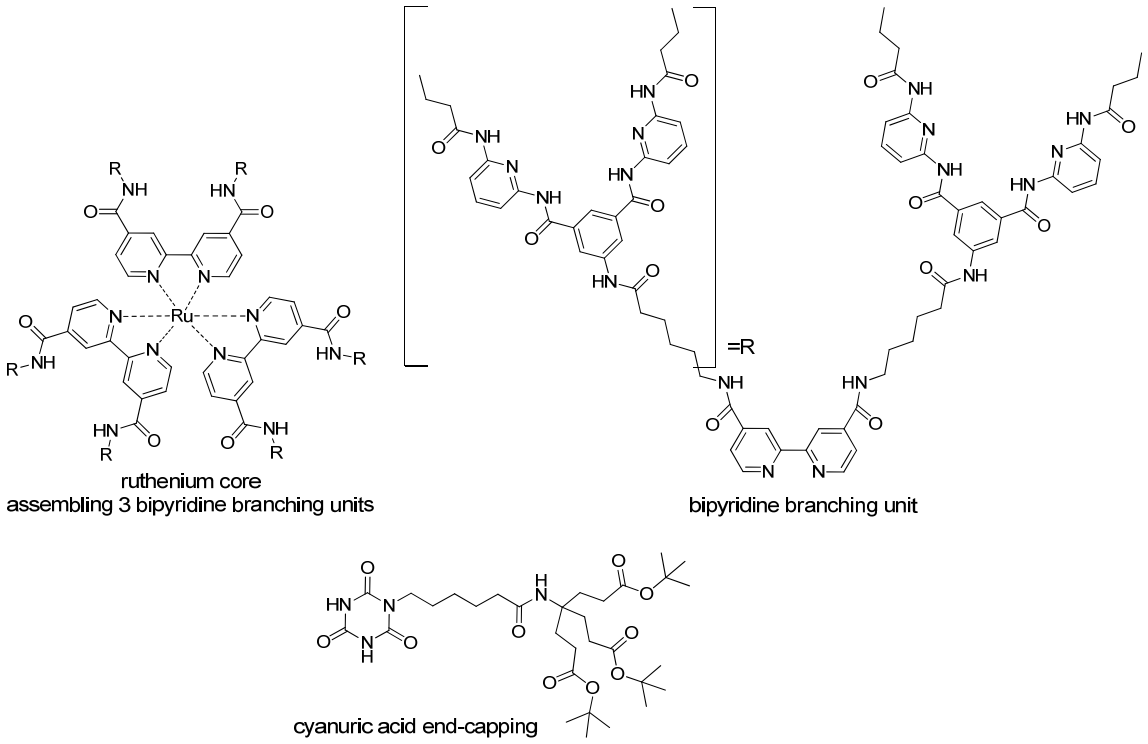

Figure 2-22: Templated self-assembly of a ruthenium coordinated bipyridine with Hamilton-Receptor units capable to form a supramolecular dendrimer with the cyanuric acid end-capping units.

[i] To what extent the self-assembly of the bipyridin around the ruthenium core is ascribed as a supramolecular complex due to the lack of reversibility is viewed differently by chemists. In fact it is sometimes addressed to coordination chemistry and not to supramolecular chemistry.[16]

There are various other examples of templated supramolecular dendrimers, for example SMITH's lysine dendrons functionalised with a carboxylic acid at the focal point interacting with the amine groups of the hydrophilic dye proflavine hydrochloride. This supramolecular dendrimer based on acid-base interactions was used to transport hydrophilic dyes suspended in dichloromethane into aqueous solution.[72, 73]

Another example for templated self-assembly are the dendritic pseudorotaxenes of GIBSON *et al.*. These researchers produced 1:3 complexes between a triply charged ammonium salt and FRÉCHET dendron-substituted dibenzo[24]crown-8 units.[i, 74, 75, 76] Based on the results of GIBSON *et al.*, a triggered self-assembled system of ammonium salts and benzo[18]crown-6 ether was later reported by SMITH and SEELEY, which will be discussed below.

The reversibility of the assembly of supramolecular dendrimers is perhaps the most interesting feature in comparison to covalent dendrimers. As mentioned above, there is the attempt to build covalent dendrimers that are cleavable in order to release enclosed guests. This is usually done by external triggers like pH or light.[43] In supramolecular dendrimer chemistry the aspect of reversibility, a logical consequence of weak bonding, allows the triggering to operate in both directions, i.e. formation and degradation of the dendrimer can be triggered back and forth. There are various external stimuli to achieve control over the self-assembly process. For instance, in case of ZIMMERMAN's rosettes (see **Chapter 2.2.2**) the self-assembly process is sensitive to temperature, concentration, as well as competing solvents, but not really reversible. The first literature example for controlled assembly and disassembly of a supramolecular dendrimer in solution was reported by SMITH and SEELEY in 2002.[77] In this study, a 1st to 3rd generation dendritic branched lysine with an benzo[18]crown-6 functionalised focal point was assembled around a bis-ammonium cation core (**Figure 2-23**). The templated self-assembly could be controlled by the addition of potassium ions to achieve a controlled release of the encapsulated core. Binding constants for 1:1 complexes of the benzylammonium core with the three different dendron generations were determined in deuterated methanol, revealing that with increasing generation the binding constant decreases. The 1st generation dendron has a binding constant of K = 3800 M^{-1}, the binding constant for the 2nd generation dendron is K = 1900 M^{-1} and the 3rd generation dendron has an association constant of only K = 200 M^{-1}. It was assumed that the decrease of the binding constants might be due to unselective binding in the branching of the dendron, but further examinations showed only a very weak non-selective binding. The finding that 1st to 3rd generation dendrons bind potassium ions more strongly, with K = 100 000 M^{-1} to 12 000 M^{-1} for 1st to 3rd generation, was utilised to displace

[i] Based on the findings of STODDART *et al.* to use crown ether complexes for interlocked molecules, GIBSON *et al.* used dibenzo[24]crown-8 to self-assemble dendrons around a triply charged ammonium salt.

the benzylammonium function. As expected, one equivalent of potassium ions was necessary to displace the benzylammonium from the 1st generation crown ether dendron.

The 1,4-bis(aminomethyl)benzene was complexed by two 2nd generation crown ether dendrons in a 1:2 stoichiometry, with a first binding constant of K = 115 M^{-1} and a second one of K = 18 M^{-1}, which indicated a non-cooperative binding in deuterated methanol. The 1:2 supramolecular complex could be disassembled by addition of potassium ions to release the bis-ammonium core.

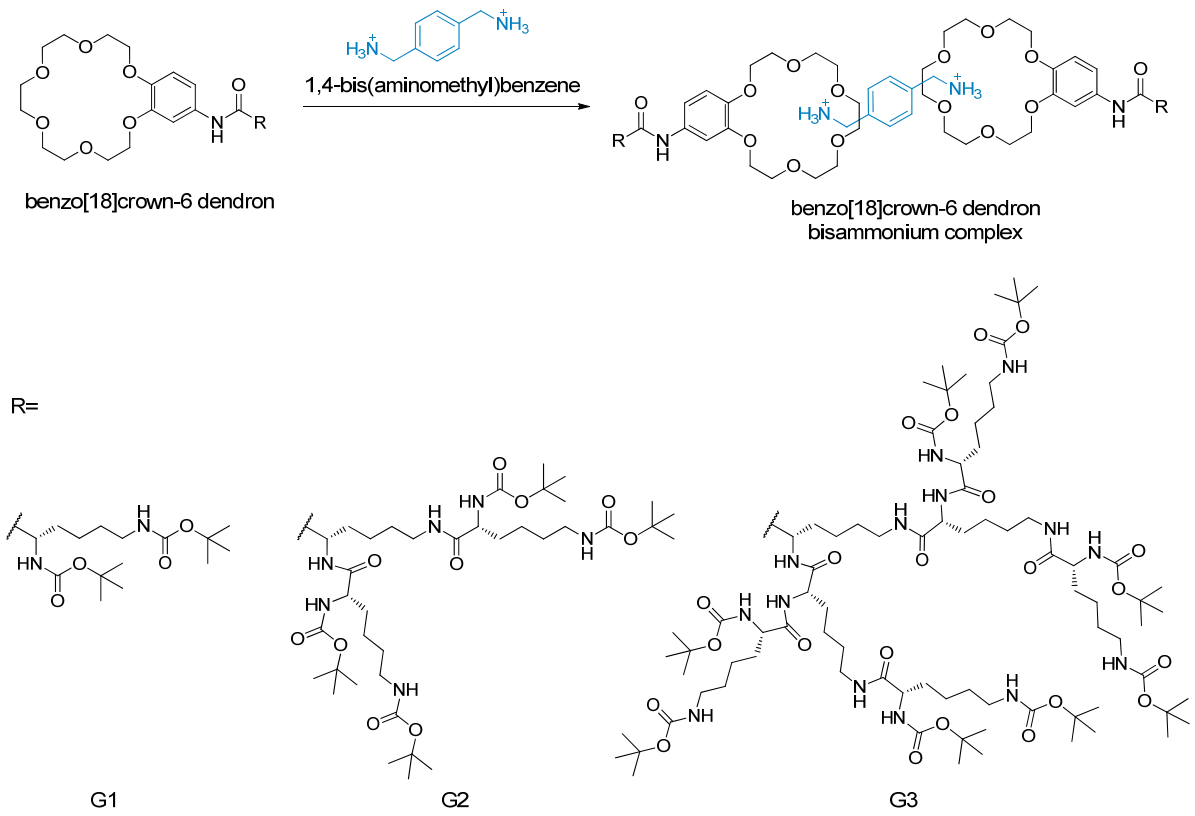

Figure 2-23: Illustration of 1st to 3rd generation dendritic branched l-lysine with a benzo[18]crown-6 moiety at the focal point forming 2:1 hetero-complexes with a bis-ammonium core according to reference 77.

Although the foregoing system represents a nice example for a triggered system in a competitive polar solvent one disadvantage is the problem of reassembling the supramolecular dendron. This would need either a complexation of the potassium ion by a stronger receptor than the crown ether, or the precipitation of potassium as a salt. A better way would be to trigger the self-assembly process by pH changes of the solution as it is easier to switch reversibly between acidic, neutral, and basic conditions by the addition of acid or base.

As demonstrated by the discussed examples of the templated and untemplated self-assembly, the concept of triggering is promising but so far often restricted to apolar solvents. To use such

systems someday as nanotransporters in aqueous media requires further research to get more information about the binding strengths and the influence of the dendritic surrounding on the self-assembly process. The next sections will discuss literature examples with regard to influence of the self-assembly process by generation size and polarity of the dendrons.

2.2.4 Influence of Polarity and Generation Size

The group of FRÉCHET was the first to publish a systematic study on self-assembly of dendritic "bow-ties", showing exciting effects of the peripheral functionality on association constants.[78] The aim of their work was to adjust the strength of complexation by altering the periphery groups of the dendrons without changing the generation size. The approach used an untemplated self-assembly based on a glycinylurea and the complementary bis(adamantylurea) as depicted in **Figure 2-24**.[i]

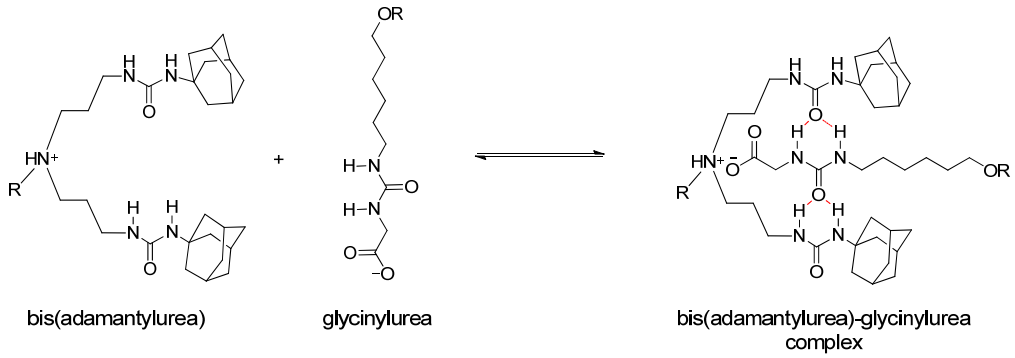

Figure 2-24: Schematic illustration of the bis(adamantylurea) and complementary glycinylurea binding motif invented by MEIJER *et al.*.[79]

The system was chosen to open the opportunity to self-assemble two orthogonal dendrons with different functionalised periphery groups. The influence of the periphery on the association constant of the binding site in the focal point was determined by NMR. Downfield shifts of the adamantylurea hydrogen atoms and the methylene protons adjacent to the tertiary amine were observed in the binding process as also described by MEIJER *et al.*.[79] An association constant of K = 520 M^{-1} in dry chloroform was measured for the bow tie with benzyliden acetal groups on the bis(adamantylurea) wedge and acetal groups at the glycinylurea wedge, as shown in **Figure 2-25**.

[i] The group of MEIJER *et al.* developed the binding motif and used it in the self-assembly of a functionalised dendrimer with 32 bis(adamantylurea) units on the periphery assembling glycinylurea building blocks.[79]

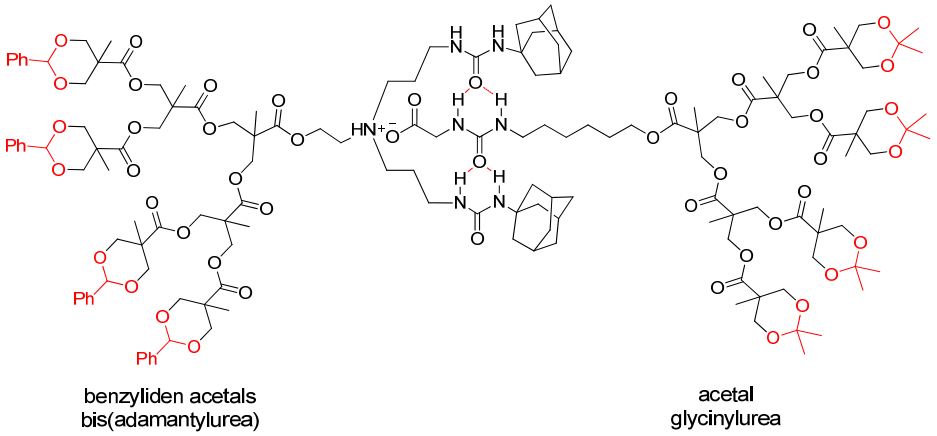

Figure 2-25: Self assembled "bow tie" dendrimer with K = 520 M^{-1} in dry chloroform.

The first variation of the "bow ties" was the deprotection of the benzyliden acetal groups. Combining the deprotected dendron with the acetal protected glycinylurea dendron leads to a bow tie as depicted in **Figure 2-26**. An increase of one order of magnitude was measured for the association constant (K = 6800 M^{-1}) in dry chloroform, which was explained in terms of the free energy gained when the rather insoluble polar dendron forms a soluble complex with the complementary dendron. This experiment shows that the periphery even at same generation size can have a significant influence on the binding site and thus on the stability of the self-assembled dendrimer.

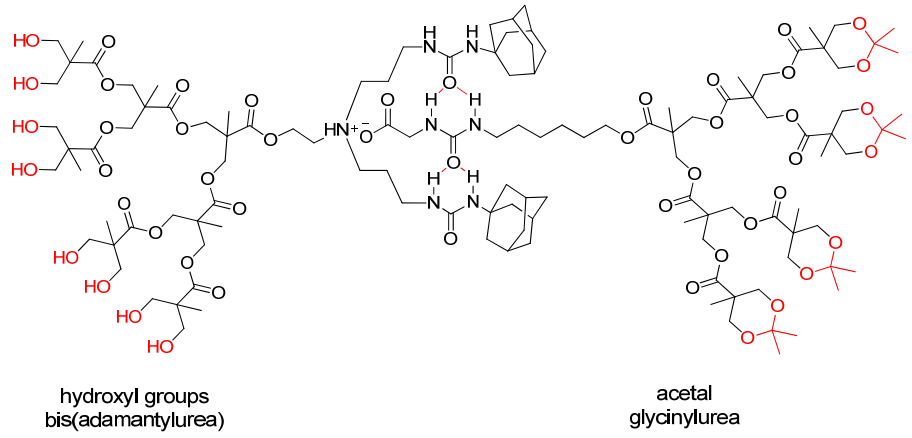

Figure 2-26: Self assembled "bow tie" dendrimer with the highest observed binding constant K = 6800 M^{-1} in chloroform.

Further investigations also with the deprotected glycinylurea dendron were hampered due to the fact that the more polar dendron was completely insoluble and no complex formation could

be observed. The better solubility of the deprotected adamantylurea dendron with same periphery is obviously due to the large apolar adamantyl residues.

As shown by the previous examples, the generation size can have a positive as well as a negative or even no effect on the stability of supramolecular aggregates. To test the influence of a higher generation dendron with high steric influence on the aggregation process, the glycinylurea dendron was functionalised with triethylenoxide chains (**Figure 2-27**). The association constant of the resulting bow tie dendrimer, K = 70 M^{-1}, was the lowest observed for this type of dendrimers indicating that a possible backfolding of the triethyleneoxide chains in the relative flexible dendron to the focal point hinders complex formation.

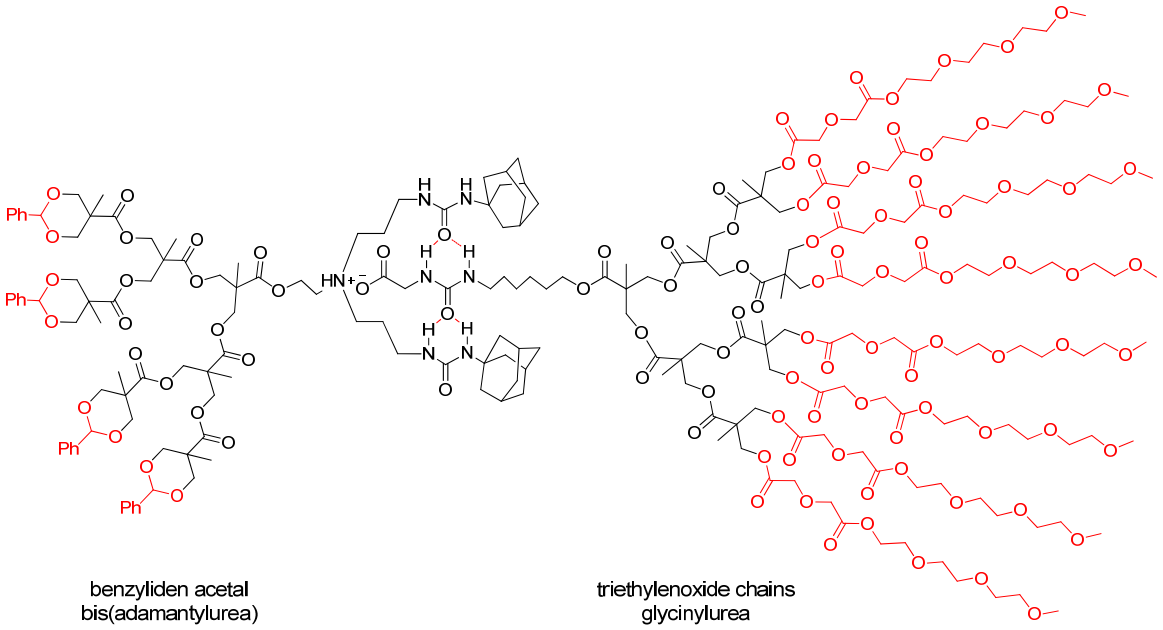

Figure 2-27: Self assembled "bow tie" dendrimer with a low binding constant (K = 70 M^{-1} in chloroform), possibly due to backfolding.

When the benzylidene acetal groups in the foregoing dendrimer were hydrolysed, an association constant of K = 1000 M^{-1} was determined for the resulting complex (**Figure 2-28**), in correspondence with observations made with the other "bow tie" dendrimers. The one order of magnitude higher association constant again can be attributed to the hydroxyl-functionalised periphery.

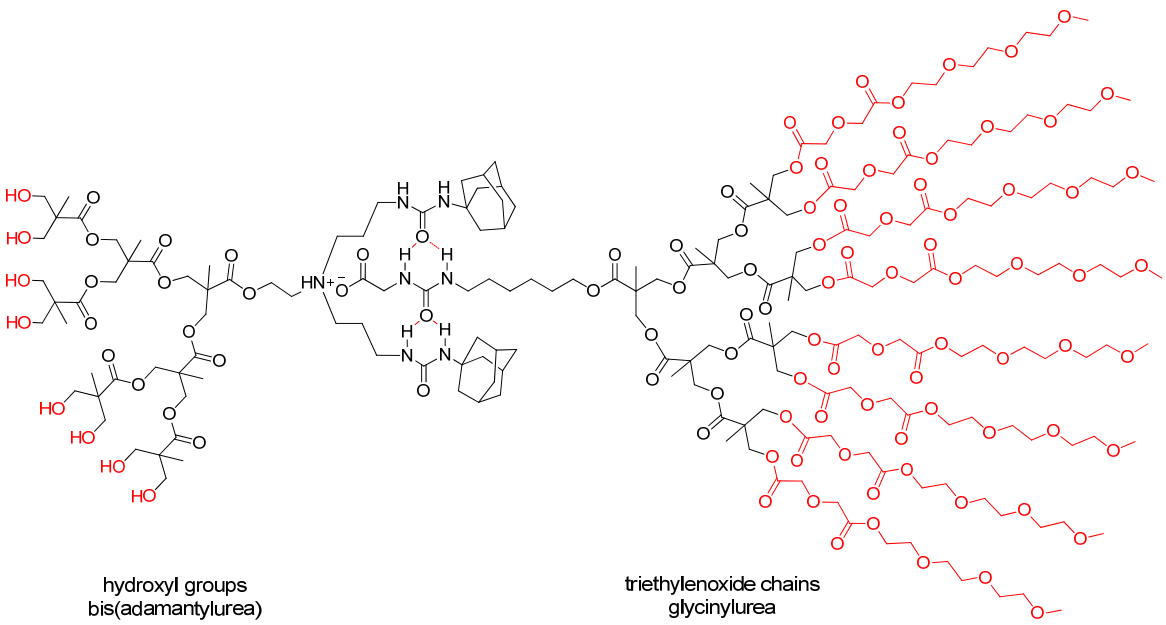

Figure 2-28: Self assembled "bow tie" dendrimer with K = 1000 M^{-1} in chloroform.

The discussed findings show that self-assembly of dendrons to supramolecular dendrimers is a challenging task and numerous possible influences of the utilised functional groups in the branching and the periphery of the dendrons have taken into account.

The influence of the generation size of the used dendron on the micropolarity and its enormous impact on the binding site was also reported by KAIFER *et al.*.[80] The authors employed the 2-ureido-4-pyrimidine binding motif developed by MEIJER *et al.* shown in **Figure 2-29**[81, 82] and attached NEWKOME-type dendrimers to achieve the self-assembled dimers as displayed in **Figure 2-30**.

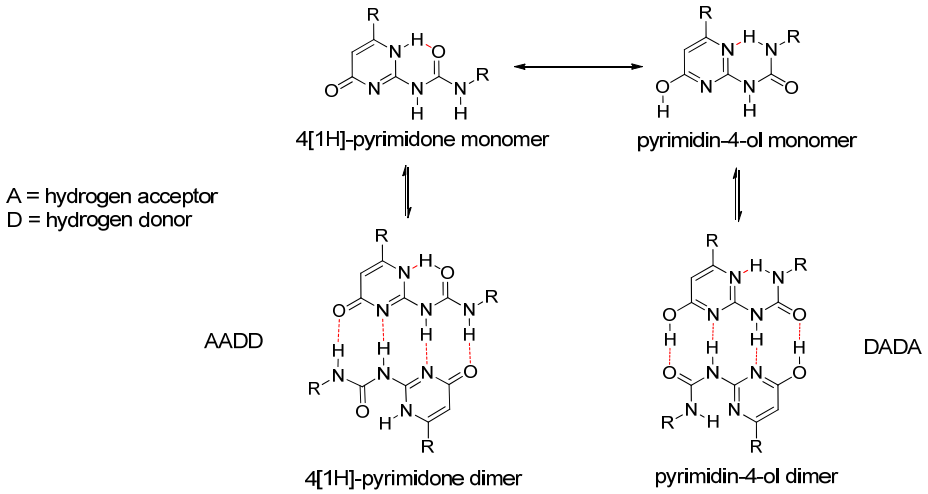

Figure 2-29: Tautomers of MEIJER's 2-ureido-4-pyrimidine binding motif.[81, 82] The keto form has a AADD hydrogen binding array and the enol tautomer a DADA hydrogen pattern.

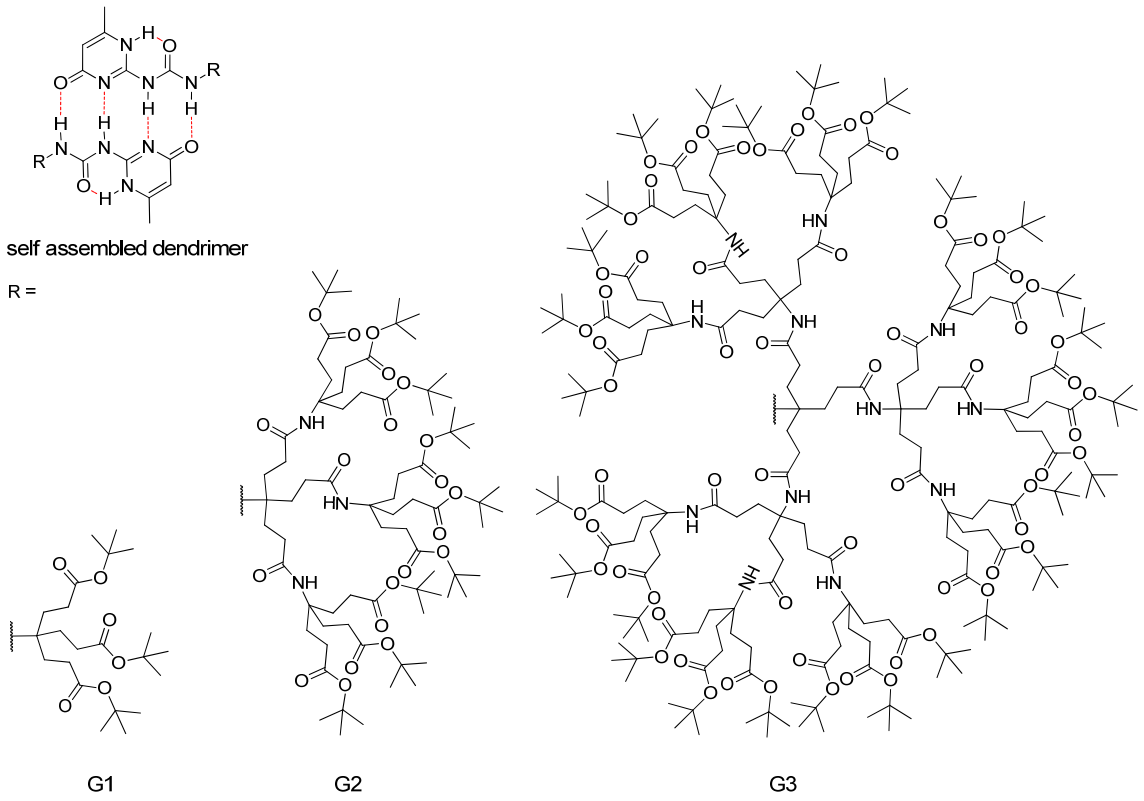

Figure 2-30: Self assembled uridopyrimidine dendrimers of KAIFER *et al.*.[80]

The NH proton NMR signals of the ureidopyrimidine unit showed a large downfield shift for 1st and 2nd generation dendrons, consistent with strong hydrogen bonding in the dimers. For the 1st and 2nd generation dimers binding constants in chloroform were determined by NMR dilution measurements. However, no significant difference was observed down to a concentration of 10^{-5} M, thus indicating association constants of $K > 10^6\ M^{-1}$. In marked contrast, a low dimerisation constant of $K = 2.6\ M^{-1}$ was found for 3rd generation dendrons (8.0 mM in $CDCl_3$), corresponding to only about 2 % dimerisation. This unexpected result was ascribed to a more polar micro-environment, i.e. polar enough to weaken the hydrogen bonding motif attached at the focal point, similar to what has been observed in other studies on NEWKOME dendrons.[83] Steric repulsion was also discussed to be responsible for the low association constant, but additional experimental data suggest only moderate steric hindrance. The effect of the micro-polarity around the binding motif can be directly seen in the NMR spectra. Beside the signals for the 4[1H]-pyrimidinone, a second set of signals for the pyrimidin-4-ol tautomer is also observed (**Figure 2-29**). The relative ratio of the two sets of signals was compared for the 1st to the 2nd generation dimers in chloroform and in the less polar solvent toluene (**Table 2–2**). As previously reported in the literature, the abundance of the pyrimidinol tautomer is higher in toluene than in polar chloroform. This can be related to the

micro-environment generated by the dendron. Also the abundance of the pyrimidinol tautomer is higher in the 1st generation dendron than in the more polar 2nd generation dendron. This is a clear hint for an increasing polar micro-environment through the increased generation size of the NEWKOME dendrons.

Table 2–2: Keto-enol tautomer ratio of 2-ureido-4-pyrimidine from ^{1}H-NMR measurements.

dendrimer generation size	keto:enol ratio in $CDCl_3$	keto:enol ratio in $toluene_{d8}$
G1	6:1	3:1
G2	99:1	7:1

CHOW and co-workers[84] used the same binding motif as KAIFER *et al.* but replaced the NEWKOME dendrons by apolar FRÉCHET dendrons at the ureidopyrimidine unit. No noticeable difference in the association constant of the different generation dendrons was observed. All three generations formed stable dimers with binding constants $K > 10^7$ M^{-1} in chloroform.[i] Since the FRÉCHET dendrons differ from the NEWKOME dendrons in size, branching pattern (3 vs. 2), and especially branch length (4 vs. 2), the steric influences cannot be directly compared (the 3rd generation NEWKOME dendron is more sterically crowded than the 3rd generation FRÉCHET dendron).

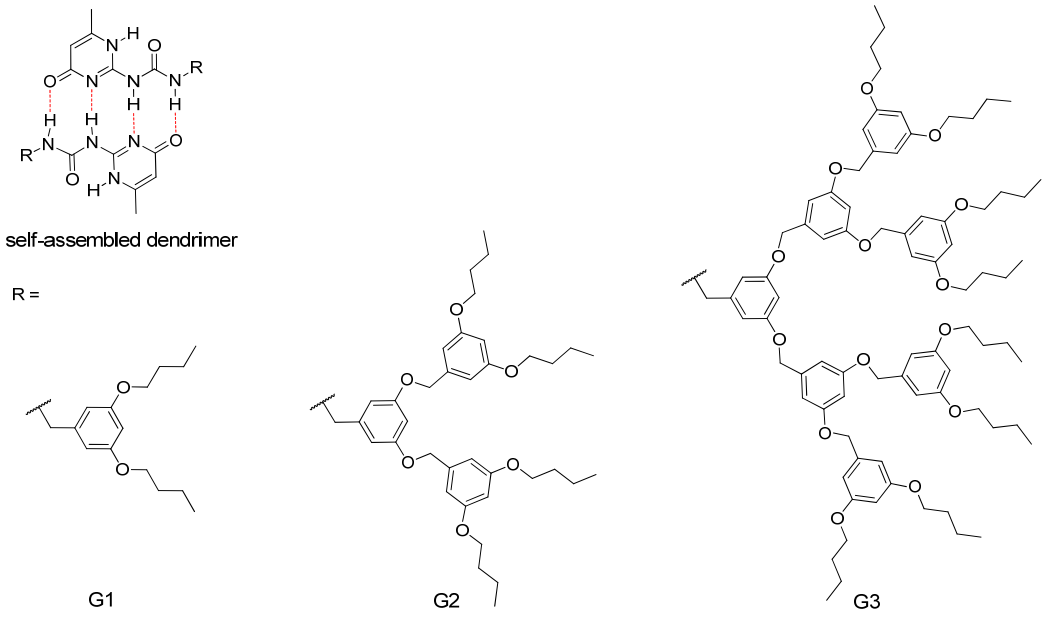

Figure 2-31: Structures of self-assembling dendronised dimers of CHOW *et al.*.[84]

[i] Additional measurements in a solvent of higher polarity (10 % dimethylsulfoxide in chloroform) led to a strong decrease in the dimerisation constants to $K = 10^2$ M^{-1} for all three generations.

Inconsistent is the fact that in the aggregates of KAIFER a second set of NMR signals for the pyrimidinol tautomer was observed in less polar solvents or for less polar generation shell. For the apolar dendrons of CHOW *et al.* one would expect a more intens signal for the pyrimidinol tautomer, but this was not observed.[i] Consequently, the effect of micro-polarity induced by the dendrons is not directly comparable in this case, hence, it is difficult to draw a conclusion. Clearly, the different effects indicate a completely different micro-environment. Perhaps, in case of KAIFER's system the higher micro-polarity is not only responsible for the sizable fraction of the pyrimidinol tautomer and the reduced stability of 3rd generation dendrimer. Another explanation could be that the hydrogen bonding interactions of the binding site are competing with the 9 amide and 27 ester functionalities surrounding the binding motif of the 3rd generation dendron. Such "backfolding" is well known in the literature for polar dendrimers such as polyamidoamine.[85]

In conclusion, dendrons with modest polarity in apolar solvents compete with the hydrogen bonding array of the binding site. This causes big problems for building stable supramolecular dendrimers of higher generations. In order to obtain water-soluble supramolecular dendrimers, the periphery has to be polar to achieve sufficient solubility in water. Therefore, the periphery has to be functionalised with groups that increase solubility but do not compete with the binding motif. Thus amide, ester, or carboxyl groups can be unfavourable for formation of supramolecular dendrimers. In the next section oligoethylenoxide chains will be discussed because they are widely used to increase the solubility in aqueous media.[ii]

2.2.5 Competitive Intramolecular Hydrogen Bonding

The influence of polar oligo-ethyleneoxide chains on formation of non-covalent assemblies was recently investigated by the group of MEIJER.[86] It is recommended to consult the original article for details because only a small part of the comprehensive examination is given here. Although the compounds investigated by MEIJER *et al.* are not dendrimers, the reported results regarding the backfolding of the polar chains onto the hydrogen bonding array are of interest because in dendrimers a multiplicity of such interactions can be expected.

Like in some of the systems described before, the ureidopyrimidone binding motif was used. The binding motif is capable of creating quadruple hydrogen bonding interactions. The related binding constant was determined to be $K = 6 \cdot 10^7\ M^{-1}$ in chloroform for alkyl-substituted

[i] As reported in the literature, the highest fractions of the pyrimidinol tautomers were observed for strong electron withdrawing groups at the 6-position of the pyrimidine.[81] In the derivatives of KAIFER and CHOW a methyl group is in the 6-position of the pyrimidine, so the same influence is expected.

[ii] The oligo-ethyleneoxide chains were not only used because of the solubilising capabilities, but also because of low toxicity and biocompatibility.

derivatives. MEIJER *et al.* observed that incorporation of a triethyleneglycol chain connected *via* an aliphatic C2 spacer lead to a dimerisation constant about 2000 times weaker than before. In contrast, no change in the binding constant was observed for the linkage of the triethylene-glycol chain *via* an aliphatic C6 spacer. To study the influence of the spacer lengths m and ethyleneoxide chain lengths n, several pyrimidone derivatives were synthesised (**Figure 2-32**).

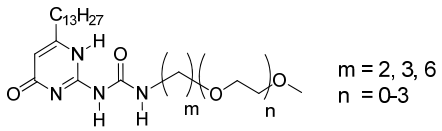

Figure 2-32: Structure of oligo-ethyleneoxide substituted 2-ureido-pyrimidinones according to reference 86.

The dimerisation constant, as determined by ^{1}H-NMR spectrometry in anhydrous deuterated chloroform, span a range of two orders of magnitude (**Table 2–3**). Significantly lower binding constants were observed for entries 5 and 6.

Table 2–3: Dimerisation constants of the ureidopyrimidone binding motif determined by ^{1}H-NMR spectrometry in anhydrous $CDCl_3$ according to reference 86.

entry	m	n	K_{dim} M^{-1}
1	**2**	0	$> 10^6$
2	**3**	0	$> 10^6$
3	**2**	1	$> 10^6$
4	**3**	1	$5 \pm 1\ 10^5$
5	**2**	2	$3 \pm 0.5\ 10^4$
6	**3**	2	$7.7 \pm 0.6\ 10^4$
7	**6**	2	$> 10^6$

From further NMR, IR, and UV studies it was concluded that these low values are a result of backfolding of the ethyleneoxide chain by building up hydrogen bonds to the ureido NH protons. Intramolecular hydrogen bonds can strongly differ in their enthalpic contributions, depending largely on the strength and spatial arrangement of the hydrogen bond donor and acceptor. The hydrogen bond strength between the oxygen of the ethyleneoxide and the urea NH proton is much lower compared to an amide-amide hydrogen bond. This is due to the fact that the carbonyl group is a better electron donor for hydrogen bonding compared to the oxygen. If the ethyleneoxide will be replaced by a side chain with stronger hydrogen bond donor and acceptor moieties, like the NEWKOME type dendrons in the above discussed example

of KAIFER, it is getting more difficult to obtain a strong dimer formation of the ureidopyrimidone binding motif.

The foregoing sections made clear that attempts to produce stable and water-soluble supramolecular dendrimers will heavily be influenced by all the discussed effects, namely of polarity, generation size of dendrons, and possible interactions with the binding site by backfolding of the periphery groups.

In the next chapter the research project of the present thesis is outlined and the employed dendrons and binding site are presented.

3. PROJECT AND OBJECTIVES

3.1 From Small Molecules Towards Supramolecular Dendrimers

As outlined in **Chapter 2** –Background Information– dendrimers are an interesting class of macromolecules which are currently intensely explored for various applications in chemistry, material sciences, biology, and medicine. An important advantage of self-assembled dendrimers in contrast to covalent ones is the possibility to trigger aggregate formation using external stimuli like solvent polarity, pH, the presence of metal ions, and various others. Self-assembly is based on reversible, non-covalent interactions that allows, in favourable cases, to control the conditions under which the macromolecules are formed or disaggregated. However, a supramolecular assembly of dendrons most often results in polymeric aggregates such as columnar stacks, fibres, or hollow spheres. Achieving control over the exact size and probably even the shape of these polymeric aggregates is difficult and challenging. With the help of structurally well-defined templates, discrete self-assembled dendrimers have been obtained. The templates organise and assemble a given number of dendrons with complementary binding sites around themselves, thus forming well-defined templated supramolecular aggregates. Direct and untemplated self-assembly of dendrons into well-defined, specific aggregates is much less explored and only a few examples exist. However, most of the supramolecular dendrimers prepared so far are only stable in organic solvents like chloroform but dissociate into their monomers in more polar solvents.[i] Self-assembly of small monomers into discrete and well-defined supramolecular dendrimers which can be deliberately switched back and forth between monomer and self-assembled aggregate in water is still a major challenge.

The objective of this thesis is to investigate the self-assembly process of a dendron-modified binding site in aqueous media with the aim to obtain well-defined and highly stable supramolecular dendrimers, and to control the assembly and disassembly process by changing the pH value. For this project two main building blocks are necessary:

- Dendrons of different generations providing water solubility of the assembled dendrimers.
- A binding site that exhibits properties for efficient self-assembly in aqueous solution and sensitive to pH changes, i.e. owns acid-base properties.

[i] Based on amphiphilic molecules there are examples reported for defined micellular structures and pH dependent molecular arrangements in water.[87]

The dendrons will be attached covalently to the binding site, and the acquired building blocks are used in the self-assembly approach to obtain supramolecular dendrimers. In the following two sections the selected dendrons and binding sites are presented.

3.1.1 Dendrons

Promising types of dendrons are the polyglycerol systems invented by the research group of HAAG.[88, 89, i] The polyglycerol dendrons **1**, **2**, and **3** have, in contrast to often used amide or ester based dendrons, only ether functionalities in the branches, which may be beneficial in preventing strong intramolecular hydrogen bonding to the binding site, compare **Section 2.2**. The polyglycerol dendrons have been used by HAAG *et al.* as building blocks for the synthesis of covalent dendrimers. The polyglycerol dendrons are functionalised at the focal point with an azide[ii] group because the synthesis of covalent systems *via* click chemistry[90, 91, 92] turned out to be an efficient method to obtain high yields, especially for higher generations of dendrons. Therefore the 1st to 3rd generation polyglycerol dendrons **1**, **2**, and **3** depicted in **Figure 3-1** were employed in the present thesis as water soluble and highly biocompatible[88, 93, 94] building blocks. In the following, the structural presentations of the dendrons are simplified as shown in the lower right corner of **Figure 3-1**.

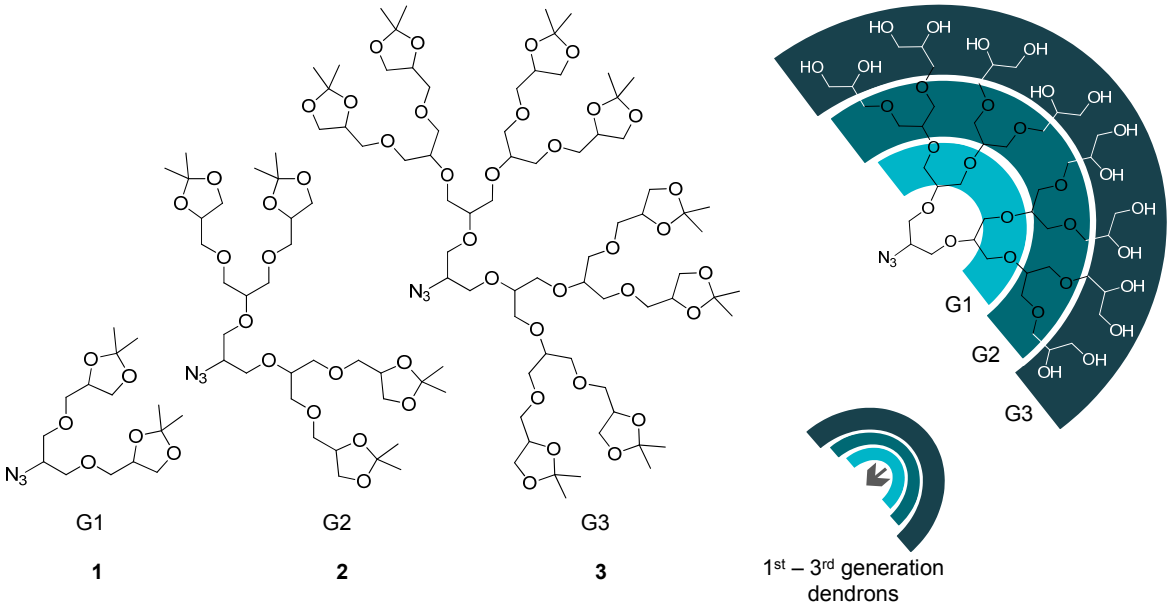

Figure 3-1: The 1st to 3rd generation polyglycerol dendrons invented by HAAG *et al.*. Hydroxyl groups are protected as acetals. The schematic simplification on the right is used in the following text to symbolise either unprotected or protected dendrons. The generation size is illustrated by colouring of the rings.

[i] The work presented here is based on a cooperation project of Prof Dr. Carsten Schmuck and Prof. Dr. Rainer Haag, FU Berlin. The initial synthesis of polyglycerol dendrons was carried out by Dr. Monika Wyszogrodzka, a former member of the Haag group.
[ii] Organic azides can be handled relatively safely if the "rule of six" is fulfilled: six carbons or other atoms of about the same size per azide provide a sufficient diluted atom ratio of nitrogen compared to other atoms.

3.1.2 Binding Site

As stated above, the aim of this thesis is to generate supramolecular dendrimers in aqueous solution.[i, 95, 96] But the question is, why is an efficient self-assembly in water so interesting? Beside the fact that water is a "green", inexpensive reaction medium, it provides the environment for life and regulates many processes in nature. The idea is to use supramolecular dendrimers as nanotransporters for biomedical applications. Therefore it is indispensable to target water as medium to form such self-assembled aggregates. The main problem of supramolecular chemistry in water is to confer sufficient water solubility to the supramolecular entity and also to minimise the involvement of water in the non-covalent self-assembly process. As an efficient binding site, the guanidiniocarbonyl pyrrole invented by SCHMUCK[97] was used to connect the 1st to 3rd generation dendrons. In the past 10 years SCHMUCK *et al.* has used the pH dependent complexation ability of the guanidiniocarbonyl pyrrole structure (**Figure 3-2**, top) to obtain strong association constants with oxo-anions even in polar media.[98] With a special variant of a self-complementary guanidiniocarbonyl pyrrole carboxylate zwitterion (**Figure 3-2**, bottom) different types of nanostructures such as vesicles or supramolecular polymers have been obtained by the dimerisation process.[99] The stability of the aggregates is primarily based on the formation of hydrogen-bond enforced ion pairs and thus limited to a pH in the range of 5–8.

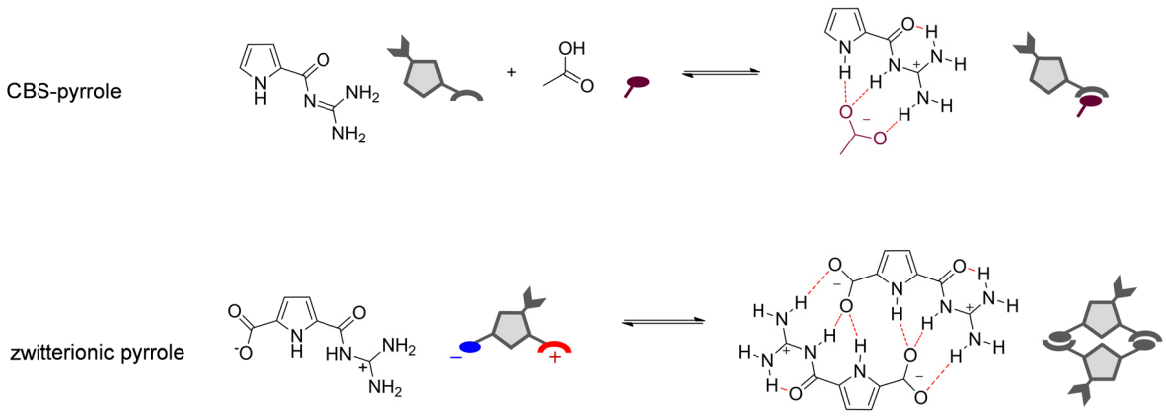

Figure 3-2: **Top**: Guanidiniocarbonyl pyrrole as efficient carboxylate binding site (CBS), and the schematic illustration used in the work; **Bottom**: The self-complementary zwitterionic guanidiniocarbonyl pyrrole carboxylate and its schematic illustration.

For use in this work, the binding site had to be functionalised with an alkyne moiety in order to perform click reactions with the azide-functionalised dendrons.

[i] A comprehensive review on "Supramolecular Chemistry in Water" was written by VERBOOM *et al.*[95] The reader is recommended to this article as this topic will not be discuss in detail.

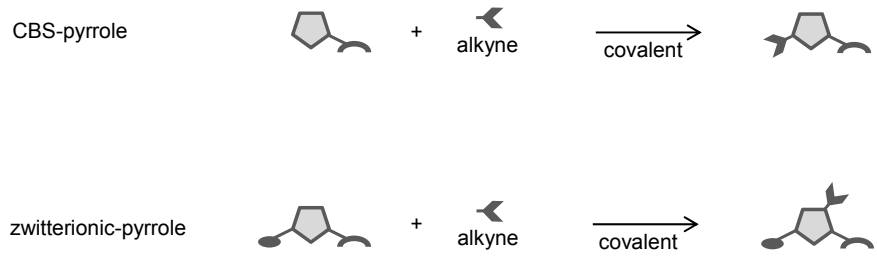

Figure 3-3: Covalent synthesis to introduce an alkyne moiety in the pyrrole binding sites.

3.2 Self-Assembly Approaches

This work is based on the covalent combination of the 1st to 3rd generation dendrons **1–3** shown above and the guanidiniocarbonyl pyrrole binding site to create building blocks used for the non-covalent self-assembly procedure. Three different approaches were performed to elucidate the potential of each method in forming supramolecular dendrimers. The first utilises the carboxylate binding site (CBS), in the other two approaches zwitterionic binding sites are employed:

- CBS Templated Supramolecular Dendrimer (CBS-T-SD)
- Zwitterionic Untemplated Supramolecular Dendrimers (ZU-SD)
- Zwitterionic Templated Supramolecular Dendrimers (ZT-SD)

3.2.1 CBS Templated Supramolecular Dendrimers (CBS-T-SD)

As mentioned above, the building blocks for self-assembly are synthesised by a click reaction between the alkyne substituted pyrrole and the azide functionalised 1st to 3rd generation dendrons. The thus obtained CBS-dendron building block is then used in the CBS-T-SD approach to form supramolecular water stable complexes by the interaction of the guanidiniocarbonyl pyrrole with carboxylic acids or phosphonic acid functionalised cores (**Figure 3-4**). Here, an AB system avoids undesired aggregation, i.e. neither the dendrons nor the cores should undergo self-assembly.

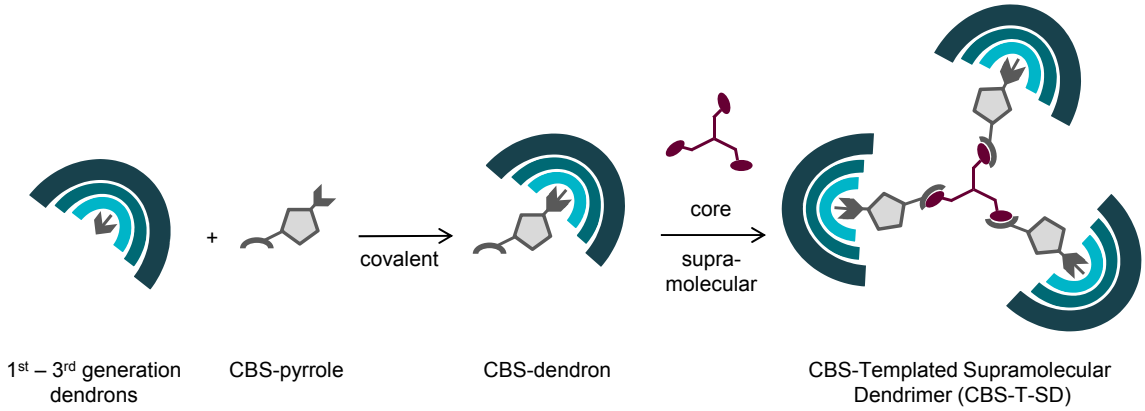

Figure 3-4: Schematic illustration of the CBS Templated Supramolecular Dendrimer approach.

The capability of the CBS-dendron building blocks to coordinate to various carboxylic acid or phosphonic acid substituted molecules renders this approach more general applicable than the zwitterionic approach. However, the zwitterionic approach is in case of complex stability very interesting, because it has a higher complexation strength compared to the CBS-pyrrole oxo-anion interactions.

3.2.2 Zwitterionic Untemplated Supramolecular Dendrimers (ZU-SD)

The zwitterionic-dendron building blocks are again prepared by click reactions between 1st to 3rd generation dendrons **1–3** and the alkyne functionalised zwitterionic bindingsite. Producing supramolecular dendrimers *via* untemplated self-assembly is a challenging approach, but in view of the synthetic complexity interesting. Only one self-complementary building block has to be synthesised in order to obtain a supramolecular dendrimer based on a homo-dimer of zwitterionic-dendrons. **Figure 3-5** demonstrates how the dendrons of 1st to 3rd generation can be covalently attached to the backbone of the bindingsite. The self-assembly process to give the supramolecular dendrimer is than achieved by non-covalent interactions.

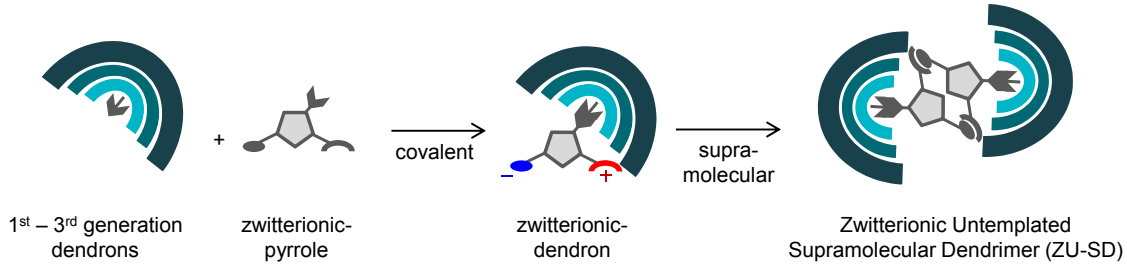

Figure 3-5: Schematic illustration of the Zwitterionic Untemplated Supramolecular Dendrimer approach.

3.2.3 Zwitterionic Templated Supramolecular Dendrimers (ZT-SD)

For use of zwitterionic-dendrons in the ZT-SD approach, a zwitterionic templating core is necessary in order to get a 2:1 hetero-associate as shown in **Figure 3-6**.

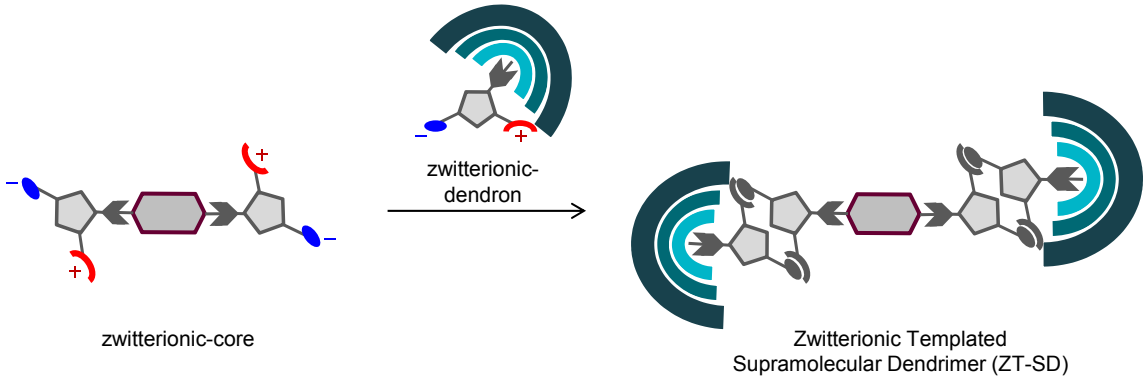

Figure 3-6: Schematic illustration of the Zwitterionic Templated Supramolecular Dendrimer approach.

The problem of self-assembly with self-complementary binding sites are the facts that the zwitterionic dendrons can build homo-dimers and that the core may undergo self-association to form a supramolecular network. Thus, an AB system as shown in **Section 3.2.1** for the CBS approach is in general more suitable.

4. Results and Discussion

4.1 Overview

An overview of the three possible pathways to supramolecular dendrimers *via* the guanidiniocarbonyl pyrrol binding motif as discussed in **Chapter 3** –Project and Objectives– is shown in **Figure 4-1**.

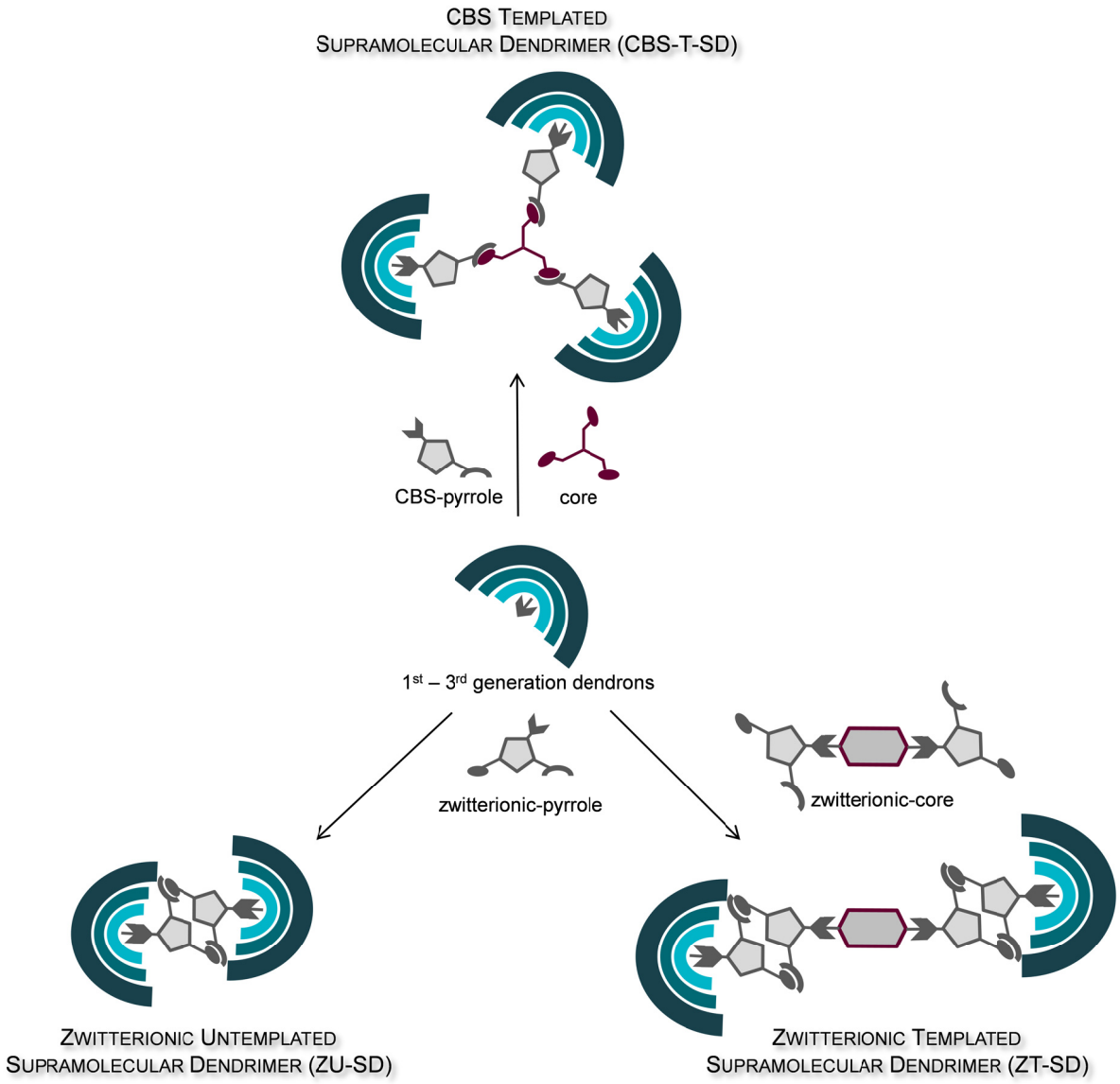

Figure 4-1: Schematic illustration of the three different approaches studied in this thesis to produce supramolecular dendrimers.

4.2 CBS Templated Supramolecular Dendrimers (CBS-T-SD)

4.2.1 Introduction

In this section the work concerning the CBS-T-SD approach is reported. The idea was to self-assemble an efficient carboxylate binding site around different oxo-anionic cores by non-covalent interactions. CBS-dendrons were prepared by connecting the guanidiniocarbonyl pyrrole binding site covalently to polyglycerol dendrons of different generations (**Figure** 4-2).

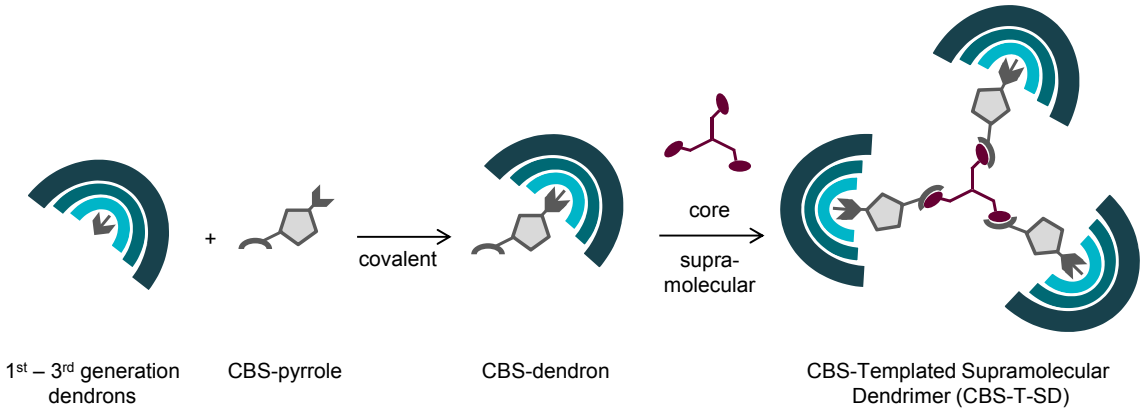

Figure 4-2: Schematic illustration of the CBS-T-SD approach.

Experiments to test the potential of templated self-assembly were performed with trivalent trimesic-acid (TMA, 4),[100] tetravalent ethylene-diamine-tetracarboxylic-acid (EDTA, 5),[101] and trivalent nitrilo-tri-methylene-phosphonic-acid (NTMP, 6)[102] as template core precursors. The actual entities undergoing self-assembly, CBS-cation and core-anion, are formed by an instantaneous acid-base reaction between CBS-dendron and core precursor. Pyrrole-acetylguanidines have pK_a values of about 6.8, the pK_a values of the used core acids are given in **Figure** 4-3. Since the pK_a values differ at least by 2 units, complete proton transfer between the reactants is guaranteed.

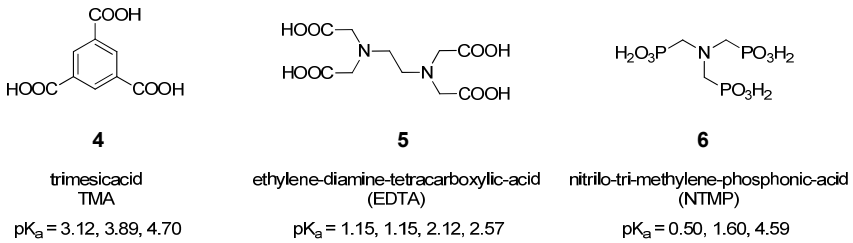

Figure 4-3: Core molecules used in the CBS-T-SD approach with the guanidiniocarbonyl pyrrole binding site.

4.2.2 The 2,5-Substituted CBS-Dendrons

4.2.2.1 Synthesis

The synthesis of CBS-dendron **13** is illustrated in **Scheme 4–1**. The alkyne functionalised guanidiniocarbonyl pyrrole building block **11** is based on the 2,5-substituted pyrrole **10**.[103] Differently to the reported synthetic procedure for **10** *via* a benzyl ester, the methyl ester **7**[i] was used as starting material. After hydrolysis of methyl ester **7**, a standard coupling reaction with PyBOP and Boc-guanidine[104] in dimethylformamide was performed.[ii] Carboxylic acid **10** was obtained after permanganate oxidation of aldehyde **9** and care has to be taken in the acidic work up of **10** to prevent decomposition of the Boc-protecting group. Reaction of pyrrole **10** with propargylamine was performed in nearly quantitative yield by a standard coupling reaction with PyBOP in dimethylformamide. The click reaction of 2nd generation dendron **2** and pyrrole **11** was carried out in a 1:1 water/tetrahydrofuran mixture in the presence of diisopropylamine, sodium ascorbate, and copper(II)sulphate pentahydrate. Reaction control by thin-layer-chromatography (TLC) showed complete transformation after 2.5 hours. After purification, the protected pyrrole **12** was isolated in 55 % yield. The moderate yield results from necessary purification procedures. For purification, the reaction mixture was diluted with dichloromethane and extracted with saturated EDTA solution to remove the copper salts, followed by reversed-phase and normal-phase chromatography. Deprotection of the Boc- and acetal-protecting groups was done with tri-fluoroacetic-acid (TFA). High-performance-liquid-chromatography (HPLC) reaction control showed incomplete deprotection at room temperature after 2 days. Therefore, the solution was further stirred at elevated temperature until complete deprotection was achieved after 3 days. After purification *via* reversed-phase chromatography, the CBS-dendron **13** was isolated as chloride salt in a yield of 78 %. The CBS-dendron **13** was transformed to the salt-free unprotonated state by additional reversed-phase chromatography with triethylamine as additive.

[i] Synthesised according to literature procedure.[103]
[ii] The Boc-protected guanidine was used to perform a acidic deprotection of the Boc-group and the acetal-protecting groups of the dendron in one step.

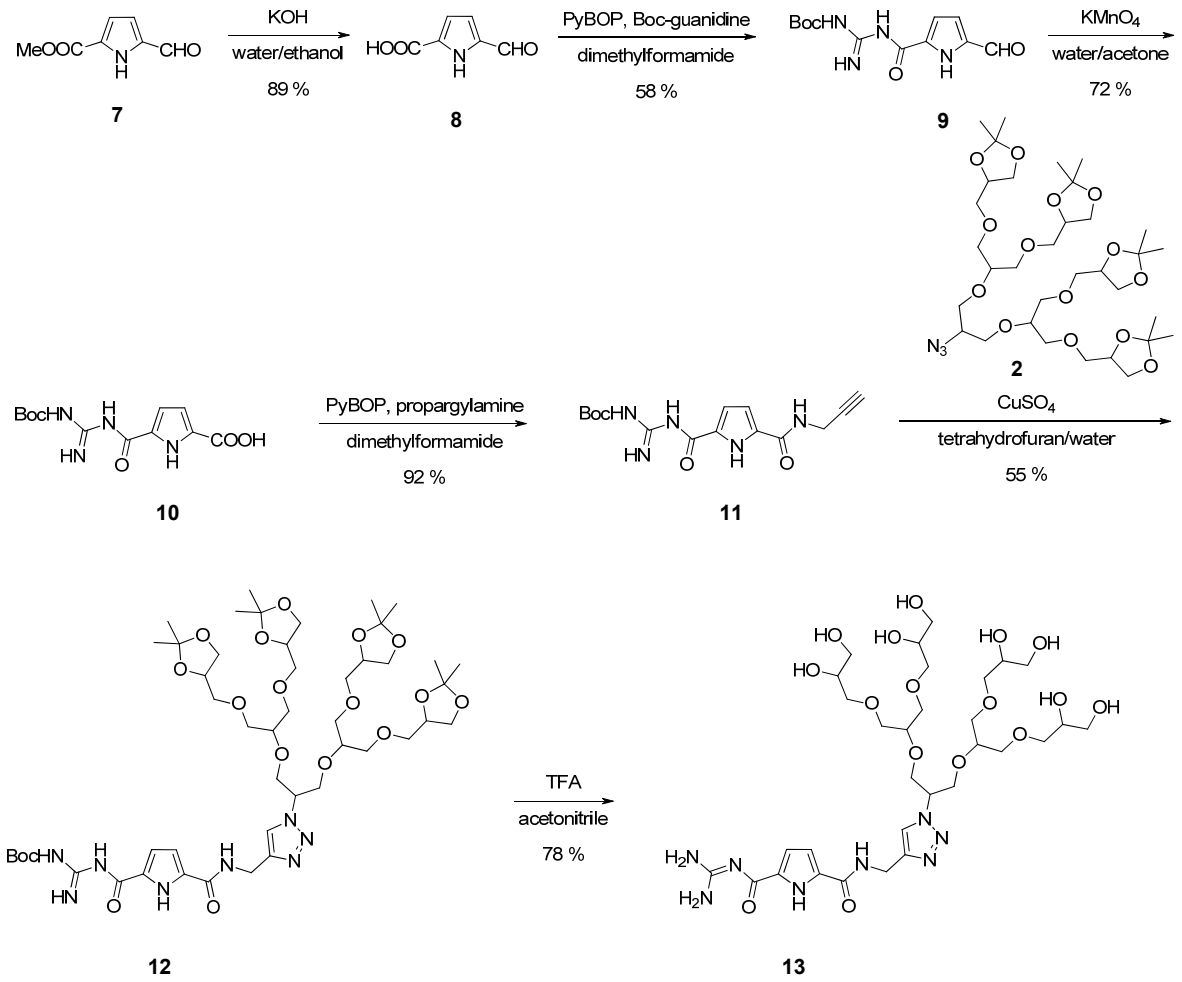

Scheme 4–1: Synthesis of 2,5-substituted CBS-dendron 13.

With CBS-dendron 13 at hand, the self-assembly experiments with core molecules TMA, NTMP, and EDTA were performed, and the results are discussed in the next section.

4.2.2.2 Physicochemical Characterisation

In order to determine the sizes of monomeric CBS-dendron 13 and core molecules 4–6 and to find out whether larger hetero-aggregates may have been formed, diffusion-ordered-spectroscopy (DOSY)[105, 106] experiments in deuterated dimethylsulfoxide were performed. The principle to measure the size of molecules by DOSY-NMR technique is based on the fact that molecules in solution move. This is called translational motion, Brownian molecular motion, or simply diffusion of the molecules. In the DOSY experiment, pulsed magnetic field gradients are used to measure the diffusion coefficient *D*. The diffusion coefficient depends on the effective molecular weight, size, and shape of a molecule under given conditions like solvent viscosity ($DMSO_{d6}$ η = $1.987 \cdot 10^{-3}$ $Ns \cdot m^{-2}$)[107] and temperature (297 K) (**Equation** 4–1).

$$D = \frac{kT}{f} = \frac{RT}{Nf} \qquad f = 6\pi\eta r$$

Equation 4–1: **Left**: Von Smoluchowski equation for correlation of diffusion coefficient and molecular size; D = diffusion coefficient [$m^2 \cdot s^{-1}$], k = Boltzmann constant [$J \cdot K^{-1}$], T = temperature [K], N = Avogadro's constant [mol^{-1}], R = gas constant [$J \cdot mol^{-1} \cdot K^{-1}$], f = hydrodynamic friction coefficient; **Right**: Einstein equation for spherical objects in a homogenous medium of defined viscosity for f, η = viscosity [$Ns \cdot m^{-2}$].

Based on the measured diffusion coefficients *D,* the hydrodynamic radii *r* were calculated using the Stokes-Einstein equation for spherical particles (**Equation 4–2**).

$$D = \frac{kT}{6\pi\eta r}$$

Equation 4–2: Stokes-Einstein equation for spherical objects in a constant medium of distinct viscosity.

With DOSY-NMR experiments it is possible to detect the diffusion coefficients of each compound in a reaction mixture of different compounds. Due to that it is possible to differentiate between aggregated species, showing one diffusion coefficient, and non-aggregated molecules with distinct diffusion coefficients for each compound.

To support the results of the DOSY experiments, molecular modelling (force-field molecular mechanics, MM) computations of the theoretical size of the monomeric building blocks and the expected supramolecular self-assembled dendrimers were performed. The results are listed in **Table 4–1**. As can easily be seen the experimentally determined and the MM-calculated sizes of core molecules **4**, **5**, and **6** (entries 2, 3, 4) as well as the one of the monomeric CBS-dendron **13** (entry 1) are in a good agreement. However, the experimental diameters for mixtures of **13** and cores **4**–**6** deviate only slightly from the values of the isolated monomeric cores. Thus, these data do not indicate significant, if at all, formation of supramolecular 3:1 (expected for TMA, NTMP) or 4:1 (expected for EDTA), respectively, hetero-complexes. The data from all self-assembly experiments show a dendron size (entries 2a, 3a, 4a) comparable to that of the monomer (entry 1). Additionally in each mixture the core (entries 2b, 3b, 4b) has a smaller size compared to the dendron (entries 2a, 3a, 4a) which indicates not even formation of a 1:1 complex. For example, trimesic acid in the reaction mixture with CBS-dendron [$(\mathbf{13})_3 \cdot \mathbf{4}$] (entry 2b) has a size of 1.1 nm, which is essentially the size of pure trimesic acid **4** (1.0 nm, entry 2). It is obvious that no self-assembly has taken place.

Table 4–1: Experimental hydrodynamic diameters from DOSY measurements in $DMSO_{d6}$ at 25 °C and theoretical values calculated with the OPLS2005 force field. Entries **Xa** are the values for the dendron and **Xb** for the core molecule in the reaction mixture.

entry	compound		DOSY diameter/nm	MM diameter/nm
1	**G–P–G2-$(OH)_8$** 15 mM	**13**	**1.8**	1.9
2	**TMA** 15 mM	**4**	**1.0**	1.0
2a	**G–P–G2-$(OH)_8$** 15 mM – trimesic acid 5 mM	[(**13**)$_3$ 4]	**1.9**	3.4
2b	G–P–G2-$(OH)_8$ 15 mM – **TMA** 5 mM	[(13)$_3$ **4**]	**1.1**	3.4
3	**EDTA** 3.75 mM	**5**	**1.2**	1.0
3a	**G–P–G2-$(OH)_8$** 15 mM – EDTA 3.75 mM	[(**13**)$_3$ 5]	**2.0**	3.6
3b	G–P–G2-$(OH)_8$ 15 mM – **EDTA** 3.75 mM	[(13)$_3$ **5**]	**1.5**	3.6
4	**NTMP** 5 mM	**6**	**1.2**	0.9
4a	**G–P–G2-$(OH)_8$** 7.5 mM – NTMP 2.5 mM	[(**13**)$_3$ 6]	**1.8**	
4b	G–P–G2-$(OH)_8$ 7.5 mM – **NTMP** 2.5 mM	[(13)$_3$ **6**]	n.d.	

Calculated structures of monomeric CBS-dendron 13 and the complex of CBS-dendron with trimesic acid [$(13)_3$·4] indicate a possible problem in the formation of higher aggregates due to sterical reasons. The calculated structure of the theoretical 3:1 complex with trimesic acid is shown on the left side of **Figure** 4-4. As schematically illustrated, there might be a steric problem for arranging three dendron units around the trimesic acid core. The 2,5-substitution pattern of the pyrrole is of a sickle-like shape and therefore, might interfere with the neighbouring dendron in the complex. Additionally the similarly sickle-like shape of the dendron seems also be unfavourable for bringing the periphery of the dendron close to the binding site as shown in **Figure** 4-4, right.

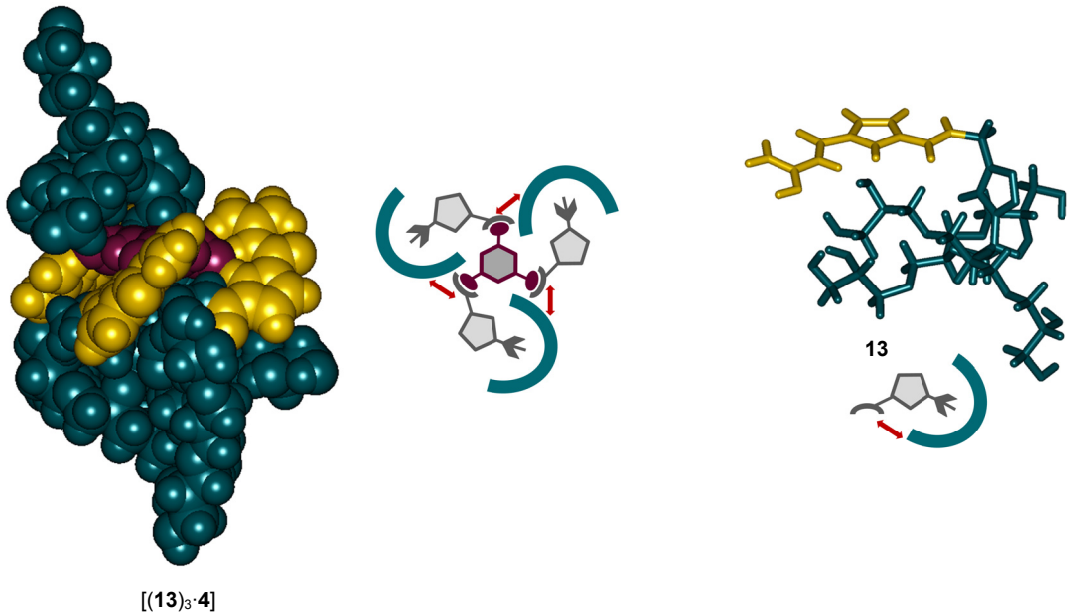

[(**13**)$_3$·**4**]

Figure 4-4: **Left**: Molecular mechanics modelling of a 3:1 complex of CBS-dendron 13 and trimesic acid 4 [$(13)_3$·4]; **Right**: Illustration of molecular-modelled monomeric CBS-dendron 13.

Further molecular modelling calculations predicted that if the pyrrole substitution pattern would be changed from a 2,5 to a 2,4 arrangement, the CBS-dendron periphery should not interfere with the binding site, but also the space around the trimesic acid core should not be so crowded, as shown in **Figure 4-5**, left. Therefore, attempts were made to synthesise compound 14 (**Figure 4-5**, right).

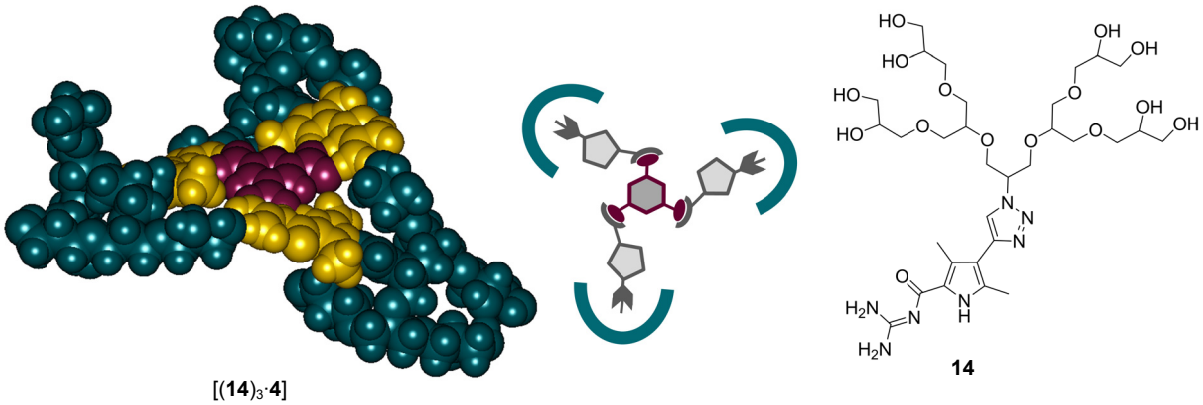

Figure 4-5: Molecular modelling of dendrimer 14 and the 3:1 complex with trimesic acid 4, indicating a less crowded and a more planar arrangement of the CBS-dendron 14 around the trimesic acid core 4.

4.2.3 The 2,4-Substituted CBS-Dendrons

4.2.3.1 Synthesis

Alkyne Functionality in the 4-Position of the Pyrrole

Due to the intended change of the pyrrole substitution pattern a new "bottom up" synthesis was carried out. The starting material was selected in a way to obtain the alkyne functionality by a simple conversion reported in the literature. An acetyl group was introduced in the 4-position of the pyrrole, which then could be converted by a COREY-FUCHS-like reaction into the desired alkyne.[108, 109, 110] Instead of a benzylester protecting group as used in the literature procedure, an ethylester was chosen as starting material, thereby enabling the deprotection of the ester without reducing the alkyne moiety. This synthesis route was chosen to introduce first the guanidine building block and in the last step the synthetically more valuable polyglycerol dendrons (**Scheme 4–2**).

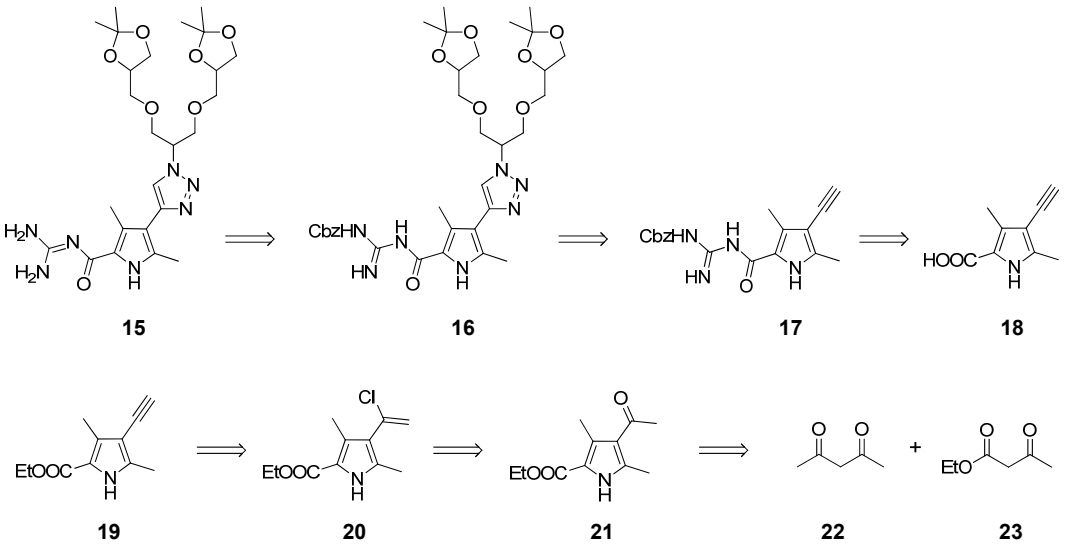

Scheme 4–2: Retrosynthetic illustration of 2,4-substituted pyrrole CBS-dendron 15.

The straightforward synthesis of pyrrole 19 was performed on a multi-gram scale. No column chromatography purification was necessary because all products could be purified by crystallisation.

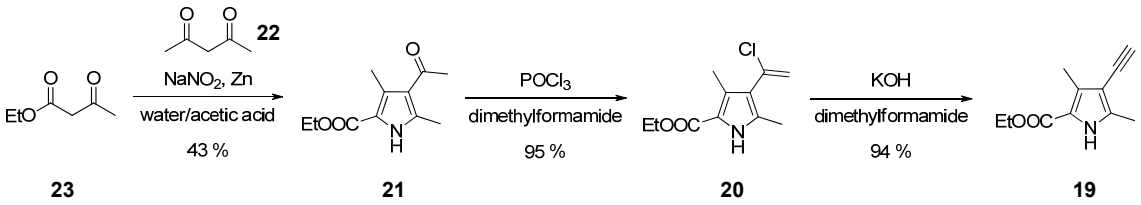

Scheme 4–3: Synthesis of pyrrole building block 19.

It should be mentioned that pyrrole 20 is not stable and is about 50 % reconverted to starting material 21 during a 4 hour ^{13}C-NMR measurement in $DMSO_{d6}$ containing traces of water. It can be imagined that nucleophilic substitution of the chloride by water is assisted by the aromatic system in conjugation with the vinyl chloride moiety, as shown in **Scheme** 4–4. Pyrrole 20 is also not stable as solid after a few weeks it is completely reconverted to the starting material, if it is not stored under protecting gas. Therefore, the elimination reaction leading to alkyne 19 was performed immediately after isolation.

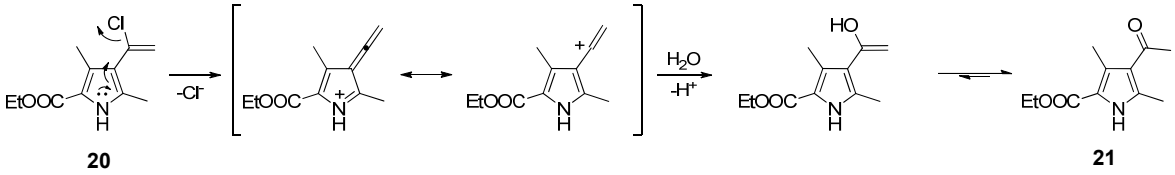

20 21

Scheme 4–4: Possible hydrolysis mechanism of **20**.

A major problem of the synthetic route depicted in **Scheme** 4–2 was the cleavage of the ethylester **19** to give the free carboxylic acid **18**. Ester hydrolysis was attempted under standard conditions with lithium hydroxide and sodium hydroxide in tetrahydrofuran/water mixtures but no deprotection could be detected. Instead, decomposition occurred during long reaction times. Hydrolysis of pyrrole ethylester accompanied by sensitive moieties is in general very difficult and sometimes requires extended reaction times, as experienced for other systems investigated in our group. The ratio of tetrahydrofuran/water mixtures, the concentrations of reaction solutions, and the equivalents of lithium hydroxide are known to play a crucial role.

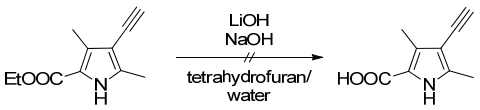

19 18

Scheme 4–5: Unsuccessful hydrolysis of ethylester **19**.

An additional problem was the high reactivity of the pyrrole system during acidic work-up. The alkyne reacts immediately with acids back to the starting material **21**. Even purification conditions of normal-phase chromatography are too acidic, leading to partial transformation of the alkyne. A possible reaction mechanism is depicted in **Figure** 4-7.

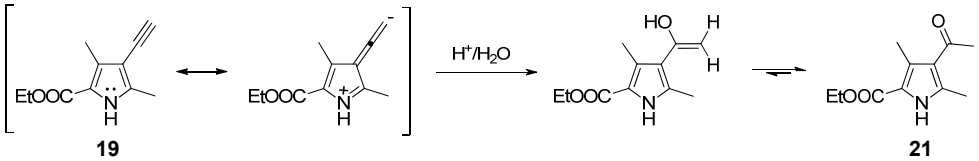

19 21

Scheme 4–6: Possible mechanism of the acid-catalysed hydrolysis of **19**.

Because attempts to prepare acid **18** *via* ester **19** were unsuccessful, a new synthetic route was followed, as is shown in **Scheme** 4–7. To circumvent the problems of the instable alkyne functionality, the dendron is introduced by click chemistry prior to ester cleavage. By this change also the ester hydrolysis problem can be avoided by exchanging the ethylester with a

benzylester group. In the proposed synthetic route, the benzylester can be used as protecting group due to the fact that the alkyne is already converted, and the hydrogenolysis of the benzylester is not interfering.

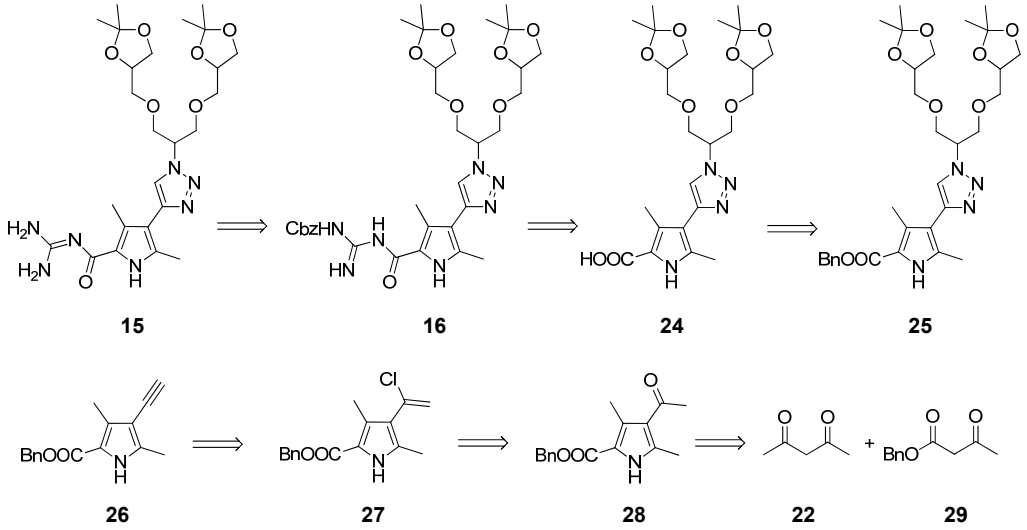

Scheme 4–7: Alternative synthesis of CBS-dendron 15.

Preparation of the benzylester protected pyrrole 26 followed the same route as described for the ethylester protected pyrrole 19 (p. 50). The unstable vinyl chlorid 27 was immediately converted to 26.

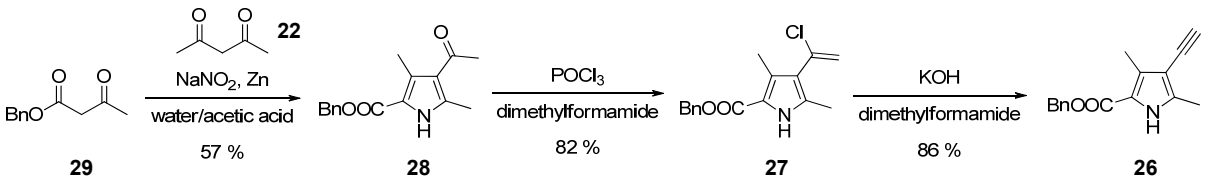

Scheme 4–8: Synthesis of benzylester protected pyrrole 26.

In the next step, the click reaction of compound 26 with the 1st generation polyglycerol dendron 1 was performed. The reaction conditions were the same as described on page 45 for the synthesis of 2,5-pyrrole based CBS-dendron 16. The reaction was monitored by HPLC. However, only starting material could be detected after 24 hours. Additional supplementation of sodium ascorbate and copper(II)sulphate was also unsuccessful. After extended reaction times a multitude of peaks were observed in the HPLC, indicating decomposition of starting material 26.

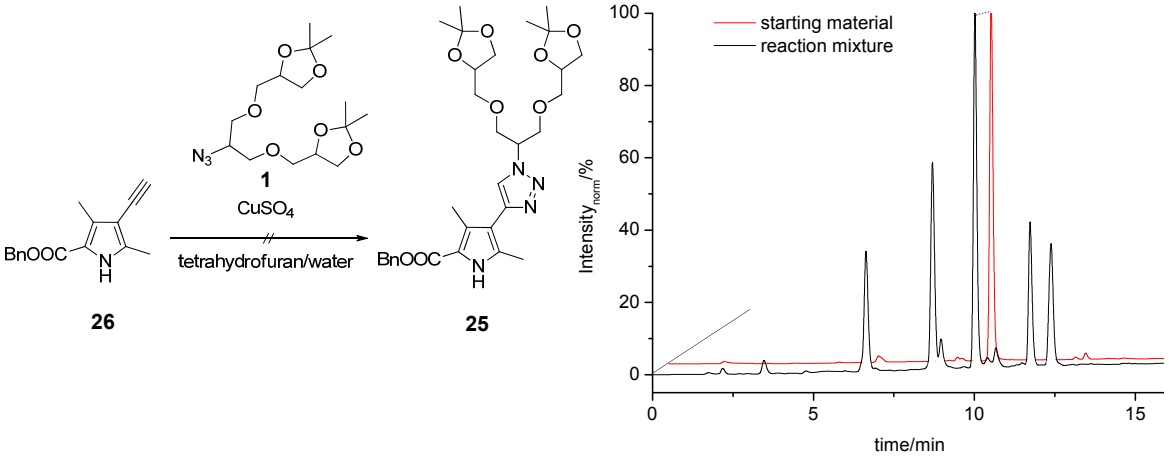

Scheme 4–9: **Left**: Unsuccessful click chemistry synthesis of **25**; **Right**: HPLC reaction control after 2 days. Starting material **26** in **red** and reaction mixture in **black**. Conditions: Reversed-phase YMC-ODSA 150 x 3 mm, 5 µm, 12 nm, 0.43 ml min^{-1}, gradient from 50 % acetonitrile to 100 % during 15 minutes and 5 minutes 100 % acetonitrile, detection wavelength 220 nm. The HPLC intensities are normalised to 100 % for the most intense peak.

As depicted in **Scheme 4–10**, the first step of a click reaction is the insertion of copper into the CH bond of the alkyne. This step should lead to a reaction intermediate that should be distinguishable from the starting material by reversed-phase HPLC. As the reaction control detected only starting material until decomposition occurred, it is obvious that the first step of the click reaction did not took place. A possible explanation for this failure is that the alkyne is in conjugation with the aromatic pyrrole ring, resulting in a reduced acidity of the alkyne proton, thereby reducing the driving force for the insertion of the copper ion.[i]

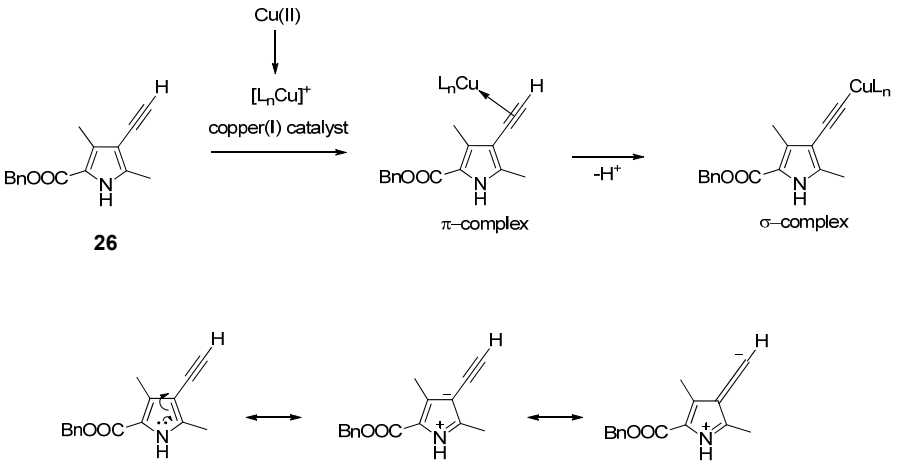

Scheme 4–10: **Top**: Illustration of the copper(I) promoted click chemistry reaction mechanism; **Bottom**: Resonance structures of pyrrole **26**.

[i] Another explanation for the unsuccessful click reaction could be a possible complexation of the copper(II) by the pyrrole, however, other performed click reactions with similar pyrrole systems further discussed below show good reactivity.

As a consequence of the described problems with the synthesis of 2,4-substituted CBS-pyrrole **15**, the synthetic route to the 2,5-substituted CBS-dendron **13** *via* successful click chemistry transformation of the propargylamine-substituted pyrrole **11**, see **Section 4.2.2**, was readopted for the preparation of 2,4-substituted pyrroles. The change in the synthetic strategy is displayed in **Figure 4-6**.

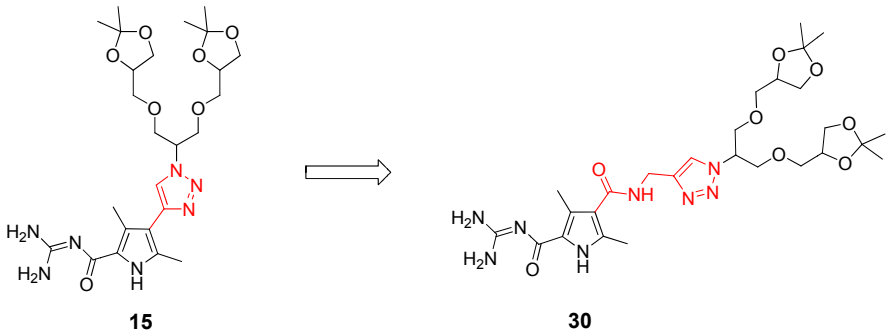

Figure 4-6: Synthetic route from 4-alkyne-substituted pyrrole to 4-carboxylic acid-substituted pyrrole. The alkyne group will be introduced by a coupling reaction with propargylamine to afford CBS-dendron **30** by a subsequent click reaction.

Exploratory molecular modelling predicted an almost planar arrangement of three CBS-dendrons **31** attached to the trimesic acid core (**Figure 4-7**). Thus, the CBS-dendrons expected to be accessible *via* this strategy seemed to be promising candidates for a successful self-assembly process.

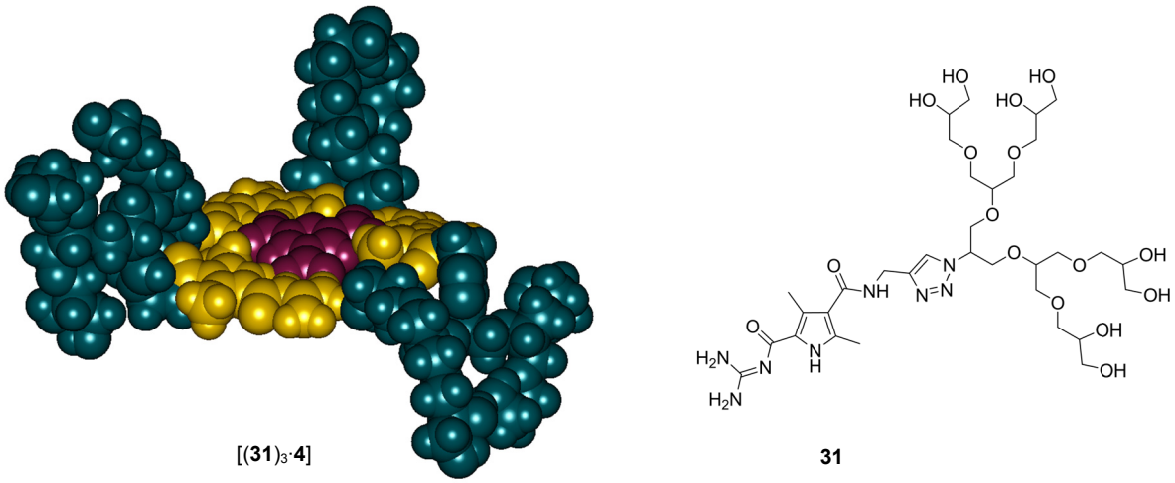

Figure 4-7: MM-calculated 3:1 complex of CBS-dendron **31** and trimesic acid **4**.

Carboxylic Acid Functionality in the 4-Position of the Pyrrole

The synthetic route is depicted in **Scheme 4–11**. The 1st generation dendron 1 was chosen in order to minimise possible steric hindrance in the formation of the self-assembled hetero-associates. Instead of the previously used Boc-protected guanidine, the Cbz-protected derivative was used to allow the deprotection of the guanidine without affecting the acetal groups of the dendron, the initial self-assembly studies were planned to be carried out with acetal-protected hydroxyl groups to avoid possible hydrogen-bonding interactions with the binding site. With the exception of the first step all reactions could be performed in good yields.

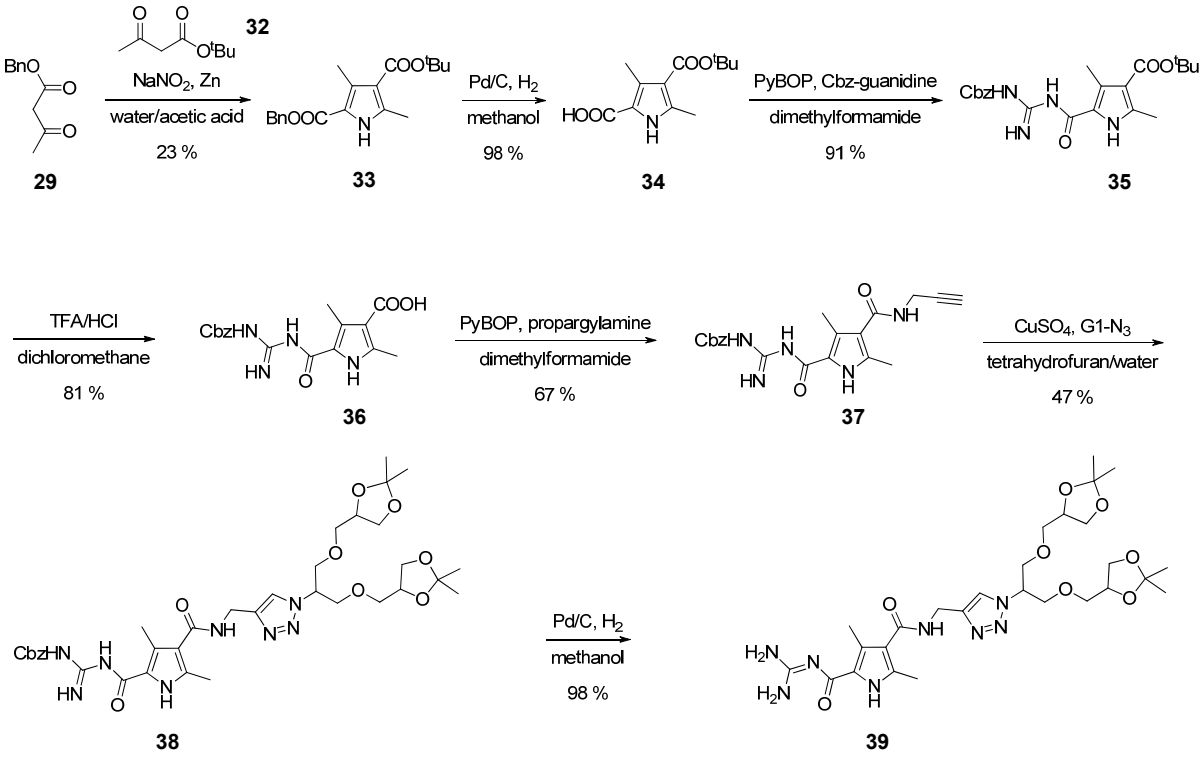

Scheme 4–11: Synthesis of acetal-protected 1st generation CBS-dendron 39.

The click reaction with the 1st generation dendron 1 was monitored by normal-phase HPLC, showing that contrary to the unsuccessful reaction of **25** (**Scheme 4–1**, p. 53) the starting material **37** was completely converted after 10 minutes. Only one new HPLC peak was detected. Further reaction control was carried out by reversed-phase HPLC in order to elute intermediates that possibly have not been eluted on the normal-phase column. However, here also, only one new signal was observed after a reaction period of 10 minutes. After 30 minutes the reaction solution had turned dark green, and a new peak of a side product appeared in the HPLC control.

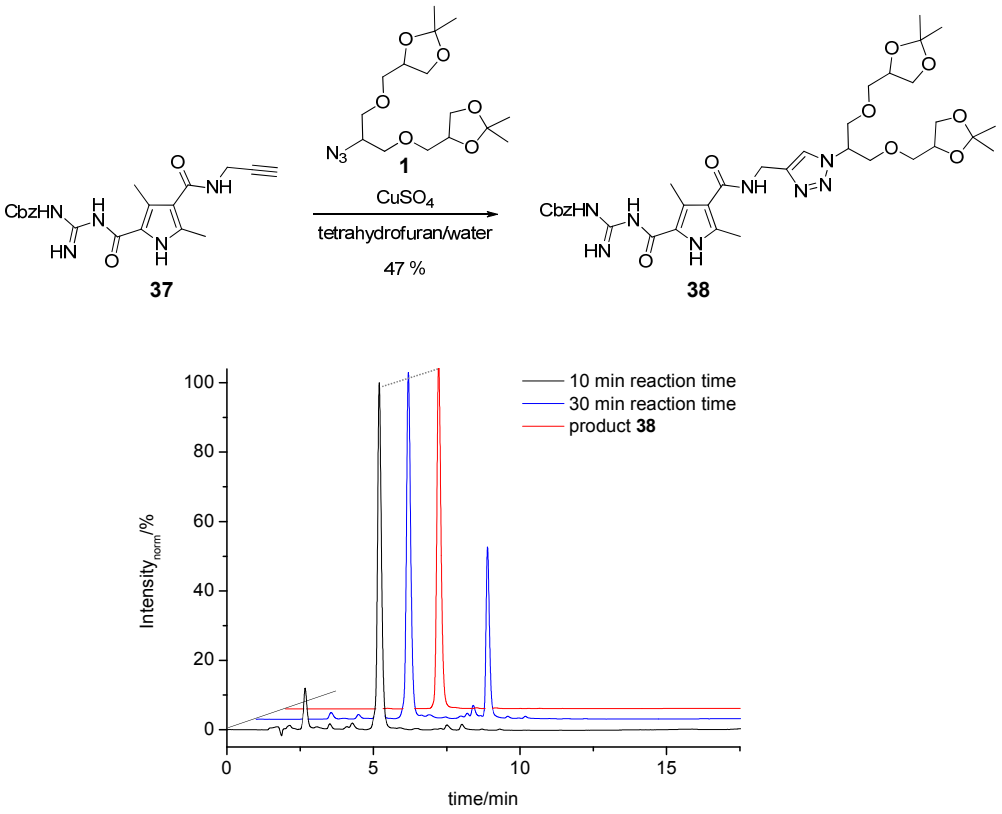

Figure 4-8: HPLC reaction control, for a reaction time of 10 minutes (**black**), 30 minutes (**blue**), and isolated product **38** (**red**). Conditions: Reversed-phase YMC-ODSA 150 x 3 mm, 5 µm, 12 nm, 0.43 ml min^{-1}, gradient from 50 % acetonitrile to 100 % during 15 minutes and 5 minutes 100 % acetonitrile, detection wavelength 220 nm. The HPLC intensities are normalised to 100 % for the most intense peak of each run.

After work-up the protected CBS-dendron **38** was isolated in a yield of 43 %. After deprotection of the Cbz-protecting group by hydrogenolysis the desired protected 1st generation dendron was isolated in an overall yield of 5 % over all steps.

After successful synthesis of 2,4 substituted CBS-dendron **39** the self-assembly experiments with core molecules TMA, NTMP, and EDTA were performed, and the results are discussed in the next section.

4.2.3.2 Physicochemical Characterisation

The results of the DOSY-NMR experiments in $DMSO_{d6}$ and of the molecular modelling studies on the acetal-protected CBS-dendron **39** are summarised in **Table 4–2**. The calculated diameter (1.7 nm) of the monomeric CBS-dendron **39** (entry 5) is in a good agreement with the size derived from the DOSY experiments (1.5 nm). This indicates that the shape of CBS-dendron **39** adopts a globular conformation in DMSO solution (**Figure 4-9**) like the higher generation unprotected polar dendron **13** (see page 48).

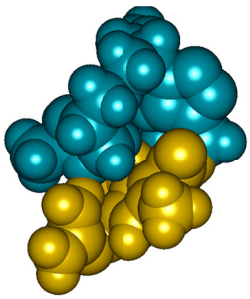

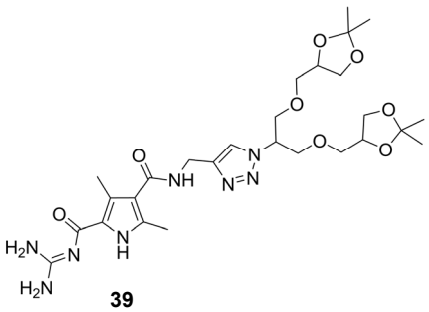

39

Figure 4-9: Acetal-protected 1st generation CBS-dendron **39**. Calculated size 1.7 nm in diameter for a spherical sphere enclosing the whole molecule.

The sizes of **39** (entries 6a, 7a, 8a) and cores **4**, **5**, and **6** (entries 6b, 7b, 8b) in the assembly mixtures show that there is not the expected increase in size for 3:1 or 4:1 assemblies. The sizes of cores and dendron are consistent, which indicates some complexation of the cores by CBS-dendron **39**. In case of the trimesic acid **4** (entries 6 and 6b) the size increases from 1.0 nm to 1.5 nm. However, the size of CBS-dendron **39** (1.6 nm) (entry 6a) is not significantly increased compared to that of the monomer (1.5 nm) (entry 5).

Table 4–2: Experimental hydrodynamic diameters from DOSY-NMR measurements in $DMSO_{d6}$ at 25 °C and theoretical values calculated with the OPLS2005 force field. Entries **Xa** are for the dendron and **Xb** for the core molecule in the reaction mixture. Entries X^* are for calculated 1:1 and $X^{\#}$ for calculated 2:1 hetero-complexes.

entry	compound		DOSY diameter/nm	MM diameter/nm
5	**G–P[^{3}Me^{4}G1]–Me** 15 mM	**39**	**1.5**	1.7
6	**TMA** 15mM	**4**	**1.0**	1.0
6*		[(39)$_1$·4]		1.8
6$^{\#}$		[(39)$_2$·4]		2.2
6a	**G–P[^{3}Me^{4}G1]–Me** 15 mM – trimesic acid 5 mM	[(**39**)$_3$·4]	**1.6**	2.4
6b	G–P[^{3}Me^{4}G1]–Me 15 mM – **TMA** 5 mM	[(39)$_3$·**4**]	**1.5**	2.4
7	**EDTA** 3.75 mM	**5**	**1.2**	1.0
7*		[(39)$_1$·5]		1.8
7$^{\#}$		[(39)$_2$·5]		2.2
7a	**G–P[^{3}Me^{4}G1]–Me** 15 mM – EDTA 3.75 mM	[(**39**)$_4$·5]	**1.5**	2.8
7b	G–P[^{3}Me^{4}G1]–Me 15 mM – **EDTA** 3.75 mM	[(39)$_4$·**5**]	**1.4**	2.8
8	**NTMP** 5 mM	**6**	**1.2**	0.9
8*		[(39)$_1$·6]		1.7
8$^{\#}$		[(39)$_2$·6]		2.4
8a	**G–P[^{3}Me^{4}G1]–Me** 15 mM – NTMP 5 mM	[(**39**)$_3$·6]	**1.7**	2.6
8b	G–P[^{3}Me^{4}G1]–Me 15 mM – **NTMP** 5 mM	[(39)$_3$·**6**]	**1.7**	2.6

A possible explanation is the presence of a 1:1 complex of trimesic acid 4 and CBS-dendron 39. This would increase the size of the smaller core but should not significantly increase the size of the dendron. Considering the calculated size of the monomeric dendron 39 (entry 5) with 1.7 nm the size of the calculated 1:1 complex (entry 6*) with 1.8 nm shown in **Figure 4-10**, makes a 1:1 complexation most likely.

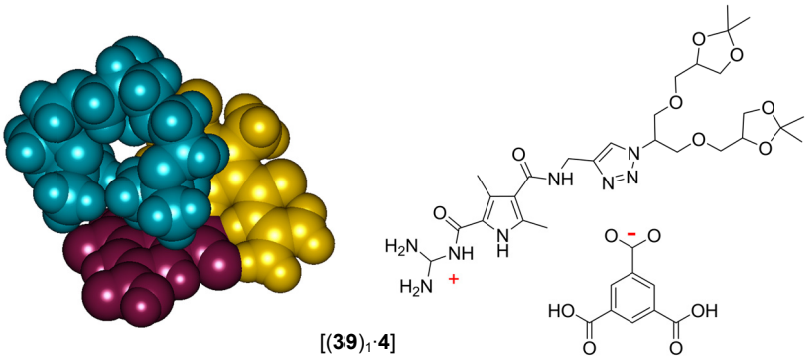

Figure 4-10: Calculated 1:1 complex of CBS-dendron and trimesic acid [$(39)_1$·4]. Calculated size 1.8 nm in diameter for a spherical sphere enclosing the complex.

The results of the DOSY-NMR experiments with EDTA (5) are comparable to the results for the trimesic acid core. Only for complex mixture [$(39)_3$·6] with NTMP an increase of the size of the dendron from 1.5 nm in the monomeric solution (entry 5) to 1.7 nm in the complex mixture [$(39)_3$·6] (entry 8a) was found. Similarly, the core 6 showed an increases from 1.2 nm in the monomeric (entry 8) to 1.7 nm in the complex solution [$(39)_3$·6] (entry 8b). The diameter by DOSY-NMR with 1.7 nm is smaller than that of the calculated 3:1 complex (2.6 nm). The structure of calculated 1:1 complex is shown in **Figure 4-11** and fits with its 1.7 nm diameter (entry 8*) to the experimental DOSY value indicating also a 1:1 complexation.

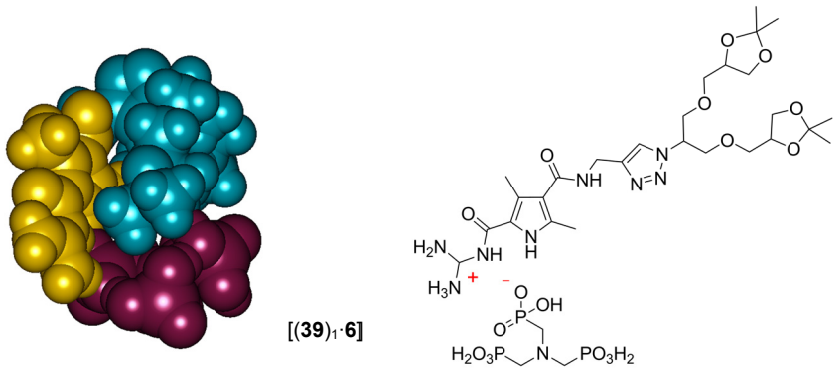

Figure 4-11: Calculated 1:1 complex of CBS-dendron 39 and NTMP 6 forming [$(39)_1$·6].

A look at the ^{1}H-NMR of NTMP reveals a highfield shift and a change from a doublet to a broad singlet, of the NTMP methylene groups, when the dendron is added (see **Figure 4-12**). The highfield shift can be assigned to the deprotonation of the phosphonic acids by the guanidine of the dendron. The former doublet at 3.18 ppm caused by a proton-phosphor coupling is obviously affected by a complexation with dendron **39**, however, an additional ^{31}P NMR shows for both the monomeric NTMP as well as for the 3:1 mixture [(**39**)$_3$·**6**] only one signal and is hence not indicating any complexation stoichiometry.

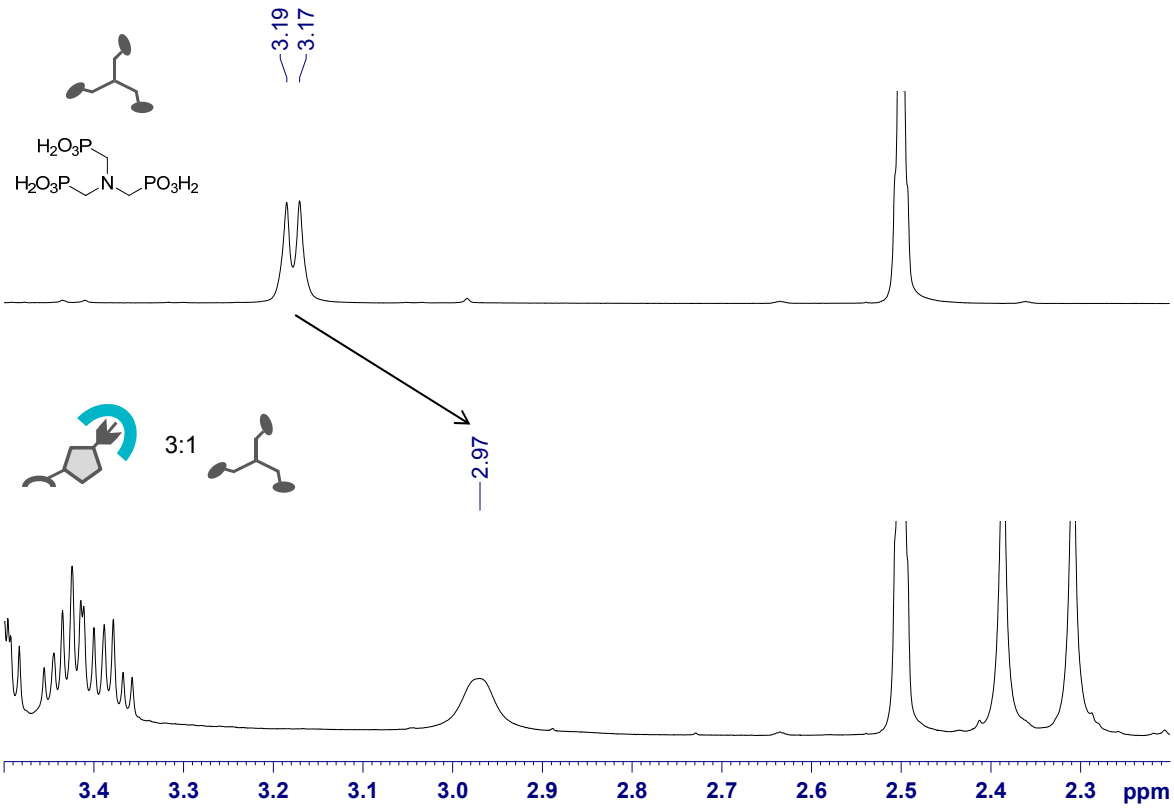

Figure 4-12: **Top**: ^{1}H-NMR of NTMP (**6**) in DMSO$_{d6}$. **Bottom**: ^{1}H-NMR of 3:1 mixture [(**39**)$_3$·**6**] of CBS-dendron **39** and NTMP (**6**) in DMSO$_{d6}$.

If the ^{1}H-NMR of the pure dendron is compared with that of the 3:1 compound mixture, i.e. possible formation of [(**39**)$_3$·**6**], a lowfield shift of the NH signals is observed, as expected for the protonated binding site. The NH$_2$ proton signals of the protonated guanidine would be expected to split up from an uncomplexed broad singlet at 8.1 ppm to two singlets at 9.1 ppm and 7.7 ppm, respectively, for the guanidiniocarbonyl pyrrole complexing an oxo-anion. A small split up to 8.3 ppm and 7.9 ppm indicate a partly complexation in the 3:1 mixture, and possible formation of a 1:1 aggregate as discussed above.

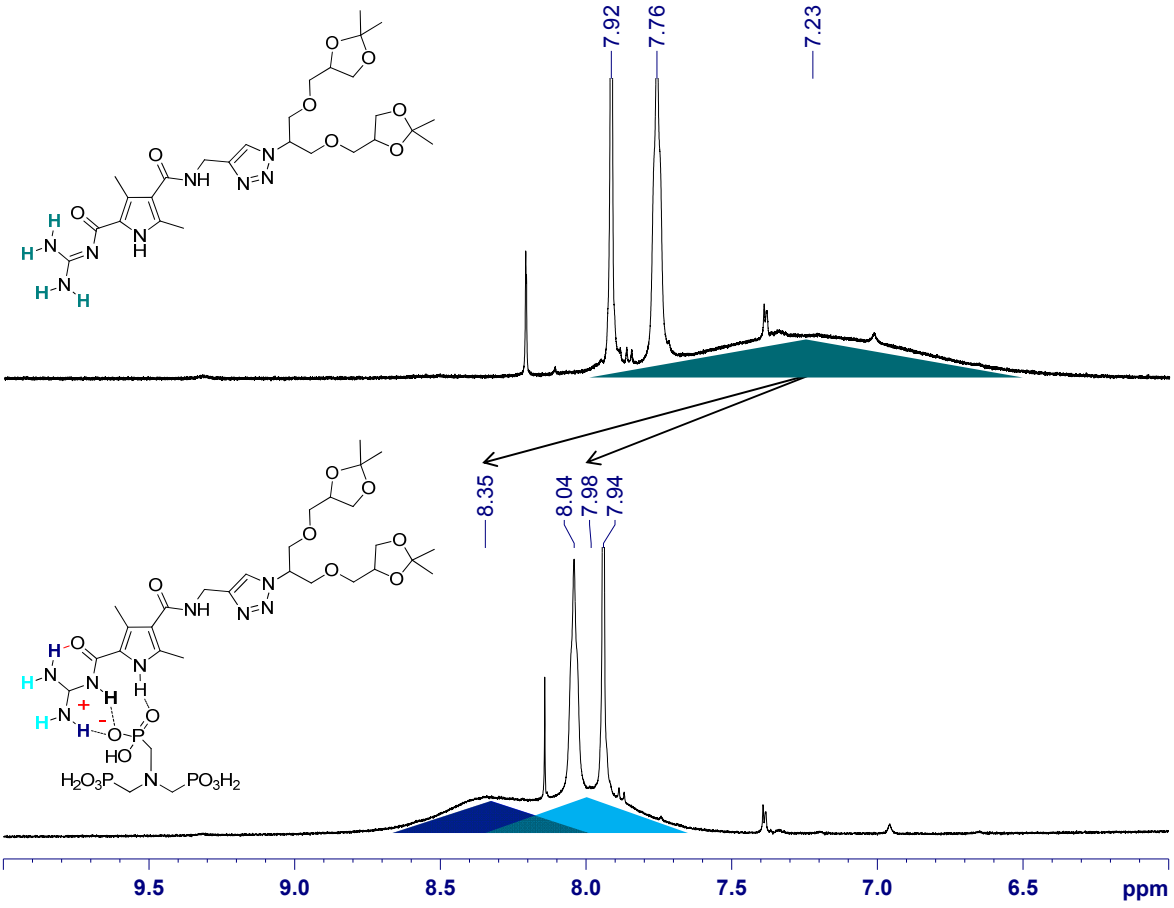

Figure 4-13: **Top**: ^{1}H-NMR of CBS-dendron **39** in $DMSO_{d6}$. **Bottom**: ^{1}H-NMR of a 3:1 mixture of CBS-dendron and NTMP [$(\mathbf{39})_3$·**6**] in $DMSO_{d6}$.

Because the ^{1}H-NMR experiments provided the first hints for a possible positive self-assembly, the results were sought to be confirmed by Dynamic Light Scattering (DLS)[111] experiments. DLS measures the Brownian motion of particles in solution and relates this to the size of the particles. This is done by analysing the intensity fluctuations of the scattered light from a laser illuminated particle. As small particles move faster than bigger ones, the relationship between the Brownian motion of a particle and its size, as defined in the Stokes-Einstein equation, can be used to calculate the size by the intensity fluctuations. Like in DOSY-NMR measurements, the solvent viscosity and constant temperature are important experimental conditions. The DLS experiments were performed at 298 K in dimethylsulfoxide. Unfortunately, no useful data could be obtained, possibly due to the high refractive index of dimethylsulfoxide in combination with the small size of the measured particles. Because good experiences had been made with DLS measurements in water and the aim of this work in fact was to achieve supramolecular dendrimers in water, the acetal-protected CBS-dendron **39** was deprotected to obtain dendron **41** with free hydroxyl groups in the periphery (**Scheme 4–12**). First, the acetal groups of compound **38** were cleaved with a mixture of hydrochloric and trifluoroacetic acid.

After purification *via* reversed-phase MPLC pyrrole **40** was isolated in almost quantitative yield. After further hydrogenolytic deprotection of the Cbz-group the water soluble 1st generation CBS-dendron **41** was isolated in a yield of 98 %.

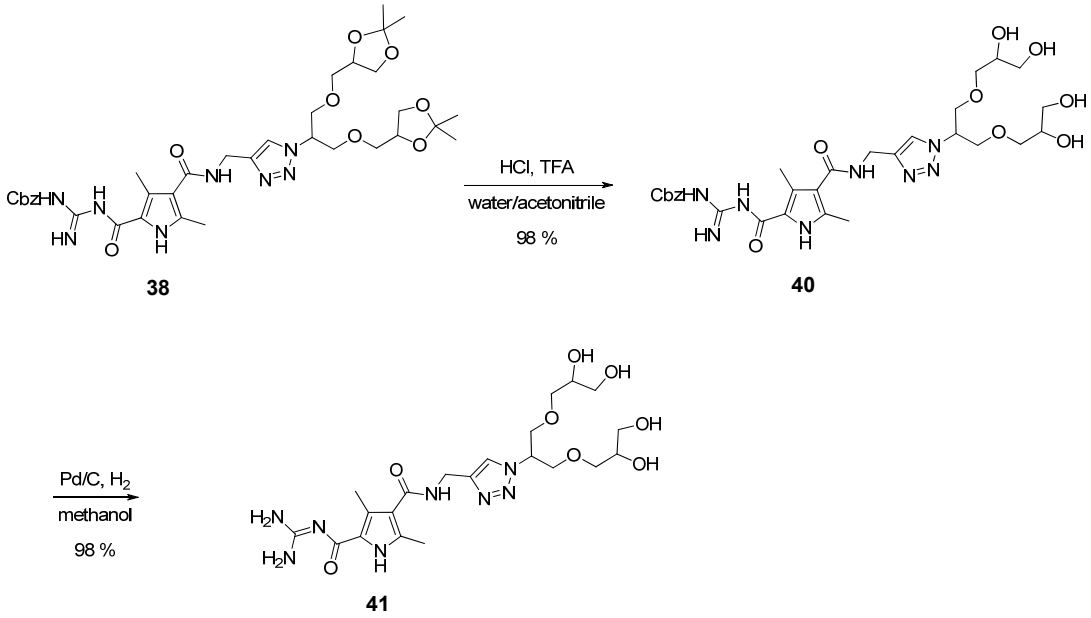

Scheme 4–12: Synthesis of unprotected 1st generation CBS-dendron **41**.

DLS measurements of 5 mM solutions of dendron **41** were performed in water (**Figure** 4-14). Unexpectedly no signal attributable to the monomeric CBS-dendron **41** was observed. The DLS trace of **41** shows a maximum at 99 nm and a small amount of higher aggregates in the range of 500–700 nm. Noticeable, for a 3:1 mixture of the CBS-dendron and NTMP core [(**41**)$_3$**6**] no significant change of the size was monitored. The maximum was still located at 105 nm with a small amount of higher aggregates in the range of 300–500 nm.

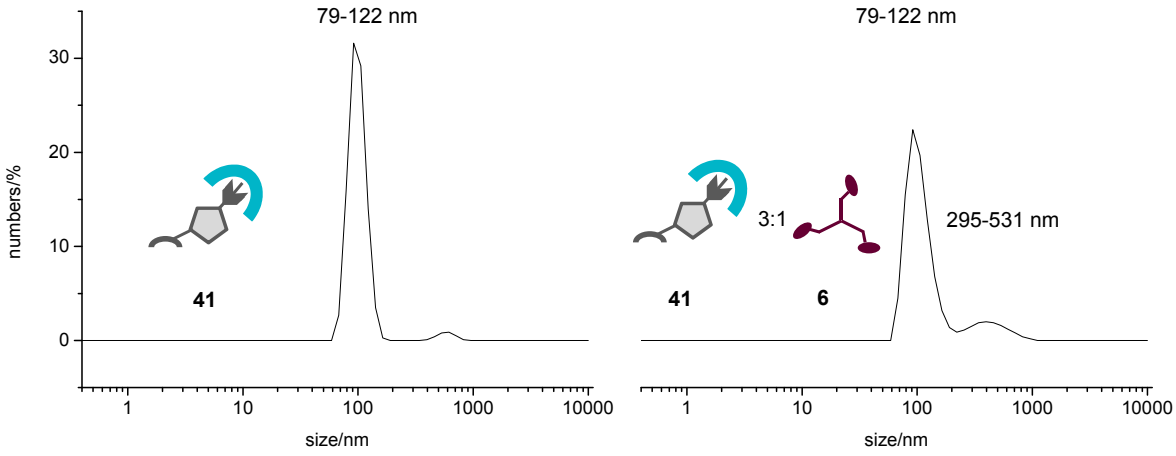

Figure 4-14: **Left**: DLS measurement of unprotected 1st generation CBS-dendron **41** (5 mM) in water at 25 °C, 91 % of all particles are in the range of 79–122 nm; **Right**: DLS measurement of 3:1 mixture of CBS-dendron **41** (15 mM) and NTMP **6** (5 mM) in water at 25 °C, 70 % of all particles are in the range of 79–122 nm and 9 % of all particles in the range of 295–531 nm.

The self-assembly around an oxo-anionic core seems to be not the dominating force. In a control experiment the dendron was treated with 4 equivalents of hydrochloric acid to obtain the protonated dendron 41. As shown in **Figure 4-15** the protonated dendron and the size distribution of the higher aggregates is comparable as above observed for the complex mixture [$(41)_3$6].

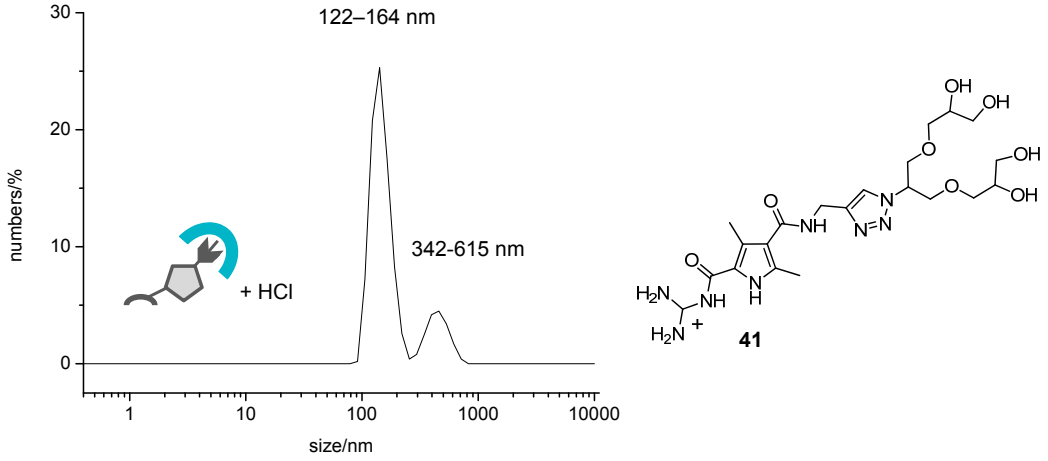

Figure 4-15: DLS measurement of unprotected 1st generation CBS-dendron 41 (5 mM) in water and 4 equivalents of HCl, 64 % of all particles are in the range of 122–164 nm and 16 % of the particles are in the range of 342–615 nm.

The DLS measurements with the CBS-dendron 41 were repeated after addition of sodium hydroxide. Now, only a single, quite narrow peak at 312 nm was detected (**Figure 4-16**) for the 1st generation dendron, also indicating higher aggregates.

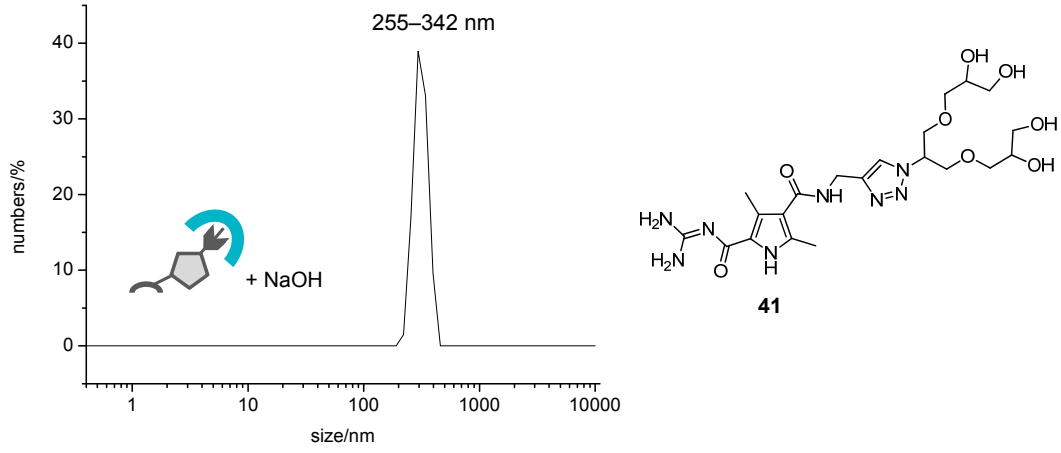

Figure 4-16: DLS measurement of CBS-dendron 41 (5 mM) in water and 4 equivalents of sodium hydroxide, 89 % of all particles are in the range of 255–342 nm.

In conclusion, the foregoing attempts to build self-assembled structures of CBS-dendrons around various oxo-anionic cores were unsuccessful. Formation of higher aggregates of the water soluble 1st generation dendron 41 itself rather than formation of small hetero-complexes dominates in aqueous solution. The dendron 41 seems to build higher aggregates depending on the protonation state of the guanidine moiety of the dendron. Various aspects of this issue are still to be uncovered, like testing different generation sizes of dendrons and concentration dependencies. However, the prospect of success, to obtain discrete supramolecular dendrimers, seemed not to be possible in the discussed approach, even though some interesting results of dendron 41 were observed. The formation of self-assembled dendrons was further investigated in the zwitterionic self-complementary approach discussed in the next section.

4.3 Zwitterionic Supramolecular Dendrimers

4.3.1 Zwitterionic Untemplated Supramolecular Dendrimers (ZU-SD)

4.3.1.1 Introduction

In the past few years the research group of SCHMUCK has utilised the pH dependent dimerisation of the self-complementary guanidiniocarbonyl pyrrole carboxylate zwitterion (**Figure 3-2**) to obtain different types of nanostructures such as vesicles or supramolecular polymers. By taking advantage of the dimerisation property of the guanidiniocarbonyl pyrrole carboxylate zwitterion, the objective of this section is to show how the dimerisation of a polyglycerol dendron-modified self-complementary zwitterionic binding site can be used to form well-defined, pH switchable supramolecular dendrimers in water.

The syntheses of zwitterionic pyrrole systems are based on the combination of 1st to 3rd generation polyglycerol dendrons with an alkyne-functionalised guanidiniocarbonyl pyrrole carboxylate by click chemistry as discussed above (p. 45).

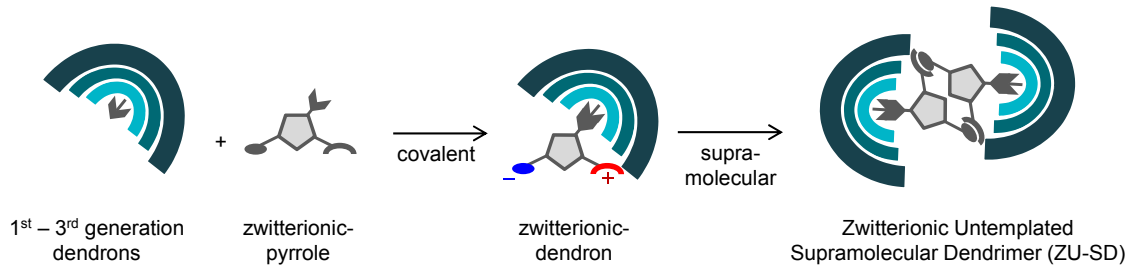

Figure 4-17: Schematic illustration of the Zwitterionic Untemplated Supramolecular Dendrimer approach.

4.3.1.2 Synthesis

On the first stage of the synthetic route, an alkyne functionality had to be introduced in the zwitterionic pyrrole system. Compound 42 was chosen as precursor for the zwitterionic pyrrole because the synthesis of pyrroles carrying propionic acid side chains in the β-position are well known in the literature,[112, 113, 114] and the derived pyrrole carboxylic acid 43 had been prepared earlier by RUPPRECHT[115, 116] in SCHMUCK's group (**Scheme 4–13**). The critical step towards compound 43 is the oxidation of the α-methyl group of pyrrole 42 to obtain the carboxylic acid of pyrrole 43. The ^{t}butylester protecting group is acid labile and due to that it has to be acted with caution to prevent the formation of hydrochloric acid during synthesis. Preparation

and work-up of compound **43** was carried out with minimal modifications[i] of the literature procedure, with a yield of 60 %. Boc-guanidine was attached at the carboxylic acid of **43** by standard coupling reactions. Pyrrole **44** was purified by normal-phase chromatography. Hydrolysis of the methyl ester group in **44** was achieved by using 6 equivalents of lithium hydroxide in a tetrahydrofuran/water mixture (6/5),[ii] to give the free carboxylic acid **45** with 92 % yield. The last step to the alkyne functionalised building block **46** was again a standard coupling reaction with propargylamine. The product **46** was isolated after normal-phase chromatography as colourless solid. The 1st to 3rd generation polyglycerol azides **1–3** were attached to alkyne **46** using the copper promoted click reaction described in **Chapter 4.2** to obtain the 1st (**47**), 2nd (**48**), and 3rd (**49**) generation protected zwitterionic-dendrons.[iii] The Boc- and acetal-protecting groups were cleaved under acidic conditions. However, this deprotection step proved to be more difficult than expected, requiring continuous reaction monitoring by HPLC. Standard deprotection conditions with trifluoroacetic acid as well as hydrochloric acid at room temperature were insufficient to cleave all protecting groups within a reasonable reaction period (46 h). Finally, a trifluoroacetic/hydrochloric acid mixture proved to be most efficient to ensure complete deprotection of all 1st to 3rd generation precursors within 24 h at room temperature.

The deprotected dendrons were first dissolved in water by addition of sodium hydroxide to give a pH of 9, and then the pH was adjusted to pH 6 by addition of hydrochloric acid to obtain the zwitterionic dendrons **50**, **51**, and **52**. Unfortunately, the 1st generation dendron **50** precipitated from the aqueous solution, whereas the 2nd **51** and 3rd **52** generation zwitterionic dendrons were completely water-soluble, as expected. The latter compounds were purified by reversed-phase MPLC with water/methanol gradients. Purification of **50** was done by precipitation from water at pH 6. The desired 1st to 3rd generation zwitterionic dendrons were isolated in an overall yield of 12 % for the 1st generation, 10 % for 2nd, and 10% for the 3rd generation dendron.

[i] Hydrolysis with sodium acetate in a dioxane/water mixture was performed by stirring for 15 hours at room temperature, followed by heating to 110 °C, and the amount of solvent for extraction was minimised.

[ii] Cleavage of the methyl ester was first attempted with trimethyltin hydroxide to avoid the possible nucleophilic attack of hydroxide anions on the carbonyl group of the acylguanidine. However, during hydrolysis with lithium hydroxide there was no indication for cleavage of the Boc-guanidine, thus the expensive and hazardous tin reagent could be replaced.[117]

[iii] This preparation was performed by Dr. Monika Wyszogrodzka, a former working group member of Prof. Dr. Rainer Haag, FU Berlin.

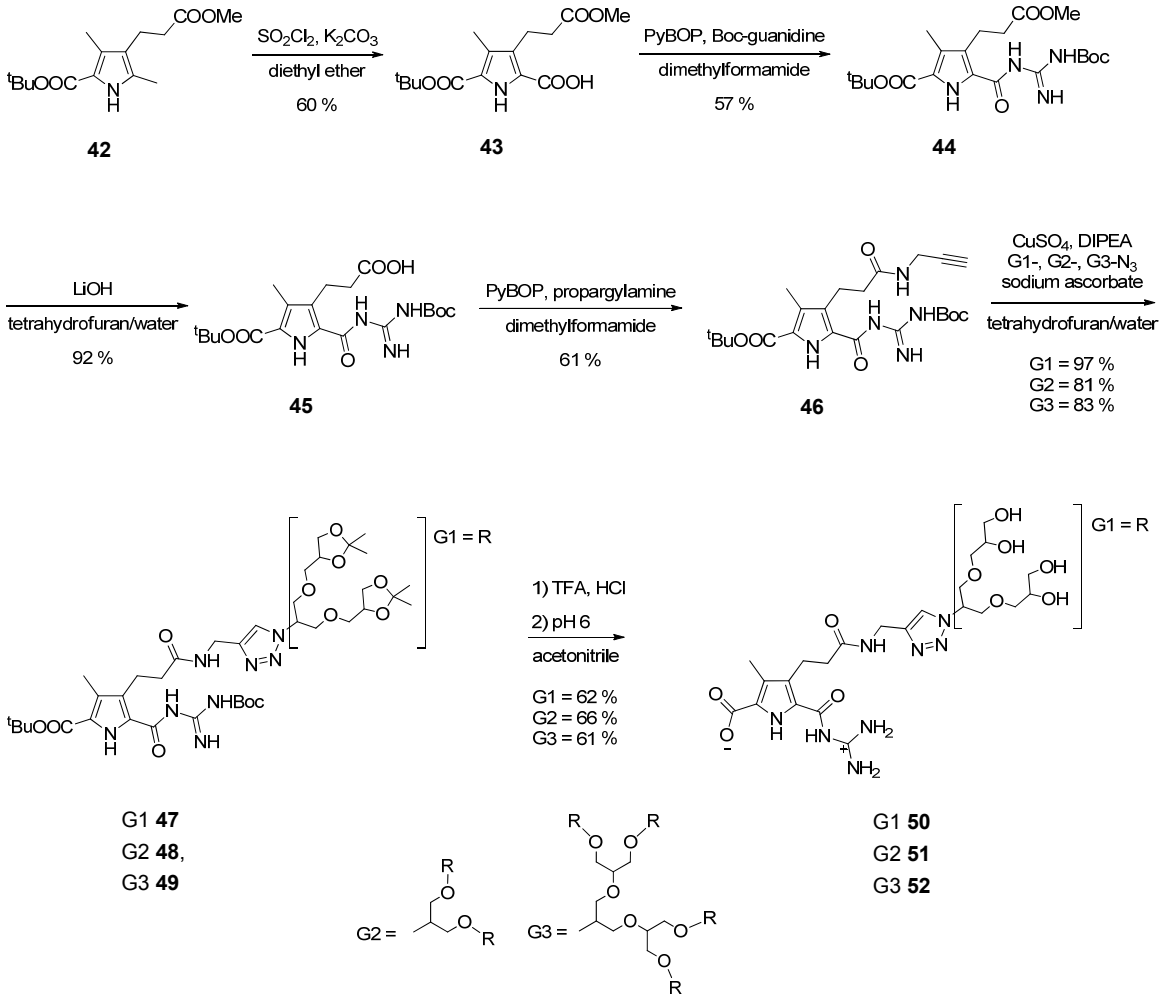

Scheme 4–13: Synthesis of 1st to 3rd generation zwitterionic dendrons **50**, **51**, and **52**.

4.3.1.3 Physicochemical Characterisation

The dimerisation of zwitterionic dendrons **50–52** in water is immediately evident from characteristic shifts of certain resonances in the ^{1}H-NMR spectrum, as demonstrated for **52** in **Figure** 4-18. The NH shifts that are specific indicators for dimer formation have already been established for this type of zwitterions in previous studies.[118] Specifically upon dimerisation the guanidinio NH of **52** shifts from 11.9 ppm to 14.6 ppm, whereas the four guanidinio NH_2 protons, which show a broad signal at 8.3 ppm in the monomer, split into two signals, one being shifted downfield to 10.1 ppm, the other shows a small highfield shift to 8.2 ppm. Such characteristic shifts were observed for all three generations of zwitterionic-dendrons **50–52**.

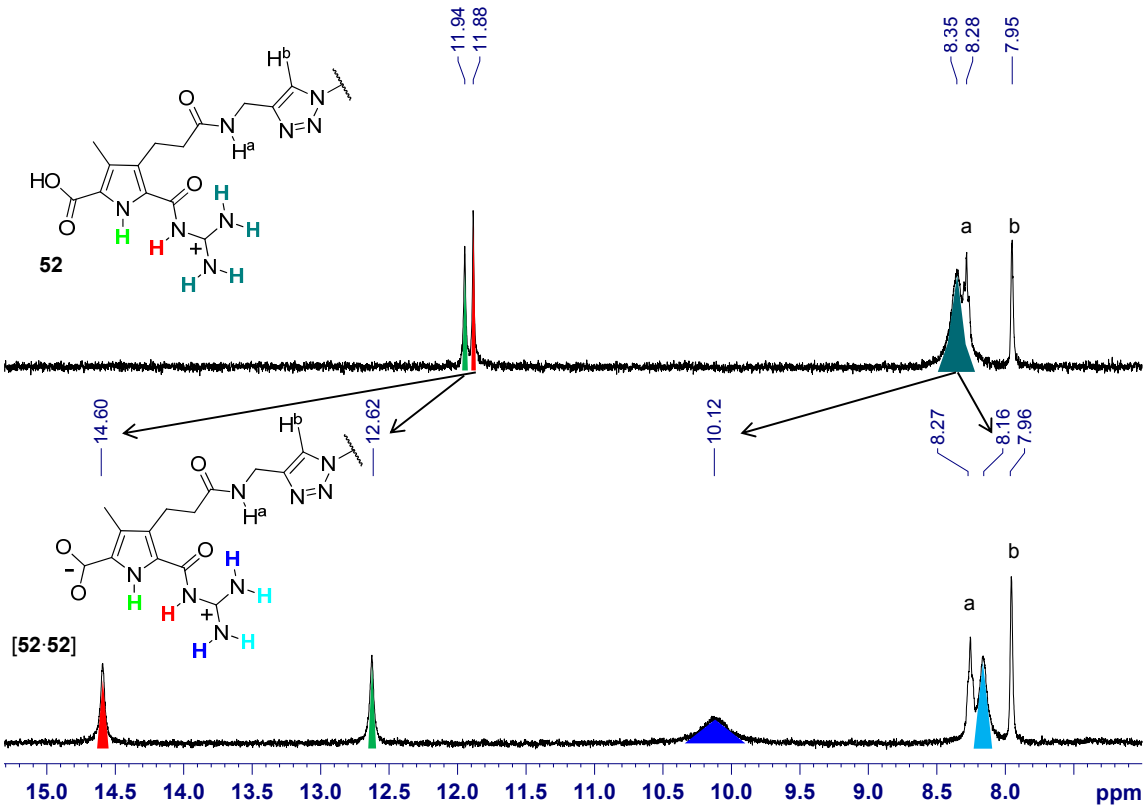

Figure 4-18: ^{1}H-NMR spectra of 3rd generation dendron **52** in $DMSO_{d6}$, the specific downfield shifts for example of the guanidinio NH proton confirm dimerisation and thus the formation of self-assembled dendrimers. **Top**: Protonated, monomeric form of **52**; **Bottom**: Zwitterionic, dimeric form of **52**.

Previously, by monitoring such shift changes quantitatively in a NMR dilution study, the dimerisation constant of the related non-dendritic pyrrole carboxylate zwitterion **53** (**Figure** 4-19) was determined to K_{dim} = 170 M^{-1} in water containing 2.5 vol. % $DMSO_{d6}$.[118]

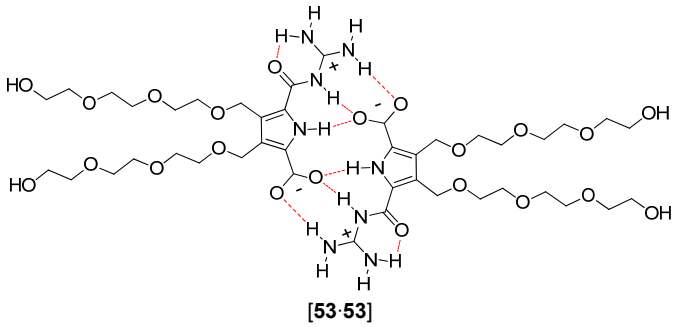

Figure 4-19: Water soluble zwitterionic pyrrole [**53**·**53**] with a binding constant of K = 170 M^{-1} in $H_2O/DMSO_{d6}$ 97.5/2.5 (v/v).

Surprisingly, the dimers of the self-assembling zwitterionic dendrimers turned out to be significantly more stable than [**53**·**53**]. Down to a concentration of 0.1 mM in $H_2O/DMSO_{d6}$

97.5/2.5 (v/v) no shift changes were observed.[i] As shown in **Figure 4-20**, this result clearly indicates complete dimerisation, even at this low concentration. Hence, the dimerisation constant is at least in the order of $K = 10^4\ M^{-1}$ and thus two orders of magnitude larger than for the non-dendritic zwitterion [**53**·**53**]. An exact value of the binding constant could not be determined because of the limitations of measuring such highly diluted aqueous solutions by ^{1}H-NMR.[ii]

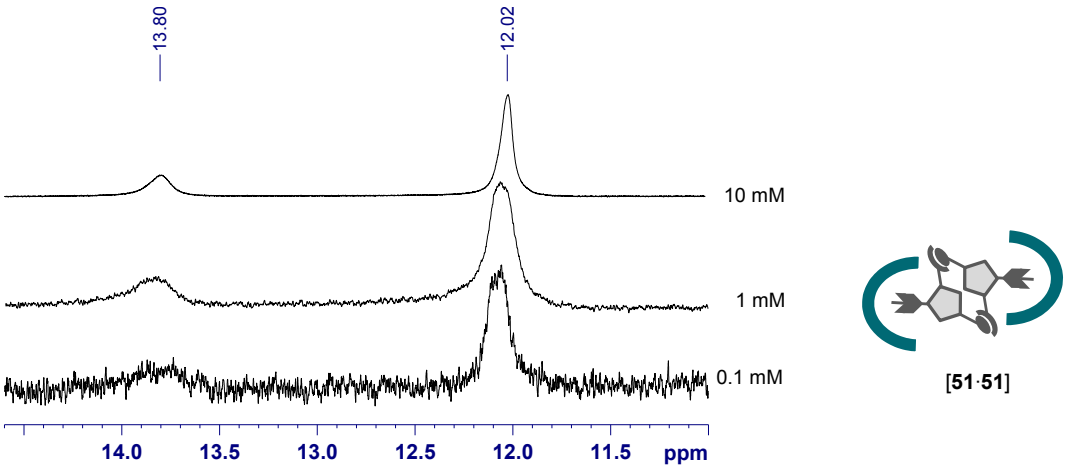

Figure 4-20: 700 MHz ^{1}H-NMR dilution experiment of 2nd generation dendrimer [**51**·**51**] in $H_2O/DMSO_{d6}$ 97.5/2.5 (v/v) with water suppression by excitation sculpting.[119] No significant shifts were observed by dilution.[iii]

The increased stability of the dendron dimers was also confirmed for 2nd generation dimer [**51**·**51**] by isothermal titration calorimetry (ITC)[106] measurements in water. A dimerisation constant of $K_{dim} = 8196\ M^{-1} \pm 1164$ was obtained, in good agreement with the results from the ^{1}H-NMR dilution studies described above. As depicted in **Figure 4-21**, the dimerisation process is exothermic with a $\Delta H = -84\ kJ \cdot mol^{-1}$ but entropically unfavoured by $-T\Delta S = 61\ kJ \cdot mol^{-1}$.

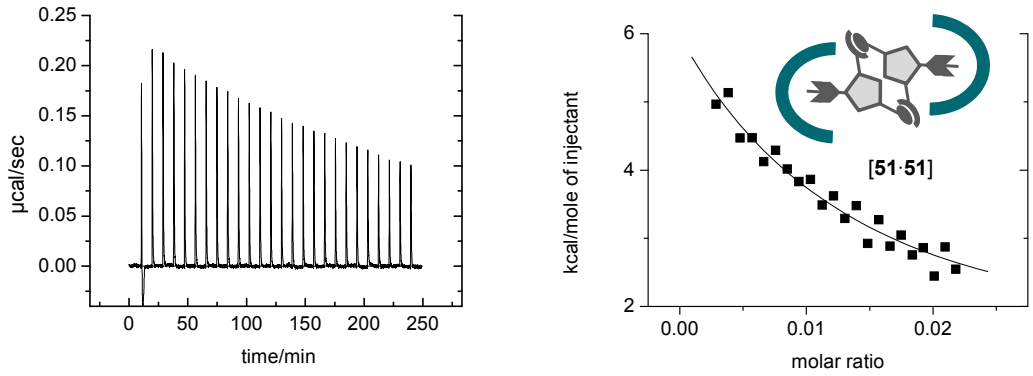

Figure 4-21: ITC dilution experiment of a 2nd generation dimer [**51**·**51**] (0.2 mM in water).

[i] A NMR dilution study for 1st generation dimer [**50**·**50**] in 50 % water and 50 % dimethylsulfoxide$_{d6}$ showed also no shift of signals down to a concentration of 0.4 mM performed at a 500 MHz Bruker NMR spectrometer.
[ii] The ^{1}H-NMR measurement of [**51**·**51**] was performed on a 700 MHz Bruker NMR spectrometer.
[iii] The observed highfield shift of both NH signals compared to **Figure 4–18** is due to the solvent change from pure $DMSO_{d6}$ to 97.5 % H_2O.

The increased stability of the dendritic dimer most likely reflects an effective shielding of the zwitterion from the aqueous surrounding by the dendritic branches. The dendrimer creates a less polar micro-environment around the zwitterion, which enforces hydrogen-bond assisted ion pair formation. Similar dendritic effects on supramolecular complex stabilities have also been reported by other groups. The proposed shielding of the zwitterionic dimers from the aqueous phase within the self-assembled dendrimer is also supported by the calculated structures of the dimers. A Monte Carlo conformational search with subsequent stochastic dynamics calculations provided the energy-minimised structures shown in **Figure** 4-22 and **Figure** 4-23. The two zwitterions (yellow) are completely covered by the polyglycerol dendrons with their less polar ethylene ether units (dark cyan). Hence, a more stable dimerisation in this less polar micro-environment compared to pure water is conceivable because the stability of the H-bond-enforced ion pairs depends strongly on the polarity of the surrounding.

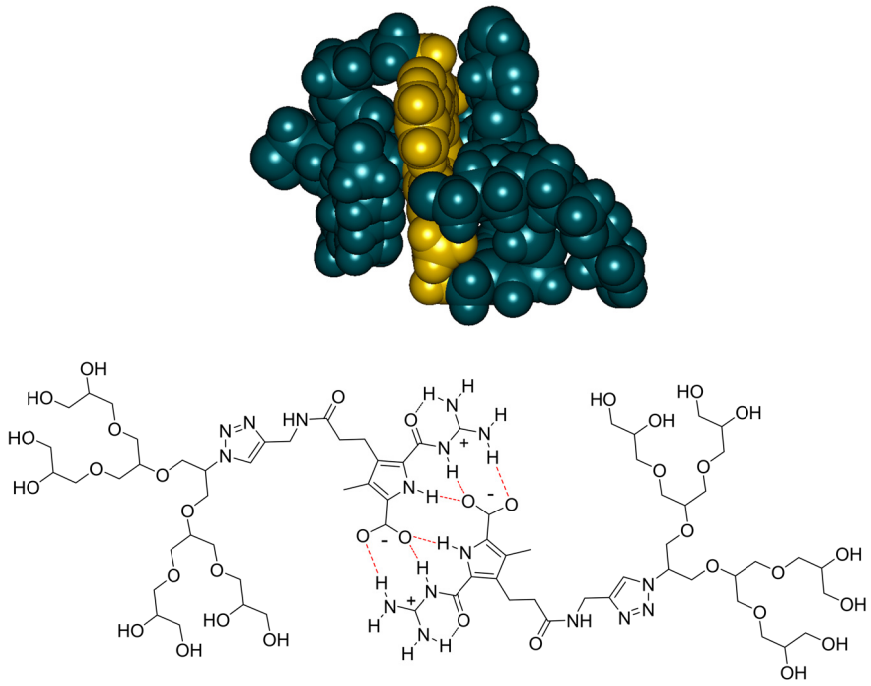

[51·51]

Figure 4-22: Energy-minimised structures of the self-assembled 2nd generation dendrimer dimeric complex [51·51]. Macromodel, OPLS 2005 force field, water solvation model, equilibration time = 1 ps, time step = 1.5 fs, run time = 20 ps, temperature = 300 K.

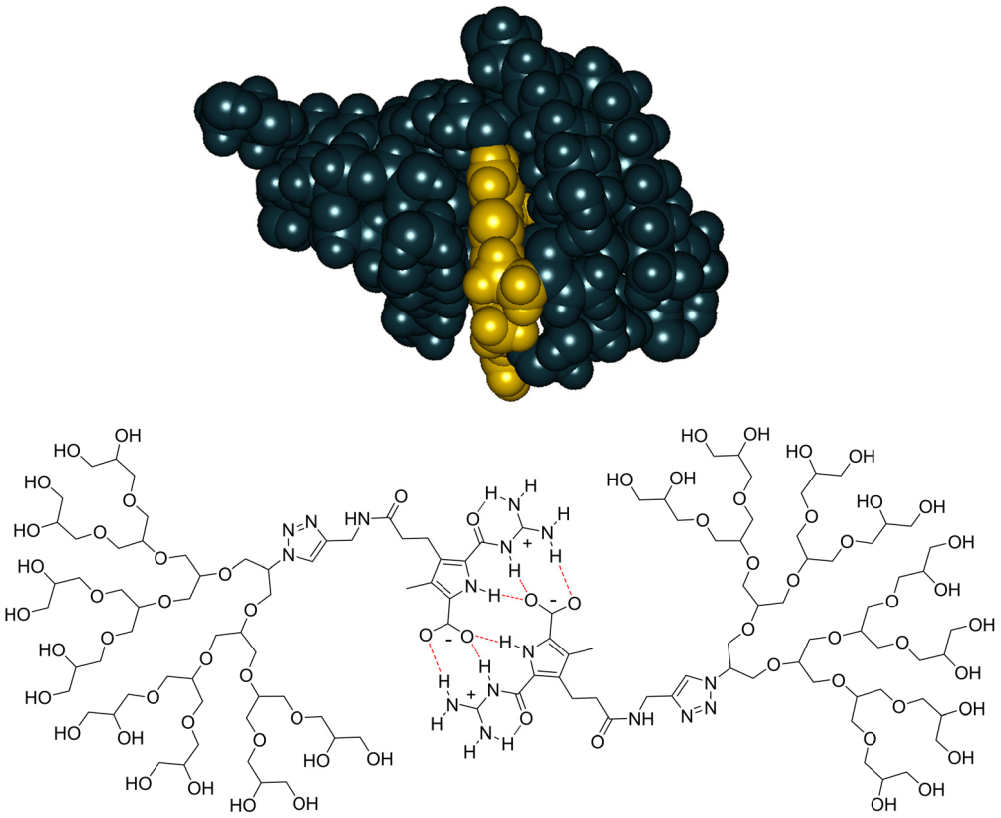

[52·52]

Figure 4-23: Energy-minimised structures of the self-assembled 3rd generation dendrimer dimeric complex [52·52]. Macromodel, OPLS 2005 force field, water solvation model, equilibration time = 1 ps, time step = 1.5 fs, run time = 20 ps, temperature = 300 K.

As mentioned above, it was found that the 1st generation dendrimer **50** is insoluble in water. A force field calculation of the related dimer is shown in **Figure 4-24**, indicating that the hydroxyl groups are orientated toward the binding site and form intramolecular hydrogen bonds. This finding implies that no "free" hydroxyl groups are available for interactions with the solvent. Thus, despite the presence of eight hydroxyl groups, dimer [**50**·**50**] must be considered to be relatively apolar. On the other side, the binding motif is effectively shielded from the solvent, which results in the observed higher binding strength. **In Section 4.3.2** below, soluble zwitterionic templated hetero-associates based on the 1st generation dendron are described underlining the decrease of the solubility caused by dimer formation. In case of the 2nd generation dimer [**51**·**51**] – which is completely water soluble[i] – the calculations show an arrangement comparable to the 1st generation dimer, with two polyglycerol branches orientated above and below the binding site. However, due to the presence of additional branches in the

[i] 2nd generation zwitterion **51** is not soluble in methanol, tetrahydrofuran, or chloroform (1 mg·ml^{-1}).

2nd generation dendron having four hydroxyl groups each orientated away from the binding site solubility is conferred, in contrast to the 1st generation dendron.

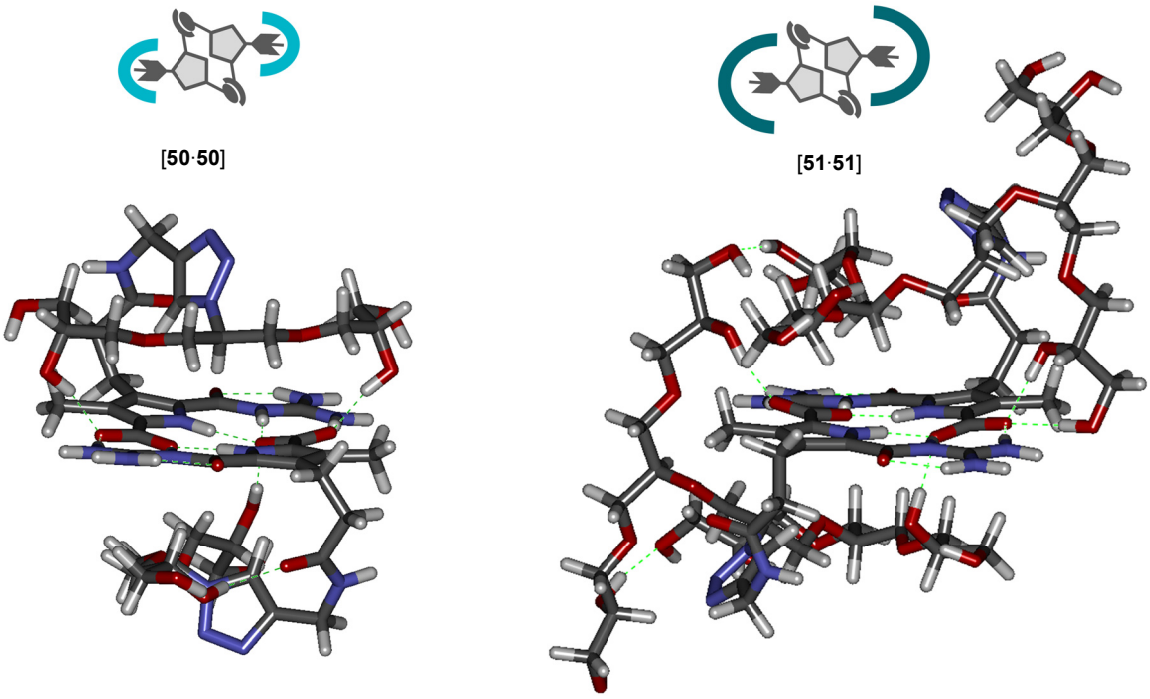

Figure 4-24: Calculated zwitterionic structures of 1st [**50·50**] and 2nd [**51·51**] generation dendritic dimers. Macromodel, OPLS 2005 force field, water solvation model, hydrogen-bonds are depicted up to a distance of 2.5 nm.

Formation of such discrete self-assembled dimers was confirmed by DOSY-NMR studies and DLS. DOSY-NMR experiments in dimethylsulfoxide$_{d6}$ also provided evidence for the presence of dimers in solution. The hydrodynamic diameters evaluated by means of the Stokes-Einstein equation (**Equation 4–2**) for spherical particles are in good agreement with the size of precursors **47**, **48**, and **49** and dimers [**50·50**], [**51·51**], and [**52·52**] predicted by the molecular modelling calculations. The dimers present in solution are also significantly larger than the protected precursors of **50**, **51**, and **52**, which cannot self-assemble and thus are present as monomers (see **Table 4–3**).

Essentially same dimer sizes were obtained from dynamic light scattering studies. Only one signal was observed in 4.5 mM solutions of either 2nd [**51·51**] or 3rd [**52·52**] generation dendrimers in pure water, corresponding to particles with a diameter of 2.7 nm and 3.4 nm, respectively (**Figure 4-25**).[i] No larger particles than these dimers were detected. Differently to the DOSY experiments, the sizes of the monomers were determined after addition of sodium hydroxide in order to deprotonate the zwitterion and to obtain the monomeric anionic

[i] Due to the water insolubility of 1st generation dendrimer [**50·50**] DLS measurements could not be performed. DLS measurements in dimethylsulfoxide were not possible, as discussed in **Chapter 4.2.3.2**.

dendrons 51^- and 52^-. As expected, the monomeric anions are smaller than the dimers [51·51], [52·52], and the 2nd generation anion 51^- is smaller than the 3rd generation anion 52^- (see **Table** 4–3).

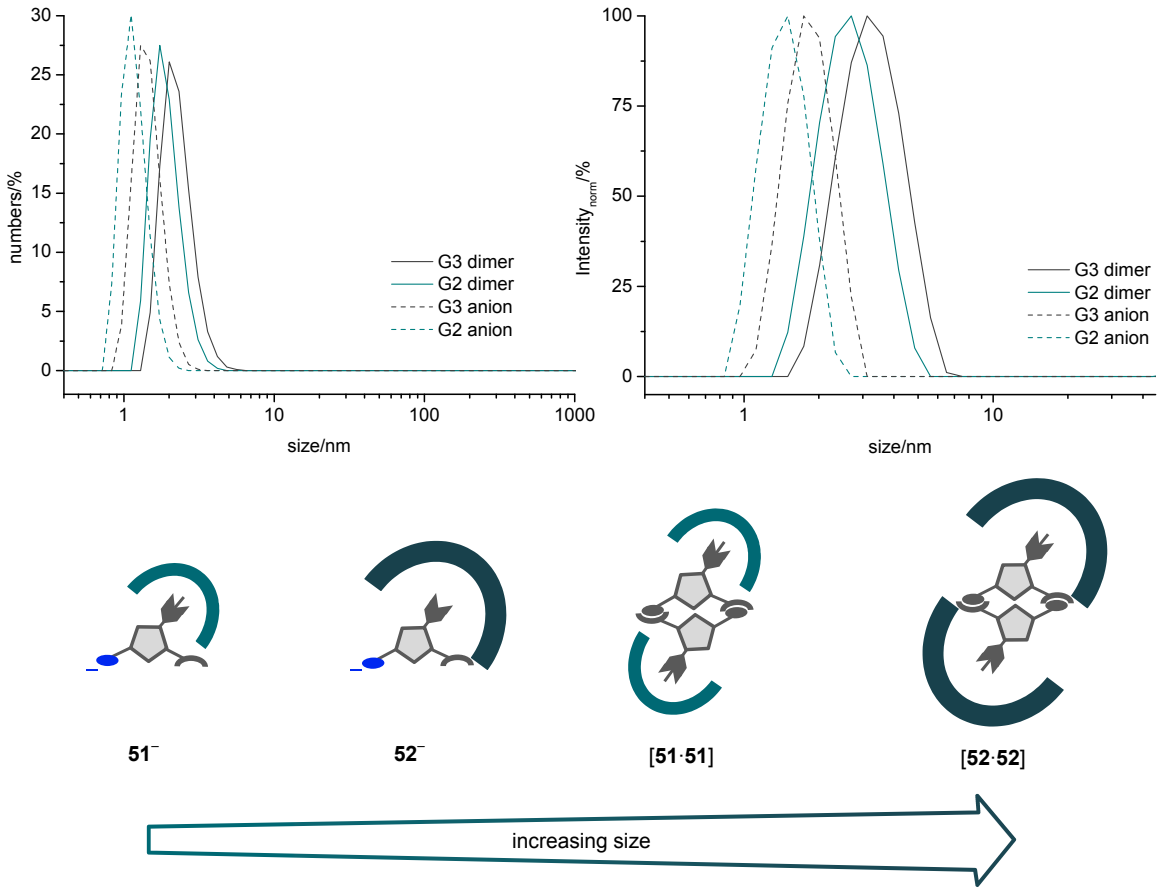

Figure 4-25: Size distribution by numbers and intensity of 4.5 mM aqueous solutions of 2nd and 3rd generation anions 51^-, 52^- and 2nd and 3rd generation dimers [51·51], [52·52]. Dimers were deprotonated by the addition of 2 equivalents of 1 M NaOH to monomers.

In **Table** 4–3 the hydrodynamic diameters determined by the DOSY and DLS measurements are compared to the calculated sizes of monomers and dimers. Except for the calculated value of the 1st generation monomeric precursor 47 (entry 1a), the data of all results are in good correspondence, confirming the predicted tendencies of the sizes of the molecules as illustrated in **Figure** 4-26. The overestimated size of entry 1a can be explained by a rather stretched than spherical structure of 47.

Table 4–3: Experimental hydrodynamic diameters from DOSY measurements of 15 mM solutions in $DMSO_{d6}$ at 25 °C, DLS measurements of 4.5 mM solutions in water at 25 °C. Theoretical size was calculated by molecular modelling with Macromodel force field OPLS2005. *(dimers were deprotonated by the addition of 2 equivalents of NaOH (1 N) to monomers 51^- and 52^-).

entry	compound	DOSY diameter/nm	DLS diameter nm	MM diameter/nm
1a	**47**	1.6	n.s.	2.2
1b	**[50·50]**	2.3	n.s.	1.9
2a	**48**	1.8	1.5*	2.1
2b	**[51·51]**	2.8	2.7	2.5
3a	**49**	2.3	1.8*	2.6
3b	**[52·52]**	3.7	3.4	3.3

For easier rationalisation of the experimental results reported above the molecular mechanics calculations of all three generation monomeric precursors **47**, **48**, and **49** and dimers [50·50], [51·51], and [52·52] are summarised in **Figure 4-26**.

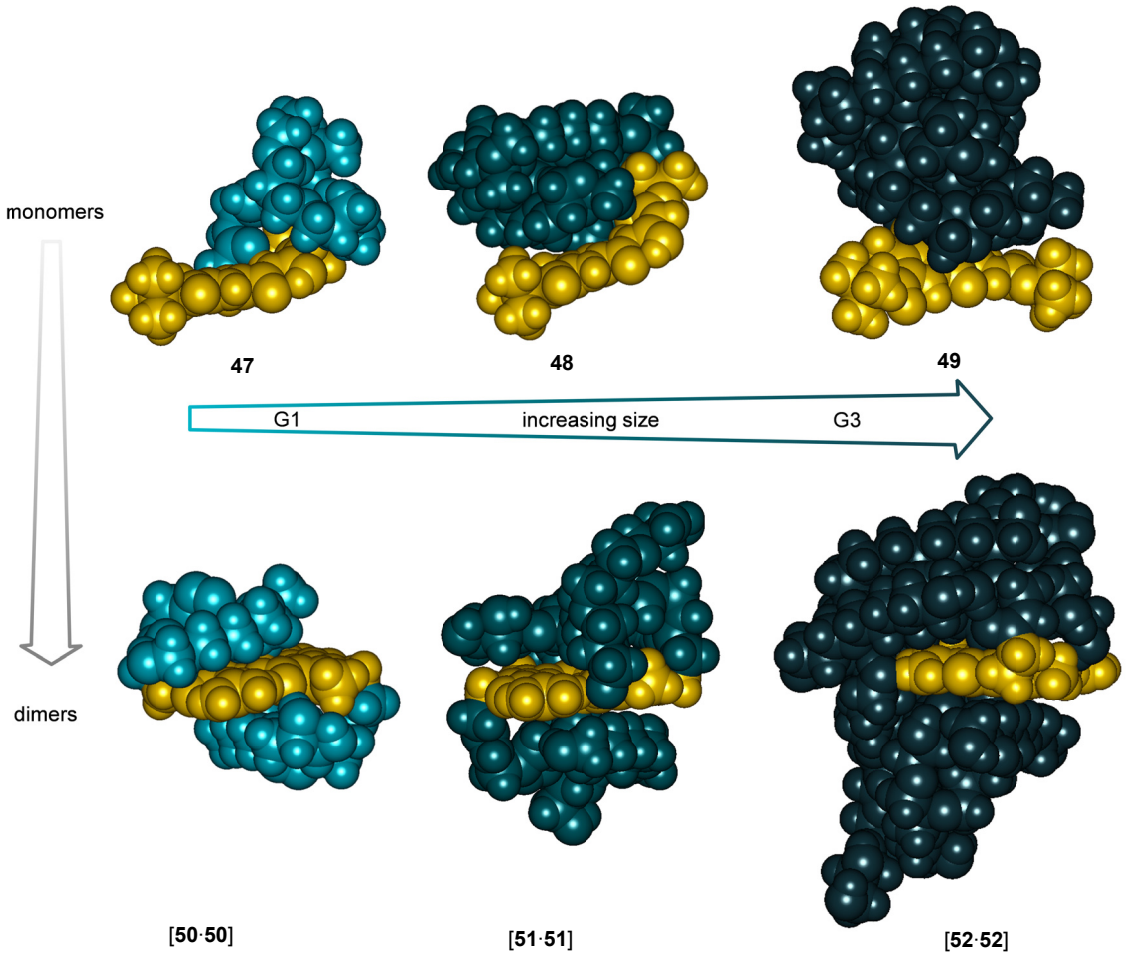

Figure 4-26: **Top**: Left to right: Calculated structures of protected 1st to 3rd generation monomeric dendritic precursors 47, 48, and 49; **Bottom**: Left to right: Calculated zwitterionic structures of 1st to 3rd generation dendritic dimers [50·50], [51·51], and [52·52]. Macromodel, OPLS 2005 force field, water solvation model.

The results of the DOSY and DLS measurements are further supported by cryo-electron-microscopy (cryo-EM). Cryo-EM is a variant of transmission electron microscopy performed at cryogenic temperatures. The main principle of electron microscopy is based on the inelastic and elastic scattering of electrons by the electron shell and the atomic nuclei of the sample. In cryo-EM the sample preparation is more complex but the sample is always in solution and not in contact with adhering surfaces. Therefore, the shape of the aggregate that is observed during cryo-EM is the same like in solution. Cryo-EM images obtained for the 2nd [51·51] and 3rd [52·52] generation self-assembled dendrimers in pure water are shown in **Figure** 4-27. Even though the resolution of cryo-EM is close to the detection limit and only allows to roughly estimate the size of the particles, being circa 3–4 nm for the 3rd generation dimer [52·52] and even smaller for the 2nd generation dimer [51·51], it is clearly evident that no larger aggregates of any kind are present.

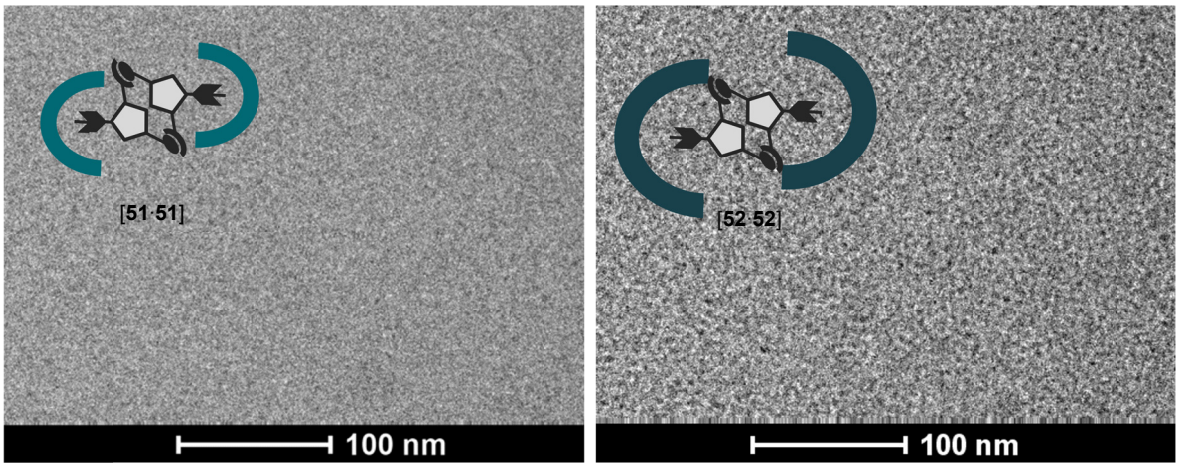

Figure 4-27: **Left**: Cryo-EM measurements of 2nd generation dendrimer [51·51] (1 mM) in water; **Right**: Cryo-EM measurements of 3rd generation dendrimer [52·52] (1 mM) in water.

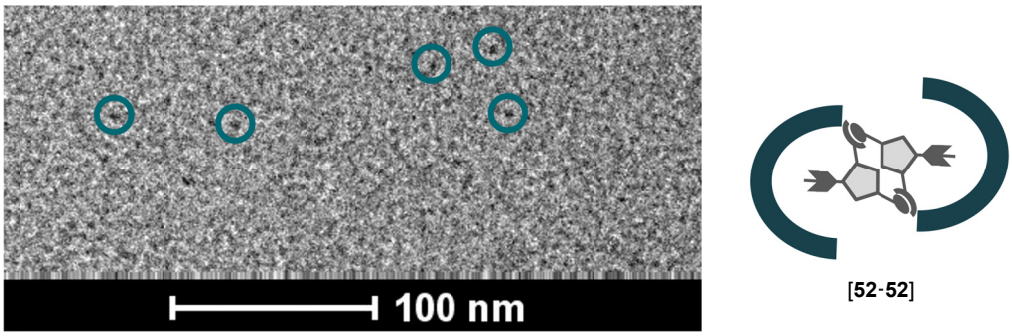

Figure 4-28: Cryo-EM image of 1 mM aqueous solution of the self-assembled 3rd generation dendrimer [52·52]. Only small spherical particles of *ca*. 3–4 nm diameter are observed (some highlighted by circles) but not any larger aggregates.

Size Exclusion Chromatography (SEC)[120] experiments underline the foregoing results. An aqueous 10 mM LiBr eluent showed intense peaks for self-assembled dimers [**51**·**51**] and [**52**·**52**], accompanied by small traces of monomers as depicted in **Figure 4-29**. The average molecular weight of the dimers obtained from these SEC runs ([**51**·**51**]: 2315 g·mol^{-1}, [**52**·**52**]: 3251 g·mol^{-1}; calibrated with narrowly distributed pullulan) are in good agreement with the calculated values ([**51**·**51**]: 1762 g·mol^{-1}, [**52**·**52**]: 2948 g·mol^{-1}, respectively). The high dimerisation strength, enforcing dimerisation down to concentrations as low as 0.1 mM, as derived from the ITC and NMR dilution studies, is also confirmed by the SEC experiments, where in highly diluted solutions of 0.23 mM and 0.14 mM of 2nd [**51**·**51**] and 3rd generation dimer [**52**·**52**], respectively, almost exclusively the dimers are detected.

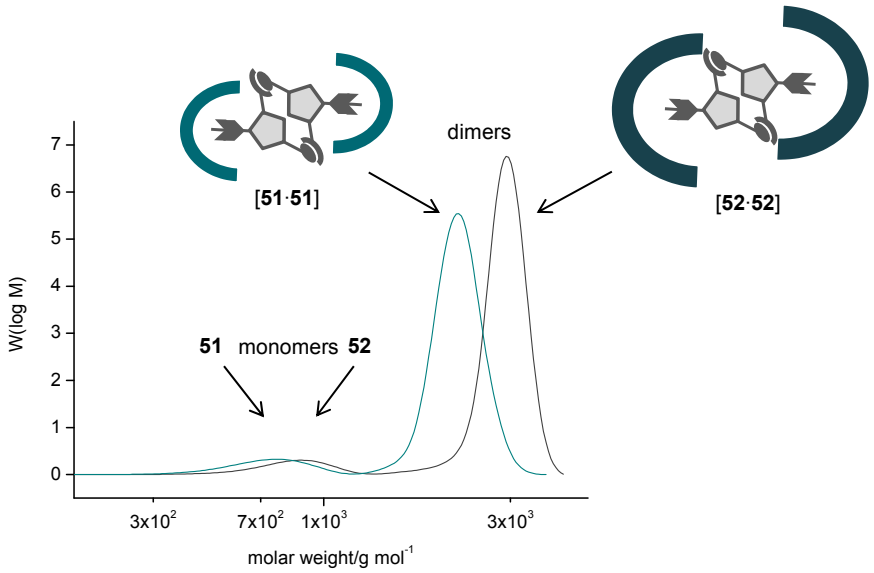

Figure 4-29: **Dark cyan**: SEC trace of 2nd generation dimer [**51**·**51**] (0.23 mM); **Dark green**: SEC trace of 3rd generation dimer [**52**·**52**]·(0.14 mM); SEC-conditions: 10 mM LiBr aqueous solution, pH 7.1; column: PSS Proteema-1000 and PSS Proteema-100; calibrated with narrow distributed pullulan.

A further SEC experiment was carried out with the protonated, cationic monomeric 3rd generation dendron **52**$^+$ (**Figure 4-30**). At pH 7.1 only a small increase of the monomer peak was observed, and again the dimer represented the major component. This, of course, reflects the attainment of the acid-base equilibrium of **52**, in which the zwitterionic form of **52** predominates, leading to formation of dimer [**52**·**52**].[i] In order to achieve weakly acidic conditions, a 1 % acetic acid solution was employed as eluent. Unfortunately, as evident from **Figure 4-30**, these conditions lead to interactions of the molecule with the column material. Thus, in the present case SEC cannot be applied as it is based on simple size exclusion, and no significant interactions of sample and stationary phase should take place. Anyway, the shown

[i] Same results were obtained for the 2nd generation dendron **51**.

SEC experiments confirm the strong tendency of the zwitterions to form dimers in aqueous solvents at pH 6–7.

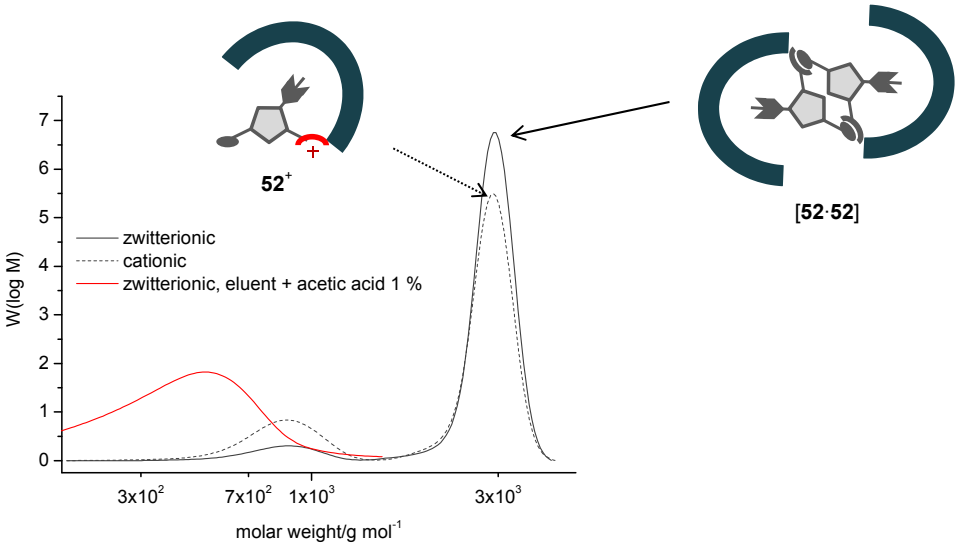

Figure 4-30: **Dark green**: (—) SEC of a solution of 3rd generation dimer [**52**·**52**] (0.14 mM); (---) Solution of 3rd generation monomeric cation **52**+ (0.14 mM), SEC-conditions: 10 mM LiBr aqueous solution, pH 7.1; **Red**: 3rd Generation dimer [**52**·**52**] (0.14 mM), SEC-conditions: Aqueous solution of acetic acid 99:1 (v/v).

As shown above, the formation of self-assembled dendrimers can be controlled by the pH of the solution. For example, at pH > 8 the zwitterion is deprotonated to the anionic dendron which cannot self-assemble. Accordingly, DLS confirms the presence of monomeric dendrons in solution at pH > 8. This underlines that the observed formation of self-assembled dendrimers is due to specific interactions of two zwitterions and not due to unspecific aggregation, e.g. of the dendritic polyglycol chains of the molecules. As a consequence, self-assembly of the dendrons can be switched on and off by reversibly changing the pH of the solution. This is demonstrated in **Figure 4-31** for the 2nd and 3rd generation dendrimers.

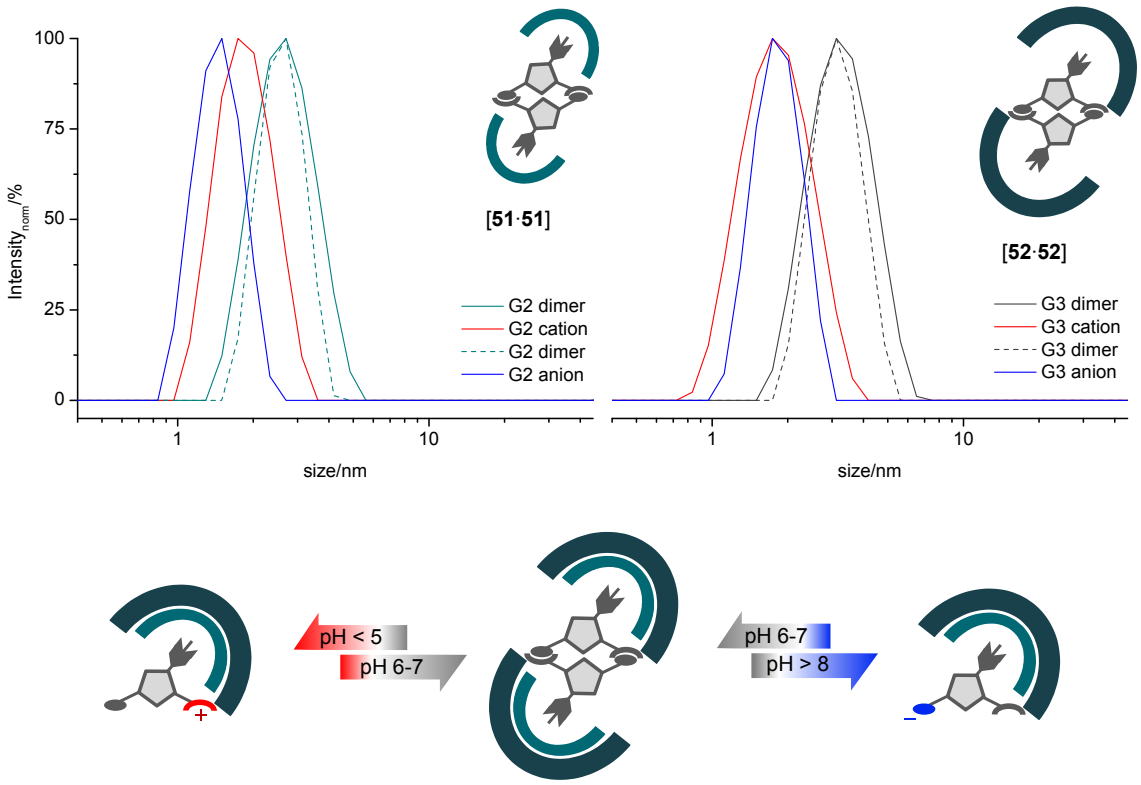

Figure 4-31: **Bottom**: Reversible pH dependent switching of 2nd and 3rd generation dendrimeric dimers to cationic and anionic monomers, respectively, from DLS measurements of 4.5 mM aqueous solutions of 2nd **51** and 3rd **52** generation dendrons at different pH values (**top**). Self-assembled dimers are only formed at neutral pH whereas at pH < 5 and > 8 only the monomers are present.

At neutral pH only dimers with a diameter of 2.7 nm for [**51**·**51**] (entry 2a) and 3.4 nm for [**52**·**52**] (entry 3a), respectively, are present. When two equivalents of HCl were added to the solutions, the size for the 2nd generation particles decreases by a factor of about 1.5 to a diameter of 1.8 nm (entry 2b), reflecting formation of the monomeric cation **51**$^+$. In case of the 3rd generation dendron, the size decreases by a factor of 1.7 to a diameter of 1.9 nm (entry 3b) indicating formation of the monomeric cation **52**$^+$. When the pH was readjusted back to neutral by addition of NaOH, reassembling to the supramolecular dendrimers [**51**·**51**] and [**52**·**52**] occurs. Further addition of two equivalents of sodium hydroxide induced disassembly to the monomeric anions **51**$^-$ and **52**$^-$ with sizes of 1.5 nm (entry 2c) and 1.8 nm (entry 3c).

Table 4–4: DLS measurements of 4.5 mM aqueous solutions of 2nd and 3rd generation dendrons. Anions and cations were formed by the addition of HCl (1 N) and NaOH (1 N), respectively.

entry	compound	diameter/nm	ratio [dimer]/ [monomer]
2a	**[51·51]**	2.7	
2b	**51$^+$**	1.8	1.5
2c	**51$^-$**	1.5	1.8
3a	**[52·52]**	3.4	
3b	**52$^+$**	1.9	1.8
3c	**52$^-$**	1.8	1.9

In conclusion, it is demonstrated that the combination of the guanidiniocarbonyl pyrrole carboxylate and 1st to 3rd generation dendrons results in a significantly enhanced stability of the resulting dimeric complexes **[50·50]**, **[51·51]**, and **[52·52]**. Besides steric shielding, the dendritic ligand also provides a more hydrophobic environment, enforcing self-assembly of the polar core. Furthermore, the switching behaviour of the embedded binding site is conserved in the dimer, thus providing novel, reversibly pH-switchable supramolecular 2nd and 3rd generation dendrimers. This unique property in combination with the high biocompatibility of the dendritic polyglycerol groups offers a new platform for stimulus-responsive nanotransporters for biomedical applications.

.

4.3.2 Zwitterionic Templated Supramolecular Dendrimers (ZT-SD)

4.3.2.1 Introduction

Guided by the results of the zwitterionic untemplated supramolecular dendrimers **50–52** as described in **Section 4.3.1**, the potential of a templated self-assembly as schematically shown in **Figure 4-32** was investigated. The results of the ZT-SD approach are reported in this chapter.

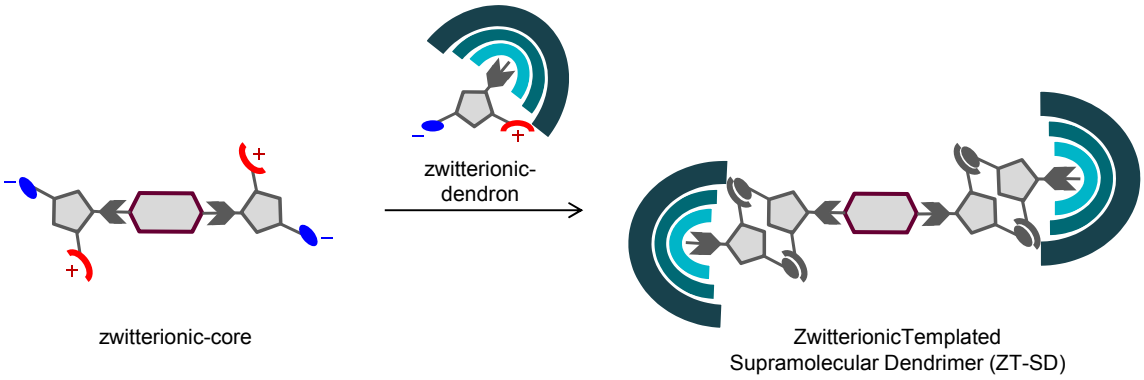

Figure 4-32: Schematic illustration of a templated self-assembly of a zwitterionic core and a zwitterionic dendron to yield a zwitterionic templated supramolecular dendrimer.

The idea to build up distinct monodisperse hetero-associates with a self-compatible binding site is a challenging task because such non-orthogonal building blocks are prone to self-assembling to hetero- as well as to homo-associates or mixtures of both. However, since supramolecular association processes can be influenced by concentration, temperature, or polarity of solvents, such external stimuli may be utilised to direct the aggregation path towards the desired assemblies. Perylene-diimide (PDI) dyes are often used in the literature as probes in UV/Vis studies to gain information on aggregation mechanisms of supramolecular dye assemblies. The UV/Vis absorption spectrum of monomeric perylene diimide shows a characteristic vibronic fine structure that is different from aggregated (π-stacked) perylene diimide. As one of the most thoroughly studied chromophores in supramolecular assembly processes, the perylene diimide is an ideal candidate to act as a central core for templated supramolecular dendrimers, allowing easy monitoring of the self-assembly processes by means of UV/Vis-spectroscopy. [121, 122, 123, 124] In the present thesis perylene-tetra-carboxylic-acid-di-anhydride (PTCDA) (**54**) was selected as central core unit. It is possible to build symmetrical PDIs by imidisation of PTCDA with 2 amine functionalised zwitterionic pyrrole binding sites as shown in **Scheme 4–14**.

4.3.2.2 Synthesis

The synthetic route to the divalent zwitterionic core **55** is outlined in **Scheme** 4–14. Pyrrole **45**, which had previously been used as starting material for the preparation of zwitterionic dendrons **50–52,** was modified by a standard coupling reaction with the Cbz-protected ethylene diamine **56** to give pyrrole **57**. The Cbz-protecting group in **56** is essential since a free amine group is necessary for the subsequent reaction with PTCDA. Hydrogenolysis of **57** afforded amine **58**, which then was reacted with dianhydride **54** (PTCDA) according to the procedure reported by LANGHALS *et al.*.[125, 126] After dilution with ethanol and aqueous work-up with 1 M hydrochloric acid the perylene diimide **59** was isolated. The ^{t}butyl-ester **59** was deprotected by addition of concentrated hydrochloric acid in methanol, the precipitated hydrochloride of **55** isolated by filtration, dissolved by addition of sodium hydroxide, and zwitterionic perylene diimide **55** precipitated by addition of hydrochloric acid to give a pH 5.9. Zwitterionic perylene diimide **55** was isolated in a yield of 72 %.[i]

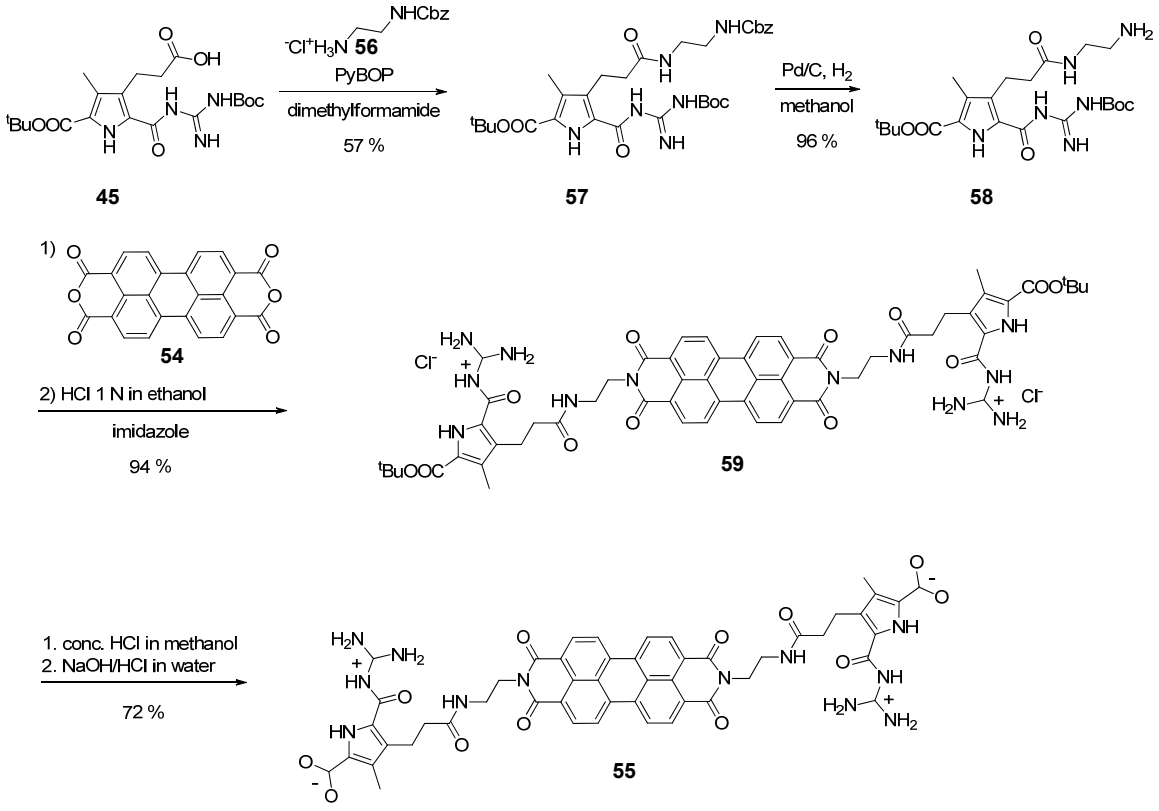

Scheme 4–14: Synthetic route to zwitterionic perylene diimide **55** starting from pyrrole compound **45**.

[i] The zwitterionic perylene diimide **55** is completely insoluble in water and even only slightly soluble in dimethylsulfoxide at elevated temperatures. A ^{1}H-NMR could only be recorded at 80 °C showing the significant lowfield shifts of the guanidine NH protons as characteristic for the zwitterionic structure.

4.3.2.3 Physicochemical Characterisation

Reaction of the Zwitterionic Perylene Diimide with Zwitterionic Dendrons

The water-insoluble zwitterionic perylene diimide **55** (Z-PDI) could not be solubilised by simple addition of 1st to 3rd generation zwitterionic dendrons **50–52**. Obviously, **55** is trapped kinetically in an aggregated state due to its bad solubility in water. To circumvent the insolubility problem, the pH switchable properties of the guanidiniocarbonyl pyrrole carboxylate binding motif were taken in advantage.

As learned from the synthetic work, Z-PDI **55** can be dissolved in aqueous sodium hydroxide solution to give the anion of **55** (A-PDI, $\mathbf{55}^-$). To the basic solution the supramolecular dendrimers **50**, **51**, and **52**, respectively, were added. Their deprotonation caused them to disassemble to the monomeric anionic dendrons. The mixture then was treated with hydrochloric acid to a final pH of 6–7, thereby the zwitterions of the core and the dendrons were regenerated. The solution was filtered through a syringe filter to remove the precipitated aggregates. However, by inspection with the naked eye it became already evident that a significant amount of the zwitterionic perylene **55** remained solubilised in the aqueous phase by association to dendrons **50**, **51**, or **52**, respectively, as demonstrated in **Figure 4-33**.[i] The experiment was repeated in the absence of 1st to 3rd generation dendrons to verify this observation by a negative cross-check. As expected, after filtration no zwitterionic perylene diimide **55** was found in the aqueous phase as shown in **Figure 4-33**. Hence, the zwitterionic perylene diimide **55** is solubilised by forming hetero-aggregates with dendrons **50–52**, while in the absence of the dendrons the perylene diimide **55** self-assembles to water-insoluble larger homo-aggregates. Noteworthy, the same observations were made if both kinds of reaction mixtures were allowed to stand overnight, the mixture containing dendrons **50–52** provided a stable solution of zwitterionic perylene **55**, and no precipitation was observed, whereas from the reaction mixture containing solely zwitterionic perylene diimide **55** the aggregated Z-PDI (**55**) precipitated. For further characterisation, UV/Vis, AFM, and DLS measurements of anionic, zwitterionic, and dendron-solubilised perylene diimides were performed.

[i] Even the 1st generation dendron **50**, the dimer of which is not soluble in water as discussed in **Chapter 4.3.1** is able to solubilise perylene diimide **55**.

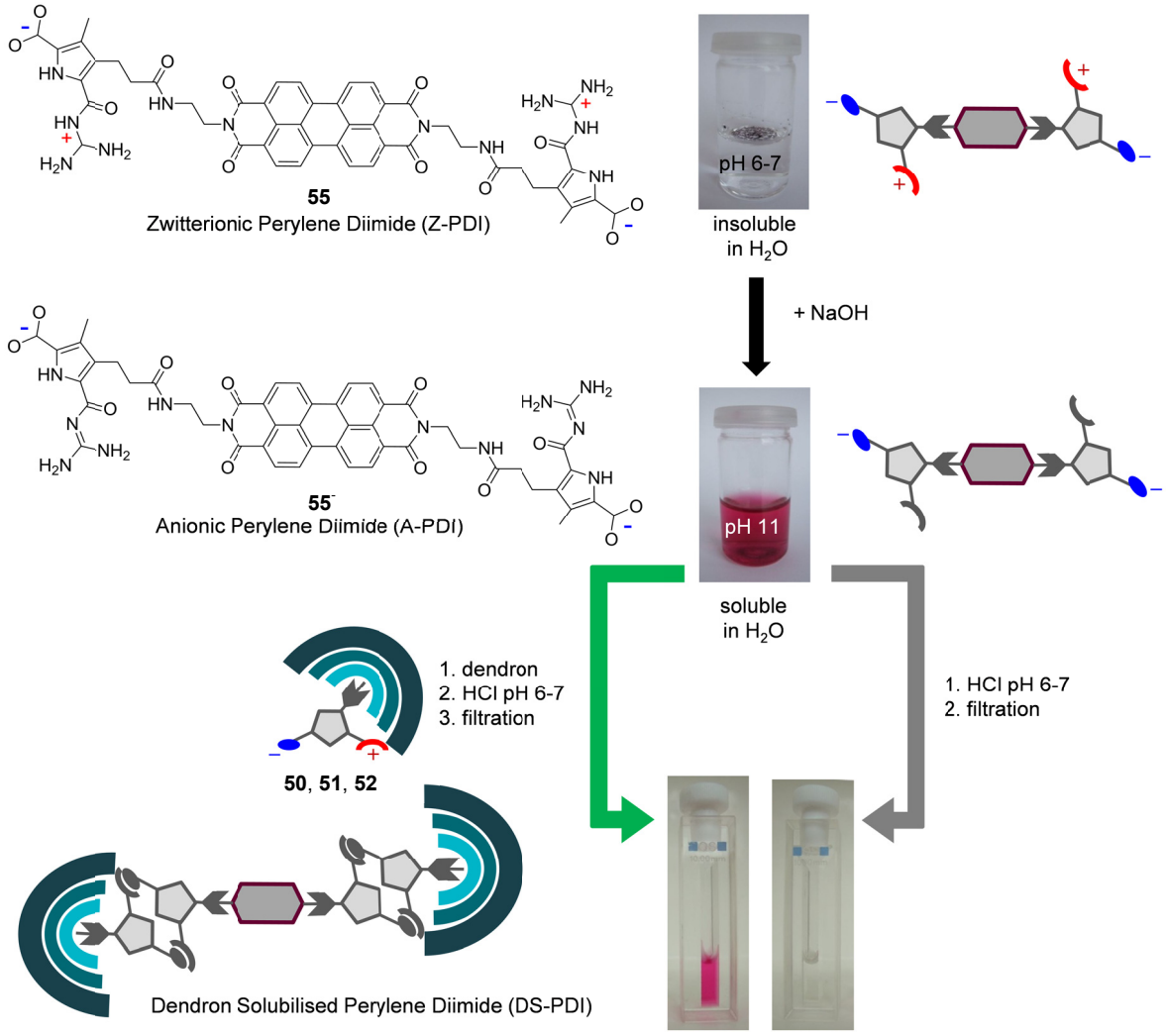

Figure 4-33: Solubility test of perylene diimide **55** in water. Water insoluble zwitterionic perylene diimide **55** was dissolved with 40 equivalents of NaOH; **Green:** The aqueous solutions of **55** was treated with 1st to 3rd generation dendrons **50–52** (4 equivalents for each generation). After pH adjustment with HCl to pH 6–7, the solution was filtered through a PTFE syringe filter of 0.45 µm pore size; **Grey:** The pH was adjusted to pH 6–7 by hydrochloric acid, and the 0.1 mM solution of **55** was filtered through a PTFE syringe filter of 0.45 µm pore size.

UV/Vis Measurements

As discussed in the introduction, the UV/Vis spectra of perylene diimides show significant differences for monomeric and aggregated chromophores. The qualitative proof of solubilisation as shown in **Figure 4-33** was also established in a quantitative manner by pH titration experiments monitored by UV/Vis spectroscopy. As noted, the zwitterionic perylene diimide **55** is not water-soluble and thus can be filtered off. This holds for solutions in the range of 0.05 mM to 0.2 mM and above, while a 0.01 mM solution of **55** was found to be stable over a longer period of time. Obviously, the aggregation process is slowed down at low concentrations. In **Figure 4-34** the pH dependence of the aggregation process in the range of pH 11 to pH 6 induced by stepwise addition of hydrochloric acid is depicted. The absorption

spectra of perylene diimide **55** in the absence and in the presence of 2nd generation dendron **51**, respectively, are presented.

The electronic absorption spectra at pH 11 in both cases show the typical shape for H-aggregated perylene diimides, with a maximum absorbance at 507 nm. The addition of hydrochloric acid to a final pH of 9 led to the same spectral changes in the absence and presence of the dendron. In both cases a hypochromic and bathochromic shift of the absorption maximum is observed.

While the shape of the UV/Vis spectra in the absence of a dendron did not change dramatically on lowering the pH to 9, a significant hyperchromic shift was observed for the perylene diimide dendron mixture [**55**·**51**], displaying a new maximum at 560 nm. The spectra observed at pH 7 of (**Figure 4-34**, right) are typical for monomeric perylene diimides (S_0–S_1 transition of the PDI chromophore with well resolved vibronic fine structure). The absorption spectra did not further change on lowering the pH to 5.7, in agreement with the fact that in the pH region 7.3 to 5.7 the binding site remains in the zwitterionic state. Further lowering of the pH to values below 5 causes protonation of the carboxylate groups, resulting in precipitation of the cationic perylene diimide **55**$^+$ from both solutions, i.e. with or without added dendron.

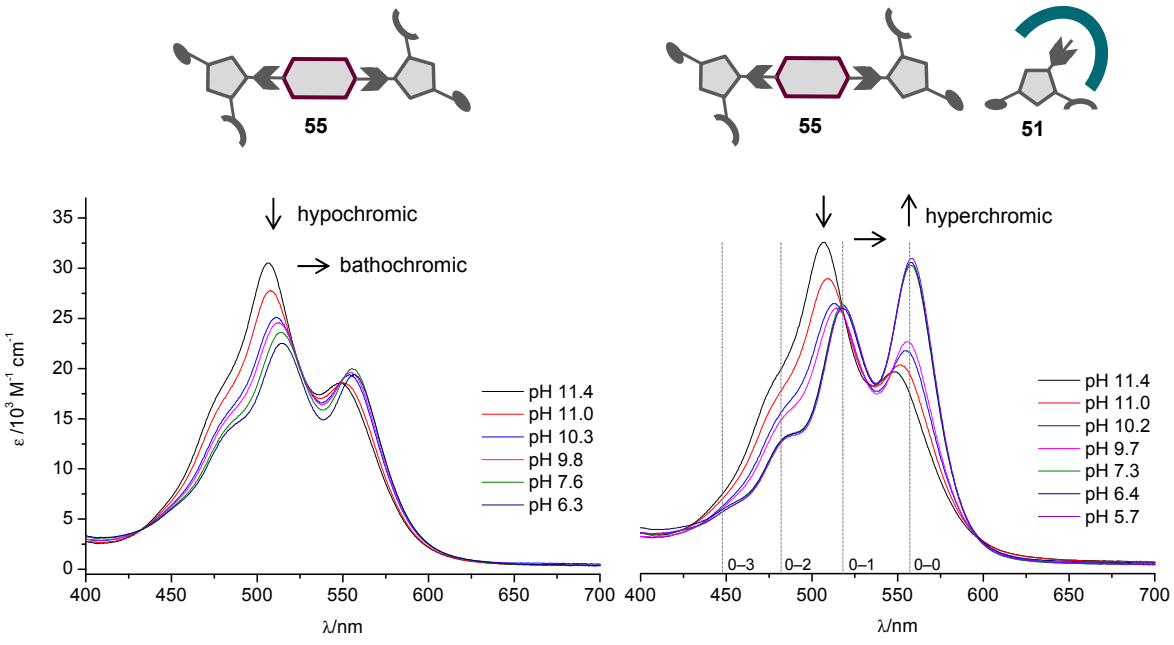

Figure 4-34: pH Titration: **Left**: Perylene diimide **55** (0.01 mM) and sodium hydroxide (0.4 mM)–pH adjusted by the addition of 0.1 N HCl; **Right**: Perylene diimide **55** (0.01 mM), sodium hydroxide (0.4 mM), and 10 equivalents of 2nd generation dendron **51** (0.1 mM)–pH change adjusted by addition of 0.1 N HCl.

The experiment of **Figure 4-34** clearly demonstrates the effect of 2nd generation dendron **51** on the aggregation state of the zwitterionic perylene diimide **55**. A switch of the pH from 11

to 6 caused solubilisation of **55** as monomer in water. The non-aggregated PDI species are most likely hetero-aggregates of **55** and 2nd generation zwitterionic dendron **51**, forming a dendron-solubilised PDI. To shed some light on the thermodynamics of the aggregation processes of the PDIs, temperature-dependent UV/Vis studies were performed.

Temperature or concentration dependent UV/Vis measurements using perylene diimides as probes have frequently been carried out in the literature with the goal to gain information about the degree of supramolecular polymerisation. As demonstrated in **Figure 4-34**, the resolved 1st vibronic band in the UV/Vis spectra most clearly distinguishes the monomeric PDI from dimeric or aggregated perylene diimide. Depending on the association constant, the absorption spectrum of aggregated PDI will gradually change to that of the monomeric form by lowering the concentration of the perylene diimide or by increasing the temperature.[124, 127] Temperature dependent UV/Vis spectra of anionic perylene diimide **55**$^-$ and 2nd generation dendron-solubilised perylene diimide [**55**·**51**] are shown in **Figure 4-35**.[i] On the left, the characteristic spectrum of aggregated anionic diimide **55**$^-$ with a λ_{max} at 500 nm is shown. The characteristic maximum at 500 nm has frequently been reported in the literature for aggregated perylene diimides in organic and as well in aqueous solvents. These aggregates are bound by weak aromatic interactions, thus they increasingly dissociate at elevated temperatures. Thereby the UV/Vis absorption changes to show the well-known electronic absorption of monomeric perylene diimide with a λ_{max} at 530 nm. On the right side of **Figure 4-35**, the temperature-dependent spectra of the 2nd generation dendron-solubilised perylene diimide [**55**·**51**] at pH 6–7 is reproduced, showing the vibronic fine structure characteristic for monomeric perylene diimides.[127, 128] An unexpected observation is the hypochromic change of the spectrum on increasing the temperature.

For a better understanding of these results a comparison to similar systems described in literature will be discussed and subsequently more detailed investigations of the aggregated anionic perylene diimide **55**$^-$ and dendron-solubilised perylene diimides are presented.

[i] The temperature-dependent measurements were all repeated twice. After the first heating and cooling the initial and final absorption spectra at 25 °C were slightly different in shape. This was ascribed to a tempering effect due to the supramolecular nature of the systems. The spectra displayed in **Figure 4-35** are those recorded after tempering, thus as expected, the UV absorption at 25 °C for the initial and final stage are identical.

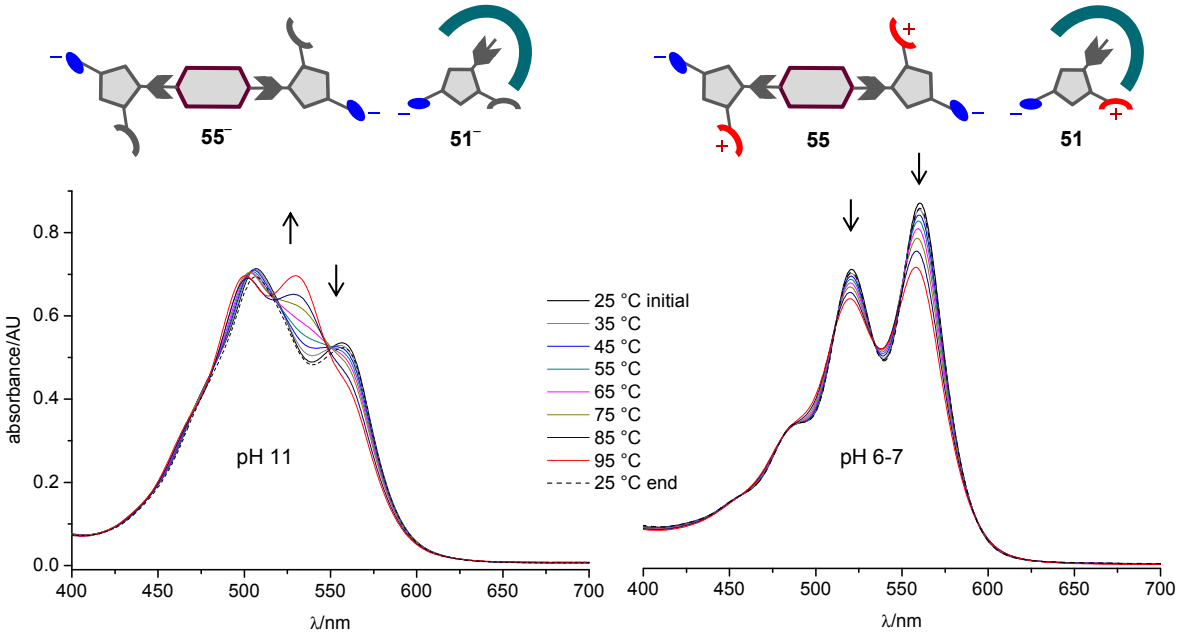

Figure 4-35: Temperature-dependent UV/Vis spectra starting at 25 °C and heating in 10 °C intervals to 95 °C; **Left**: Aqueous solutions of perylene diimide **55** (0.1 mM), sodium hydroxide (4 mM) filtered through a 0.45 µm PTFE syringe filter at pH 11; **Right**: Aqueous solutions of perylene diimide **55** (0.1 mM), sodium hydroxide (0.4 mM) and 2nd generation dendron **51** (0.4 mM) filtered through a 0.45 µm PTFE syringe filter after pH was adjusted with 1 N HCl to pH 6–7.

FORD investigated the aggregation process of perylene diimide dicarboxylate **60** (**Figure 4-36**)[128] by means of concentration dependent UV/Vis measurements.[i] At high concentrations, the absorption maximum for aggregated perylene **60** was observed at 500 nm, in good agreement with the above noted maximum at 507 nm of **55**⁻ at 25 °C. With decreasing concentration, favouring the dissociation into monomeric dye **60**, the shape of the spectrum changes with a new maximum appearing near 532 nm, again in good agreement with the maximum at 530 nm of **55**⁻ recorded at 95 °C. The extinction coefficient ε of the 0–0 vibronic transition of monomeric perylene compounds is in the range of 75 000 to 85 000 $M^{-1} \cdot cm^{-1}$. The vibronic fine structure of the S_0–S_1 transition has been used in the literature as an indicator for the presence of monomeric perylene diimide entities in solution. For entirely monomeric perylene diimides, the ratio of 2nd vibronic (0–1) transition to the 1st vibronic (0–0) transition is generally found in the literature to be close to 0.63, as depicted in **Figure 4-36**, right.[129] If this ratio increases above 0.63, dimeric and possibly higher aggregates of perylene diimide are co-existent with the monomeric ones.

[i] An recommendable article describing the use of temperature and concentration depending measurements to distinguish isodesmic from cooperative supramolecular polymerisation is published by MEIJER *et al.*.[121]

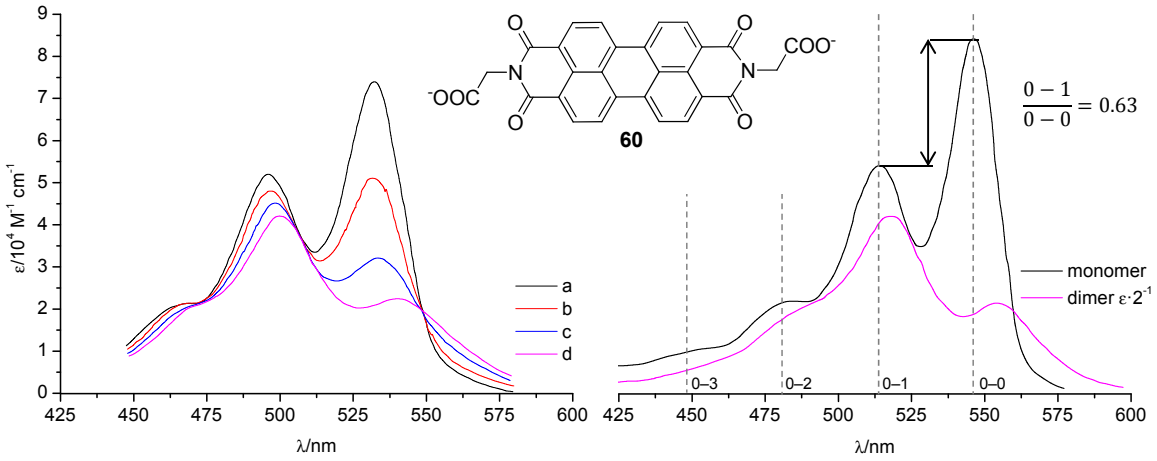

Figure 4-36: **Left**: Electronic absorption spectra of solutions of **60** and NaOH (10^{-3} M) in H_2O at 24 °C; a: $8.7 \cdot 10^{-9}$ M path length 9.93 cm; b: $1.1 \cdot 10^{-7}$ M path length 9.93 cm; c: $8.2 \cdot 10^{-7}$ M path length 9.93 cm; d: $2.4 \cdot 10^{-5}$ M path length 1.00 cm; **Right**: Extrapolated absorption spectra of the monomer and dimer of **60** in H_2O and NaOH (10^{-3} M). The extinction coefficient of the dimer is given per monomer component. Schematic illustration depicted according to reference **128** (Ford W. E., "Photochemistry of 3,4,9,10-Perylenetetracarboxylic Dianhydride Dyes", *J. Photochem.*, **1987**, *37*, 189–204.).

In the majority of the literature examples the absorption maxima of the monomeric perylene diimide derivatives are reported to be close to 530 nm. This is in good agreement with the maximum of the anionic perylene diimide **55**$^-$ found here (**Figure 4-35**) at elevated temperatures, even though at 95 °C complete disaggregation of the A-PDI has not yet been achieved.[i]

The solubilisation of perylene derivatives in organic solvents was often realised by covalently linked solubilising groups at the perylene core or at the imide positions. However, examples for water-soluble perylene systems are rare in the literature. One example was published very recently by the research groups of HAAG and WÜRTHNER,[127] who covalently attached the 1st to 3rd generation polyglycerol dendrons that are also used in the present thesis to the imide positions, as shown in **Figure 4-37**. At low concentrations the typical UV/Vis spectra for monomeric perylene diimides with an absorption maximum at 534 nm were detected. For the 1st and 2nd generation dendrons, a strong aggregation *via* π-stacking occurred at higher concentrations, as evident from the appearance of an absorption maximum at 501 nm. In marked contrast, for the 3rd generation PDI no spectral changes could be detected over the entire concentration range. These observations can straightforwardly be explained by the degree of shielding of the perylene chromophore by the dendritic side chains, that is, the 1st and 2nd generation dendrons extend in the plane of the perylene diimide unit and cannot

[i] Dilution experiments by addition of ethanol provided the absorption spectrum of the monomer. This experiment is presented on page 89.

effectively shield the π-face of the chromophore. In case of the 3rd generation PDI backfolding of the long dendritic side chains causes effective shielding of the π-faces.[i]

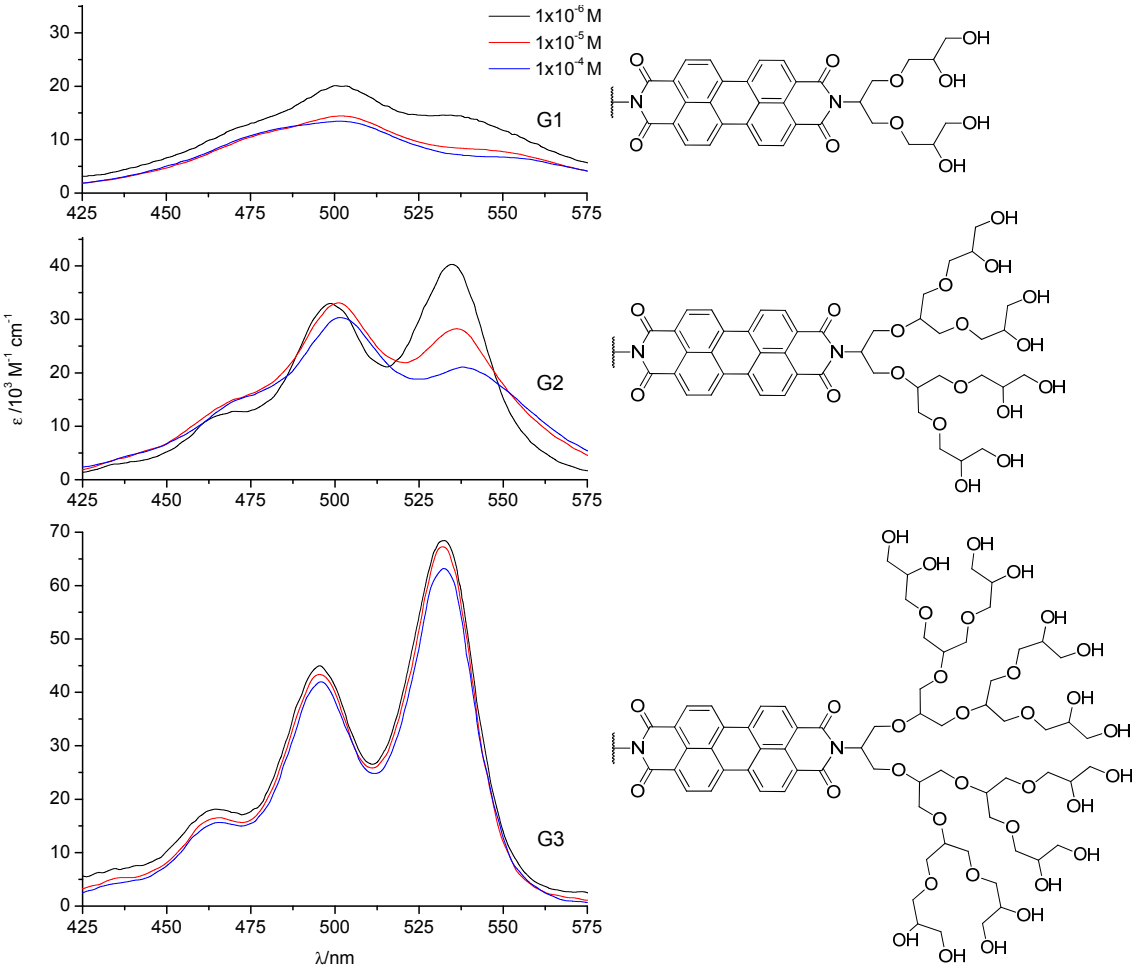

Figure 4-37: **Left**: UV/Vis spectra of aqueous solutions of 1st (top), 2nd (middle) to 3rd (bottom) generation PDIs in the concentration range 10^{-4} to 10^{-6} M at 25 °C; **Right**: Structures of symmetric 1st to 3rd generation PDIs. Schematic illustration depicted according to reference **127** (Heek T., Fasting C., Rest C., Zhang X., Würthner F., Haag R., "Highly fluorescent water-soluble polyglycerol-dendronized perylene bisimide dyes", *Chem. Comm.*, **2010**, *46*, 1884–1886.).

In analogy to the foregoing system, the spectral changes observed here for the dendron-solubilised perylene diimide **[55·51]** and the anionic perylene diimide **55**$^-$ (**Figure 4-34** and **Figure 4-35**) can be explained by help of molecular modelled structures, as shown in **Figure 4-38**. As displayed on the left, the 2nd generation dendron-solubilised perylene diimide **[55·(51)$_2$]** is predicted to form sandwich-type structure, enclosing the perylene component between the dimer of the pyrrole binding sites. The pyrrole fragment itself is shielded by the 2nd generation dendron wedges. This arrangement is believed to inhibit the typical aggregation

[i] This is visualised by the AM1 modelled structures structure of the 1st to 3rd generation PDI as depicted in the electronic supplementary information of reference 127.

process of apolar molecules in water predominantly forced by the hydrophobic effect. The anionic perylene diimide **55**$^-$ shown on the right of **Figure 4-38**, has a sterically unhindered π-face, which enables an effective π-stacking that leads to aggregated structures as deduced from the absorption spectrum. The observations made for the deprotonated system **55**$^-$, namely, an absorption maximum at 500 nm for the aggregated anionic perylene diimide **55**$^-$ and a maximum at 530 nm for monomeric anionic perylene diimide **55**$^-$ are in agreement with literature data. The thermodynamics of the aggregation processes of the anionic perylene diimide will be discussed in more detail before further investigations on the dendron-solubilised perylene diimides are described.

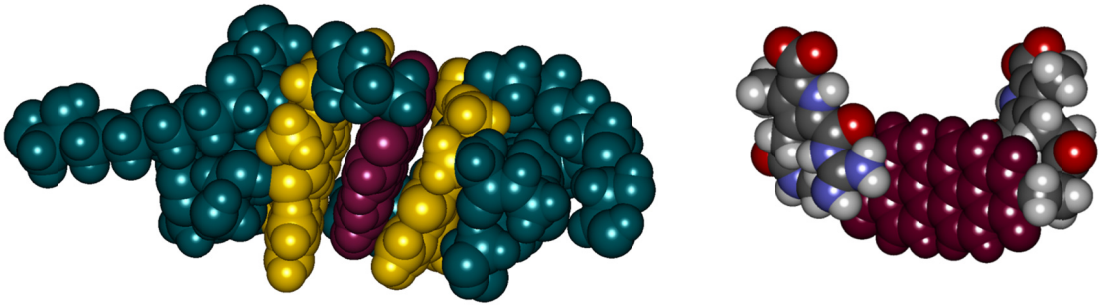

Figure 4-38: Molecular modelling with the OPLS 2005 force field in water; **Left**: Predicted structure of a 1:2 complex of zwitterionic perylene diimide and 2nd generation zwitterionic dendron [**55**·(**51**)$_2$]; **Right**: Anionic perylene diimide **55**$^-$.

Anionic Perylene Diimide

To acquire information on the size and the number of stacked perylene cores it is necessary to know the unperturbed absorption spectra of the fully aggregated and the monomeric perylene diimide **55**. Due to the fact that in 0.01 mM solutions at 95 °C the anionic perylene diimide **55**$^-$ exists still partly aggregated, it was attempted to enhance the disaggregation process by the addition of ethanol. Because the apolar π-faces of perylene diimide **55**$^-$ can reasonably be assumed to have the highest tendency to form π-stacks in water, a decrease of the polarity by addition of ethanol was expected to reduce the aggregation tendency of the PDIs.[Fehler! Textmarke nicht definiert.] In **Figure 4-39**, the results of a dilution and temperature variation experiment with ethanol are displayed, revealing that with increasing amounts of added ethanol, the absorption maximum of the monomer at 530 nm increases, similar to the temperature-dependent measurements discussed before. However, even at a concentration of **55**$^-$ as low as $6.67 \cdot 10^{-6}$ M and in the presence of 67 % ethanol the shape of the spectrum still indicates the presence of aggregates. An absorption spectrum attributed to essentially complete dissociation of the aggregates into monomeric **55**$^-$ was recorded after heating the solution to 95 °C. In this

spectrum the ratio of the 2nd and 1st vibronic transition amounted to 0.80. As discussed before, a ratio of 0.63 is commonly observed for entirely monomeric PDIs. Differently to the perylene derivatives investigated in the literature, in **55**$^-$ as well as in the dendron-solubilised perylene diimids an intramolecular stacking of the pyrrole binding site is still possible even in the monomer. Such a stacking could be responsible for the difference to the ratio of the vibronic bands compared to previous studies. A further difference is also observed for the intensity of the 1st vibronic band, which has uniformly been reported to be in the range of 75 000 to 85 000 $M^{-1}\cdot cm^{-1}$, whereas the values observed here are between 30 000 and 35 000 $M^{-1}\cdot cm^{-1}$. This reduction of the transition probability may also be related to the interaction of the perylene chromophore with the pyrrole binding site and will be discussed by means of quantum-chemically calculated absorption spectra below (p. 94–95).

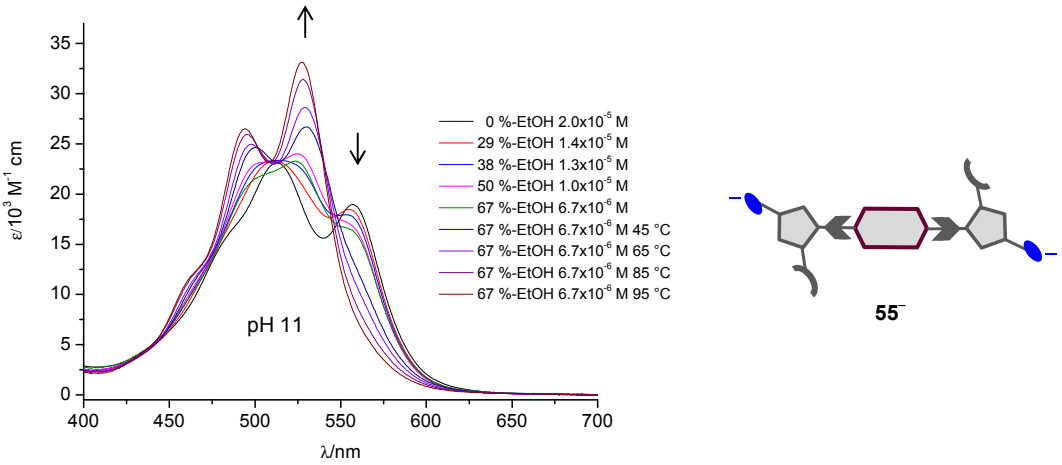

Figure 4-39: UV/Vis monitoring of dilution of a solution of anionic perylene diimide **55**$^-$ (0.02 mM), sodium hydroxide (0.8 mM in 500 µl H_2O; pH 11.4) with ethanol (100 µl each spectra).

Successive dilution of a $2.00\cdot10^{-5}$ M aqueous solution of **55**$^-$ with water did not lead to general change of the shape of the absorption spectrum, indicating that the anionic perylene diimide has at a concentration of $6.67\cdot10^{-6}$ M still the same aggregation degree as in case of a $2.00\cdot10^{-5}$ M solution. Thus, the experiment described below was performed on the assumption of a polymerisation degree = 100% (α = 1) for a $6.67\cdot10^{-6}$ M solution. As described by MEYER *et al.*,[121] the average stack length DP_N of aggregates can be calculated by measuring the absorbance change at a fixed wavelength in a temperature variation experiment. In **Figure 4-40** the temperature dependence of the polymerisation degree α and the derived average stack length DP_N are shown in the left and the right graphs, respectively. The polymerisation degree α was measured by heating the anionic perylene diimide **55**$^-$ in steps of 2 K per minute and reading the absorbance at 527 nm. The absorbance of the ethanol-diluted solution at 95 °C

(**Figure** 4-39) was taken as a first approximation for that of monomeric perylene **55**$^-$ (α = 0). For aggregated **55**$^-$ a lower limit of the stack length of about 35 molecules was estimated for a temperature of 30 °C (**Figure** 4-40, right). At 95 °C still dimers of the anionic perylene diimide **55**$^-$ seems to exist because a stack length of 2 was extrapolated. Thus perylene **55**$^-$ exhibits a much stronger stacking behaviour than PDI compound **60**, for which the highest observed aggregates were dimers.

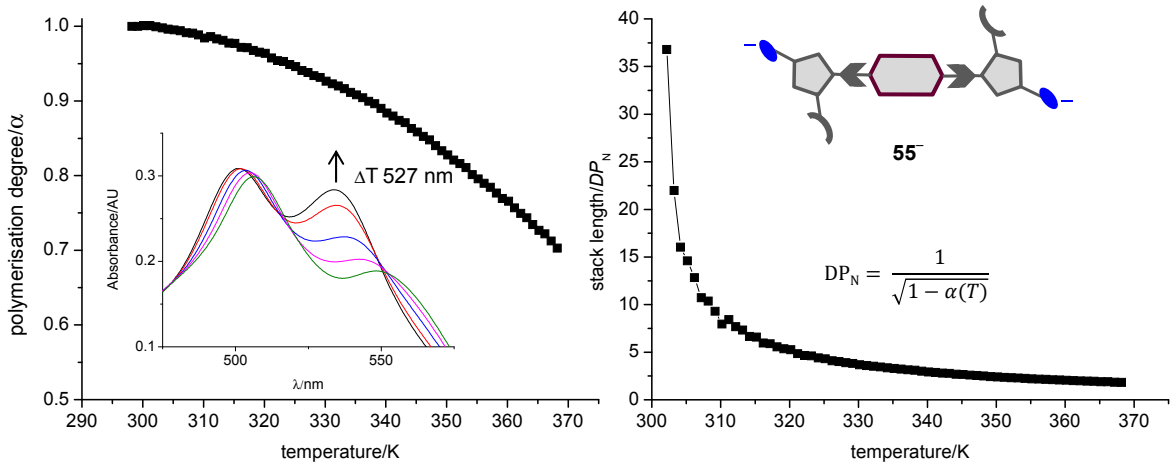

Figure 4-40: **Left**: Temperature-dependence of the polymerisation (aggregation) degree α of anionic perylene diimide **55**$^-$ ($6.67 \cdot 10^{-6}$ M) in water determined from the UV/Vis absorption at 527 nm. The value α = 0 was estimated from a 67 % ethanolic solution of anionic perylene diimide **55**$^-$ ($6.67 \cdot 10^{-6}$ M); **Right**: Number-average degree of polymerisation DP_N, as a function of temperature.

To gain further insight in the morphology of these particles, Atomic Force Microscopy (AFM)[130] measurements were performed. AFM is a scanning technique based on the measurement of ultra-small forces (< 1 nN) between the AFM tip and the sample. There exist different modes (static, dynamic) to measure sample surfaces. For soft surfaces like organic molecules on MICA the AFM can be operated in the tapping mode (intermittent contact mode). In this mode the cantilever/tip vibrates sinusoidally and the oscillating tip slightly taps the soft surface.[i] The contact of the tip with the surface is recognised by a laser beam reflected from the cantilever/tip as shown in **Figure** 4-41. By this technique very high resolution three dimensional images of sample surfaces can be produced.

[i] This is done to minimise forces between the tip and the soft surface to avoid structural changes of the surface.

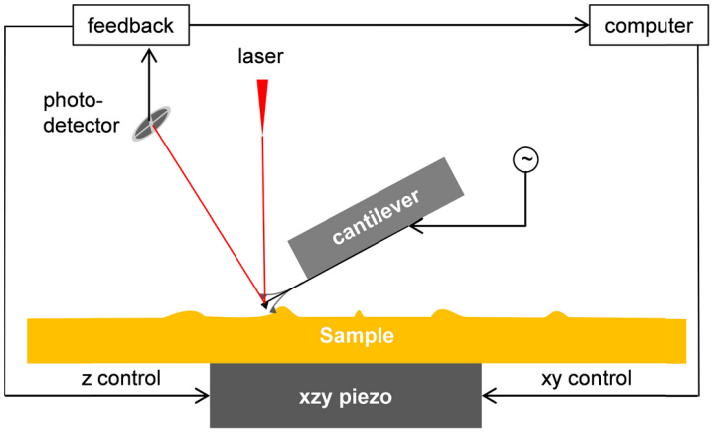

Figure 4-41: Schematic illustration of tapping mode according to literature 130.

The AFM measurements of anionic perylene diimide **55**$^-$ indicated the presence of particles of predominantly two different sizes. The larger ones were 485 nm in diameter and 65 nm in height, the smaller ones were in the range of 265 nm in diameter and 85 nm in height, as displayed in **Figure** 4-42, left. The large particles are actually agglomerates of smaller particles of a diameter of about 30 nm, as can be deduced from the phase image shown in grey. On the MICA surface the small particles were observed sporadically as individual particles. To a first approximation, the shape of the agglomerates observed on the MICA surface are flattened spheres, thus, particles of diameters of about 285 nm, 180 nm, and 16 nm can be estimated to exist in solution.[i] The 16 nm particles are estimated to be composed of circa 15 individual perylene diimide units because 2 monomers of **55**$^-$ fit in a sphere of 2.2 nm. This is in agreement with the calculated degree of polymerisation as shown in **Figure** 4-40.

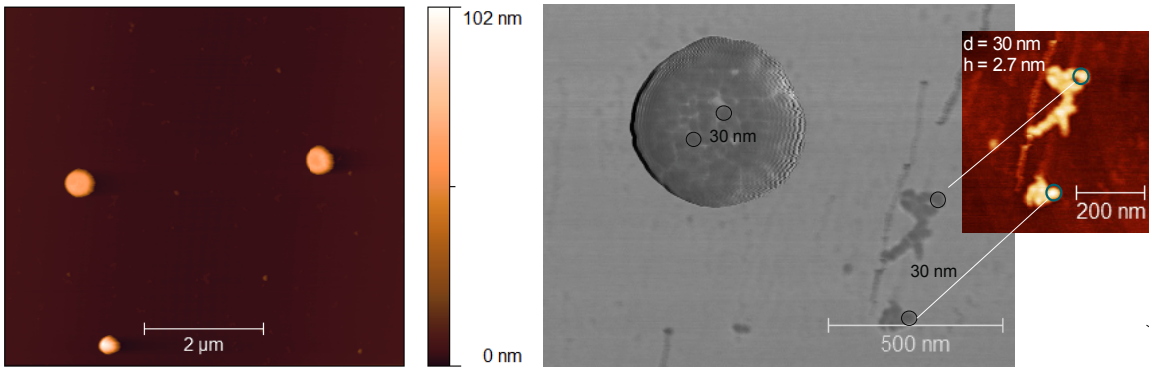

Figure 4-42: AFM images of aggregates of **55**$^-$; **Left**: Scan of 0.02 mM solution of **55**$^-$, spin coated on MICA showing aggregates of three different sizes: 485 nm·65 nm; 265 nm·85 nm; 30 nm·2.7 nm – very weak, (diameter·height); **Right**: Phase image (in grey) shows that bigger aggregates are mainly composed of particles with 30 nm diameter.

[i] It was estimated that the flattened particle on MICA is spherical in solution. The size of the particle in solution was estimated by an increase in height together with the same amount of nm decrease in diameter until height and diameter are identical: 285 nm can be calculated as follows: 485 nm diameter – 200 nm = 285 nm and 85 nm height + 200 nm = 285 nm.

DLS measurements of a 0.02 mM solution **55**$^-$ revealed mainly particles of an average diameter of 255 nm diameter (**Figure 4-43**), which agrees very well with the 285 nm observed for the larger particles from the AFM measurements. In addition to the larger particles also smaller ones, in the range of 90–164 nm, were detected. The related data from the UV/Vis, AFM, and DLS measurements are all of the same magnitude. Formation of these large agglomerates is inhibited by the addition of 2nd generation zwitterionic dendron **51**, as outlined above. In the following, further properties of the dendron-solubilised perylene diimide are given.

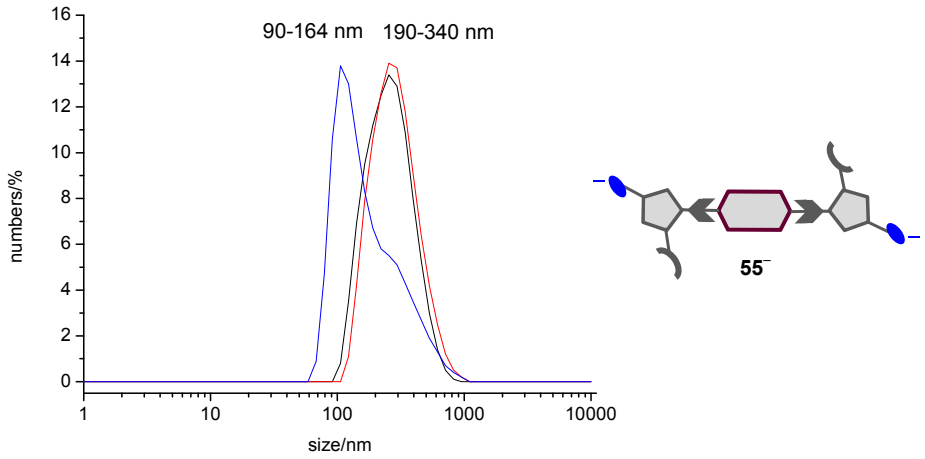

Figure 4-43: Three individual DLS measurements of a 0.02 mM solution of anionic perylene diimide **55**$^-$ in water at pH 11.4; Two of the three measurements with 60 % of all particles of 190–340 nm, diameter are shown in **black** and red; the **blue** trace represents a measurement indicating 45 % of the particles having diameters in the range of 90–164 nm.

Dendron-Solubilised Perylene Diimide

In contrast to the anionic perylene diimide **55**$^-$ exhibiting a degree of high polymerisation, UV/Vis measurements indicate that the dendron-solubilised perylene diimides exist as monomeric entities under similar conditions. Initial molecular modelling calculations suggest that the perylene diimide units may be complexed in a sandwich-like manner between the dimer of the pyrrole binding sites (**Figure 4-38**). The temperature-dependent UV/Vis measurements of dendron-solubilised perylene diimide show two characteristic features (**Figure 4-35** right, p. 85). First, although the shape of the absorption spectrum is as expected, showing the well-known vibronic fine structure for a monomeric perylene diimide chromophore, i.e. an unusual bathochromic shift of circa 30 nm of the whole spectra compared to those reported in the literature is observed. Second, the absorption bands show a pronounced hypochromic shift at elevated temperatures. This hypochromic effect will be discussed first.

A small hypochromic change of absorption bands would easily be explained by the temperature dependence of the density of water. At the present conditions, this would cause only a small increase of the volume by about 3.7 % as calculated from the density change of

water at 25 °C compared to 95 °C. This should result in an identical reduction of the absorbances. However, the observed decrease in intensity amounts to 17 % and 9 % at 560 and 520 nm, respectively. In addition, the maximum at 560 nm shows a small hypsochromic shift of about 2 nm. These observations are tentatively attributed to a higher mobility of the dendron wedges and partial breakup of the sandwich-like structure at higher temperatures. This reduces the shielding of the perylene core and may allow increased π–π-interactions with other perylene cores resulting in reduction of the monomer absorption[i]. Thus, the increase of temperature, which normally leads to a disaggregation of π-stacked chromophores, operates in the opposite direction in case of the present dendron-solubilised zwitterionic perylene diimide [**55**·**51**]. This explanation is in accord with observations made when ethanol was added to the aqueous solution of [**55**·**51**] (**Figure 4-44**). Addition of increasing amounts of ethanol led to virtually identical spectral changes as was monitored on elevating the temperature. Hence the more apolar solvent obviously leads to a less shielded perylene core, probably by a more expanded structure due to a better solubility of the glycerol branches of the dendron in ethanol. The foregoing observations clearly demonstrate that the monomeric nature of the supramolecular adducts [**55**·**51**] is strongly favoured by highly polar solvents.

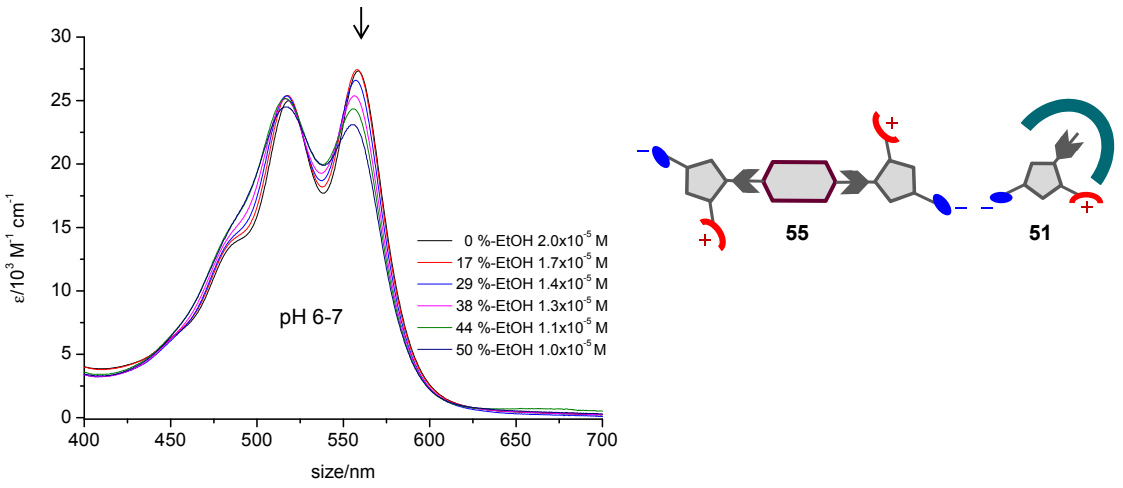

Figure 4-44: Solvent dilution experiment by the addition of ethanol (100 µl each) to perylene diimide **55** (0.02 mM) and 10 equivalents of 2nd generation dendron **51** in 500 µl H_2O at pH 6.5.

As follows, the observed bathochromic shift (**Figure 4-35**, **Figure 4-44**) of the UV/Vis absorption spectrum of dendron-solubilised perylene diimide [**55**·**51**] in regard to those reported in the literature for monomeric perylene diimides will be discussed. This discussion

[i] In the case of the anionic perylene diimide **55**$^-$ even at 95°C the absorption spectrum shows π-stacking.

also pertains to the spectroscopic changes of anionic perylene diimide **55**$^-$ at elevated temperature.

The pronounced bathochromic shift of the dendron-shielded complex certainly has to be related to interactions of the perylene chromophore with the zwitterionic binding site and/or the dendron wedges. As known from theoretical studies, the HOMOs and the LUMOs of perylene diimides have nodes at the imide nitrogens. As a consequence, the electronic coupling (electron delocalisation) between substituents at the imide positions and the aromatic perylene π-system is reduced.[121]

As expected the covalently attached glycerol dendrons at the diimide positions of the perylene moiety do not shift the absorption maximum in water from its parent value at 530 nm, as published by WÜRTHNER and HAAG.[127] Thus, the bathochromic shift is more likely to derive from an interaction of the pyrrole binding motif with the perylene core. Considering to the fact that the anionic perylene diimide **55**$^-$ does not show a related spectroscopic change, it must be concluded that the bathochromic shift is induced by interaction with the aromatic pyrrole system of the zwitterionic binding site.[i] Aromatic systems of opposite electron demand show a strong tendency to attract each other and to form stacked arrangements by alternating electron-poor and electron-rich aromatic molecules.[132, 133]

Such an electronic situation is assumed to be responsible for the observed spectroscopic shift. In order to check whether this would be supported by theory, a 1:2 complex of the perylene diimide and two zwitterionic pyrrole dendrons [**55**·(**51**)$_2$] was computed by molecular mechanics force-field, as shown in **Figure 4-38** above. Using the optimised structure from the molecular mechanics calculation, the electronic excitation energies of [**55**·(**51**)$_2$] as well as the isolated perylene diimide **55** were calculated by time-dependent density functional theory (TD-DFT) on the B3LYP/6-31G(d,p) level of theory. As seen in **Figure 4-45**, the maximum is shifted from 494 nm for the uncomplexed perylene diimide **55** to 527 nm for the one forming a stack by attaching the pyrrole binding motif to both sides.[ii]

The numerical correspondence of the calculated shift (33 nm) with the experimentally observed one (30 nm) should be considered rather fortuitous, but nevertheless clearly confirms the bathochromic shift observed for the dendron-solubilised perylene diimide [**55**·**51**].[iii]

---

[i] A similar bathochromic shift was also observed by WAGENKNECHT et al. with DNA incorporated perylene diimides.[131]

[ii] The complex was calculated in the gas phase because in water the calculations for stacked systems in aqueous environment are highly time consuming. In water the maximum for perylene diimide monomer was calculated to be at 515 nm.

[iii] As already noted above, the extinction coefficient of the 0–0 vibronic transition of monomeric perylene compounds has uniformly been reported to be in the range of 75 000 to 85 000 $M^{-1}\cdot cm^{-1}$, whereas the extinction coefficient of the dendron-solubilised perylene diimides presented here are between 30 000 and 35 000 $M^{-1}\cdot cm^{-1}$. A decrease of the same order of magnitude was calculated for the pyrrole dimer enclosed PDI compared to the monomeric PDI shown in Figure 4 45. Since the 1st vibrational transition of the perylene diimide is influenced strongly by stacked arrangements it is possible that extinction coefficient of the present monomeric PDI is influenced by the pyrrole binding motif.

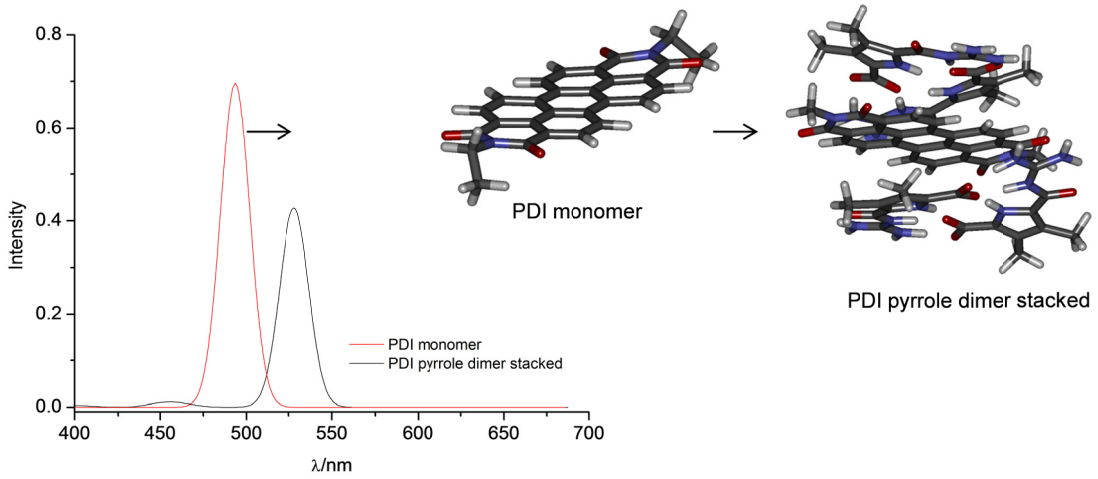

Figure 4-45: TD-DFT-calculated absorption maxima of PDI monomer (red trace) and pyrrole dimer stacked complex (black trace) in the gas phase. Electronic excitation energies calculated on the B3LYP/6-31G(d,p) level on the OPLS2005 force-field optimised structure.[134]

The bathochromic shift was also observed in a pH titration experiment with zwitterionic perylene diimide **55** having no dendron side chains. To draw further conclusions in regard to relate the bathochromic shift to possible structures of the perylene diimide **55** a further experiment will be discussed. Temperature-dependent UV/Vis measurements of the anionic perylene diimide $\mathbf{55}^-$ at pH 11 and of the zwitterionic perylene diimide **55** at pH 6 are compared in **Figure** 4-46. As expected, the zwitterionic system shows only small changes in the UV/Vis absorptions, indicating more stable aggregates than in the anionic case. Almost no significant change to monomeric perylene diimide was observed at 95 °C for the zwitterionic system.

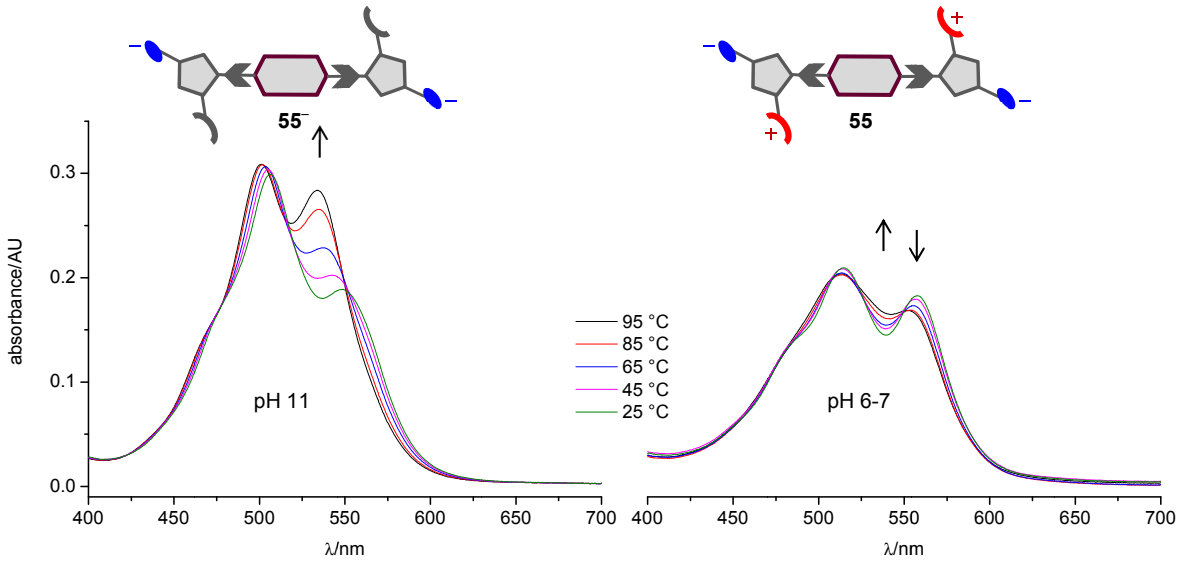

Figure 4-46: Temperature-dependent UV/Vis measurement; **Left**: Perylene diimide **55** (0.01 mM) in sodium hydroxide solution (0.4 mM) at pH 11.4. **Right**: Perylene diimide **55** (0.01 mM), sodium hydroxide (0.4 mM) at pH 6.4, adjusted by addition of 0.1 N hydrochloric acid.

A plausible explanation for this observation are the strong interactions between the zwitterionic binding sites, forming stable perylene-stacked aggregates in water even at 95 °C. Derived from the fact that the zwitterionic perylene diimide **55** exhibits the same bathochromic shift as discussed before and that the calculations favour a perylene chromophore stacked between the pyrrole dimer, a ladder like structure as depicted in **Figure 4-47**, left, is suggested as a possible structure for the aggregates of Z-PDI **55**.[i] As mentioned before, all these aggregates are very sensitive with respect to, concentration, temperature, and the polarity of solvents. Unfortunately, since these zwitterionic aggregates are only soluble in the range of 0.01 mM and show only small changes in the temperature-dependent measurements, it was not possible to measure polymerisation degrees or to calculate stack lengths.

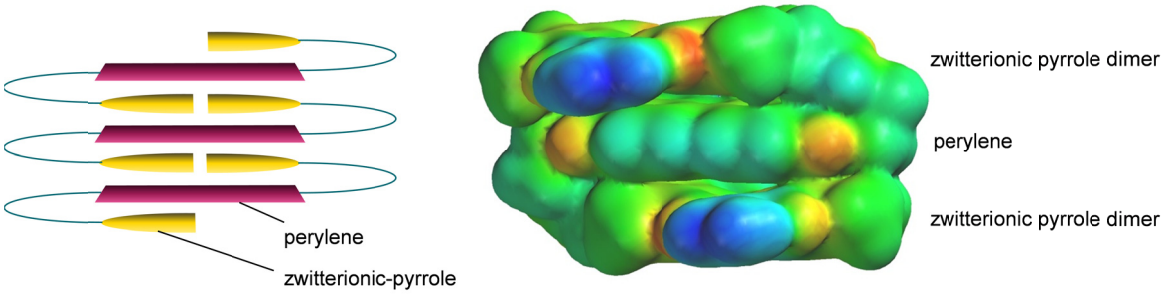

Figure 4-47: **Left**: Schematic illustration of the postulated ladder like structure of zwitterionic perylene diimide **55**; **Right**: Electron densities (AM1) of the ladder-like structure.

1st and 3rd Generation Dendron-Solubilised Perylene Diimides

The above discussed effects for 2nd generation DS-PDIs [**55**·**51**] were as well observed in the UV/Vis spectra of 1st and 3rd generation DS-PDIs [**55**·**50**] and [**55**·**52**] (**Figure 4-48**). The spectra show a well-resolved vibronic fine structure with maxima at 560 nm, characteristic for monomeric perylene diimides. The temperature-dependence of the UV/Vis spectra indicated a somewhat different stability of the 1st and 3rd generation hetero associates compared to the 2nd generation PDI [**55**·**51**]. As can be seen on the left side, the 1st generation assembly [**55**·**50**] was not stable over the whole temperature range. At 95°C a jump in the UV/Vis absorbance was observed,[ii] indicating that at this temperature the 1st and the 3rd generation supramolecular complexes start to disassemble causing the perylene diimide to precipitate. (Photographs of the cuvettes are reproduced in the center of **Figure 4-48** from which the precipitation of the perylene diimide is apparent.) In case of the 3rd generation dendron-solubilised perylene diimide [**55**·**52**] no discrete temperature range was observed for the disassembly process.

[i] Beside the ladder liker structure built up by intermolecular interactions of the zwitterionic binding site also an intramolecular dimer of the guanidiniocarbonyl pyrrole carboxylate is possible, forming dimers or oligomers by π-interactions. However, due to the small changes in the temperature measurements shown in **Figure 4-46**, indicating strong interactions, the postulated ladder like structure is more plausible.
[ii] As mentioned the temperature-dependent measurements were done twice with the same solution, due to a temper effect.

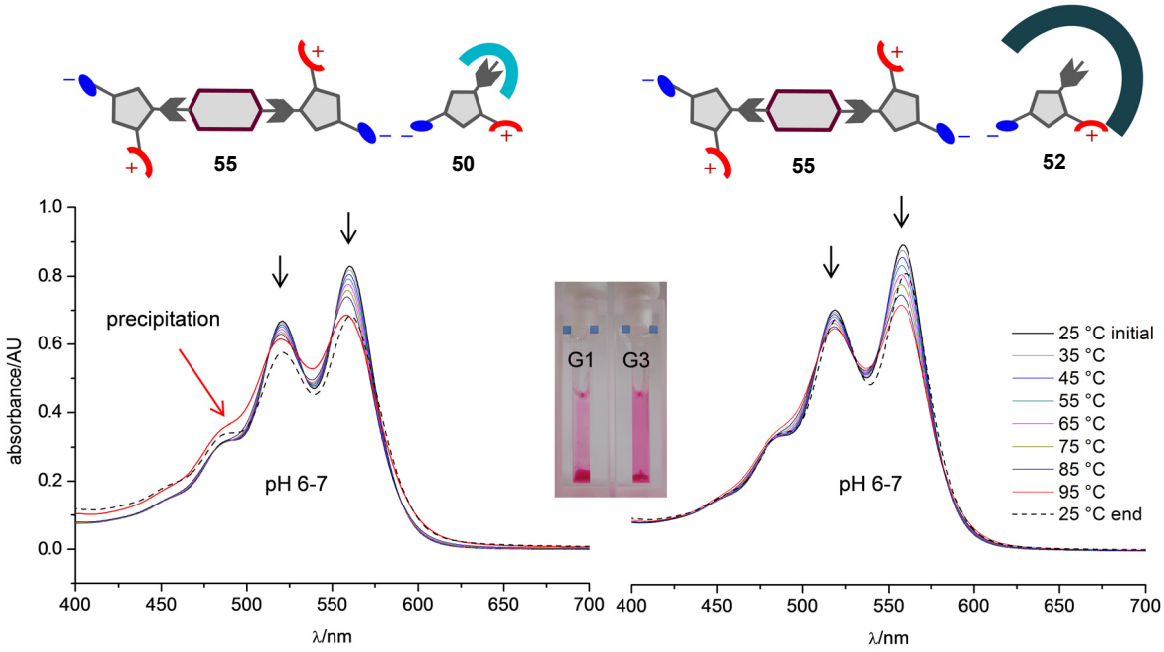

Figure 4-48: Temperature-dependent UV/Vis measurement starting at 25 °C and heating in 10 °C intervals to 95 °C; **Left:** Zwitterionic perylene diimide **55** (0.1 mM), sodium hydroxide (4 mM), 1st generation zwitterionic dendron **50** (0.4 mM), adjustment with hydrochloric acid to pH 6–7 and filtered through a 0.45 µm PTFE syringe filter; **Right:** Zwitterionic perylene diimide **55** (0.1 mM), sodium hydroxide (4 mM), 3rd generation zwitterionic dendron **52** (0.4 mM), adjustment with hydrochloric acid to pH 6–7 and filtered through a 0.45 µm PTFE syringe filter; **Middle**: Photographs of cuvettes from both runs to 95 °C.

Molecular modelling of the 1st and 3rd generation dendron-solubilised perylene diimides [**55**·(**50**)$_2$] and [**55**·(**52**)$_2$] predicts minimum structures that are similar to that of the 2nd generation one [**55**·(**51**)$_2$]. Again, the chromophore is enclosed between the guanidiniocarbonyl pyrrole carboxylate dimer, thereby hindering the self-aggregation process in pure water. The 2nd generation solubilised perylene diimide [**55**·(**51**)$_2$] appears to be the most stable hetero-complex, but also the 1st and 3rd are quite stable at elevated temperatures. The following measurements were performed in order to establish the solubilising potential of the three different generation dendrons.

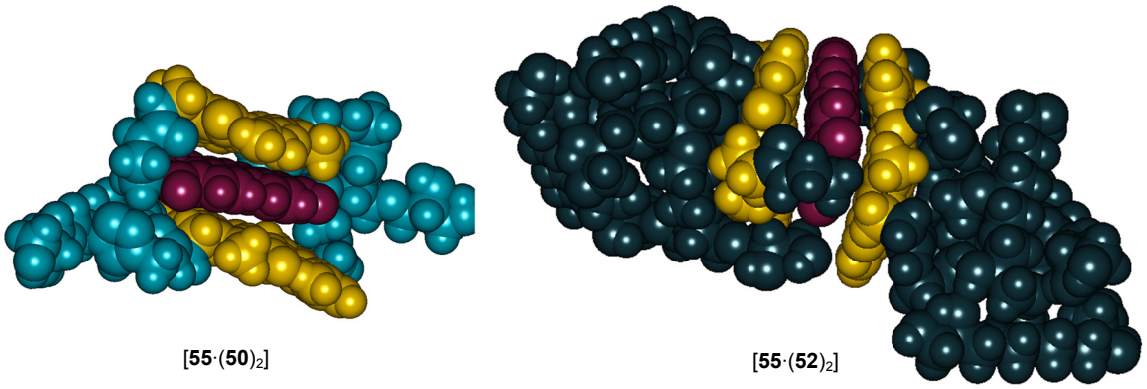

Figure 4-49: Molecular modelling with the OPLS 2005 force field in water. **Left**: Predicted 1:2 complex of zwitterionic perylene diimide and 1st generation dendron [**55**·(**50**)$_2$]. **Right**: Predicted 1:2 complex of Z-PDI and 3rd generation dendron [**55**·(**52**)$_2$].

To test how many equivalents of the dendron are necessary to obtain non-aggregated perylene diimides, varying equivalents of 2nd generation dendrons were added to a 0.01 mM solution of zwitterionic perylene diimide **55**. In **Figure 4-50** the absorption spectra recorded with 10, 5 and 3 equivalents of added **51** are typically for non-aggregated perylene diimides. The measurement with 2 equivalents of dendron **51** shows a less resolved vibronic fine structure and with only 1 equivalent of **51** the shape of the absorption spectrum is typically for aggregated perylenes diimide.

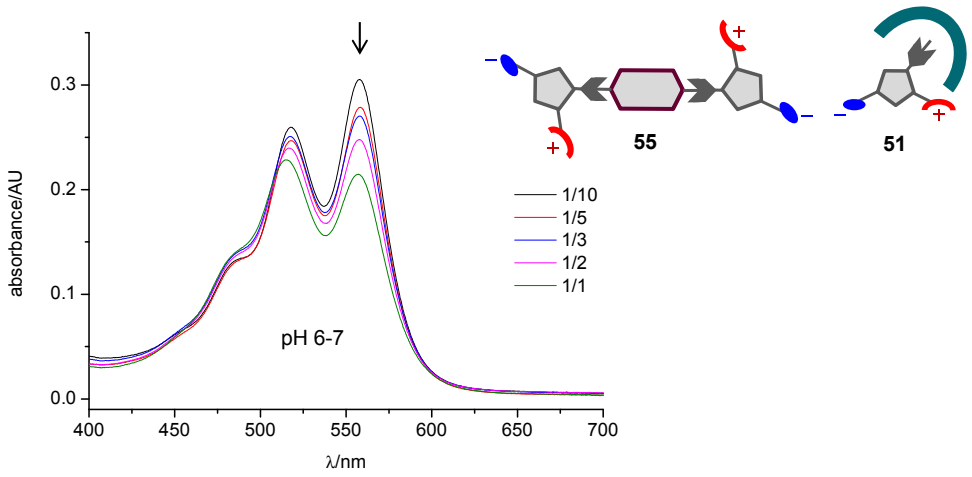

Figure 4-50: Solution of zwitterionic perylene diimide **55** 0.01 mM and sodium hydroxide 0.4 mM was treated with 10, 5, 3, 2, and 1 equivalents of 2nd generation dendron **51** before pH was set with hydrochloric acid to 6.4.

Figure 4-51 shows the result of a dilution experiment to generate a calibration line for the calculation of the maximal solubilisation of perylene diimide **55** by the 1st–3rd generation dendrons **50–52**.

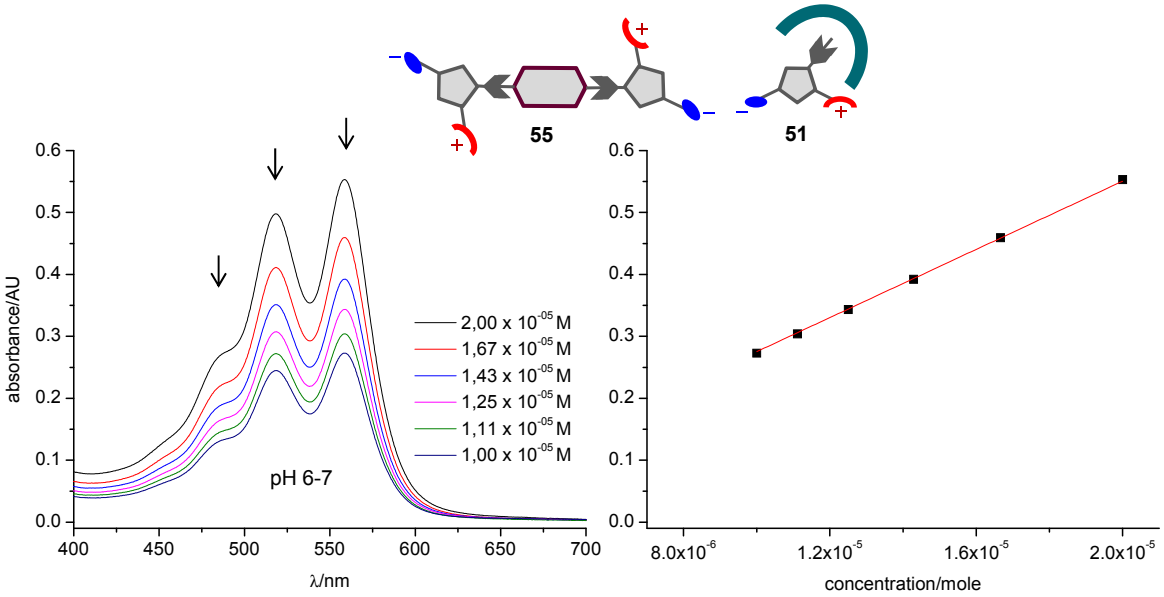

Figure 4-51: **Left**: Dilution experiment of perylene diimide **55** (0.02 mM) and 2nd generation dendron **51** (0.2 mM) in 500 µl H_2O by the addition of H_2O (100 µl each); **Right**: Calibration line from the dilution experiment: r^2 = 0.99998; y = 27529 ± 53. The calculation was based on the absorbance maximum at 559 nm.

The amount of solubilised perylene **55** obtained from the calibration lines are shown in **Table 4–5**. The values for dendrons **50**, **51**, and **52** are all in the same order of magnitude, so that they exhibit very similar solubilising properties, slightly favouring the 2nd generation dendron. The comparison between 10 and 4 equivalents of 2nd generation dendron **51** demonstrates that with 10 equivalents of 2nd generation dendron 48 % perylene diimide can be solubilised, with 4 equivalents 33 %.

Table 4–5: Calculated values of solubilised perylene diimide **55** by the addition of 1st to 3rd generation dendrons. A solution of 55^- ($1.00\ 10^{-4}$ M^{-1}) and 40 equivalents of sodium hydroxide were treated with different equivalents of dendrons **50–52**. The pH was adjusted to 6–7 by addition of hydrochloric acid and the mixture was filtered through a PTFE 0.45 µm syringe filter.

compound	dendron generation	concentration of PDI 55^- /M	equivalents of dendron	solubilised PDI 55/M
50	G1	$1.00\ 10^{-4}$	4	$2.99\ 10^{-5}$
51	G2	$1.00\ 10^{-4}$	4	$3.33\ 10^{-5}$
52	G3	$1.00\ 10^{-4}$	4	$3.26\ 10^{-5}$
51	G2	$1.00\ 10^{-4}$	10	$4.81\ 10^{-5}$

DLS Measurements

In AFM studies with 2nd generation dendron-solubilised perylene diimide {**55**·**51**} no agglomerates were observed, and additional DLS studies showed the presence of small particles. The calculated diameter of a discrete 1:2 hetero-complex {**55**·(**51**)$_2$} is 4 nm. In the DLS experiments particles of mainly 7.5 nm and 18 nm in diameter were observed, as shown in **Figure 4-52**.

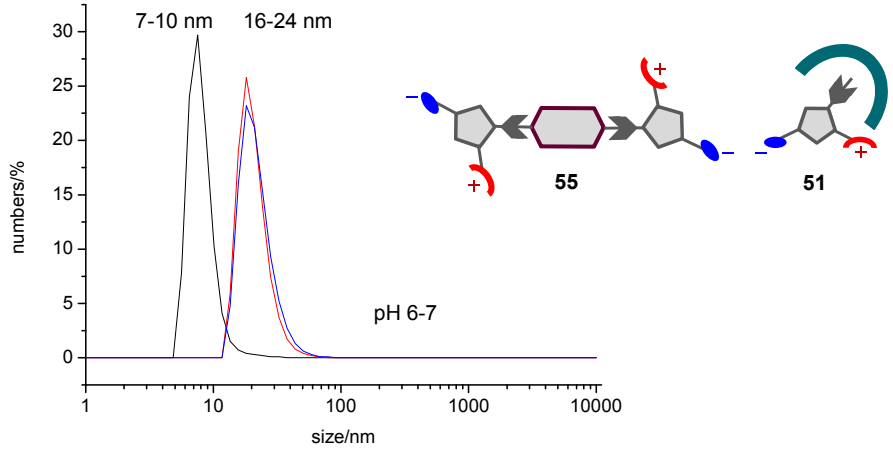

Figure 4-52: DLS measurement of perylene diimide **55** (0.02 mM), sodium hydroxide (0.8 mM) and 2nd generation dendron **51** (0.2 mM) in water, addition of hydrochloric acid to pH 6.5 and filtration through a 0.45 PTFE syringe filter; 3 individual measurements with 75–80 % particles in the range of 16–24 nm for **red** and **blue** curves; 85 % particles in the range of 7–10 nm for **black** curve.

As each supramolecular process can be described as coupled equilibrium reactions between the monomers and the supramolecular aggregates, the size and structure of the aggregates can strongly be affected by external factors like temperature, solvent polarity, or time. Because all experiments described in this thesis were performed in aqueous solution under which circumstances solvophobic effects play a crucial role, there is a strong tendency for self-aggregation. Molecular modelling studies indicate the polar 2nd generation dendron shield mainly the π-face of the guanidiniocarbonyl pyrrole carboxylate dimer. It therefore seems possible that oligomers as schematically displayed in **Figure 4-53** are formed with time, due to the fact that the possible 1:2 hetero-aggregates [**55**·(**51**)$_2$] are polar on the top and the bottom, respectively, through the hydroxyl groups of the dendron, whereas the side of the cylinder-shaped molecule is relatively apolar.

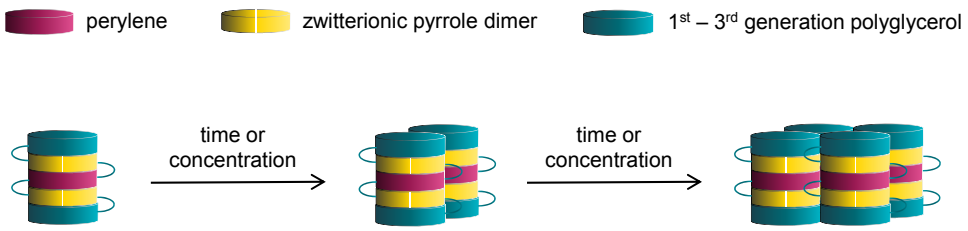

Figure 4-53: Possible aggregation behaviour of cylinder like 2nd generation solubilised zwitterionic perylene diimide [**55**·(**51**)$_2$]. Apolar faces attract in polar solvent.

As the solubilities of the foregoing systems are restricted to the low mM range, there are limitations for further experiments like cryo-EM or SANS to determine the exact sizes of the aggregates and to gain proof for the postulated 1:2 hetero-associates [**55**·(**51**)$_2$]. However, as the UV/Vis spectral characteristics for perylene diimides are well established, the UV/Vis spectra provide strong evidence for a high quantity of monomeric perylene diimide **55**, solubilised by pH-triggered zwitterionic 1st to 3rd generation dendrons **50**, **51**, and **52**. The most reasonable explanation for the experimental observations is the formation of a 1:2 hetero-associate with the perylene diimide enclosed between two zwitterionic pyrrole dimers. Quantum-chemically calculated excitation energies (absorption maxima) and pH effects underline the hypothesis of such a discrete supramolecular dendrimer. In conclusion, the principle to build such zwitterionic templated supramolecular dendrimers seems to work but due to the presence of non-orthogonal building blocks appears to be more complicated compared to the highly monodisperse homodimers discussed in **Chapter 4.3.1**.

5. Summary and Outlook

The present thesis is based on the idea to combine the principles of supramolecular chemistry and dendrimer chemistry. Therefore, individual, covalently bound dendrons were synthesised, which were expected to self-assemble in aqueous solution *via* non-covalent interactions to provide supramolecular dendrimers.

Self-assembly is based on reversible interactions, a property that would allow in favourable cases to control the conditions under which the dendrimers are formed or disaggregated. One aim of the present thesis was to trigger such aggregation processes by a binding site which exhibits acid-base properties, in order to induce the assembly and disassembly of the supramolecular dendrimer by changes of the pH value.

The synthesis concept entirely followed was the covalent combination of 1st to 3rd generation polyglycerols with a guanidiniocarbonyl pyrrole carboxylate binding site. The polyglycerol provides water solubility to the self-assembled aggregates, the zwitterionic pyrrole unit inherits efficient self-assembly in water, and is sensitive to pH changes (**Figure 5-1**).

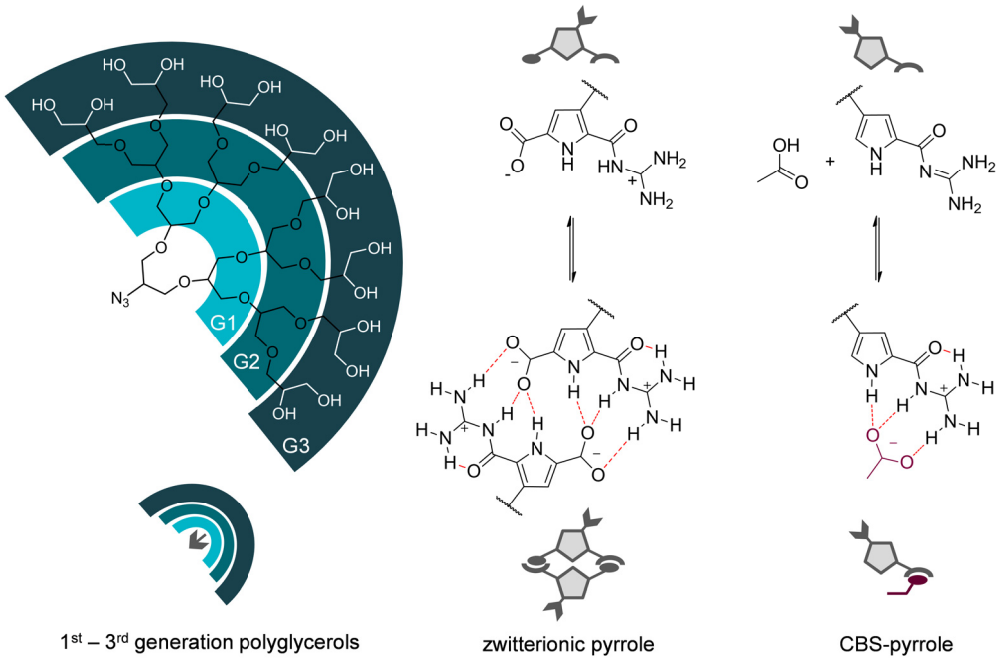

Figure 5-1: 1st–3rd polyglycerol dendrons and guanidiniocarbonyl pyrrole binding sites used in this thesis.

The covalent combination of the polyglycerols and guanidiniocarbonyl pyrroles lead to different dendron subunits, which were investigated for their self-assembly properties in the CBS-templated, zwitterionic untemplated, and the zwitterionic templated approach.

The aim of the present thesis was to investigate which of these self-assembly approaches is the most promising one and fulfils all of the following criteria:

- **formation of discrete** supramolecular dendrimers, which are
- **stable** and **soluble** in water for biological applications, and show
- **switchable** assembly and disassembly by pH changes

The different approaches are discussed in detail in **Section** 4 –Results and Discussion–; in the following the investigated self-assembly methods are briefly summarised, the CBS-templated dendrimer approach is presented first.

CBS Templated Supramolecular Dendrimers

The CBS-templated method is based on the concept to form supramolecular dendrimers by the self-assembly of a CBS-dendron with multitopic carboxylic- or phosphonic acid cores, as schematically illustrated in **Figure** 5-2.

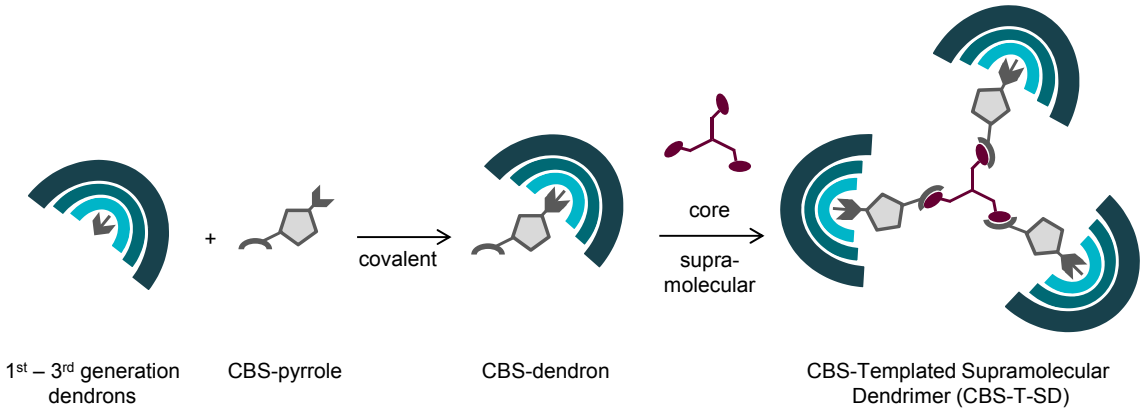

Figure 5-2: Schematic illustration of the CBS templated supramolecular dendrimer approach.

The cores used for the self-assembly process were TMA (4), EDTA (5), and NTMP (6). Due to unfavourable steric interactions or problems in the synthetic procedures for the CBS-dendrons, several strategies towards various polyglycerol substituted pyrroles were followed. The most promising CBS-dendron was the 2,4-substituted pyrrole 41 (**Figure** 5-3).

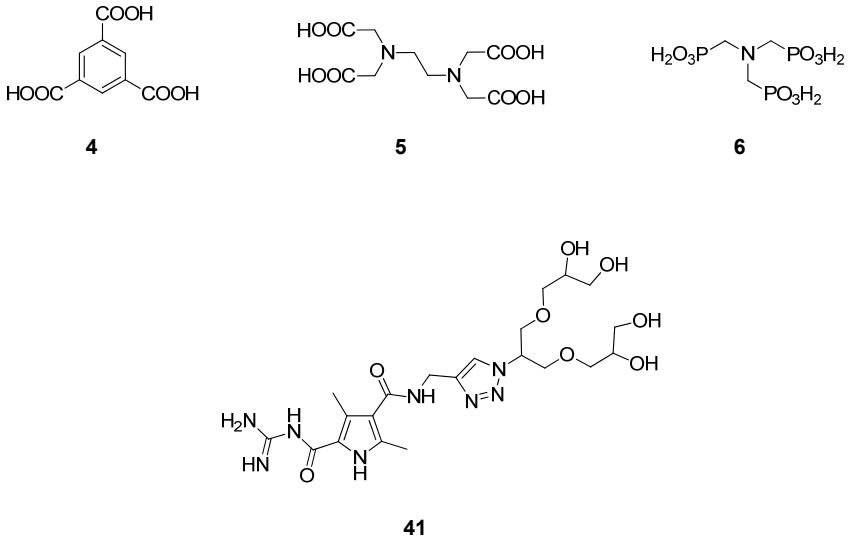

Figure 5-3: **Top**: Carboxylic- and phosphonic acid cores, (TMA, 4), EDTA (5), and NTMP (6).; **Bottom**: The 1st generation CBS-dendron 41 based on a 2,4-pyrrole substitution pattern.

The self-assembly experiments revealed that dendron 41 is obviously not able to self-assemble around the cores 4–6 to form discrete 3:1 or 4:1 hetero-complexes, respectively, in water. DLS experiments indicated that predominantly higher aggregates of dendron 41 were formed, independent of the employed core. It was observed that the protonation state of the CBS-dendron influences the size of the produced aggregates. The protonated dendron shows particles of diameters in the range of 122 to 164 nm, whereas the unprotonated dendron shows aggregates of a size of 255–342 nm (**Figure 5-4**).

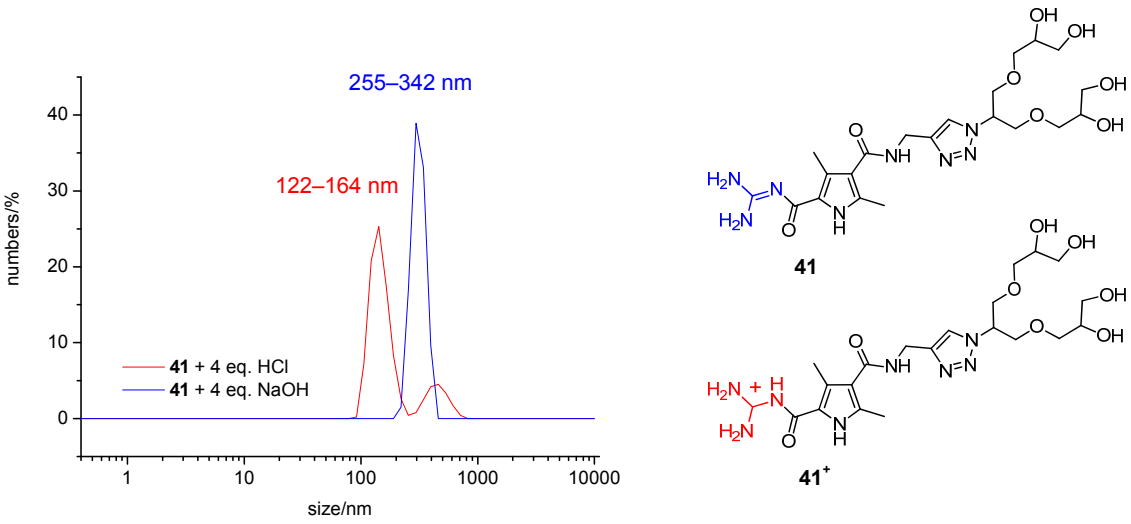

Figure 5-4: DLS experiments of unprotected 1st generation CBS-dendron 41 (5 mM) in water; **Red**: Addition of 4 equivalents HCl, **Blue**: Addition of 4 equivalents NaOH.

The CBS-dendron **41** has to be further investigated by AFM, DSL, cryo-EM, and SANS experiments to clarify what kind of structures these nano-aggregates have. Size and structure of the aggregates may probably be controlled by pH changes, as indicated by the initial DLS experiments. During the present thesis the CBS-T-SD approach was not further investigated, because the results obtained so far seemed unpromising in achieving distinct supramolecular dendrimers. The work was focused on the zwitterionic untemplated supramolecular dendrimer approach to achieve the above noted aims. The results, achieved with the ZU-SD, are most auspicious of all investigated systems, and will be briefly summarised in the following.

Zwitterionic Untemplated Supramolecular Dendrimers

In the present approach only one self-complementary building block has to be synthesised in order to obtain a supramolecular dendrimer based on a homo-dimer of zwitterionic-dendrons (**Figure 5-5**).

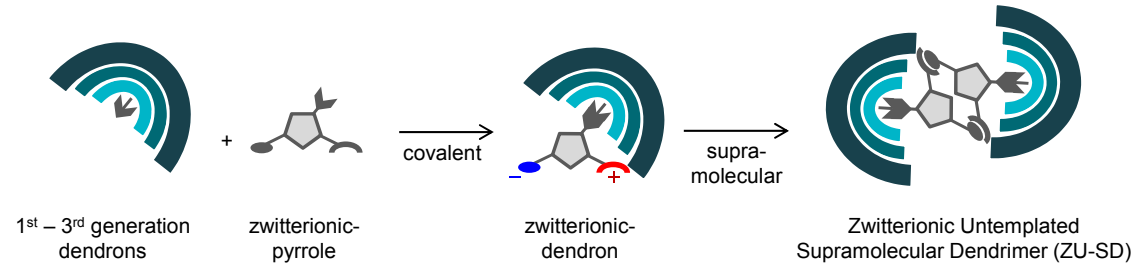

Figure 5-5: Schematic illustration of the zwitterionic untemplated supramolecular dendrimer approach.

The 1st to 3rd generation polyglycerol dendrons were attached *via* a click reaction to the propionic acid side chain in the β-position of the pyrrole. The prepared zwitterionic dendrons **50**–**52** are shown in **Figure 5-7**.

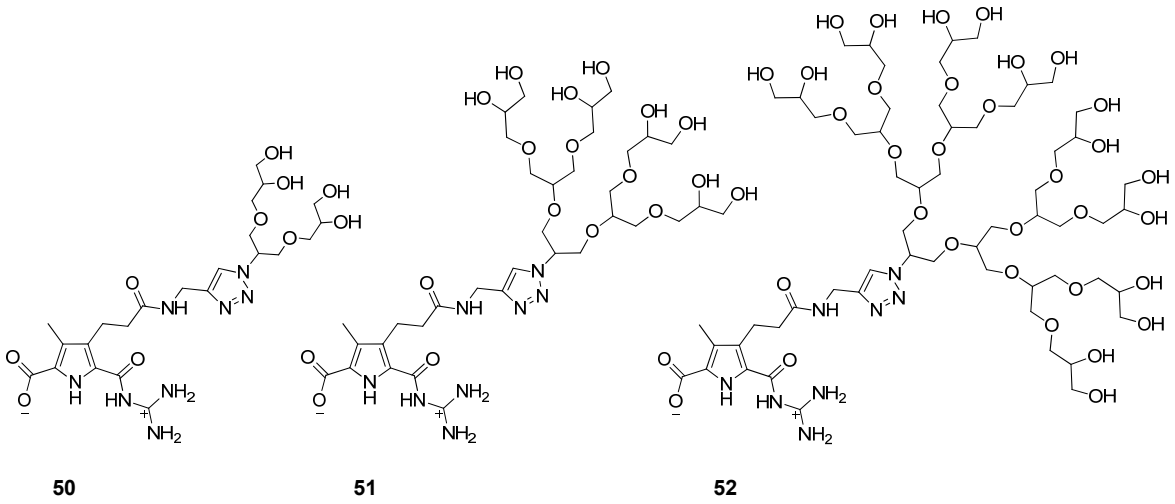

Figure 5-6: 1st to 3rd generation zwitterionic dendrons **50**–**52**.

By combination of various analytical methods, namely DOSY-NMR, DLS, cryo-EM, SEC, and ITC it was proven that all the zwitterionic dendrons show a strong tendency to dimerise to discrete 1:1 homo-associates with sizes in the low nanometre range (**Figure 5-7**).

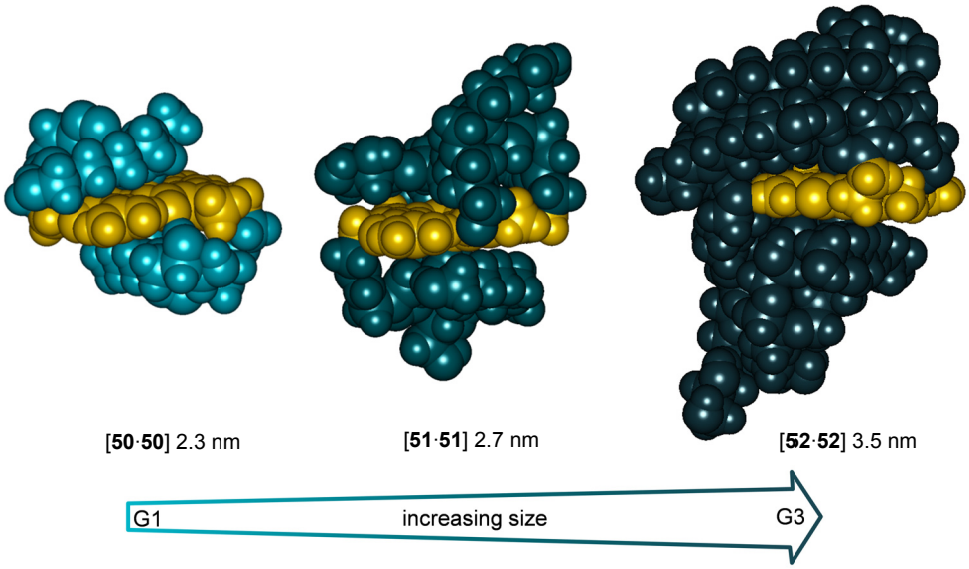

Figure 5-7: Left to right: calculated zwitterionic structures of dimers [50·50]–[52·52]. Macromodel, OPLS 2005 force field, water solvation model.

pH-Dependent DLS measurements show a reversible assembly–disassembly process of the 2nd (51) and 3rd (52) generation dendrons, in aqueous solution, as illustrated in **Figure 5-8**.

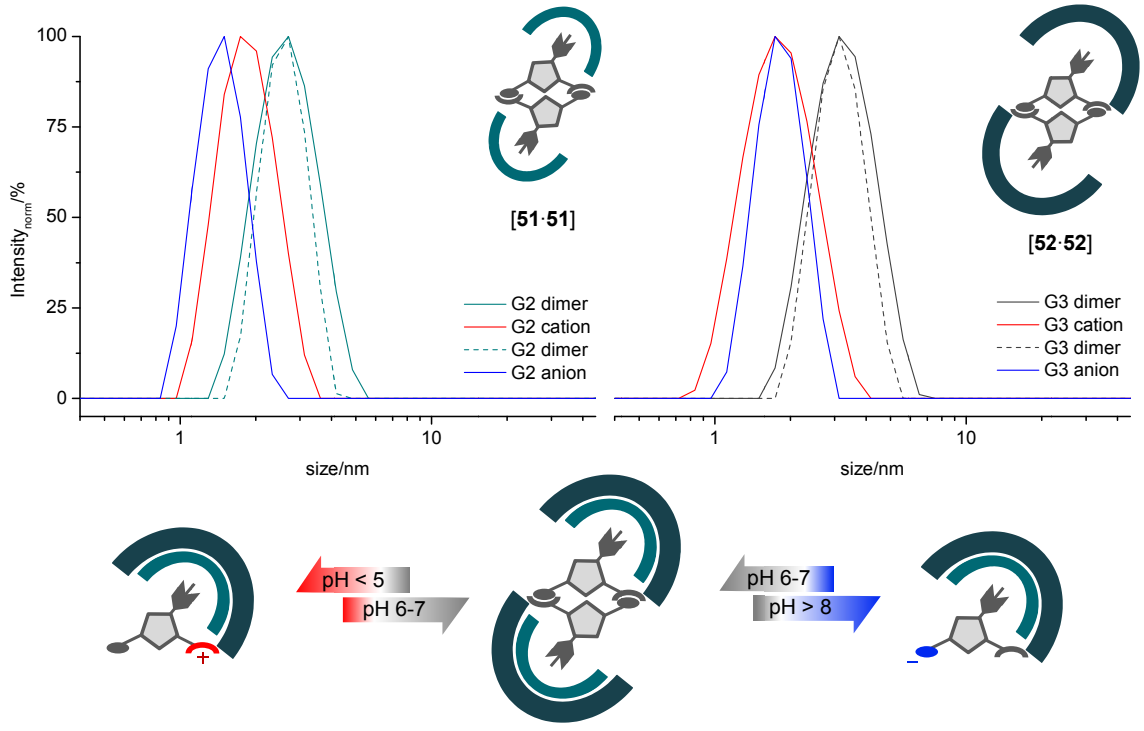

Figure 5-8: **Bottom**: Reversible pH dependent switching of 2nd and 3rd generation dendrimeric dimers to cationic and anionic monomers, respectively, from DLS measurements of 4.5 mM aqueous solutions of 2nd **51** and 3rd **52** generation dendrons (**top**). Self-assembled dimers are only formed at neutral pH, whereas at pH < 5 and pH > 8 only the protonated and deprotonated monomers are present.

This is the first example of an untemplated self-assembly of two biocompatible polyglycerol dendrons into discrete well-defined supramolecular dendrimers in water.[i] The acid-base properties of the embedded guanidiniocarbonyl pyrrole carboxylate zwitterion lead to new reversible, pH-switchable supramolecular dendrimers. These unique characteristics in combination with the high biocompatibility of the dendritic polyglycerol offer a new platform for stimulus-responsive nanotransporters for biomedical applications.

In summary, the untemplated zwitterionic supramolecular dendrimers produced here are DISCRETE, STABLE, and SWITCHABLE in aqueous solution.

Continuing work on this topic will focus on the further development of the zwitterionic dendrons with the goal to use them as nano-carriers. The size and the interior polarity of the dimer may be modified by the following alterations: The size of the dendrimer, an important feature for the encapsulation of molecules, can be increased by a second propionic acid group in the β-position of the pyrrole to introduce two polyglycerol units, as illustrated in **Figure 5-9**. The calculated structure of the dimer has a theoretical diameter of 4.5 nm and indicates a less dense packed interior, important for the encapsulation of guest molecules.

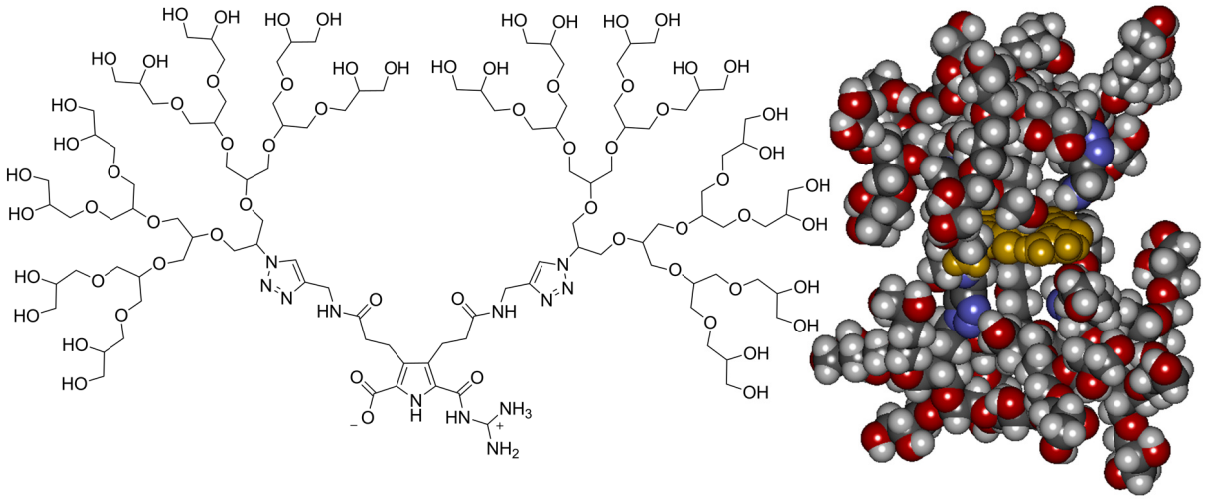

Figure 5-9: Size increase of the dendron by two polygglycerol units attached at the β-positions of the pyrrole. **Left**: Schematic illustrated monomer; **Right**: Molecular modelled dimer, size 4.5 nm in diameter.

Another promising modification for successful application as nanotransporters is the variation of the interior polarity. This may be altered by combining apolar branching residues (FRÉCHET type dendrons) in the vicinity of the binding site with polar polyglycerol dendrons in the periphery, as shown in **Figure 5-10**. The calculated structure of the dimer has a theoretical diameter of 4.6 nm and indicates like above a less dense packed interior, in which

[i] Based on hydrophobic effects and micelle formation, the groups of HIRSCH and BÖTTCHER published structurally defined switchable micelles.[87]

the aromatic branching units are orientated above and below the zwitterionic pyrrole dimer, with free space between the aromatic moieties. This can be beneficial in encapsulation of apolar guest molecules by π-stacking interactions.

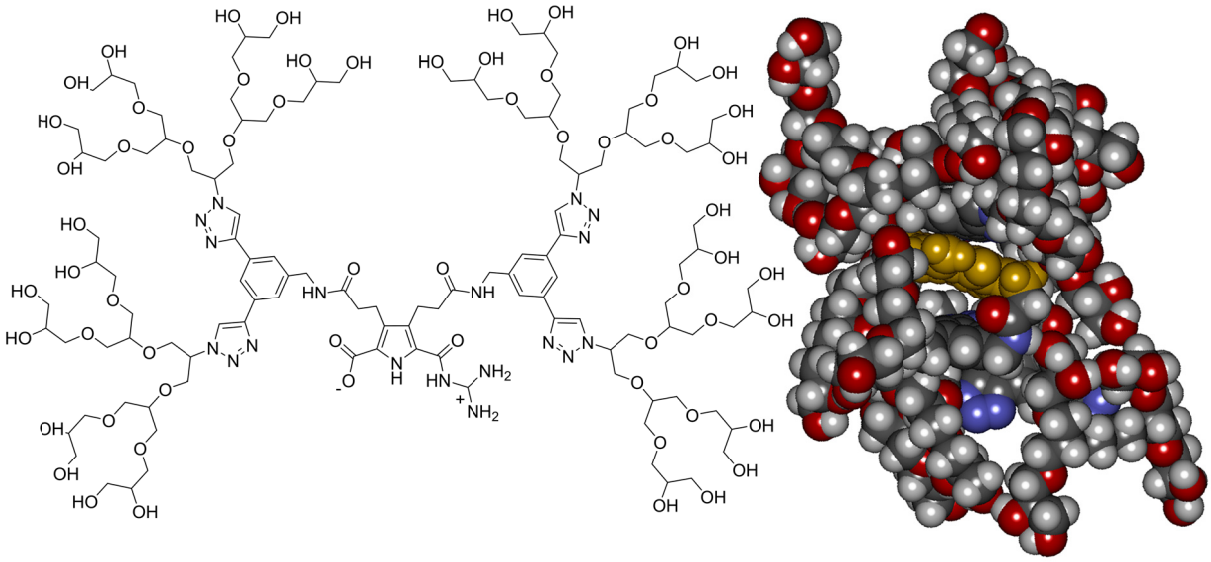

Figure 5-10: Alteration of the interior polarity by apolar aromatic spacers between the binding site and the polyglycerol units. **Left**: Schematic illustrated monomer; **Right**: Molecular modelled dimer, size 4.6 nm in diameter.

In addition to the zwitterionic untemplated approach shown above the 1st to 3rd generation zwitterionic dendrimers **50–52** were also used in a zwitterionic templated approach by assembling them around a zwitterionic core.

Zwitterionic Templated Supramolecular Dendrimers

For use of zwitterionic dendrons in the ZT-SD approach, a zwitterionic templating core is necessary in order to get a 1:2 hetero-associate (**Figure 3-6**).

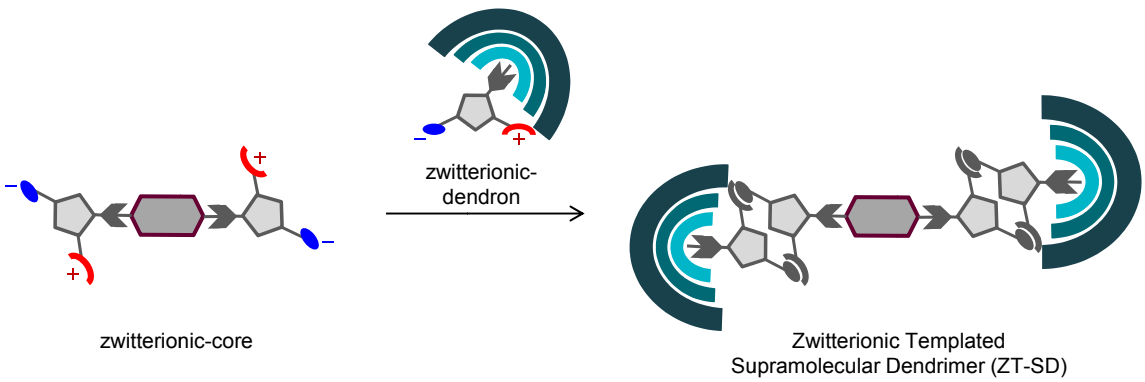

Figure 5-11: Schematic illustration of the Zwitterionic Templated Supramolecular Dendrimer approach.

For the assembly of two dendrons around a zwitterionic core, a perylene diimide derivative carrying two zwitterionic pyrroles at the imide positions was synthesised. The zwitterionic core was solubilised by association with the 1st to 3rd generation dendrons, as illustrated in **Figure 5-12**.

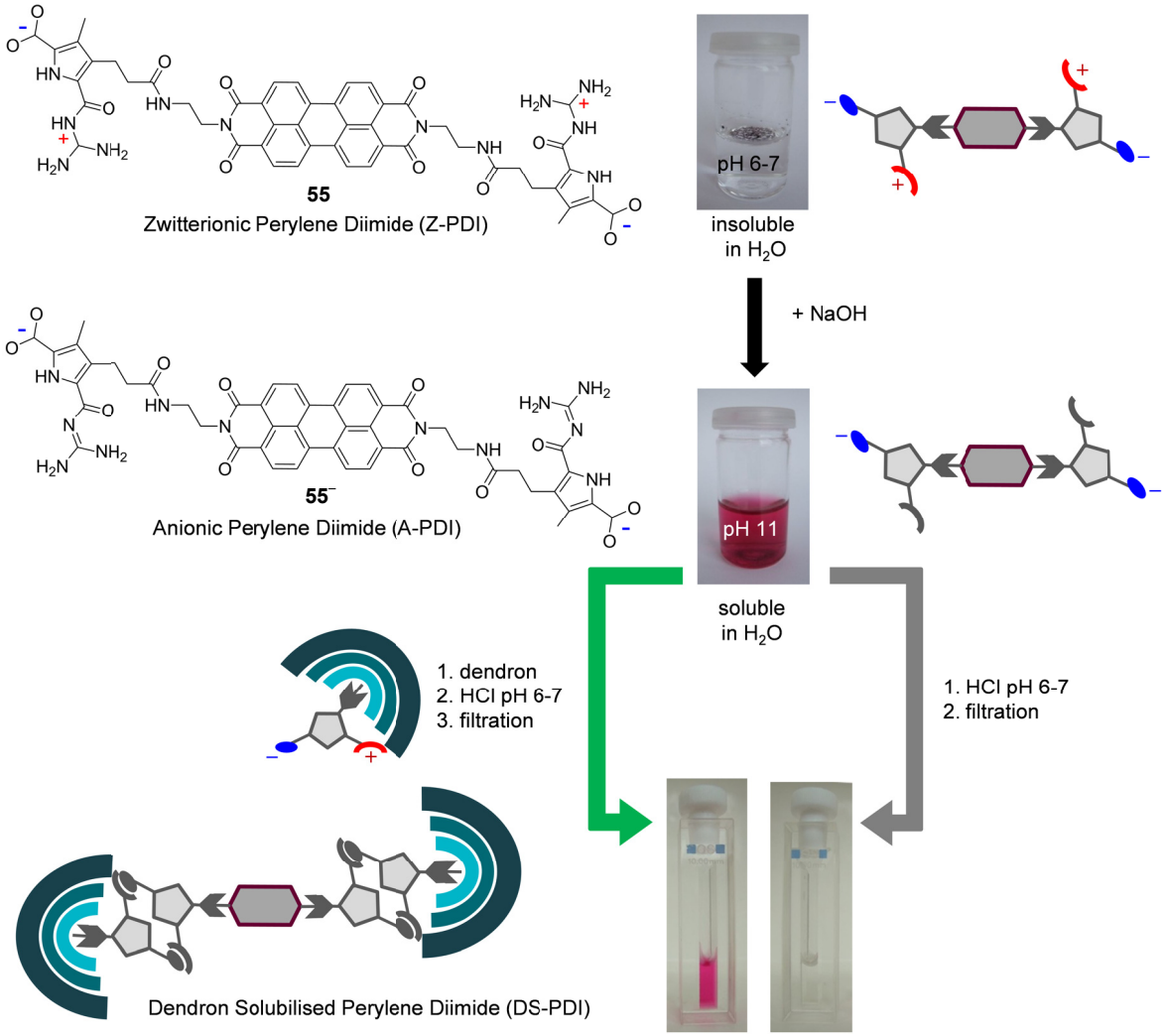

Figure 5-12: Solubility test of perylene diimide **55** in water; **Black**: Water-insoluble zwitterionic perylene diimide **55** was dissolved with 40 equivalents of sodium hydroxide; **Green**: The aqueous solutions of **55** was treated with 1st to 3rd generation dendrons **50**, **51**, and **52** (4 equivalents for each generation). After pH adjustment with HCl to pH 6–7, the solution was filtered through a PTFE syringe filter of 0.45 µm pore size; **Grey**: The pH was adjusted to pH 6–7 by hydrochloric acid, and the 0.1 mM solution of **55** was filtered through a PTFE syringe filter of 0.45 µm pore size.

The solubilisation of the perylene core by association with the dendron as qualitatively proven according to **Figure 5-12** was also established in a quantitative manner by pH titration experiments monitored by UV/Vis spectroscopy. The recorded electronic absorption spectra reflect the solubilisation of the monomeric perylene diimide by 1st to 3rd generation zwitterionic dendrons, as illustrated in **Figure 5-13**.

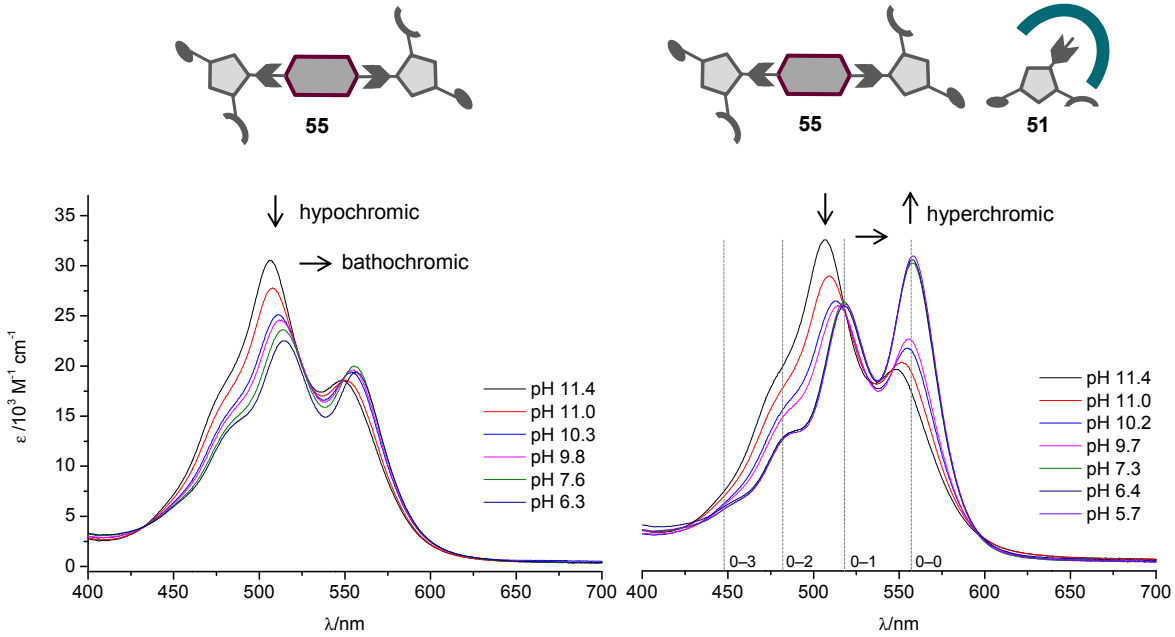

Figure 5-13: UV/Vis pH titration: **Left**: Perylene diimide **55** (0.01 mM) and sodium hydroxide (0.4 mM) – pH adjusted by the addition of 0.1 N HCl; **Right**: Perylene diimide **55** (0.01 mM), sodium hydroxide (0.4 mM), and 10 equivalents of 2nd generation dendron **51** (0.1 mM) – pH change adjusted by addition of 0.1 N HCl.

The UV/Vis characteristics of perylene diimides are well established and provide strong evidence for the solubilisation of monomeric perylene diimide **55** by dendrons **50**–**52**. The most reasonable explanation for the experimental observations is the formation of a 2:1 hetero-associate with the perylene diimide enclosed between the zwitterionic pyrrole dimers (**Figure 5-14**). Quantum-chemically calculated excitation energies (absorption maxima) and pH effects underline the hypothesis of such a discrete supramolecular dendrimer.

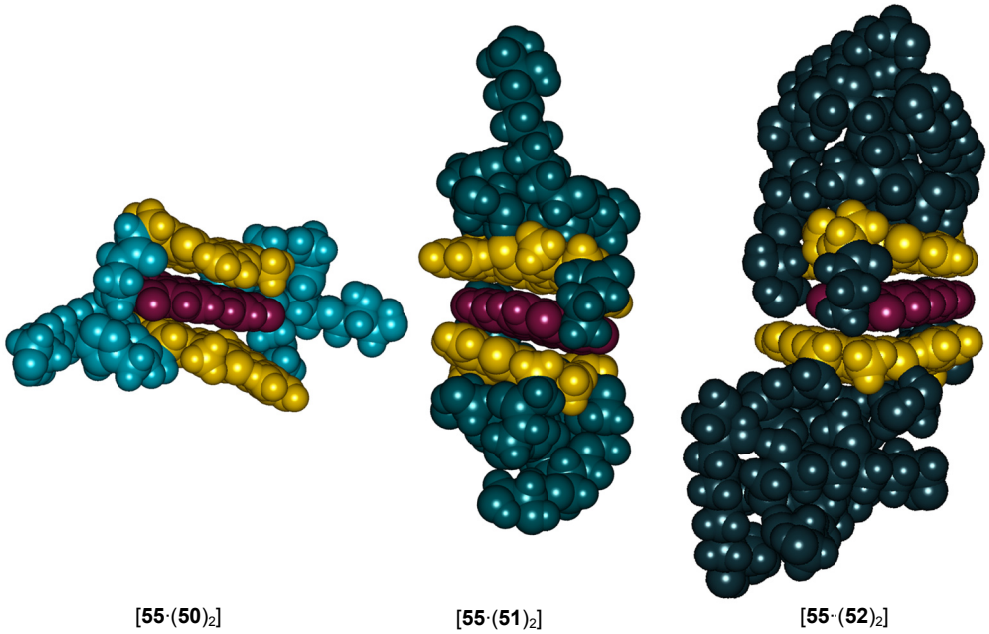

Figure 5-14: Molecular Modelling with OPLS 2005 force field in water; Possible 1:2 complex of zwitterionic perylene diimide and 1st to 3rd generation zwitterionic dendron.

A major deficiency of these systems are the non-orthogonal binding modes of zwitterionic cores and dendrons. Therefore it is difficult to achieve well defined systems like in the untemplated zwitterionic approach. A possible new concept for an orthogonal binding motif (AB system) based on the guanidiniocarbonyl pyrrole binding site, is depicted in **Figure 5-15**.

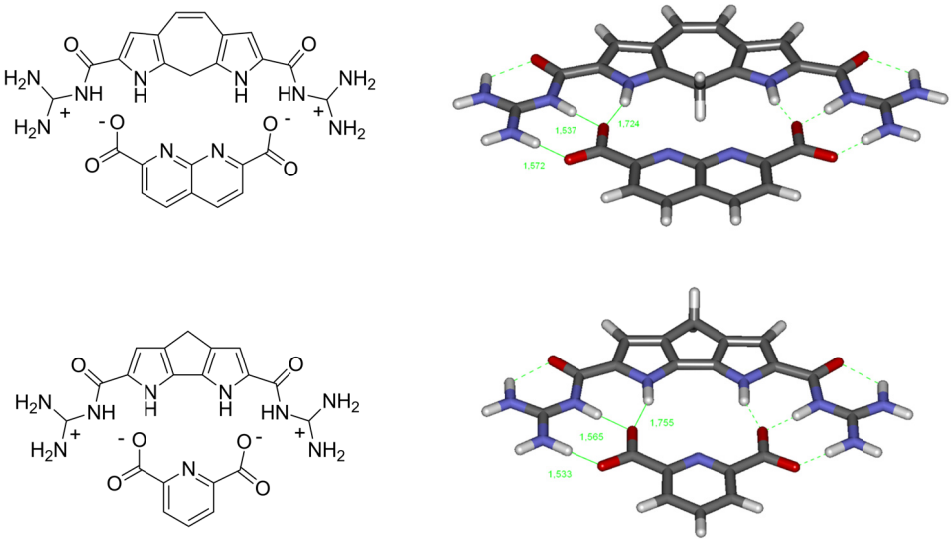

Figure 5-15: Possible new orthogonal binding motifs based on the zwitterionic guanidiniocarbonyl pyrrole of SCHMUCK.

The aim of this work was to obtain monodisperse supramolecular dendrimers, which are stable and switchable by pH changes in water. This goal was achieved in the case of untemplated zwitterionic concept discussed in **Chapter 4.3.1** by the combination of HAAG'S polyglycerols and the guanidiniocarbonyl pyrrole carboxylate binding site of SCHMUCK. Further investigations for the purpose to use these supramolecular complexes as nanotransporters in biomedical applications will follow and are expected to provide exciting results.

6. EXPERIMENTAL SECTION

6.1 General Experimental and Analytical Methods

Solvents and Chemicals

All solvents were dried according to literature procedures.[135] Dichloromethane and N,N-dimethylformamide were dried by distillation from calcium hydride. Diethyl ether and tetrahydrofuran were distilled from sodium with benzophenone as indicator. Dry methanol was distilled from magnesium, methanol for MPLC was distilled with ILUDEST MICROPURE distillation system. Water for chromatographic and spectroscopic measurements was purified with a TKA MicroPure ultrapure water system. All other commercial reagents were purchased and used as received unless otherwise specified.

Rotary Evaporation

Equipment: Heidolph Laborota 4000 efficient and HB digital water bath. Concentration under reduced pressure was performed by rotary evaporation at 40 °C at the appropriate pressure for the solvent used.

Inert Gas

Reactions with humidity-sensitive compounds were carried out under technical argon, which was dried with orange gel and calcium chloride.

Vacuum Pumps

Equipment: Vacuubrand PC2002 Vario with CVC 2000, MD1C, Vacuubrand Sliding vane rotary vacuum pump RZ 5

Lyophilisation

All lyophilisations were performed from ultrapure water with a Christ Alpha 1-4 LD plus freeze dryer. If necessary, the substances were dissolved in a few milliliters of methanol.

Melting Point (mp)

Melting points were determined on a Reichert Thermovar type 300429 Kofler hot stage melting apparatus and are uncorrected.

Cryostatic Temperature Regulator

Equipment: Julabo F12; ED

pH Measurement

Equipment: Knick pH-Meter 766 Calimatic

The pH-meter was calibrated with commercial available buffer standards (pH = 4.00 and pH = 7.00).

Thin Layer Chromatography (TLC)

Equipment: Benda Nu-4 KL UV lamp (wavelengths: 254 nm, 366 nm)

Material: Macherey-Nagel POLYGRAM SIL/UV_{254}

Reactions were monitored by TLC on silica gel precoated plates. Visualization of the spots was carried out by fluorescence quenching with 254 nm UV light. The TLC elution mixtures are reported in volume percent (v/v) except otherwise stated.

Medium Performance Liquid Chromatography (MPLC), Normal-Phase, Preparative

Equipment: Kronlab KD50/100 SS pump; Kronlab UV/Vis 2.5 detector

Column: Kronlab laboratory scale glass column ECO^{PLUS}, TAC25/500LS0-SR-2

Material: Macherey Nagel Silica Gel 60M for chromatography, 0.04–0.063, 230–400 mesh ASTM

Flash chromatography was performed with vacuum packed silica Kronlab glass columns with 25 mm diameter and 250–500 mm length. Solvent mixtures used for flash chromatography are reported in volume percent. Yields refer to chromatographically purified and spectroscopical pure compounds, unless otherwise stated.

Medium Performance Liquid Chromatography (MPLC), Reversed-Phase, Preparative

Equipment: Teledyne Isco, Inc. CombiFlash Companion

Column: Kronlab laboratory scale glass columns ECO^{PLUS}, TAC25/500LS0-SR-2 and TAC25/250LS0-SR-2

Material: YMC GEL ODS-A 12 nm, S-50 µm, AA12S50

Reversed-phase chromatography was performed on self-packed Kronlab glass columns with 25 mm diameter and 250–500 mm length. All eluents were distilled prior use. Solvent mixtures used for liquid chromatography are reported in volume percent. Yields refer to chromatographically purified and spectroscopical pure compounds, unless otherwise stated.

High Performance Liquid Chromatography (HPLC), Normal-Phase, Analytical[136]

Equipment: Merck Hitachi L-6200A Intelligent Pump, Erma Degasser ERC-3512, Knauer UV Detector 2600, Erma RI-Detektor ERC-7512

Software: SCPA Chromstar 7.0

Column: Macherey Nagel, 250 mm length, 4 mm diameter, 7 µm, 10 nm; type: EC250/4 NUCLEOSIL 100-7

All eluents used for liquid chromatography were commercial available and in "HPLC - Gradient Grade" quality. Solvent mixtures are reported in volume percent.

High Performance Liquid Chromatography (HPLC), Reversed-Phase, Analytical[136]

Equipment: Dionex HPLC system: P680 pump, ASI-100 automated sample injector, UVD-340U UV detector, UltiMate 3000 Column Compartment

Software: Dionex Chromeleon 6.80

Column: YMC-Pack ODS-A, 150 mm length, 3.0 mm diameter, 5 µm, 12 nm; AA12S05-1503

Size Exclusion Chromatography (SEC)[120]

Equipment: Jasco PU-880 (BT-8100) pump, Knauer A0263 injector, Shodex RI-101 detector, PSS degasser

Column: PSS-Proteema 1000 nm, 5 µm, 300/8 mm [100–150 000 $g \cdot mol^{-1}$], Proteema 10000 nm, 5 µm, 300/8 mm [1000–7 500 000 $g \cdot mol^{-1}$]

System was calibrated with narrow distributed pullullan. All measurements were performed with 1.0 ml/min flow at 23 °C with sodium azide in ultrapure water (0.01 M) as eluent.

Nuclear Magnetic Resonance Spectrometry (NMR)[137]

Equipment: Bruker DMX 300 (1H: 300 MHz; 13C: 100 MHz), Bruker Avance 400 (1H: 400 MHz; 13C: 100 MHz), Bruker DRX 500 (1H: 500 MHz; 13C: 125 MHz)

All measurements were performed at room temperature, using $DMSO_{d6}$ or $CDCl_3$ as solvents. The chemical shifts were measured against the solvent signal and are reported in ppm from TMS (*d* scale). The coupling constants are given in Hertz. The following abbreviations for the description of the fine structure were used: s = singlet, bs = broad singlet, d = doublet, t = triplet, q = quartet, m = multiplet, br = broad signal. Peak assignments are based on DEPT, 2D NMR studies and/or comparison with literature data.

High Resolution Mass Spectrometry (HR-MS)

Equipment: High resolution ESI: Bruker BioTOF III, Bruker Daltonik MicroTOF focus

Fourier Transform Infrared Spectroscopy (FT-IR)

Equipment: Jasco FT-IR 430 spectrophotometer, Jasco FT-IR 410 spectrophotometer

The compounds were measured in pure form with the Pike Miracle or JASCO ATR-500M unit. The maxima are classified in four intensities: s (strong), m (middle), w (weak), br (broad) and are reported in cm^{-1}.

Atomic Force Microscopy (AFM)

Equipment: Veeco Innova Scanning Probe Microscope, Veeco NanoDrive Controller, HALCYONICS Micro 40 active vibration isolation unit, AC 160TS OLYMPUS cantilever

Software: Gwyddion-2.18

Sample solutions were spin coated (40 rps) on a freshly cleaved mica surface. AFM measurements were performed in tapping mode.

Dynamic Light Scattering (DLS)

Equipment: Malvern Zetasizer nano zs

Software: Dispersion Technology Software 5.03

Measurements were performed with sample solutions (ultrapure water) in glass cuvettes (round aperture) at 25 °C with 2 min equilibration time.

Isothermal Titration Calorimetry (ITC)

Equipment: MicroCal VP-ITC MicroCalorimeter

Software: Implemented plugin in ORIGIN 7 (Origin Lab)

Dilution experiments were performed with ultrapure degassed water.

Molecular Modelling (MM)

Software: Schrödinger Maestro, MacroModel Vers. 9.6

The structure calculations with MacroModel were performed based on the forcefield OPLS 2005 and water as solvent.

Time-Dependet Density Functional Theory (TD-DFT)

Software: Gaussian 03 Revision E.01[134]

The calculations were performed on the B3LYP/6-31G(d,p) level of theory.

6.2 Construction of a Chromatography System

6.2.1 Construction Plan

During the present work a self-constructed chromatographic system was built together with Dr. Rolf Janiak. The construction scheme is illustrated in **Figure 6-1**.[138]

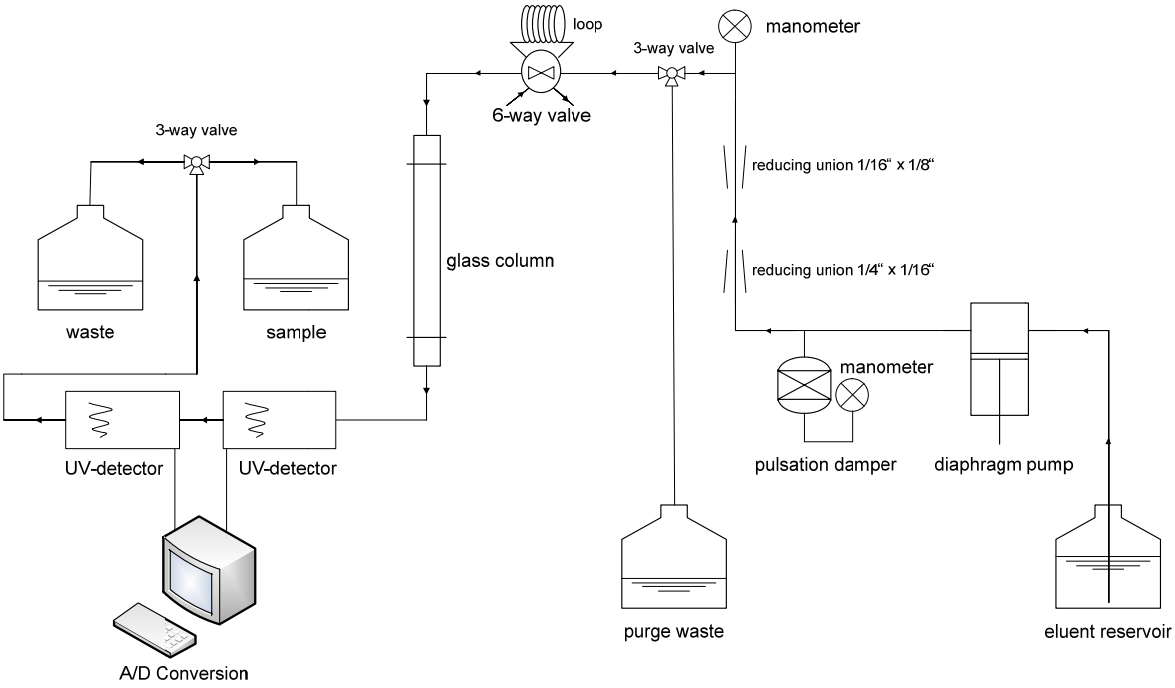

Figure 6-1: **Top**: Schematic illustration of self-constructed chromatographic system. **Bottom**: Picture of the chromatographic system.

6.2.2 List of Component Parts

company	component		order number
Swagelok	stainless steel tubing	1/4 x 0.035“	SS-T4-S-035
		1/8 x 0.028“	SS-T4-S-028
		1/16 x 0.014“	SS-T4-S-014
	nut and ferrule set:	1/4“ tube fitting	SS-400-NFSET
		1/8“ tube fitting	SS-200-NFSET
		1/16“ tube fitting	SS-100-NFSET
	union tee	3 x 1/8“	SS-200-3
		3 x 1/4“	SS-400-3
	reducing union	1/4“ x 1/16“	SS-400-6-1
		1/8“ x 1/16“	SS-200-6-1
	male connector:	1/4“ x G3/8“	SS-400-1-6RS
		1/4“ x G1/2“	SS-400-1-8RS
		1/8“ x G1/8“	SS-200-7-2RG
	3-way ball valve	1/8“	SS-41GXS2
	manometer	40 bar	PGI-63B-BG40-LAOX
Kronlab	Laboflon PTFE tubing	4.75 x 6.35 mm	PT4,75NA6,35
	Laboflon FEP tubing	1.6 x 3.2 mm	PT1,6FE3,2
	ECOplus glass column	50 x 500 mm, PTFE, 30 bar	TAC50/500LSO-SR-1
Lewa	diaphragm metering pump	max. oper. pres. 40 bar	LDB-M-9XX-1
	pulsation damper	0.2 l, 40 bar SBO HYDAC	090058.0584
Rheodyne	rotary 6-Position teflon valve	model 5012	
Merck-Hitachi	UV-detector	L4000A	
SCPA	A/D conversion ISA card		
	ChromStar 3		

6.3 Syntheses

6.3.1 CBS-Dendrons

6.3.1.1 Synthesis of HOOC–P–CHO (8)

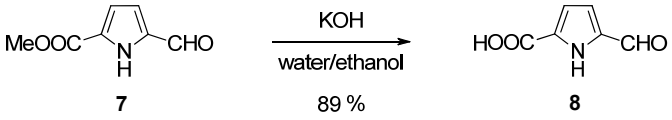

7 89 % **8**

reactants		formula	g·mol^{-1}	eq.	mmol	g
MeOOC–P–CHO[i]	**7**	$C_7H_7NO_3$	153.14	1.00	65.3	10.0
potassium hydroxide		HKO	56.11	1.10	71.8	4.03

A suspension of MeOOC–P–CHO (7) (10.0 g, 65.3 mmol, 1.00 eq.) and potassium hydroxide (4.03 g, 71.8 mmol, 1.10 eq.) in an ethanol/water mixture (8/2, 100 ml) was heated to reflux for 3 hours. The reaction mixture was concentrated in vacuum and the residue was dissolved in water (20 ml). Hydrochloric acid (37 %) was added to precipitate the product. The suspension was filtered through a Buechner funnel, the filtration residue was washed with water (100 ml), and dried in vacuum. The product HOOC–P–CHO (**8**) (8.13 g, 58.4 mmol, 89 % yield) was isolated as pale orange solid.

product		formula	g·mol^{-1}	%	mmol	g
HOOC–P–CHO	**8**	$C_6H_5NO_3$	139.11	89	58.4	8.13

mp = 188 °C (decomposition); ^{1}**H-NMR** (400 MHz, $DMSO_{d6}$) δ = 6.82–6.84 (m, 1H, CH), 6.93–6.95 (m, 1H, CH), 9.69 (s, 1H, CH), 12.85 (br.s, 1H, NH), 13.06 (br.s, 1H, OH); ^{13}**C-NMR** (100 MHz, $DMSO_{d6}$) δ = 115.4, 116.4 (CH), 129.1, 135.3 (C_q) 161.4, 181.3 (CO); **HR-MS** (pos. ESI) m/z = calculated 138.019–measured 138.019 for $C_6H_5NO_3$ -H^+.

[i] MeOOC–P–CHO (7) was synthesised according to literature procedure.[103]

6.3.1.2 Synthesis of BocG–P–CHO (9)

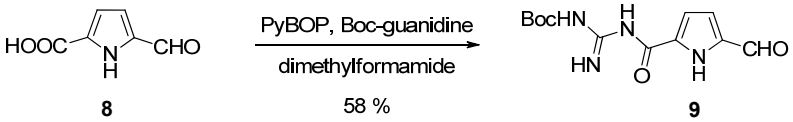

8 **9**

reactants		formula	g·mol^{-1}	eq.	mmol	ml	g·ml^{-1}	g
HOOC–P–CHO	**8**	$C_6H_5NO_3$	139.11	1.00	7.19			1.00
PyBOP		$C_{18}H_{28}F_6N_6OP_2$	520.40	1.00	7.19			3.74
4-methylmorpholine		$C_5H_{11}NO$	101.15	1.27	9.10	1.00	0.92	0.920
Boc-guanidine[i]		$C_6H_{13}N_3O_2$	159.19	1.00	7.19			1.14
4-dimethylaminopyridine		$C_7H_{10}N_2$	122.17	0.200	1.44			0.176

HOOC–P–CHO (**8**) (1.00 g, 7.19 mmol, 1.00 eq.) and PyBOP (3.74 g, 7.19 mmol, 1.00 eq.) were dissolved in a dimethylformamide/dichloromethane mixture (1/1, 10 ml). After addition of 4-methylmorpholine (1.00 ml, 9.10 mmol, 1.27 eq.) the reaction mixture was stirred for 10 minutes. Boc-guanidine (1.14 g, 7.19 mmol, 1.00 eq.) and 4-dimethylaminopyridine (0.18 g, 1.44 mmol, 0.20 eq.) were added, and the reaction solution was stirred for 24 hours at room temperature. Subsequently the reaction mixture was poured into ice cold water (100 ml) and the precipitated solid was filtered through a Buechner funnel. The filtration residue was washed with water (100 ml) and ice cold methanol (25 ml). When dried in vacuum the BocG–P–CHO (**9**) (1.18 g, 4.21 mmol, 58 % yield) was obtained as pale yellow solid.

product		formula	g mol^{-1}	%	mmol	g
BocG–P–CHO	**9**	$C_{12}H_{16}N_4O_4$	280.28	58	4.21	1.18

mp = 170 °C (decomposition); ^{1}**H-NMR** (400 MHz, $DMSO_{d6}$) δ = 1.47 (s, 9H, CH_3), 6.87, 6.94 (s, 1H, CH), 8.57, 9.36 (br.s, 1H, NH), 9.66 (s, 1H, CH), 10.75, 12.11 (br.s, 1H, NH); ^{13}**C-NMR** (100 MHz, $DMSO_{d6}$) δ = 27.7 (CH_3), 81.6 (C_q), 114.0, 117.3 (CH), 134.3 (C_q), 158.4, 181.1 (CO); **FT-IR** (KBr) [cm^{-1}] = 3387 s, 3265 s, 2981 w, 1728 s, 1679 m, 1645 s, 1532 s, 1339 m, 1238 s, 1147 s, 842 m, 767 m; **HR-MS** (pos. ESI) m/z = calculated 303.106– measured 303.106 for $C_{12}H_{16}N_4O_4$ +Na^+.

[i] Boc-guanidine was synthesised according to literature procedure.[103, 104]

6.3.1.3 Synthesis of BocG–P–COOH (10)

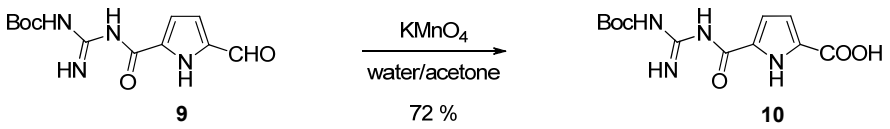

reactants		formula	g·mol^{-1}	eq.	mmol	g
BocG–P–CHO	**9**	$C_{12}H_{16}N_4O_4$	280.28	1.00	14.5	4.07
potassium permanganate		$KMnO_4$	158.03	2.50	36.3	5.74
sodium dithionite		$Na_2S_2O_4$	174.11	0.101	1.46	0.255

BocG–P–CHO (**9**) (4.07 g, 14.5 mmol, 1.00 eq.) was dissolved in acetone (50 ml) and a suspension of potassium permanganate (5.74 g, 36.3 mmol, 2.50 eq.) in a water/acetone mixture (1/1, 240 ml) was added over a period of 1 hour. The reaction mixture was stirred for 1 hour at 40 °C, and an additional hour at room temperature. Sodium dithionite (0.255 g, 1.46 mmol, 0.101 eq.) was added to the suspension before filtering it through a pad of celite®. The filter cake was washed with a sodium hydroxide solution (5 %, 350 ml). The filtrate was acidified with hydrochloric acid (5 %) until precipitation of the product was observed. The suspension was extracted with dichloromethane (3·100 ml) and the combined organic fractions were washed with water (1·100 ml) and finally concentrated in vacuum until precipitation. The resulting suspension was again filtered through a Buechner funnel and the filtration residue was washed with water and dried in vacuum. BocG–P–COOH (**10**) (3.10 g, 10.5 mmol, 72 % yield) was isolated as a pale yellow solid matter.

product		formula	g·mol^{-1}	%	mmol	g
BocG–P–COOH	**10**	$C_{12}H_{16}N_4O_5$	296.28	72	10.5	3.10

mp > 250 °C; **^{1}H-NMR** (400 MHz, $DMSO_{d6}$) δ = 1.47 (s, 9H, CH_3), 6.74, 6.79 (s, 1H, CH), 8.56, 9.30, 11.30, 11.74 (br.s, 1H, NH); **^{13}C-NMR** (100 MHz, $DMSO_{d6}$) δ = 27.7 (CH_3), 81.0 (C_q), 113.7, 114.9 (CH), 126.5, 132.5 (C_q), 155.8, 158.3, 161.5, 167.8 (CN, CO); **FT-IR** (KBr) [cm^{-1}] = 3392 m, 3322 m, 3169 s, 2982 m, 1765 s, 1683 s, 1619 s, 1322 s, 1210 s, 965 w, 753 m; **HR-MS** (pos. ESI) m/z = calculated 319.101–measured 319.101 for $C_{12}H_{16}N_4O_5$ $+Na^+$.

6.3.1.4 Synthesis of BocG–P–(prop-2-inyl) (10)

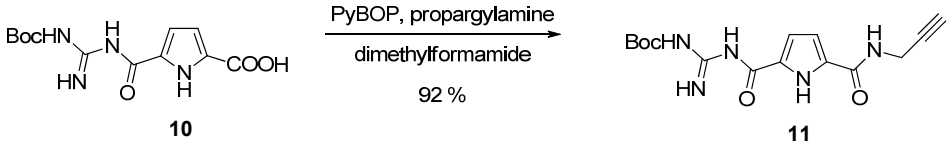

10 **11**

reactants		formula	g·mol^{-1}	eq.	mmol	µl	g·ml^{-1}	mg
BocG–P–COOH	**10**	$C_{12}H_{16}N_4O_5$	296.28	1.00	2.03			600
PyBOP		$C_{18}H_{28}F_6N_6OP_2$	520.39	1.10	2.23			1159
4-methylmorpholine		$C_5H_{11}NO$	101.15	3.00	6.08	668	0.92	615
propargylamine		C_3H_5N	55.08	1.10	2.23	143	0.86	123
4-dimethylaminopyridine		$C_7H_{10}N_2$	122.17	0.200	0.405			49.5

BocG–P–COOH (**10**) (600 mg, 2.03 mmol, 1.00 eq.) and PyBOP (1159 mg, 2.23 mmol, 1.10 eq.) were dissolved in dimethylformamide (6 ml). 4-Methylmorpholine (668 µl, 6.08 mmol, 3.00 eq.), propargylamine (143 µl, 2.23 mmol, 1.10 eq.) and 4-dimethylaminopyridine (49.5 mg, 0.405 mmol, 0.200 eq.) were added and the reaction solution was stirred for 12 hours. Water (50 ml) was poured into the reaction mixture and a solid precipitated. The suspension was filtered through a Buechner funnel and the filter cake was washed with water (100 ml) and dried in vacuum. The crude product was purified *via* normal-phase flash chromatography (triethylamine deactivated SiO_2, ethyl acetate/^{n}hexane, 3/7) to isolate BocG–P–prop-2-inyl (**11**) (620 mg, 1.86 mmol, 92 % yield) as colourless solid.

product		formula	g·mol^{-1}	%	mmol	mg
BocG–P–prop-2-inyl	**11**	$C_{15}H_{19}N_5O_4$	333.34	92	1.86	620

mp = 175–178 °C; **^{1}H-NMR** (300 MHz, $DMSO_{d6}$) δ = 1.46 (s, 9H, CH_3), 3.17 (t, ^3J = 2.34 Hz, 1H, CH), 4.04 (q, ^3J = 2.56 Hz, 2H, CH_2), 6.82 (s, 2H, CH), 8.58 (br.s, 1H, NH), 8.80 (t, ^3J = 6.17 Hz, 1H, NH), 9.34, 10.84, 11.37 (br.s, 1H, NH); **^{13}C-NMR** (62.5 MHz, $DMSO_{d6}$) δ = 27.8 (CH_3), 28.0 (CH_2), 73.3, 81.1 (C_q), 112.2, 113.7 (CH), 128.8, 131.9 (C_q), 158.4, 159.4, 161.5, 168.4 (CN, CO); **FT-IR** (ATR) [cm^{-1}] = 3416 w, 3371 s, 3333 m, 3277 m, 3120 w, 2979 w, 2933 w, 1665 s, 1617 s, 1526 m, 1282 s, 1253 s, 1158 s, 1128 s, 807 s, 754 s; **HR-MS** (pos. ESI) m/z = calculated 334.151–measured 334.155 for $C_{15}H_{19}N_5O_4$ +H^+.

6.3.1.5 Synthesis of BocG–P–G2 (12)[89]

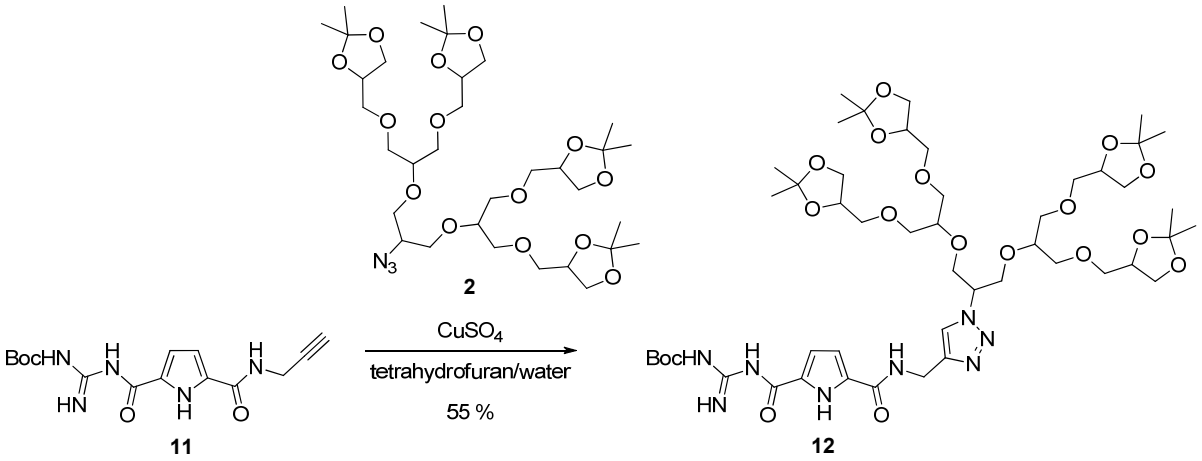

reactants		formula	g·mol^{-1}	eq.	µmol	µl	g·ml^{-1}	mg
BocG–P–prop-2-inyl	**11**	$C_{15}H_{19}N_5O_4$	333.34	1.00	480			160
G2–N_3	**2**	$C_{33}H_{59}N_3O_{14}$	721.83	1.10	528			381
diisopropylethylamine		$C_8H_{19}N$	129.24	0.300	144	25.0	0.74	18.6
sodium ascorbate		$C_6H_7NaO_6$	198.11	0.300	144			28.5
copper(II)sulphate pentahydrate		$CuH_{10}O_9S$	249.68	0.150	72.0			18.0

BocG–P–prop-2-inyl (**11**) (160 mg, 480 µmol, 1.00 eq.) and G2–N_3 (**2**) (381 mg, 528 µmol, 1.10 eq.) were suspended in tetrahydrofuran (2.5 ml). Diisopropylethylamine (25.0 µl, 144 µmol, 0.300 eq.) and freshly prepared aqueous solutions of sodium ascorbate (28.5 mg, 144 mmol, 0.300 eq.) and copper(II)sulphate pentahydrate (18.0 mg, 72.0 µmol, 0.15 eq.) were added to the reaction mixture. The reaction mixture was adjusted to a tetrahydrofuran/water 1/1 ratio by an additional amount of water (400 µl). After 15 minutes the colour of the reaction solution changed to deep green. Thin layer chromatography control showed complete conversion after 2.5 hours. The reaction mixture was diluted with water (50 ml) and extracted with dichloromethane (3·35 ml). The combined organic fractions were washed with saturated EDTA solution (2·20 ml) and water (20 ml). The organic solvent was dried with sodium sulphate and evaporated in vacuum. The crude product was purified *via* reversed-phase chromatography (MPLC, RP18, 50 g, 50 µm, 25·2.5 cm, 290 nm, 25 ml·min^{-1} gradient methanol 75 % to 100 % in 15 minutes, retention time 9 minutes). An additional normal-phase chromatography was done (MPLC, SiO_2, 50 g, 21 µm, 25·2.5 cm, 290 nm, 30 ml·min^{-1} isocratic dichloromethane/methanol 9.5/0.5). The isolated residue was freeze dried to obtain BocG–P–G2 (**12**) (283 mg, 268 µmol, 55 % yield) as colourless high viscous resin.

product		formula	g·mol^{-1}	%	µmol	mg
BocG–P–G2	**12**	$C_{48}H_{78}N_8O_{18}$	1055.18	55	268	283

mp = 38–42 °C; ^{1}**H-NMR** (500 MHz, $DMSO_{d6}$) δ = 1.24, 1.26 (s, 24H, CH_3), 1.46 (s, 9H, CH_3), 3.33–3.63 (m, 22H, CH_2, CH), 3.78–3.86 (m, 2H, CH_2), 3.89–3.99 (m, 6H, CH_2), 4.05–4.17 (m, 4H, CH), 4.48–4.49 (m, 2H, CH_2), 4.83–4.96 (m, 1H, CH), 6.81 (br.s, 2H, CH), 7.97 (s, 1H, CH), 8.49, 8.88, 9.38, 10.81, 11.00 (br.s, 1H, NH); ^{13}**C-NMR** (125 MHz, $DMSO_{d6}$) δ = 25.3, 26.6, 27.8 (CH_3), 34.2 (CH_2), 48.6, 60.2 (CH), 65.8, 68.4, 70.5, 71.7 (CH_2), 74.2 (CH), 77.6 (C_q), 77.9 (CH), 108.4 (C_q), 112.2, 122.6, 127.5 (CH), 144.3 (C_q), 154.3, 159.4, 165.1 (CO); **FT-IR** (ATR) [cm^{-1}] = 3384 w, 3274 w, 2984 w, 2875 w, 2096 w, 1725 w, 1632 m,1545 m, 1458 m, 1369 m, 1288 m, 1238 s, 1146 s, 1077 s, 1048 s, 839 m, 785 w; **HR-MS** (pos. ESI) m/z = calculated 1077.533–measured 1077.547 for $C_{48}H_{78}N_8O_{18}$ $+Na^+$.

6.3.1.6 Synthesis of $^{+}$G–P–G2(OH)$_8$ (13)

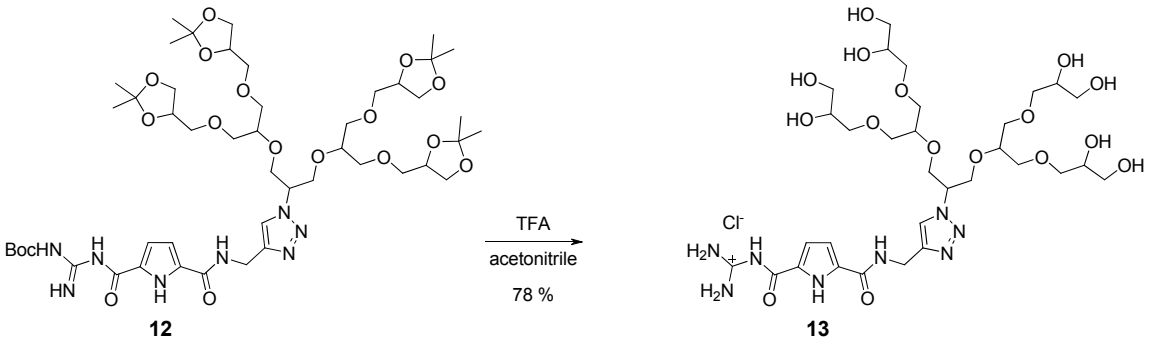

reactants		formula	g·mol^{-1}	eq.	mmol	ml	g·ml^{-1}	mg
BocG–P–G2	**12**	$C_{48}H_{78}N_8O_{18}$	1055.18	1.00	0.114			120
trifluoroacetic acid		$C_2HF_3O_2$	114.02	140	16.0	1.23	1.48	1820

BocG–P–G2 (**12**) (120 mg, 0.114 mmol, 1.00 eq.) dissolved in acetonitrile (1 ml) was treated with trifluoroacetic acid (615 µl, 8.0 mmol, 70.0 eq) and stirred for 24 hours before an additional amount of trifluoroacetic acid (615 µl, 8.0 mmol, 70.0 eq.) was added. The reaction solution was stirred for further 34 hours at room temperature, 12 hours at 40 °C and 2 hours at 60 °C until HPLC reaction control showed complete deprotection of starting material **12**. Solvent and trifluoroacetic acid were evaporated in vacuum, the residue was dissolved in water, and freeze dried. The crude product was purified *via* reversed-phase chromatography (MPLC, RP18, 50 g, 50 µm, 25·2.5 cm; 290 nm, 25 ml·min^{-1}, gradient methanol 20 % to 30 % in 15 minutes with trifluoroacetic acid 0.05 % as additive, retention time 7 minutes) and the isolated product was freeze dried twice with hydrochloric acid (1 N) to obtain the chloride salt of $^{+}$G–P–G2(OH)$_8$ (**13**) (74.0 mg, 88.9 µmol, 78 % yield).

product		formula	g·mol^{-1}	%	µmol	mg
$^{+}$G–P–G2(OH)$_8$	**13**	$C_{31}H_{55}ClN_8O_{16}$	831.27	78	88.9	74

^{1}H-NMR (300 MHz, DMSO$_{d6}$) δ = 3.24–3.59 (m, 22H, CH$_2$, CH), 3.82–3.94 (m, 4H, CH$_2$), 4.50–4.52 (m, 2H, CH), 4.97 (br.s, 17H, CH, OH), 6.90 (t, ^3J = 2.87 Hz, 1H, CH), 7.45 (t, ^3J = 3.05 Hz, 1H, CH), 8.05 (br.s., 1H, CH), 8.40–8.55 (m, 4H, NH), 8.99 (t, ^3J = 5.23 Hz, 1H, NH), 11.82, 12.40 (br.s, 1H, NH); **^{13}C-NMR** (125 MHz, DMSO$_{d6}$) δ = 34.2 (CH$_2$), 60.3, 60.6 (CH), 63.0, 68.8, 69.9, 69.9 (CH$_2$), 70.5 (CH), 70.7 (CH$_2$), 70.7 (CH), 70.7, 71.6, 72.8 (CH$_2$) 77.6, 77.7, 78.0, 78.0, 111.6, 112.2, 122.5 (CH), 134.5, 144.4, 145.6 (C$_q$), 162.6, 166.1 (CO); **HR-MS** (pos. ESI) m/z = calculated 795.373–measured 795.377 for $C_{31}H_{54}N_8O_{16}$ +H$^+$.

6.3.1.7 Synthesis of EtOOC–P[^{3}Me^{4}Ac]–Me (21)[109]

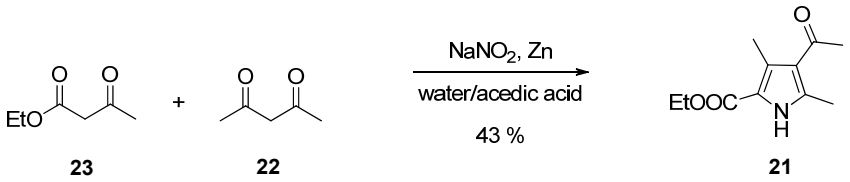

23 **22** **21**

reactants		formula	g·mol^{-1}	eq.	mmol	ml	g·ml^{-1}	g
ethyl acetoacetate	**23**	$C_6H_{10}O_3$	130.14	1.00	556	70.3	1.03	72.4
sodium nitrite		$NNaO_2$	69.00	1.50	834			57.5
acetylacetone	**22**	$C_5H_8O_2$	100.12	1.00	556	57.1	0.975	55.7
sodium acetate		$C_{11}H_{15}NO_3$	82.03	2.00	1112			91.0
zinc dust		Zn	65.41	2.03	1129			73.8

Ethyl acetoacetate (**23**) (70.3 ml, 556 mmol, 1.00 eq.) was dissolved in glacial acetic acid (100 ml) and cooled to 5–10°C. Sodium nitrite (57.5 g, 834 mmol, 1.50 eq.) dissolved in water (80 ml) was added under stirring during 90 minutes. The reaction mixture was stirred at 5 °C for 4 hours and for additional 12 hours at room temperature. Acetylacetone **22** (57.1 ml, 556 mmol, 1.00 eq.), sodium acetate (91.0 g, 1112 mmol, 2.00 eq.), and acetic acid (100 ml) were added to the reaction mixture and subsequently zinc dust (73.8 g, 1129 mmol, 2.03 eq.) in small portions keeping the temperature below 70 °C during the addition. The reaction mixture was heated to 100 °C for 2 hours before it was poured into a water/ice mixture (2 l) to precipitate the crude product. The suspension was filtered through a Buechner funnel and the filtration residue was dissolved in hot ethanol (200 ml). Unreacted zinc was separated by hot filtration through a sintered glass funnel. The product was recrystallised from ethanol and filtered through a Buechner funnel. After washing with ice cold ethanol, and drying in vacuum EtOOC–P[^{3}Me^{4}Ac]–Me (**21**) (50.6 g, 242 mmol, 43 %) was isolated as pale yellow needles.

product		formula	g·mol^{-1}	%	mmol	g
EtOOC–P[^{3}Me^{4}Ac]–Me	**21**	$C_{11}H_{15}NO_3$	209.24	43	242	50.6

mp = 143–145 °C; **^{1}H-NMR** (300 MHz, $CDCl_3$) δ = 1.37 (t, ^3J = 7.09 Hz, 3H, CH_3), 2.45, 2.52, 2.58 (s, 3H, CH_3), 4.33 (q, ^3J = 7.07 Hz, 2H, CH_2), 9.20 (br.s, 1H, NH); **^{13}C-NMR** (75 MHz, $CDCl_3$) δ = 12.8, 14.6, 15.3 (CH_3), 31.4, 60.6 (CH_2), 118.6, 123.7, 129,5, 138.5 (C_q), 161.9, 195.7 (CO); **FT-IR** (ATR) [cm^{-1}] = 3276 s, 1642 s, 1555 m, 1512 w, 1439 m, 1275 m, 1200 m, 1099 s, 1022 m, 941 m, 879 w, 793 m; **HR-MS** (pos. ESI) m/z = calculated 232.094–measured 232.094 for $C_{11}H_{15}NO_3$ +Na^+.

6.3.1.8 Synthesis of EtOOC–P[^{3}Me^{4}Cl-vinyl]–Me (20)[109]

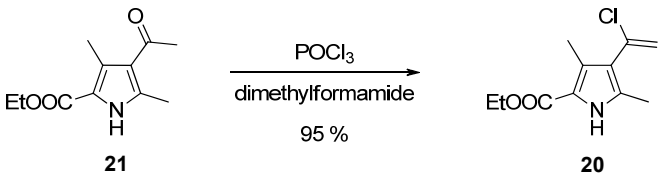

21 **20**

reactants		formula	g·mol^{-1}	eq.	mmol	ml	g·ml^{-1}	g
EtOOC–P[^{3}Me^{4}Ac]–Me	**21**	$C_{11}H_{15}NO_3$	209.24	1.00	47.8			10.0
phosphorus oxychloride		Cl_3OP	153.33	1.05	50.1	4.67	1.65	7.68

EtOOC–P[^{3}Me^{4}Ac]–Me (**21**) (10.0 g, 47.8 mmol, 1.00 eq.) was dissolved in dry dimethylformamide (50 ml) under protective gas and the solution was cooled to 0 °C. The solution of **21** was treated over a period of 40 minutes with phosphorus oxychloride (4.67 ml, 50.1 mmol, 1.00 eq.) and stirred at 0 °C for 15 minutes. The reaction mixture was stirred for additional 60 minutes at room temperature until thin layer chromatography showed complete transformation. The reaction mixture was quenched with ice water (600 ml) and the resulting precipitate was filtered off, washed with water, and dried in vacuum to afford the EtOOC–P[^{3}Me^{4}Cl-vinyl]–Me (**20**) (10.4 g, 45.5 mmol, 95 %).

product		formula	g·mol^{-1}	%	mmol	g
EtOOC–P[^{3}Me^{4}Cl-vinyl]–Me	**20**	$C_{11}H_{14}ClNO_2$	227.69	95	45.5	10.4

mp = 116 °C; **^{1}H-NMR** (300 MHz, $CDCl_3$) δ = 1.35 (t, ^{3}J = 7.11 Hz, 3H, CH_3), 2.31, 2.36 (s, 3H, CH_3), 4.30 (q, ^{3}J = 7.13 Hz, 2H, CH_2), 5.21 (d, ^{2}J = 0.78 Hz, 1H, CH_2), 5.62 (d, ^{2}J = 0.81 Hz, 1H, CH_2), 8.73 (br.s, 1H, NH); **^{13}C-NMR** (75 MHz, $CDCl_3$) δ = 11.3, 12.2, 14.7 (CH_3), 60.2, 117.2 (CH_2), 117.6, 122.2, 127.1, 131.6, 133.8 (C_q), 161.2, 195.9 (CO); **FT-IR** (ATR) [cm^{-1}] = 3273 m, 1660 s, 1503 w, 1434 s, 1370 w, 1277 s, 1185 m, 1099 m, 1069 m, 1022 m, 882 m, 771 s, 745 s, 719 m; **HR-MS** (pos. ESI) m/z = calculated 457.129–measured 457.122 for $C_{11}H_{14}ClNO_2$ +$C_{11}H_{13}NKO_2^+$.

6.3.1.9 Synthesis of EtOOC–P[^{3}Me^{4}alkyne]–Me (19)[109]

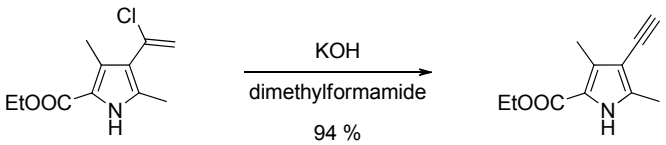

20 **19**

reactants		formula	g·mol^{-1}	eq.	mmol	g
EtOOC–P[^{3}Me^{4}Cl-vinyl]–Me	**20**	$C_{11}H_{14}ClNO_2$	227.69	1.00	43.9	10.0
potassium hydroxide		HKO	56.11	1.67	70.3	3.94

EtOOC–P[^{3}Me^{4}Cl-vinyl]–Me (**20**) (10.0 g, 43.9 mmol, 1.00 eq.) dissolved in dimethylformamide (30 ml) was treated with an aqueous solution of potassium hydroxide (3.94 g, 70.3 mmol, 1.60 eq., in 2 ml H_2O). The reaction mixture was kept at 35 °C for 2 hours until completion of the reaction was shown by thin layer chromatography. The reaction mixture was poured into ice water (600 ml), and the resulting precipitate was filtered off, washed with water, and dried in vacuum to afford the EtOOC–P[^{3}Me^{4}alkyne]–Me (**19**) (7.87 g, 41.2 mmol, 94 %).

product		formula	g·mol^{-1}	%	mmol	g
EtOOC–P[^{3}Me^{4}alkyne]–Me	**19**	$C_{11}H_{13}NO_2$	191.23	94	41.2	7.87

mp = 162 °C; ^{1}**H-NMR** (300 MHz, $CDCl_3$) δ = 1.36 (t, ^3J = 7.14 Hz, 3H, CH_3), 2.34, 2.35 (s, 3H, CH_3), 3.17 (s, 1H, CH), 4.30 (q, ^3J = 7.11 Hz, 2H, CH_2), 8.81 (br.s, 1H, NH); ^{13}**C-NMR** (75 MHz, $CDCl_3$) δ = 11.6, 12.3, 14.6 (CH_3), 60.3 (CH_2), 77.5 (CH), 80.4, 105.6, 117.5, 131.0, 137.2 (C_q), 161.8 (CO); **FT-IR** (ATR) [cm^{-1}] = 3281 s, 2107 w, 1650 s, 1435 m, 1374 w, 1277 s, 1213 m, 1177 m, 1098 m, 1020 m, 883 w, 774 s, 743 s, 670 m; **HR-MS** (pos. ESI) m/z = calculated 230.058–measured 230.051 for $C_{11}H_{13}NO_2$ +K^+.

6.3.1.10 Synthesis of BnOOC–P[^{3}Me^{4}Ac]–Me (28)[109]

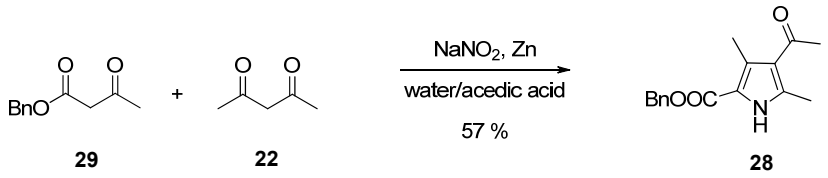

29 **22** **28**

reactants		formula	g·mol^{-1}	eq.	mmol	ml	g·ml^{-1}	g
benzyl acetoacetate	**29**	$C_{11}H_{12}O_3$	192.21	1.00	75.4	13.0	1.112	14.5
sodium nitrite		$NNaO_2$	69.00	1.25	94.2			6.50
acetylacetone	**22**	$C_5H_8O_2$	100.12	1.07	80.9	8.31	0.975	8.10
sodium acetate trihydrate		$C_{11}H_{22}NO_6$	136.08	1.37	104			14.1
zinc dust		Zn	65.41	1.42	107			7.00

Benzyl acetoacetate (**29**) (13.0 ml, 75.4 mmol, 1.00 eq.) was dissolved in glacial acetic acid (23 ml) and cooled to 5 °C. Sodium nitrite (6.50 g, 94.2 mmol, 1.25 eq.), dissolved in water (20 ml), was added under stirring over a period of 30 minutes. The mixture was stirred at room temperature for additional 22 hours, and subsequently transferred into a dropping funnel and added to a mixture of acetylacetone (**22**) (8.31 ml, 80.9 mmol, 1.07 eq.), sodium acetate trihydrate (14.1 g, 104 mmol, 1.37 eq.), and zinc dust (7.00 g, 107 mmol, 1.42 eq.), dissolved in acetic acid (50 ml). The temperature was kept at 70 °C during the addition and afterwards heated to 90 °C for 1 hour. The reaction solution was poured into a water/ice mixture (500 ml) precipitating the crude product. The suspension was filtered through a Buechner funnel and the filter cake was dissolved in hot methanol (300 ml) to remove unreacted zinc by hot filtration through a sintered glass funnel. The product was recrystallised out of methanol, filtered through a Buechner funnel, washed with ice cold methanol, and dried in vacuum to obtain BnOOC–P[^{3}Me^{4}Ac]–Me (**28**) (11.8 g, 43.5 mmol, 57 % yield).

product		formula	g·mol^{-1}	%	mmol	g
BnOOC–P[^{3}Me^{4}Ac]–Me	**28**	$C_{16}H_{17}NO_3$	271.31	57	43.5	11.8

mp = 134 °C; **^{1}H-NMR** (300 MHz, $CDCl_3$) δ = 2.45, 2.50, 2.61 (s, 3H, CH_3), 5.32 (s, 2H, CH_2), 7.35–7.43, (m, 5H, CH), 8.86 (br.s, 1H, NH); **^{13}C-NMR** (75 MHz, $CDCl_3$) δ = 12.7, 15.2, 31.3 (CH_3), 66.1 (CH_2), 117.5, 123.7 (C_q), 128.3, 128.3, 128.6 (CH), 129.9, 135.9, 138.2 (C_q), 161.1, 195.4 (CO); **FT-IR** (ATR) [cm^{-1}] = 3171 w, 1682 s, 1627 s, 1477 s, 1276 s, 952 s, 813 s, 754 s, 699 s; **HR-MS** (pos. ESI) m/z = calculated 294.110–measured 294.109 for $C_{16}H_{17}NO_3$ +Na^+.

6.3.1.11 Synthesis of BnOOC–P[^{3}Me^{4}Cl-vinyl]–Me (27)[109]

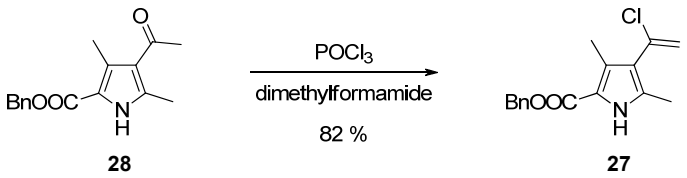

28 **27**

reactants		formula	g·mol^{-1}	eq.	mmol	µl	g·ml^{-1}	mg
BnOOC–P[^{3}Me^{4}Ac]–Me	**28**	$C_{16}H_{17}NO_3$	271.31	1.00	2.25			611
phosphorus oxychloride		Cl_3OP	153.33	1.05	2.36	219	1.65	362

BnOOC–P[^{3}Me^{4}Ac]–Me (**28**) (611 mg, 2.25 mmol, 1.00 eq.) was dissolved in dry dimethylformamide (3 ml) under protective gas and cooled to 0 °C. The solution was treated over a period of 10 minutes with phosphorus oxychloride (219 µl, 2.36 mmol, 1.05 eq.), stirred at 0 °C for 15 minutes, and additional 90 minutes at room temperature until thin layer chromatography showed complete transformation of the starting material **28**. The reaction mixture was then quenched with ice water (5 ml) and the resulting precipitate was filtered off, washed with water, and dried in vacuum to afford the BnOOC–P[^{3}Me^{4}Cl-vinyl]–Me (**27**) (537 mg, 1.85 mmol, 82 %).

product		formula	g·mol^{-1}	%	mmol	mg
BnOOC–P[^{3}Me^{4}Cl-vinyl]–Me	**27**	$C_{16}H_{16}ClNO_2$	289.76	82	1.85	537

mp = 95 °C; **^{1}H-NMR** (300 MHz, $CDCl_3$) δ = 2.30, 2.37 (s, 3H, CH_3), 5.21 (d, ^2J = 0.78 Hz 1H, CH), 5.30 (s, 2H, CH_2), 5.62 (d, ^2J = 0.72 Hz 1H, CH), 7.33–7.42, (m, 5H, CH), 8.73 (br.s, 1H, NH); **^{13}C-NMR** (75 MHz, $CDCl_3$) δ = 11.2, 12.4 (CH_3), 65.8, 117.1 (CH_2), 117.2, 122.2 (C_q), 127.5, 128.1, 128.2 (CH), 128.6, 131.6, 133.4, 136.3 (C_q), 161.2 (CO); **FT-IR** (ATR) [cm^{-1}] = 3288 s, 1660 s, 1434 s, 1272 s, 1186 s, 1102 s, 1066 s, 888 s, 772 s, 962 s.

6.3.1.12 Synthesis of BnOOC–P[^{3}Me^{4}alkyne]–Me (26)[109]

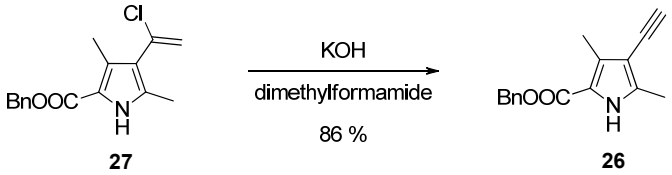

27 26

reactants		formula	g·mol^{-1}	eq.	mmol	mg
BnOOC–P[^{3}Me^{4}Cl-vinyl]–Me	**27**	$C_{16}H_{16}ClNO_2$	289.76	1.00	1.73	500
potassium hydroxide		HKO	56.11	1.21	2.09	117

BnOOC–P[^{3}Me^{4}Cl-vinyl]–Me (**27**) (500 mg, 1.73 mmol, 1.00 eq.) dissolved in dimethylformamide (5 ml) was treated with an aqueous solution of potassium hydroxide (117 mg, 2.09 mmol, 1.21 eq., in 1.4 ml H_2O). The reaction mixture was kept at 35 °C for 3 hours until thin layer chromatography reaction control showed complete conversion of **27**. The reaction mixture was diluted with dichloromethane (10 ml) and water (10 ml). The separated aqueous phase was extracted with dichloromethane (2·10 ml) and the combined organic phases were washed with water (3·10 ml), dried with sodium sulphate, and concentrated in vacuum. The resulting oily residue was purified *via* normal-phase chromatography (MPLC, SiO_2, 100 g, 50 µm, 50·2.5 cm, 280 nm, 20 ml·min^{-1} isocratic ^{n}hexane/ethyl acetate 7/3, retention time 9.5 minutes) to isolate BnOOC–P[^{3}Me^{4}alkyne]–Me (**26**) (375 mg, 1.48 mmol, 86 % yield).

product		formula	g·mol^{-1}	%	mmol	mg
BnOOC–P[^{3}Me^{4}alkyne]–Me	**26**	$C_{16}H_{15}NO_2$	253.30	86	1.48	375

mp = 113 °C; **^{1}H-NMR** (300 MHz, $CDCl_3$) δ = 2.32, 2.37 (s, 3H, CH_3), 3.17 (s, 1H, CH), 5.30 (s, 2H, CH_2), 7.33–7.42, (m, 5H, CH), 8.72 (br.s, 1H, NH); **^{13}C-NMR** (75 MHz, $CDCl_3$) δ = 11.6, 12.2 (CH_3), 65.9 (CH_2), 77.2 (C_q), 80.3 (CH), 105.6, 117.0 (C_q), 128.0, 128.2, 128.6 (CH), 131.5, 136.2, 137.4 (C_q), 161.1 (CO); **FT-IR** (ATR) [cm^{-1}] = 3290 s, 1664 s, 1431 s, 1274 s, 1093 s; 944 s, 728 s, 692 s; **HR-MS** (pos. ESI) m/z = calculated 276.100–measured 276.101 for $C_{16}H_{15}NO_2$ +Na^+.

6.3.1.13 Synthesis of BnOOC–P[^{3}Me^{4}COO^{t}Bu]–Me (33)[112]

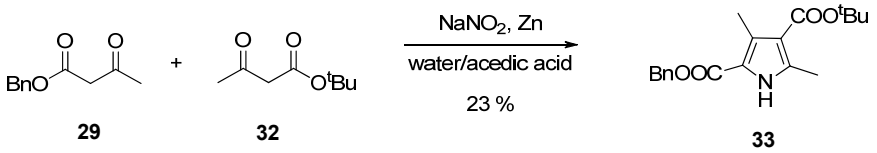

29 **32** **33**

reactants		formula	g·mol^{-1}	eq.	mmol	ml	g·ml^{-1}	g
benzyl acetoacetate	**29**	$C_6H_{10}O_3$	192.21	1.00	43.4	7.51	1.11	8.35
sodium nitrite		$NNaO_2$	69.00	1.00	43.4			3.00
^{t}butyl acetoacetate	**32**	$C_5H_8O_2$	158.19	1.00	43.4	7.20	0.954	6.87
sodium acetate		$C_{11}H_{15}NO_3$	82.03	0.845	36.7			3.01
zinc dust		Zn	65.41	2.03	117			7.67

Benzyl acetoacetate (**29**) (7.51 ml, 43.4 mmol, 1.00 eq.) diluted in glacial acetic acid (25 ml) was cooled to 5–10 °C, and a aqueous solution of sodium nitrite (3.00 g, 43.4 mmol, 1.00 eq., in 13 ml H_2O) was added by a dropping funnel. After addition and additional 15 minutes of stirring the reaction mixture was treated with a solution of ^{t}butyl acetoacetate (**32**) (7.20 ml, 43.4 mmol, 1.00 eq.) and sodium acetate (3.01 g, 36.7 mmol, 0.845 eq.) in glacial acetic acid (25 ml). Finally zinc dust (7.67 g, 117 mmol, 2.03 eq.) was added in small portions over a period of 35 minutes allowing the temperature to rise to 15 °C during the addition. To keep the product in solution an additional amount of acetic acid (25 ml) was added, and the reaction mixture was heated to reflux for 90 minutes before unreacted zinc was separated by hot filtration through a sintered glass funnel. The filtrate was poured into a water/ice mixture (400 ml), the oily residue was extracted with dichloromethane (3·100 ml), and the combined organic fractions were dried with sodium sulphate and concentrated in vacuum. The resulting oily residue was purified *via* normal-phase chromatography (MPLC, SiO_2, 100 g, 50 µm, 50·2.5 cm, 280 nm, 20 ml·min^{-1} isocratic ^{n}hexane/ethyl acetate 7/3, retention time 8.5 minutes) to isolate the BnOOC–P[^{3}Me^{4}COO^{t}Bu]–Me (**33**) (3.32 g, 10.1 mmol, 23 %) as pale yellow solid matter.

product		formula	g·mol^{-1}	%	mmol	g
BnOOC–P[^{3}Me^{4}COO^{t}Bu]–Me	**33**	$C_{19}H_{23}NO_4$	329.39	23	10.1	3.32

mp = 116 °C; ^{1}**H-NMR** (300 MHz, $CDCl_3$) δ = 1.56 (s, 9H, CH_3), 2.47, 2.56 (s, 3H, CH_3), 5.29 (s, 2H, CH_2) 7.33–7.41 (m, 5H, CH), 8.84 (br.s, 1H, NH); ^{13}**C-NMR** (75 MHz, $CDCl_3$)

δ = 12.1, 14.4, 28.5 (CH_3), 65.9 (CH_2), 80.0, 115.1, 117.3 (C_q), 128.1, 128.2, 128.6 (CH), 131.4, 136.1, 138.8 (C_q), 161.3, 164.7 (CO); **FT-IR** (ATR) [cm^{-1}] = 3303 s, 2973 w, 1687 s, 1655 s, 1425 s, 1268 s, 1167 s, 1082 s, 752 s, 698 s; **HR-MS** (pos. ESI) m/z = calculated 352.153–measured 352.101 for $C_{19}H_{23}NO_4 + Na^+$.

6.3.1.14 Synthesis of HOOC–P[^{3}Me^{4}COO^{t}Bu]–Me (34)

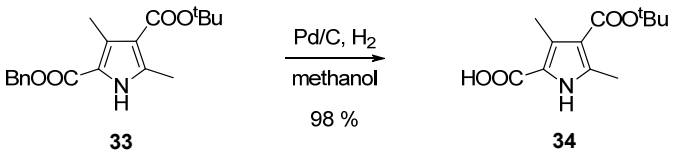

33 **34**

reactants		formula	g·mol^{-1}	eq.	mmol	g
BnOOC–P[^{3}Me^{4}COO^{t}Bu]–Me	**33**	$C_{19}H_{23}NO_4$	329.39	1.00	3.04	1.00
palladium 10 % on carbon		Pd/C	106.42	0.0310	0.0940	0.100

BnOOC–P[^{3}Me^{4}COO^{t}Bu]–Me (**33**) (1.00 g, 3.04 mmol, 1.00 eq.) and palladium 10 % on carbon (0.100 g, 0.0940 mmol, 0.0310 eq.) were suspended in methanol (50 ml) under protective gas. The suspension was stirred for 2.5 hours under hydrogen atmosphere until thin layer chromatography control showed complete transformation of the starting material. The catalyst was separated *via* filtration through a nylon filter (0.2 µm pore size) and the filtrate concentrated under reduced pressure to obtain the colourless HOOC–P[^{3}Me^{4}COO^{t}Bu]–Me (**34**) (709 mg, 2.96 mmol, 98 % yield).

product		formula	g·mol^{-1}	%	mmol	mg
HOOC–P[^{3}Me^{4}COO^{t}Bu]–Me	**34**	$C_{12}H_{17}NO_4$	239.27	98	2.96	709

mp = 97 °C; ^{1}**H-NMR** (300 MHz, $DMSO_{d6}$) δ = 1.49 (s, 9H, CH_3), 2.36, 2.42 (s, 3H, CH_3), 11.65 (br.s, 1H, NH); ^{13}**C-NMR** (75 MHz, $DMSO_{d6}$) δ = 11.8, 13.6, 28.2 (CH_3), 78.9, 113.4, 118.0, 128.9, 138.5 (C_q), 162.3, 164.2 (CO); **FT-IR** (ATR) [cm^{-1}] = 1655 s, 1570 w, 1433 m, 1366 w, 1274 s, 1169 s, 1121 s, 1084 s, 786 m, 709 w; **HR-MS** (neg. ESI) m/z = calculated 238.109–measured 238.110 for $C_{12}H_{17}NO_4$ -H^+.

6.3.1.15 Synthesis of CbzG–P[^{3}Me^{4}COO^{t}Bu]–Me (35)

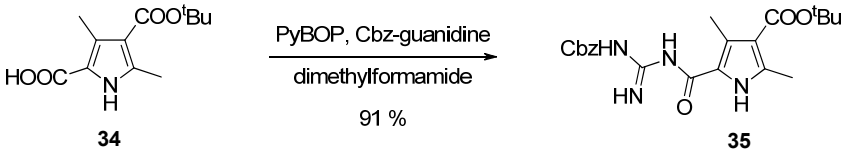

reactants		formula	g·mol^{-1}	eq.	mmol	ml	g·ml^{-1}	mg
HOOC–P[^{3}Me^{4}COO^{t}Bu]–Me	**34**	$C_{12}H_{17}NO_4$	239.27	1.00	2.72			650
PyBOP		$C_{18}H_{28}F_6N_6OP_2$	520.39	1.20	3.26			1696
diisopropylethylamine		$C_8H_{19}N$	129.24	3.00	8.15	1.42	0.74	1053
Cbz-guanidine[i]		$C_9H_{11}N_3O_2$	193.20	1.20	3.26			630
4-dimethylaminopyridine		$C_7H_{10}N_2$	122.17	0.20	0.54			66.4

HOOC–P[^{3}Me^{4}COO^{t}Bu]–Me (**34**) (650 mg, 2.72 mmol, 1.00 eq.), PyBOP (1696 mg, 3.26 mmol, 1.20 eq.) and diisopropylethylamine (1.42 ml, 8.15 mmol, 3.00 eq.) were dissolved in dimethylformamide (5 ml). Cbz-guanidine (630 mg, 3.26 mmol, 1.20 eq.) and 4-dimethylaminopyridine (66.4 mg, 0.543 mmol, 0.20 eq.) were added after 5 minutes. The reaction solution was stirred at room temperature and then poured into ice water (200 ml) after 16 hours. The resulting suspension was filtered through a Buechner funnel. The filter cake was washed with water and dried in vacuum to obtain CbzG–P[^{3}Me^{4}COO^{t}Bu]–Me (**35**) (1.03 g, 2.47 mmol, 91 % yield).

product		formula	g·mol^{-1}	%	mmol	g
CbzG–P[^{3}Me^{4}COO^{t}Bu]–Me	**35**	$C_{21}H_{26}N_4O_5$	414.45	91	2.47	1.03

mp = 79–80 °C; **^{1}H-NMR** (300 MHz, $DMSO_{d6}$) δ = 1.49 (s, 9H, CH_3), 2.37, 2.53, (s, 3H, CH_3), 5.16 (s, 2H, CH_2), 7.39–7.41 (m, 5H, CH), 8.55, 9.37, 10.69, 11.42 (br.s, 1H, NH); **^{13}C-NMR** (75 MHz, $DMSO_{d6}$) δ = 12.2, 13.8, 28.1 (CH_3), 66.4 (CH_2), 78.8, 113.7 (C_q), 127.8, 128.0, 128.4 (CH), 136.2, 138.0 (C_q), 158.1, 164.2 (CO); **FT-IR** (ATR) [cm^{-1}] = 1627 m, 1496 w, 1422 m, 1268 s, 1204 m, 1087 m, 937 w, 739 w, 696 w; **HR-MS** (pos. ESI) m/z = calculated 415.198–measured 415.199 for $C_{21}H_{26}N_4O_5$ +H^{+}.

[i] Cbz-guanidine was synthesised according to literature procedure.[103]

6.3.1.16 Synthesis of CbzG–P[^{3}Me^{4}COOH]–Me (36)

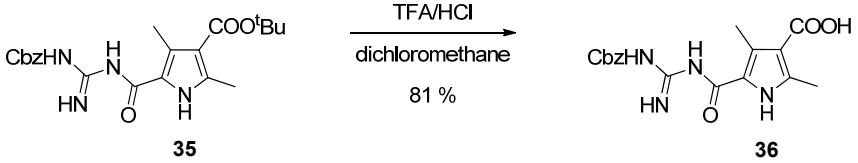

reactant		formula	g·mol^{-1}	eq.	mmol	µl	g·ml^{-1}	g
CbzG–P[^{3}Me^{4}COO^{t}Bu]–Me	**35**	$C_{21}H_{26}N_4O_5$	414.45	1.00	2.29			0.95
trifluoroacetic acid		$C_2HF_3O_2$	114.02	5.00	11.5	883	1.48	1.31
hydrochloric acid 37%		ClH	36.46	10.0	22.9	702	1.19	0.84

A solution of CbzG–P[^{3}Me^{4}COO^{t}Bu]–Me (**35**) (950 mg, 2.29 mmol, 1.00 eq.) in dichloromethane (15 ml) was treated with trifluoroacetic acid (883 µl, 11.5 mmol, 5.00 eq.) and hydrochloric acid (37 %, 702 µl, 22.9 mmol, 10.0 eq.), leading to a precipitation of a white solid. Thin layer chromatography reaction control showed complete ester cleavage after 3 hours. The reaction mixture was diluted with dichloromethane (10 ml) and sodium bicarbonate (40 ml) and filtered through a Buechner funnel. The filter cake was washed with water and dried in vacuum to afford the CbzG–P[^{3}Me^{4}COOH]–Me (**36**) (661 mg, 1.85 mmol, 80 % yield) as white solid matter.

product		formula	g·mol^{-1}	%	mmol	g
CbzG–P[^{3}Me^{4}COOH]–Me	**36**	$C_{17}H_{18}N_4O_5$	358.35	80	1.85	0.66

mp = 225–226 °C; ^{1}**H-NMR** (300 MHz, $DMSO_{d6}$) δ = 2.40, 2.55 (s, 3 H, CH_3), 5.12 (s, 2 H, CH_2), 7.32–7.34 (m, 6 H, CH, NH), 8.63, 9.41, 11.51 (br.s, 1H, NH); ^{13}**C-NMR** (75 MHz, $DMSO_{d6}$) δ = 12.3, 13.8 (CH_3), 66.1 (CH_2), 121.3, 124.2 (C_q), 127.7, 127.9, 128.4 (CH), 130.1, 136.6, 138.0 (C_q), 158.7, 160.1, 167.6 (CO); **FT-IR** (ATR) [cm^{-1}] = 3294 w, 1625 m, 1494 w, 1261 s, 1190 s, 995 w, 892 w, 831 w, 695 m; **HR-MS** (pos. ESI) m/z = calculated 359.135–measured 359.135 for $C_{17}H_{18}N_4O_5$ +H^{+}.

6.3.1.17 Synthesis of CbzG–P[^{3}Me^{4}prop-2-inyl]–Me (37)

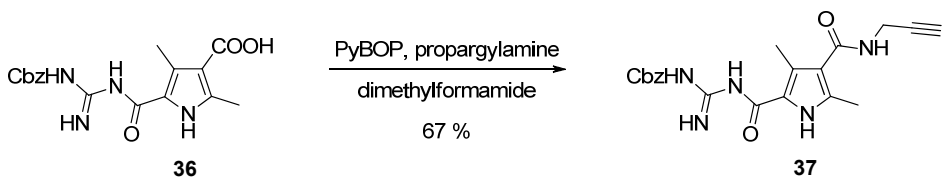

36 **37**

reactants		formula	g·mol^{-1}	eq.	mmol	ml	g·ml^{-1}	mg
CbzG–P[^{3}Me^{4}COOH]–Me	**36**	$C_{17}H_{18}N_4O_5$	358.35	1.00	1.68			600
PyBOP		$C_{18}H_{28}F_6N_6OP_2$	520.39	1.20	2.01			1046
diisopropylethylamine		$C_8H_{19}N$	129.24	3.00	5.02	0.88	0.74	649
propargylamine		C_3H_5N	55.08	1.20	2.01	0.13	0.86	111
4-dimethylaminopyridine		$C_7H_{10}N_2$	122.17	0.20	0.34			40.9

CbzG–P[^{3}Me^{4}COOH]–Me (**36**) (600 mg, 1.68 mmol, 1.00 eq.), PyBOP (1046 mg, 2.01 mmol, 1.20 eq.), and diisopropylethylamine (0.88 ml, 5.02 mmol, 3.00 eq.) were dissolved in dimethylformamide (5 ml). Propargylamine (0.13 ml, 2.01 mmol, 1.20 eq.) and 4-dimethylaminopyridine (40.9 mg, 0.34 mmol, 0.20 eq.) were added after 5 minutes, and the mixture was stirred for 12 hours at room temperature. The reaction solution was poured into ice water (150 ml) and the precipitated solid was separated by filtration and purified *via* normal-phase chromatography (MPLC, SiO_2, 100 g, 50 µm, 50· 2.5 cm, 295 nm, 20 ml·min^{-1}, isocratic dichloromethane/methanol 9.2/0.8, retention time 7.5 minutes) to isolate CbzG–P[^{3}Me^{4}prop-2-inyl]–Me (**37**) (446 mg, 1.13 mmol, 67 % yield).

product		formula	g·mol^{-1}	%	mmol	mg
CbzG–P[^{3}Me^{4}prop-2-inyl]–Me	**37**	$C_{20}H_{21}N_5O_4$	395.41	67.4	1.13	446

mp = 156 °C; **^{1}H-NMR** (300 MHz, $DMSO_{d6}$) δ = 2.28, 2.41 (s, 3 H, CH_3), 3.07 (t, ^{4}J = 2.63 Hz, 1H, CH), 3.96 (dd, ^{3}J = 5.64 Hz, ^{4}J = 2.40 Hz, 2H CH_2), 5.14 (s, 2 H, CH_2), 7.33–7.40 (m, 5 H, CH), 7.89 (t, ^{3}J = 5.67 Hz, 1H, NH), 8.58, 9.34, 11.32, 11.68 (br.s, 1H, NH); **^{13}C-NMR** (75 MHz, $DMSO_{d6}$) δ = 11.8, 12.4 (CH_3), 27.9 (CH_2), 66.3 (CH_2), 72.4 (CH), 81.8, 118.9, 121.5, 126.6 (C_q), 127.8, 128.0, 128.4 (CH), 133.6, 136.4 (C_q), 158.3, 158.7, 163.3, 164.8 (CN, CO); **FT-IR** (ATR) [cm^{-1}] = 3248 w, 1685 w, 1632 s, 1524 m, 1428 m, 1274 s, 1190 m, 1017 w, 774 m, 724 m, 690 s; **HR-MS** (pos. ESI) m/z = calculated 396.167–measured 396.169 for $C_{20}H_{21}N_5O_4$ +H^{+}.

6.3.1.18 Synthesis of CbzG–P[^{3}Me^{4}G1]–Me (38)[89]

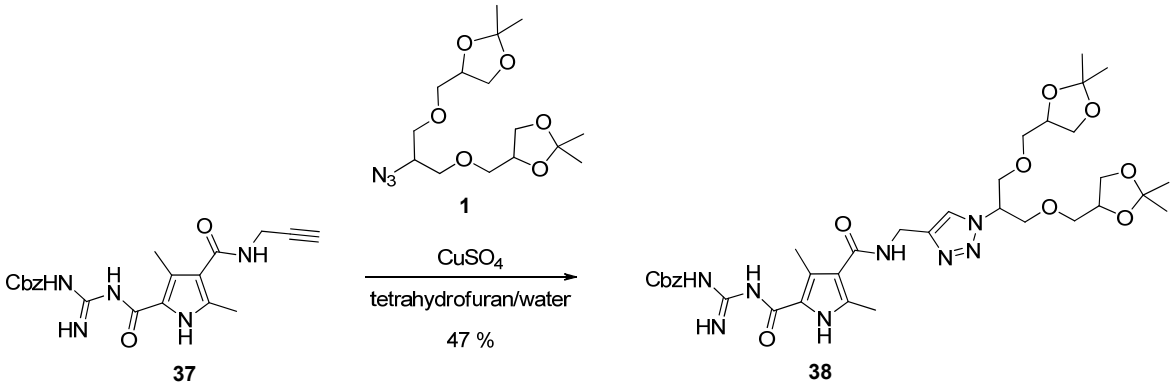

reactants		formula	g·mol^{-1}	eq.	µmol	µl	g·ml^{-1}	mg
CbzG–P[^{3}Me^{4}prop-2-inyl]–Me	**37**	$C_{20}H_{21}N_5O_4$	395.41	1.00	632			250
G1–N_3	**1**	$C_{15}H_{27}N_3O_6$	345.39	1.20	759			262
diisopropylethylamine		$C_8H_{19}N$	129.24	0.200	126	22.0	0.74	16.3
sodium ascorbate		$C_6H_7NaO_6$	198.11	0.200	126			25.1
copper(II)sulphate pentahydrate		$CuH_{10}O_9S$	249.69	0.100	63.0			15.8

CbzG–P[^{3}Me^{4}prop-2-inyl]–Me (**37**) (250 mg, 632 µmol, 1.00 eq.), G1–N_3 (**1**) (262 mg, 759 µmol, 1.20 eq.), and diisopropylethylamine (22.0 µl, 126 µmol, 0.200 eq.) were dissolved in a tetrahydrofuran (2 ml) water (1.4 ml) mixture. Sodium ascorbate (25.1 mg, 126 µmol, 0.200 eq.) and copper(II)sulphate pentahydrate (15.8 mg, 63.0 µmol, 0.100 eq.) were added after 5 minutes–as freshly prepared aqueous solutions (300 µl each). The colour of the reaction mixture changed to dark green after 30 minutes and HPLC reaction control indicated complete conversion. The solvents were evaporated by reduced pressure after 3 hours stirring time, and the crude product was purified *via* normal-phase chromatography (MPLC, SiO_2, 100 g, 50 µm, 50·2.5 cm, 300 nm, 20 ml·min^{-1}, isocratic dichloromethane/^{i}propanol 9/1 for 30 minutes, retention time 17 minutes) to afford CbzG–P[^{3}Me^{4}G1]–Me (**38**) (52.0 mg, 0.07 mmol, 27 % yield).

product		formula	g·mol^{-1}	%	µmol	mg
CbzG–P[^{3}Me^{4}G1]–Me	**38**	$C_{35}H_{48}N_8O_{10}$	740.80	47	297	220

mp = 55–57 °C; ^{1}**H-NMR** (500 MHz, $DMSO_{d6}$) δ = 1.22, 1.27 (s, 6H, CH_3), 2.29, 2.41 (s, 3 H, CH_3), 3.36–3.46 (m, 4H, CH_2), 3.48–3.52 (m, 2H, CH_2), 3.80–3.90 (m, 6H, CH_2), 4.06–4.11 (m, 2H, CH), 4.44 (d, ^{3}J = 6.30 Hz, CH_2), 4.93–4.98 (m, 1H, CH), 5.14 (s, 2H, CH_2),

7.31–7.39 (m, 5H, CH), 7.92 (s, 1H, CH), 7.96, 8.58, 9.32, 10.88, 11.30 (br.s, 1H, NH); **^{13}C-NMR** (125 MHz, $DMSO_{d6}$) δ = 11.8, 12.4, 25.3, 26.5 (CH_3), 34.5 (CH_2), 59.7 (CH), 65.7, 66.2, 69.8, 69.9, 71.4, 71.6 (CH_2), 74.0, 74.1 (CH), 108.5, 118.2 (C_q), 122.2, 127.8, 127.9, 128.4 (CH), 133.3, 136.3, 145.2, 165.0 (CO); **FT-IR** (ATR) [cm^{-1}] = 3371 w, 3268 w, 2871 w, 1739 w, 1627 m, 1531 m, 1492 m, 1371 m, 1266 s, 1207 s, 1082 m, 1044 m, 835 m, 751 m, 699 m; **HR-MS** (pos. ESI) m/z = calculated 763.387–measured 763.340 for $C_{35}H_{48}N_8O_{10} + Na^+$.

6.3.1.19 Synthesis of G–P[^{3}Me^{4}G1]–Me (39)

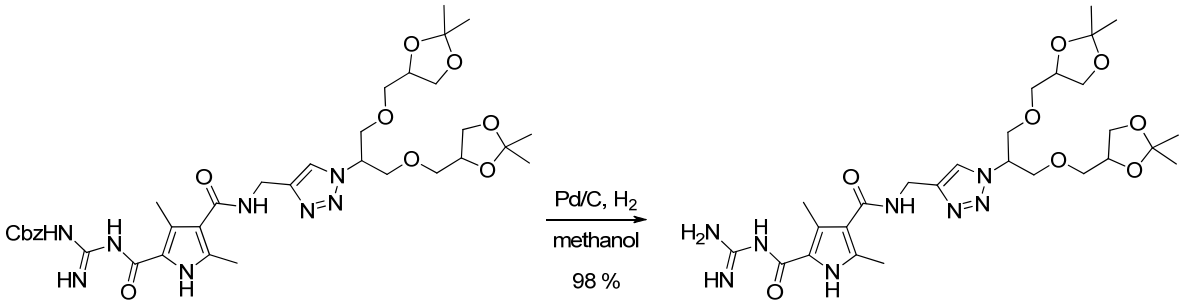

38 **39**

reactants		formula	g·mol^{-1}	eq.	µmol	mg
CbzG–P[^{3}Me^{4}G1]–Me	**38**	$C_{35}H_{48}N_8O_{10}$	740.80	1.00	60.7	45.0
palladium 10 % on carbon		Pd/C	106.42	0.100	6.07	6.46

CbzG–P[^{3}Me^{4}G1]–Me (**38**) (45.0 mg, 60.7 µmol, 1.00 eq.) and palladium 10 % on carbon (6.46 mg, 6.07 µmol, 0.100 eq.) were suspended in methanol (10 ml) under protective gas. The suspension was stirred for 2 hours in a hydrogen atmosphere until thin layer chromatography control showed complete cleavage of the Cbz-group. The catalyst was removed by a syringe filter (nylon, 0.2 µm pore size), and the solvent was evaporated under reduced pressure to obtain the colourless G–P[^{3}Me^{4}G1]–Me (**39**) (36.0 mg, 0.06 mmol, 98 % yield).

product		formula	g·mol^{-1}	%	mmol	mg
G–P[^{3}Me^{4}G1]–Me	**39**	$C_{27}H_{42}N_8O_8$	606.67	98	0.06	36.0

mp = 75–78 °C; ^{1}**H-NMR** (500 MHz, $DMSO_{d6}$) δ = 1.23 (s, 6H, CH_3), 1.27, 1.27, 2.27, 2.44 (s, 3H, CH_3), 3.36–3.46 (m, 4H, CH_2), 3.49–3.52 (m, 2H, CH_2), 3.80–3.91 (m, 6H, CH_2), 4.06–4.11 (m, 2H, CH), 4.43 (d, ^{3}J = 5.65 Hz, CH_2), 4.93–4.98 (m, 1H, CH), 7.06 (br.s, 3 H, NH), 7.70 (t, ^{3}J = 5.75 Hz, 1H, NH), 7.91 (s, 1H, CH), 10.67 (br.s, 1H, NH); ^{13}**C-NMR** (125 MHz, $DMSO_{d6}$) δ = 11.8, 12.4, 25.3, 26.6 (CH_3), 34.4 (CH_2), 59.7 (CH), 65.7, 69.9, 69.9, 71.4, 71.6 (CH_2), 74.0, 74.1 (CH), 108.5, 117.9 (C_q), 122.1 (CH), 122.3, 125.4, 130.9, 145.5 (C_q), 162.1, 165.8, 171.6 (CN, CO); **FT-IR** (ATR) [cm^{-1}] = 3346 w, 3300 w, 2949 w, 1628 w, 1523 m, 1492 s, 1429 m, 1375 m, 1303 s, 1209 m, 1085 m, 1045 m, 840 m, 796 m; **HR-MS** (pos. ESI) m/z = calculated 310.105–measured 310.106 for $C_{16}H_{17}NO_4$ +Na^+.

6.3.1.20 Synthesis of CbzG–P[^{3}Me^{4}G1(OH)$_4$]–Me (40)

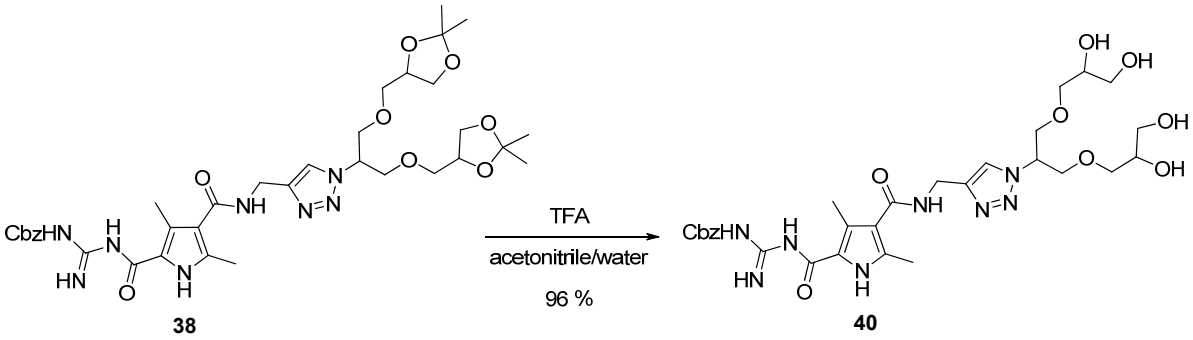

reactants		formula	g·mol^{-1}	eq.	mmol	µl	g·ml^{-1}	mg
CbzG–P[^{3}Me^{4}G1]–Me	**38**	$C_{35}H_{48}N_8O_{10}$	740.80	1.00	0.175			130
trifluoroacetic acid (TFA)		$C_2HF_3O_2$	114.02	20	3.51	270	1.48	400

A solution of CbzG–P[^{3}Me^{4}G1]–Me (**38**) (130 mg, 0.175 mmol, 1.00 eq.) in acetonitrile/water (1:1, 1 ml) was treated with trifluoroacetic acid (270 µl, 3.51 mmol, 20 eq.). The reaction was monitored *via* HPLC reaction control and a complete cleavage of acetal groups was detected after 3 hours. The crude product was purified *via* reversed-phase chromatography (MPLC, RP18, ODS-A, 50 µm, 300 nm, 25 ml·min^{-1}, gradient from 40 % to 70 % methanol in 15 min, retention time 13.5 min) to obtain colourless CbzG–P[^{3}Me^{4}G1(OH)$_4$]–Me (**40**) (111 mg, 168 µmol, 96 % yield).

product		formula	g·mol^{-1}	%	µmol	mg
CbzG–P[^{3}Me^{4}G1(OH)$_4$]–Me	**40**	$C_{29}H_{40}N_8O_{10}$	660.68	96	168	111

mp = 84 °C; ^{1}**H-NMR** (300 MHz, $DMSO_{d6}$) δ = 2.29, 2.42 (s, 3H, CH_3), 3.24, 3.26 (s, 2H, OH), 3.27–3.55 (m, 10H, CH_2), 3.77–3.87 (m, 4H, CH, CH_2), 4.43 (d, ^{3}J = 5.61 Hz, CH_2), 4.89–4.96 (m, 1H, CH), 5.14 (s, 2H, CH_2), 7.31–7.39 (m, 5H, CH), 7.95 (s, 1H, CH), 7.96, 8.58, 9.33, 10.58, 11.30 (br.s, 1H, NH); ^{13}**C-NMR** (75 MHz, $DMSO_{d6}$) δ = 11.8, 12.4, (CH_3), 34.5 (CH_2), 60.0 (CH_2), 62.9 (CH), 69.9, 70.0 (CH_2), 70.3, 70.4 (CH), 72.7, 72.8 (CH_2), 119.3 (C_q), 122.2, 127.7, 127.9, 128.4 (CH), 145.2 (C_q), 165.0 (CO); **FT-IR** (ATR) [cm^{-1}] = 3374 w, 3271 w, 2924 w, 2875 w, 1733 w, 1624 m, 1529 m, 1495 m, 1420 m, 1375 m, 1277 s, 1206 s, 1115 m, 1038 m, 934 w, 749 m, 697 m; **HR-MS** (pos. ESI) m/z = calculated 683.276–measured 683.281 for $C_{29}H_{40}N_8O_{10}$ +Na^+.

6.3.1.21 Synthesis of G–P[^{3}Me^{4}G1(OH)$_4$]–Me (41)

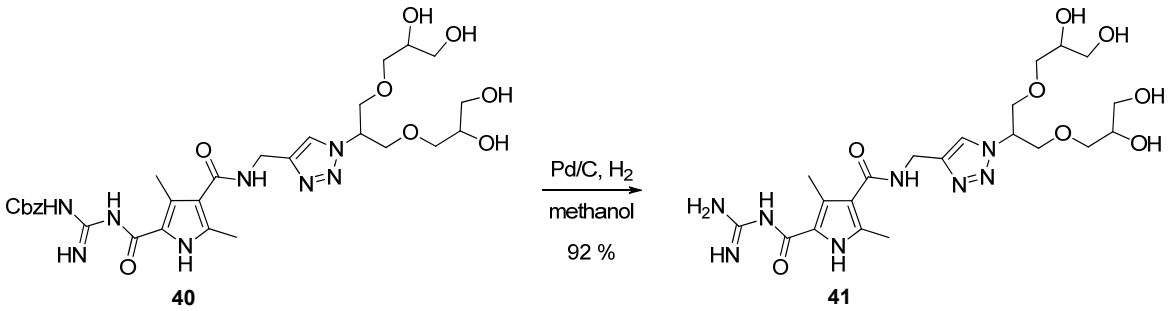

40 41

reactants		formula	g·mol^{-1}	eq.	µmol	mg
CbzG–P[^{3}Me^{4}G1OH$_4$]–Me	**40**	$C_{29}H_{40}N_8O_{10}$	660.68	1.00	136	90.0
palladium 10 % on carbon		Pd/C	106.42	0.100	13.6	14.5

A suspension of CbzG–P[^{3}Me^{4}G1(OH)$_4$]–Me (**40**) (90.0 mg, 136 µmol, 1.00 eq.) and palladium 10 % on carbon (14.5 mg, 13.6 µmol, 0.100 eq.) in methanol (15 ml) was stirred for 2 hours in a hydrogen atmosphere until HPLC reaction control indicated complete conversion of the starting material **40**. The catalyst was separated by a syringe filter (nylon, 0.2 µm pore size) and the solvent was evaporated under reduced pressure to afford colourless G–P[^{3}Me^{4}G1(OH)$_4$]–Me (**41**) (66.0 mg, 0.125 mmol, 92 % yield).

product		formula	g·mol^{-1}	%	mmol	mg
G–P[^{3}Me^{4}G1(OH)$_4$]–Me	**41**	$C_{21}H_{34}N_8O_8$	526.54	92	0.125	66.0

mp = 88–90 °C; ^{1}**H-NMR** (300 MHz, DMSO$_{d6}$) δ = 2.27, 2.44 (s, 3H, CH$_3$), 3.24–3.26 (m, 4H, OH), 3.26–3.31 (m, 2H, CH$_2$), 3.35–3.43 (m, 2H, CH$_2$), 3.50 (br.s, 2H, CH$_2$), 3.76–3.87 (m, 4H, CH$_2$), 4.43 (d, ^{3}J = 5.94 Hz, CH$_2$), 4.46 (br.s, 2H, CH$_2$), 4.62–4.64 (m, 2H, CH), 4.88–4.96 (m, 1H, CH), 7.06 (br.s, 3 H, NH), 7.70 (t, ^{3}J = 5.91 Hz, 1H, NH), 7.93 (s, 1H, CH), 10.67 (br.s, 1H, NH); ^{13}**C-NMR** (75 MHz, DMSO$_{d6}$) δ = 11.8, 12.4 (CH$_3$), 34.5 (CH$_2$), 60.0 (CH), 62.9, 69.9, 70.0 (CH$_2$), 70.3, 70.4 (CH), 72.6, 72.7 (CH$_2$), 117.9 (C$_q$), 122.1 (CH), 122.3, 125.4, 130.9, 145.3 (C$_q$), 162.0, 165.8, 171.6 (CN, CO); **FT-IR** (ATR) [cm^{-1}] = 3392 w, 3258 w, 2967 w, 2883 w, 1734 m, 1627 m, 1547 w, 1502 w, 1275 m, 1207 s, 1119 m, 1024 w, 752 m, 702 m; **HR-MS** (pos. ESI) m/z = calculated 527.257–measured 527.256 for $C_{21}H_{34}N_8O_8$ +H^{+}.

6.3.2 Zwitterionic Dendrons

6.3.2.1 Synthesis of ^{t}BuOOC–P[^{3}Me^{4}(CH$_2$)$_2$COOMe]–COOH (43)

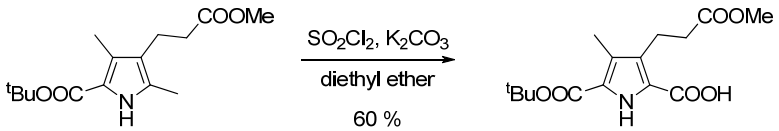

42 **43**

reactants		formula	g·mol^{-1}	eq.	mmol	ml	g ml^{-1}	g
^{t}BuOOC–P[^{3}Me^{4}(CH$_2$)$_2$COOMe]–Me[i]	**42**	$C_{15}H_{23}NO_4$	281.35	1.00	23.4			6.58
potassium carbonate		CK_2O_3	138.21	4.00	94.0			12.9
sulfuryl chloride		Cl_2O_2S	134.97	3.70	87.0	7.04	1.66	11.7
sodium acetate		$C_2H_3NaO_2$	82.03	10.4	244			20.0

A cooled (-20 °C) suspension of ^{t}BuOOC–P[^{3}Me^{4}(CH$_2$)$_2$COOMe]–Me (42) (6.58 g, 23.4 mmol, 1.00 eq.) and potassium carbonate (12.9 g, 94.0 mmol, 4.00 eq.) in dry diethyl ether (100 ml) was treated with sulfuryl chloride (7.04 ml, 87.0 mmol, 3.70 eq.) under protective gas. The reaction mixture was stirred at 40 °C for 7 hours then the organic solvent was removed under vacuum (heat bath = 30 °C), and the resulting residue was treated with a aqueous solution of sodium acetate (20.0 g, 244 mmol, 10.4 eq., in 400 ml H_2O/1,4-dioxane, 1/1). The reaction mixture was stirred at room temperature for 15 hours and at 110 °C for one further hour. The cooled (0 °C) solution was acidified to pH 2 with hydrochloric acid (5 %), and extracted with diethyl ether (8·50 ml). The combined organic phases were reextracted with a water/saturated-sodium-bicarbonate solution (1/1, 9·50 ml). The cooled (-5 °C) combined aqueous fractions were acidified under vigorous stirring to pH 2 with concentrated hydrochloric acid (37 %). The precipitated solid was filtered, washed with water (150 ml), and dried in vacuum to isolate ^{t}BuOOC–P[^{3}Me^{4}(CH$_2$)$_2$COOMe]–COOH (43) (4.40 g, 14.2 mmol, 60 % yield).

product		formula	g·mol^{-1}	%	mmol	g
^{t}BuOOC–P(^{3}Me^{4}(CH$_2$)$_2$COOMe]–COOH	**43**	$C_{15}H_{21}NO_6$	311.33	60	14.1	4.39

mp = 166 °C; **^{1}H-NMR** (400 MHz, $DMSO_{d6}$) δ = 1.52 (s, 9H, CH_3), 2.17 (s, 3H, CH_3), 2.44 (t, ^{3}J = 7.84 Hz, 2H, CH_2), 2.90 (t, ^{3}J = 7.82 Hz, 2H, CH_2), 3.57 (s, 3H, CH_3), 11.27 (br.s,

[i] ^{t}BuOOC–P[^{3}Me^{4}(CH$_2$)$_2$COOMe]–Me (42) was synthesised according to literature procedure.[116]

1H, NH), 12.70 (br.s, 1H, COOH); **^{13}C-NMR** (100 MHz, $DMSO_{d6}$) δ = 9.7 (CH_3), 19.7 (CH_2), 30.0 (CH_3), 34.3 (CH_2), 51.2 (CH_3), 80.6, 122.0, 122.7, 125.0, 128.5 (C_q), 160.0, 161.7, 172.7 (CO); **FT-IR** (ATR) [cm^{-1}] = 3473 m, 3340 m, 2977 m, 1738 s, 1697 s, 1674 s, 1565 w, 1470 m, 1369 m, 1279 s, 1154 s, 1075 m, 847 w, 783 w; **HR-MS** (pos. ESI) m/z = calculated 334.126–measured 334.126 for $C_{15}H_{21}NO_6$ +Na^+.

6.3.2.2 Synthesis of ^{t}BuOOC–P[^{3}Me^{4}(CH$_2$)$_2$COOMe]–BocG (44)[116]

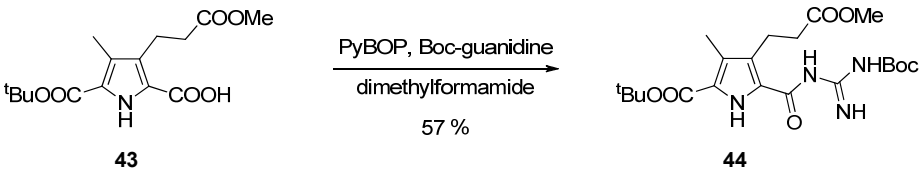

43 **44**

reactant		formula	g·mol^{-1}	eq.	mmol	ml	g·ml^{-1}	g
^{t}BuOOC–P[^{3}Me^{4}(CH$_2$)$_2$COOMe]–COOH	**43**	$C_{15}H_{21}NO_6$	311.33	1.00	5.94			1.85
4-methylmorpholine		$C_5H_{11}NO$	101.15	1.53	9.10	1.00	0.92	0.92
PyBOP		$C_{18}H_{28}F_6N_6OP_2$	520.39	1.00	5.94			3.09
Boc-guanidine		$C_6H_{13}N_3O_2$	159.19	1.00	5.94			0.95
4-dimethylaminopyridine		$C_7H_{10}N_2$	122.17	0.10	0.59			0.07

To a solution of ^{t}BuOOC–P[^{3}Me^{4}(CH$_2$)$_2$COOMe]–COOH (**43**) (1.85 g, 5.94 mmol, 1.00 eq.) and 4-methylmorpholine (1.00 ml, 9.10 mmol, 1.53 eq.) in dimethylformamide (15 ml) PyBOP (3.09 g, 5.94 mmol, 1.00 eq.), Boc-guanidine (0.95 g, 5.94 mmol, 1.00 eq.), and 4-dimethylaminopyridine (0.07 g, 0.59 mmol, 0.10 eq.) were added. The reaction mixture was stirred for 16 hours then quenched with water (100 ml), and filtered through a Buchner funnel to isolate the precipitated solid. The filtrate was extracted with dichloromethane (3·50 ml) and the solvent of the combined organic fractions was removed in vacuum. The filtered and extracted crude product was purified *via* normal phase column chromatography (SiO_2, ethyl acetate/cyclohexane, 3/7) to isolate ^{t}BuOOC–P[^{3}Me^{4}(CH$_2$)$_2$COOMe]–BocG (**44**) (1.54 g, 3.40 mmol, 60 % yield) as colourless solid matter.

product		formula	g·mol^{-1}	%	mmol	g
^{t}BuOOC–P[^{3}Me^{4}(CH$_2$)$_2$COOMe]–BocG	**44**	$C_{21}H_{32}N_4O_7$	452.50	57	3.40	1.54

mp = 133 °C; **^{1}H-NMR** (400 MHz, $DMSO_{d6}$) δ = 1.48, 1.53 (s, 9H, CH_3), 2.17 (s, 3H, CH_3), 2.47 (t, ^{3}J = 7.52 Hz, 2H, CH_2), 2.97 (t, ^{3}J = 7.80 Hz, 2H, CH_2), 3.57 (s, 3H, CH_3), 8.44, 9.42, 10.10, 10.56 (br.s, 1H, NH); **^{13}C-NMR** (100 MHz, $DMSO_{d6}$) δ = 9.7 (CH_3), 19.8 (CH_2), 27,7, 28.0 (CH_3), 34.2 (CH_2), 51.1 (CH_3), 79.8, 80.7, 125.2 (C_q), 160.2, 169.9, 172.7 (CO); **FT-IR** (ATR) [cm^{-1}] = 3378 w, 2978 w, 1727 m, 1693 m, 1628 s, 1530 m, 1454 m, 1367 m, 1290 s, 1233 s, 1137 m, 837 w, 752 w; **HR-MS** (pos. ESI) m/z = calculated 475.216– measured 475.219 for $C_{21}H_{32}N_4O_7$ +Na^+.

6.3.2.3 Synthesis of ^{t}BuOOC–P[^{3}Me^{4}(CH$_2$)$_2$COOH]–BocG (45)

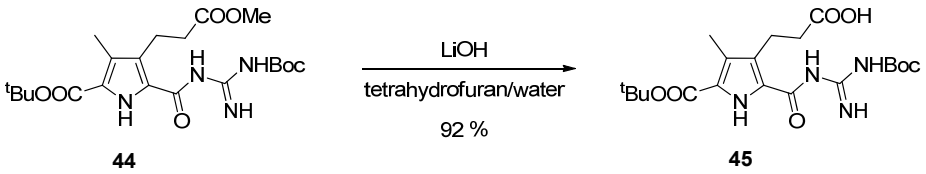

44 **45**

reactants		formula	g·mol^{-1}	eq.	mmol	g
tBuOOC–P[^{3}Me^{4}(CH$_2$)$_2$COOMe]–BocG	**44**	$C_{21}H_{32}N_4O_7$	452.50	1.00	3.54	1.60
lithium hydroxide		HLiO	23.95	6.00	21.2	0.508

A mixture of ^{t}BuOOC–P[^{3}Me^{4}(CH$_2$)$_2$COOMe]–BocG (44) (1.60 g, 3.54 mmol, 1.00 eq.) lithium hydroxide (0.508 g, 21.2 mmol, 6.00 eq.) in water/tetrahydrofuran (110 ml, 6/5) was stirred at 40 °C. Tetrahydrofuran was evaporated in vacuum after TLC reaction control indicated complete ester cleavage (after 1 hour), and the resulting aqueous suspension was acidified with hydrochloric acid (5 %). The precipitated solid was filtered off by a Buechner funnel, washed with water, and dried in vacuum to obtain ^{t}BuOOC–P[^{3}Me^{4}(CH$_2$)$_2$COOH]–BocG (45) (1.43 g, 3.26 mmol, 92 % yield).

product		formula	g·mol^{-1}	%	mmol	g
^{t}BuOOC–P[^{3}Me^{4}(CH$_2$)$_2$COOH]–BocG	**45**	$C_{20}H_{30}N_4O_7$	438.47	92	3.26	1.43

mp = 130 °C (decomposition); ^{1}**H-NMR** (400 MHz, DMSO$_{d6}$) δ = 1.48, 1.53 (s, 9H, CH$_3$), 2.18 (s, 3H, CH$_3$), 2.38 (t, ^{3}J = 7.84 Hz, 2H, CH$_2$), 2.93 (t, ^{3}J = 7.76 Hz, 2H, CH$_2$), 8.50, 9.38, 10.35 (br.s, 1H, NH), 11.41 (br.s, 2H, COOH, NH); ^{13}**C-NMR** (100 MHz, DMSO$_{d6}$) δ = 9.8 (CH$_3$), 19.8 (CH$_2$), 27,7, 28.0 (CH$_3$), 34.6 (CH$_2$), 80.7, 81.6, 120.7,125.2, 128.1 (C$_q$), 157.9, 160.2, 174.2 (CO); **FT-IR** (ATR) [cm^{-1}] = 3343 w, 2978 w, 2934 w, 1694 m, 1629 m, 1531 m, 1455 m, 1368 m, 1294 s, 1246 s, 1140 s, 839 w, 753 w; **HR-MS** (neg. ESI) m/z = calculated 437.204–measured 437.205 for $C_{20}H_{30}N_4O_7$ -H^{+}.

6.3.2.4 Synthesis of ^{t}BuOOC–P[^{3}Me^{4}(CH$_2$)$_2$prop-2-inyl]–BocG (46)

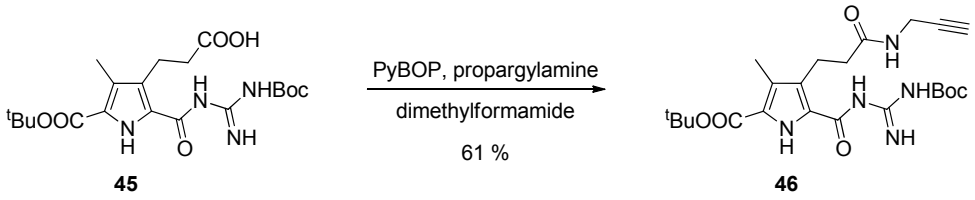

45 **46**

reactants		formula	g·mol^{-1}	eq.	mmol	µl	g·ml^{-1}	g
^{t}BuOOC–P[^{3}Me^{4}(CH$_2$)$_2$COOH]–BocG	**45**	$C_{20}H_{30}N_4O_7$	438.47	1.00	2.28			1.00
PyBOP		$C_{18}H_{28}F_6N_6OP_2$	520.39	1.10	2.51			1.31
4-methylmorpholine		$C_5H_{11}NO$	101.15	3.00	6.84	752	0.92	0.69
4-dimethylaminopyridine		$C_7H_{10}N_2$	122.17	0.20	0.46			0.06
propargylamine		C_3H_5N	55.08	1.10	2.51	161	0.86	0.14

A mixture of ^{t}BuOOC–P[^{3}Me^{4}(CH$_2$)$_2$COOH]–BocG (**45**) (1.00 g, 2.28 mmol, 1.00 eq.), PyBOP (1.31 g, 2.51 mmol, 1.10 eq.), 4-methylmorpholine (752 µl, 6.84 mmol, 3.00 eq.) and 4-dimethylaminopyridine (0.056 g, 0.456 mmol, 0.20 eq.) were dissolved in dimethylformamide (4 ml). Propargylamine (161 µl, 2.51 mmol, 1.10 eq.) was added and the reaction mixture was stirred for 12 hours. After treatment with water (50 ml) the precipitated solid matter was filtered through a Buechner funnel. The crude product was purified *via* normal-phase flash chromatography (triethylamine deactivated SiO_2, ethyl acetate/^{n}hexane 3/7) to isolate ^{t}BuOOC–P[^{3}Me^{4}(CH$_2$)$_2$prop-2-inyl]–BocG (**46**) (665 mg, 1.40 mmol, 61 % yield) as colourless solid.

product		formula	g·mol^{-1}	%	mmol	g
^{t}BuOOC–P[^{3}Me^{4}(CH$_2$)$_2$prop-2-inyl]–BocG	**46**	$C_{23}H_{33}N_5O_6$	475.54	61	3.26	0.67

mp = 109 °C; **^{1}H-NMR** (400 MHz, DMSO$_{d6}$) δ = 1.48, 1.53 (s, 9H, CH$_3$), 2.17 (s, 3H, CH$_3$), 2.26 (t, ^{3}J = 7.84 Hz, 2H, CH$_2$), 2.93 (t, ^{3}J = 7.82 Hz, 2H, CH$_2$), 3.05–3.06 (m, 1H, CH), 3.82–3.84 (m, 2H, CH$_2$), 8.21, 8.44, 9.41, 10.12, 10.59 (br.s, 1H, NH); **^{13}C-NMR** (100 MHz, DMSO$_{d6}$) δ = 9.8 (CH$_3$), 20.3 (CH$_2$), 26.3 (CH$_2$), 27.7, 28.0 (CH$_3$), 36.0 (CH$_2$), 72.7 (CH), 80.6, 81.2, 120.3, 125.3, 128.6 (C$_q$), 153.0, 157.7, 160.2, 171.6 (CO); **FT-IR** (ATR) [cm^{-1}] = 3395 w, 3285 w, 2981 w, 2933 w, 1726 m, 1626 m, 1524 m, 1453 m, 1367 m, 1294 s, 1235 s, 1140 s, 838 w, 752 w; **HR-MS** (pos. ESI) m/z = calculated 498.232–measured 498.233 for $C_{23}H_{33}N_5O_6$ +Na^{+}.

6.3.2.5 Synthesis of ^{t}BuOOC–P[^{3}Me^{4}(CH$_2$)$_2$G1]–BocG (47)[89, 139]

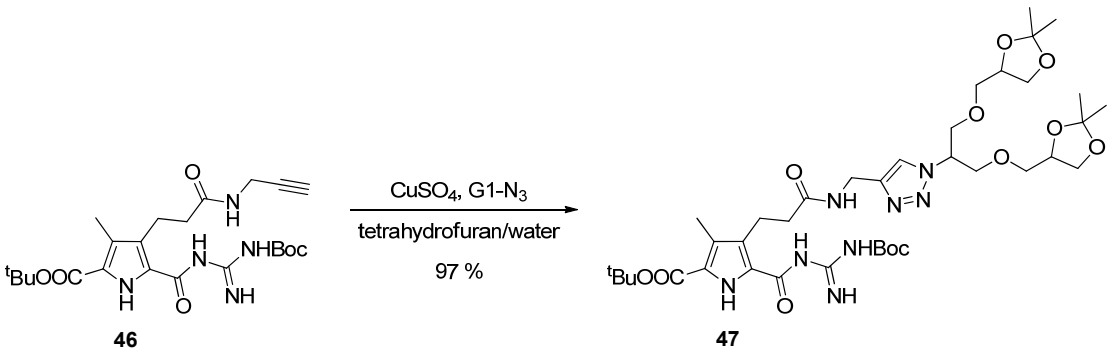

reactants		formula	g·mol^{-1}	eq.	µmol	µl	g·ml^{-1}	mg
^{t}BuOOC–P[^{3}Me^{4}(CH$_2$)$_2$prop-2-inyl]–BocG	**46**	$C_{23}H_{33}N_5O_6$	475.54	1.00	315			150
G1–N$_3$	**1**	$C_{15}H_{27}N_3O_6$	345.39	1.84	579			200
diisopropylethylamine		$C_8H_{19}N$	129.24	0.30	94.4	16.4	0.74	12.2
sodium ascorbate		$C_6H_7NaO_6$	198.11	0.30	94.4			18.7
copper(II)sulphate pentahydrate		$CuH_{10}O_9S$	249.69	0.15	47.2			11.8

A mixture of ^{t}BuOOC–P[^{3}Me^{4}(CH$_2$)$_2$prop-2-inyl]–BocG (46) (150 mg, 315 µmol, 1.00 eq.), G1–N$_3$ (1) (200 mg, 579 µmol, 1.84 eq.) and diisopropylethylamine (15.6 µl, 94.4 µmol, 0.300 eq.) in tetrahydrofuran (2.5 ml) was treated with freshly prepared aqueous solutions of sodium ascorbate (18.7 mg, 94.4 µmol, 0.300 eq.) and copper(II)sulphate pentahydrate (11.8 mg, 47.2 µmol, 0.150 eq.). The tetrahydrofuran/water mixture was set to a 1/1 ratio with water. The mixture was stirred until thin layer chromatography indicated complete conversion of the starting material. The reaction mixture was diluted with water, extracted with dichloromethane, and washed with saturated solution of EDTA. The organic fraction was dried with sodium sulphate and concentrated in vacuum. The resulting residue was purified *via* normal-phase flash chromatography (SiO$_2$, step gradient ethyl acetate/^{n}hexane 5/5, ^{i}propanol/^{n}hexane 3.5/6.5). The product ^{t}BuOOC–P[^{3}Me^{4}(CH$_2$)$_2$G1]–BocG (47) (250 mg, 305 µmol, 97 % yield) was isolated as colourless solid matter.

product		formula	g·mol^{-1}	%	µmol	mg
^{t}BuOOC–P[^{3}Me^{4}(CH$_2$)$_2$G1]–BocG	**47**	$C_{38}H_{60}N_8O_{12}$	820.93	97	305	250

mp = 54–56 °C; ^{1}**H-NMR** (500 MHz, $CDCl_3$) δ = 1.30 (s, 6H, CH_3), 1.36, 1.36 (s, 3H, CH_3), 1.51, 1.54 (s, 9H, CH_3), 2.22 (s, 3H, CH_3), 2.48 (t, ^{3}J = 7.85 Hz, 2H, CH_2), 3.11 (t,

^{3}J = 7.90 Hz, 2H, CH_2), 3.41–3.51 (m, 4H, CH, CH_2), 3.57–3.65 (m, 2H, CH_2), 3.91 (d, ^{3}J = 5.50 Hz, 4H, CH_2), 3.93–4.00 (m, 2H, CH_2), 4.11–4.25 (m, 2H, CH), 4.46–4.47 (m, 2H, CH_2), 4.83–4.88 (m, 1H, CH), 7.06 (br.s, 1H, NH), 7.61–7.63 (m, 1H, CH), 8.42, 9.05, 9.49, 9.91 (br.s, 1H, NH); **^{13}C-NMR** (125 MHz, $CDCl_3$) δ = 10.1 (CH_3), 21.4 (CH_2), 25.2, 26.7, 28.0, 28.4 (CH_3), 34.8, 37.6 (CH_2), 60.5, 66.3 (CH), 70.1, 72.1, 72.4 (CH_2), 74.5 (CH), 81.2, 83.2, 109.5, 117.4 121.7 (C_q), 122.2 (CH), 126.1, 128.2, 128.4, 144.2 (C_q), 153.2, 158.4, 160.6, 171.6 173.4 (CN, CO); **FT-IR** (ATR) [cm^{-1}] = 3386 w, 2981 w, 2879 w, 1728 w, 1629 m, 1531 m, 1454 m, 1367 m, 1298 m, 1240 s, 1213 m, 1142 s, 1076 s, 1051 s, 974 m, 839 s; **HR-MS** (pos. ESI) m/z = calculated 936.470–measured 936.481 for $C_{38}H_{60}N_8O_{12}$ $+H^+$.

6.3.2.6 Synthesis of ^{t}BuOOC–P[^{3}Me^{4}(CH$_2$)$_2$G2]–BocG (48)[89, 139]

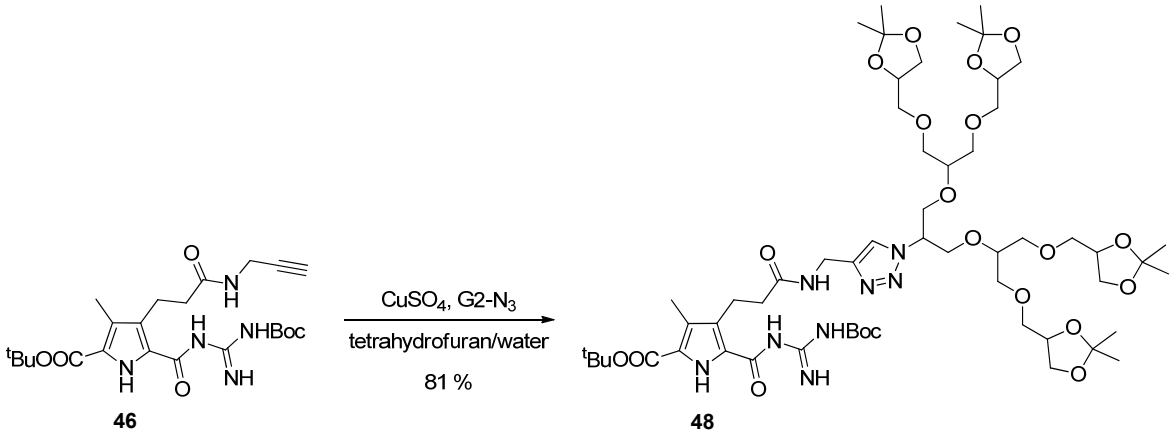

reactants		formula	g·mol^{-1}	eq.	µmol	µl	g·ml^{-1}	mg
^{t}BuOOC–P[^{3}Me^{4}(CH$_2$)$_2$prop-2-inyl]–BocG	**46**	$C_{23}H_{33}N_5O_6$	475.54	1.00	421			200
G2–N$_3$	**2**	$C_{33}H_{59}N_3O_{14}$	721.83	1.10	463			334
diisopropylethylamine		$C_8H_{19}N$	129.24	0.300	126	21.9	0.74	16.3
sodium ascorbate		$C_6H_7NaO_6$	198.11	0.300	126			25.0
copper(II)sulphate pentahydrate		$CuH_{10}O_9S$	249.69	0.150	63.0			15.7

A mixture of ^{t}BuOOC–P[^{3}Me^{4}(CH$_2$)$_2$prop-2-inyl]–BocG (**46**) (200 mg, 421 µmol, 1.00 eq.), G2–N$_3$ (**2**) (334 mg, 463 µmol, 1.10 eq.), and diisopropylethylamine (20.8 µl, 126 µmol, 0.300 eq.) in tetrahydrofuran (2.5 ml) was treated with freshly prepared aqueous solutions of sodium ascorbate (25.0 mg, 126 µmol, 0.300 eq.) and copper(II)sulphate pentahydrate (15.7 mg, 63.0 mmol, 0.150 eq.). The tetrahydrofuran/water mixture was set to 1/1 ratio with water. The mixture was stirred until thin layer chromatography indicated complete consumption of the starting material. The reaction mixture was diluted with water, extracted with dichloromethane, and washed with saturated solution of EDTA. The organic fraction was dried with sodium sulphate and concentrated in vacuum. The resulting residue was purified *via* normal–phase column chromatography (SiO_2, step gradient ethyl acetate/^{n}hexane 7.5/2.5, ^{i}propanol/^{n}hexane 3.5/6.5) to isolate ^{t}BuOOC–P[^{3}Me^{4}(CH$_2$)$_2$G2]–BocG (**48**) (410 mg, 342 µmol, 81 % yield) as colourless high viscous resin.

product		formula	g·mol^{-1}	%	µmol	mg
^{t}BuOOC–P[^{3}Me^{4}(CH$_2$)$_2$G2]–BocG	**48**	$C_{56}H_{92}N_8O_{20}$	1197.37	81	342	410

^{1}**H-NMR** (500 MHz, $CDCl_3$) δ = 1.31, 1.37 (s, 12H, CH_3), 1.50, 1.54 (s, 9H, CH_3), 2.22 (s, 3H, CH_3), 2.47 (t, ^{3}J = 7.75 Hz, 2H, CH_2), 3.11 (t, ^{3}J = 7.83 Hz, 2H, CH_2), 3.41–3.51 (m, 16H, CH_2), 3.57–3.65 (m, 2H, CH), 3.61–3.68 (m, 4H, CH_2), 3.82–3.88 (m, 2H, CH_2), 3.93–4.04 (m, 6H, CH_2), 4.13–4.21 (m, 4H, CH), 4.47 (d, ^{3}J = 5.35 Hz, 2H, CH_2), 4.78–4.84 (m, 1H, CH), 7.17 (br.s, 1H, NH), 7.58–7.68 (m, 1H, CH), 8.41, 9.05, 9.49, 9.91 (br.s, 1H, NH); ^{13}**C-NMR** (125 MHz, $CDCl_3$) δ = 10.2 (CH_3), 21.6 (CH_2), 25.5, 26.9, 28.1, 28.5 (CH_3), 34.9, 37.7 (CH_2), 61.3 (CH), 66.6, 69.4, 70.4, 71.6, 72.6 (CH_2), 74.6, 78.5, 78.8 (CH), 81.3, 83.3, 109.5, 119.3 121.8 (C_q), 122.4 (CH), 126.2, 128.3, 128.6, 144.3 (C_q), 153.4, 158.5, 160.6, 171.7 173 .6 (CN, CO); **FT-IR** (ATR) [cm^{-1}] = 2985 w, 2879 w, 1726 w, 1688 w, 1629 m, 1531 m, 1456 m, 1368 m, 1295 m, 1237 s, 1213 m, 1145 s, 1078 s, 1053 s, 975 m, 840 s; **HR-MS** (pos. ESI) m/z = calculated 1219.632–measured 1219.631 for $C_{56}H_{92}N_8O_{20}$ + Na^+.

6.3.2.7 Synthesis of ^{t}BuOOC–P[^{3}Me^{4}(CH$_2$)$_2$G3]–BocG (49)[89, 139]

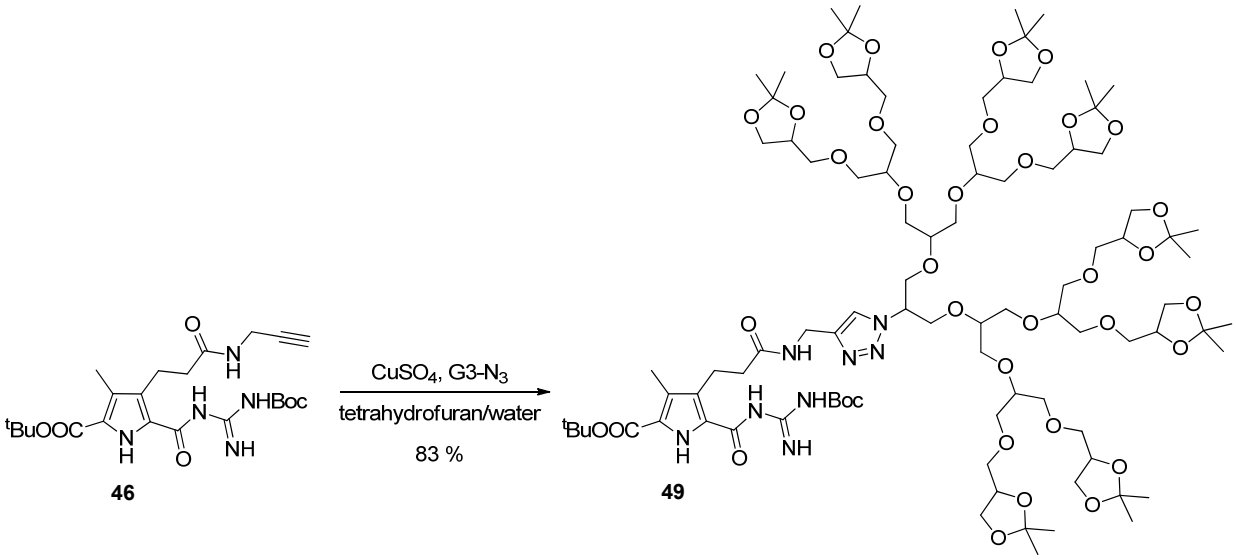

reactants		formula	g·mol^{-1}	eq.	µmol	µl	g·ml^{-1}	mg
^{t}BuOOC–P[^{3}Me^{4}(CH$_2$)$_2$prop-2-inyl]–BocG	**46**	$C_{23}H_{33}N_5O_6$	475.54	1.00	263			125
G3–N$_3$	**3**	$C_{69}H_{123}N_3O_{30}$	1464.72	1.10	289			426
diisopropylethylamine		$C_8H_{19}N$	129.24	0.300	78.9	13.8	0.74	10.2
sodium ascorbate		$C_6H_7NaO_6$	198.11	0.300	78.9			15.6
copper(II)sulphate pentahydrate		$CuH_{10}O_9S$	249.69	0.150	39.4			9.84

A mixture of ^{t}BuOOC–P[^{3}Me^{4}(CH$_2$)$_2$prop-2-inyl]–BocG (**46**) (125 mg, 263 µmol, 1.00 eq.), G3–N$_3$ (**3**) (426 mg, 289 µmol, 1.10 eq.), and diisopropylethylamine (13.8 µl, 78.9 µmol, 0.300 eq.) in tetrahydrofuran (2.5 ml) was treated with freshly prepared aqueous solutions of sodium ascorbate (15.6 mg, 78.9 µmol, 0.300 eq.) and copper(II)sulphate pentahydrate (9.84 mg, 39.4 µmol, 0.150 eq.). The tetrahydrofuran/water mixture was set to 1/1 ratio with water. The mixture was stirred until thin layer chromatography indicated complete transformation of the starting material. The reaction mixture was diluted with water, extracted with dichloromethane, and washed with saturated solution of EDTA. The organic fraction was dried with sodium sulphate and concentrated in vacuum. The resulting residue was purified *via* normal-phase column chromatography (SiO$_2$, step gradient ethyl acetate/^{n}hexane 0.1/9.9, methanol/^{n}hexane 0.5/9.5) to isolate ^{t}BuOOC–P[^{3}Me^{4}(CH$_2$)$_2$G3]–BocG (**49**) (427 mg, 219 µmol, 83 % yield) as colourless high viscous resin.

product		Formula	g mol^{-1}	%	µmol	mg
^{t}BuOOC–P[^{3}Me^{4}(CH$_2$)$_2$G3]–BocG	**49**	$C_{92}H_{156}N_8O_{36}$	1949.06	83	219	427

^{1}**H-NMR** (500 MHz, $CDCl_3$) δ = 1.31, 1.37 (s, 24H, CH_3), 1.50, 1.54 (s, 9H, CH_3), 2.23 (s, 3H, CH_3), 2.46 (t, ^{3}J = 7.40 Hz, 2H, CH_2), 3.11 (t, ^{3}J = 7.65 Hz, 2H, CH_2), 3.41–3.51 (m, 40H, CH, CH_2), 3.52–3.63 (m, 4H, CH), 3.64–3.71 (m, 10H, CH, CH_2), 3.93–4.04 (m, 12H, CH_2), 4.13–4.21 (m, 8H, CH_2), 4.47 (d, ^{3}J = 4.50 Hz, 2H, CH_2), 4.76–4.84 (m, 1H, CH), 7.14 (br.s, 1H, NH), 7.68–7.75 (m, 1H, CH), 8.38, 9.03, 9.47, 9.91 (br.s, 1H, NH); ^{13}**C-NMR** (125 MHz, $CDCl_3$) δ = 10.1 (CH_3), 21.7 (CH_2), 25.3, 26.7, 28.0, 28.3 (CH_3), 34.9, 37.5 (CH_2), 61.2 (CH), 66.6, 69.3, 70.1, 70.3, 71.1, 71.4, 71.5 72.4 (CH_2), 74.5, 74.7, 78.3, 78.5 (CH), 81.1, 83.1 (C_q), 109.3 (CH), 119.3, 121.6 (C_q), 122.5 (CH), 126.0, 128.3, 128.4, 143.8 (C_q), 153.2, 158.3, 160.5, 171.4, 173.5 (CN, CO); **FT-IR** (ATR) [cm^{-1}] = 2986 w, 2923 w, 2864 w, 1728 w, 1683 w, 1633 m, 1532 m, 1457 m, 1369 m, 1300 m, 1240 m, 1207 m, 1144 s, 1047 s, 975 m, 837 s; **HR-MS** (pos. ESI) m/z = calculated 1950.070–measured 1950.068 for $C_{92}H_{156}N_8O_{36}$ $+H^+$.

6.3.2.8 Synthesis of $^{-}$OOC–P[^{3}Me^{4}(CH$_2$)$_2$-G1(OH)$_4$]–G^{+} (50)

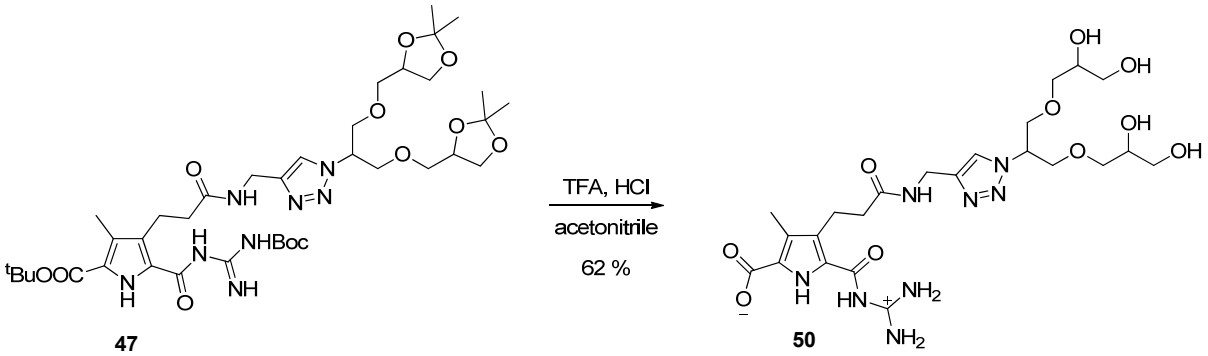

reactants		formula	g·mol^{-1}	eq.	mmol	ml	g·ml^{-1}	mg
^{t}BuOOC–P[^{3}Me^{4}(CH$_2$)$_2$G1]–BocG	**47**	$C_{38}H_{60}N_8O_{12}$	820.93	1.00	0.171			140
trifluoroacetic acid		$C_2HF_3O_2$	114.02	100	17.1	1.31	1.48	1945
hydrochloric acid 5 %		ClH	36.46	5.00	0.853	0.523	1.19	31.1

A solution of ^{t}BuOOC–P[^{3}Me^{4}(CH$_2$)$_2$G1]–BocG (**47**) (140 mg, 0.171 mmol, 1.00 eq.) in acetonitrile (2.5 ml) was treated with trifluoroacetic acid (1.31 ml, 17.1 mmol, 100 eq.) and hydrochloric acid (5 %, 0.523 ml, 0.853 mmol, 5.00 eq.). The reaction mixture was stirred until HPLC reaction control indicated complete cleavage of all protecting-groups. After evaporation of the solvent in vacuum the crude product was dissolved in hydrochloric acid (5 %) and freeze dried. The protonated product was suspended in water, sodium hydroxide (1 N) was added until pH 9.0. Hydrochloric acid (0.1 N) was added to set the pH to 5.9 precipitating the zwitterion **50**. The product was filtered off and purified *via* reversed-phase chromatography (MPLC, RP18, 50 g, 50 µm, 25·2.5 cm, 295 nm, 25 ml·min^{-1} gradient 1,4-dioxane 0% to 30 % in 15 minutes, 30 % for 10 minutes, retention time 15.5 minutes) to isolate $^{-}$OOC–P[^{3}Me^{4}(CH$_2$)$_2$G1(OH)$_4$]–G^{+} (**50**) (62.0 mg, 0.106 mmol, 62 % yield) as colourless solid matter.

product		formula	g·mol^{-1}	%	mmol	mg
$^{-}$OOC–P[^{3}Me^{4}(CH$_2$)$_2$G1(OH)$_4$]–G^{+}	**50**	$C_{23}H_{36}N_8O_{10}$	584.58	62	0.106	62.0

mp = >230 °C; **^{1}H-NMR** (500 MHz, DMSO$_{d6}$) δ = 2.29 (s, 3H, CH$_3$), 2.28 (t, ^{3}J = 7.87 Hz, 2H, CH$_2$), 2.97 (t, ^{3}J = 7.57 Hz, 2H, CH$_2$), 3.24–3.31 (br.m, 6H, CH, CH$_2$, OH), 3.36–3.42 (br.m, 2H, CH, CH$_2$), 3.48–3.54 (m, 2H, CH), 3.77–3.84 (m, 4H, CH$_2$), 4.28 (d, ^{3}J = 5.9 Hz, 2H, CH$_2$), 4.47 (t, ^{3}J = 5.07 Hz, 2H, CH$_2$), 4.64 (d, ^{3}J = 4.6 Hz, 2H, CH$_2$), 4.87–4.93 (m,

1H, CH), 7.90 (s, 1H, CH), 7.98 (s, 1H, CH), 8.21 (t, ^{3}J = 4.93 Hz, 1H, NH), 10.11, 12.65, 14.64 (br.s, 1H, NH); **^{13}C-NMR** (125 MHz, $DMSO_{d6}$) δ = 9.2 (CH_3), 20.9, 34.2, 35.4 (CH_2), 60.0 (CH), 62.8, 69.9, 70.0 (CH_2), 70.3, 70.4 (CH), 72.6, 72.7 (CH_2), 118.7 (C_q), 122.3 (CH), 122.9, 129.3, 134.2, 144.5 (C_q), 156.6, 161.1, 166.6, 171.7 (CO); **FT-IR** (ATR) [cm^{-1}]= 3388 w, 3206 w, 2947 w, 2738 w, 1722 w, 1657 s, 1554 w, 1445 w, 1330 s, 1272 s; **HR-MS** (pos. ESI) m/z = calculated 585.263–measured 585.261 for $C_{23}H_{36}N_8O_{10}$ +H^+.

6.3.2.9 Synthesis of $^{-}$OOC–P[^{3}Me^{4}(CH$_2$)$_2$G2(OH)$_8$]–G^{+} (51)

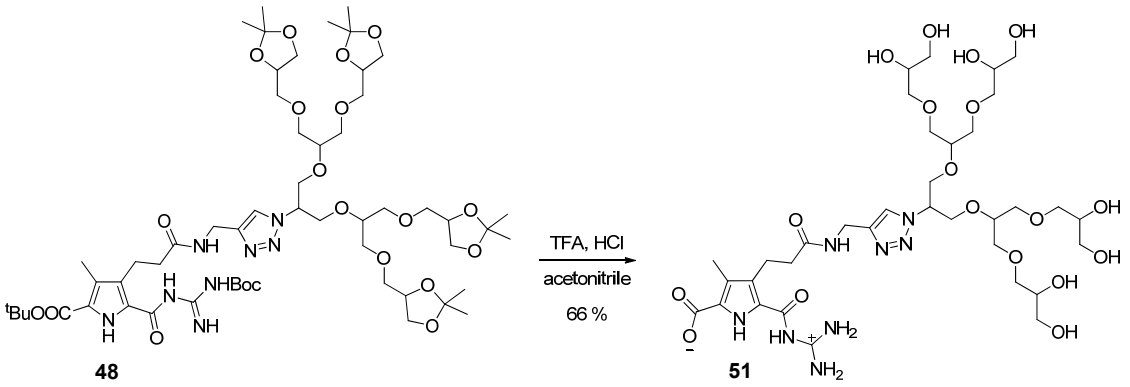

reactants		formula	g·mol^{-1}	eq.	mmol	ml	g·ml^{-1}	mg
^{t}BuOOC–P[^{3}Me^{4}(CH$_2$)$_2$G2]–BocG	**48**	$C_{56}H_{92}N_8O_{20}$	1197.37	1.00	0.20			240
trifluoroacetic acid		$C_2HF_3O_2$	114.02	100	20.0	1.54	1.48	2285
hydrochloric acid 5 %		ClH	36.46	2.44	0.49	0.30	1.19	17.9

A solution of ^{t}BuOOC–P[^{3}Me^{4}(CH$_2$)$_2$G2]–BocG (**48**) (240 mg, 0.20 mmol, 1.00 eq.) in acetonitrile (2.5 ml) was treated with trifluoroacetic acid (1.54 ml, 20.0 mmol, 100 eq.) and hydrochloric acid (5 %, 0.30 ml, 0.49 mmol, 2.44 eq.). The reaction mixture was stirred until HPLC control indicated complete cleavage of all protecting groups. After evaporation of the solvent in vacuum the crude product was dissolved in hydrochloric acid (5 %) and freeze dried. The protonated product was dissolved in water and sodium hydroxide (1 N) was added until pH 9.0. Hydrochloric acid (0.1 N) was added to set the pH to 5.9. The solution was freeze dried and the crude zwitterion was purified *via* an reversed-phase chromatography (MPLC, RP18, 50 g, 50 µm, 25·2.5 cm, 295 nm, 25 ml·min^{-1}, gradient methanol 40 % to 70 % in 8 minutes, 70 % for 10 minutes retention time 8.5 minutes) to isolate $^{-}$OOC–P[^{3}Me^{4}(CH$_2$)$_2$G2(OH)$_8$]–G^{+} (**51**) (117 mg, 0.13 mmol, 66 % yield) as colourless solid matter.

product		formula	g·mol^{-1}	%	mmol	mg
$^{-}$OOC–P[^{3}Me^{4}(CH$_2$)$_2$G2(OH)$_8$]–G^{+}	**51**	$C_{35}H_{60}N_8O_{18}$	880.89	66	0.13	117

mp = 195–205 °C; **^{1}H-NMR** (500 MHz, $DMSO_{d6}$) δ = 2.23 (s, 3H, CH_3), 2.29 (br.s, 2H, CH_2), 2.97 (t, ^{3}J = 7.86 Hz, 2H, CH_2), 3.29–3.58 (br.m, 58H, CH, CH_2, OH), 3.93 (br.s, 4H, CH), 4.30 (br.s, 2H, CH), 4.55–4.59 (m, 8H, CH_2), 4.60 (d, ^{3}J = 4.86 Hz, 2H, CH_2), 4.66–4.68 (m, 6H, CH_2), 4.84 (t, ^{3}J = 5.55 Hz, 1H, CH), 7.96 (s, 1H, CH), 8.16 (br. s, 2H, NH),

8.26 (t, ^{3}J = 5.34 Hz, 1H, NH), 10.12, 12.62, 14.60 (br.s, 1H, NH); **^{13}C-NMR** (125 MHz, $DMSO_{d6}$) δ = 9.2 (CH_3), 20.9, 34.2, 35.4 (CH_2), 59.9, 60.2, 60.6 (CH), 63.0, 68.8, 69.9 (CH_2), 70.4 (CH), 70.6 (CH_2), 70.7 (CH), 70.7, 71.2, 72.8 (CH_2), 77.6, 78.0, 78.0 (CH), 118.6 (C_q), 122.3 (CH), 122.9, 129.2, 134.2, 144.3, 144.4 (C_q), 156.5, 161.0, 166.5, 171.6 (CN, CO); **FT-IR** (ATR) [cm^{-1}] = 3354 m, 3208 m, 2919 w, 2877 w, 1717 w, 1653 m, 1555 w, 1464 w, 1334 s,1276 s, 1041 s; **HR-MS** (pos. ESI) m/z = calculated 818.411–measured 818.413 for $C_{35}H_{60}N_8O_{18}$ $+H^+$.

6.3.2.10 Synthesis of $^{-}$OOC–P[^{3}Me^{4}(CH$_2$)$_2$G3(OH)$_{16}$]–G^{+} (52)

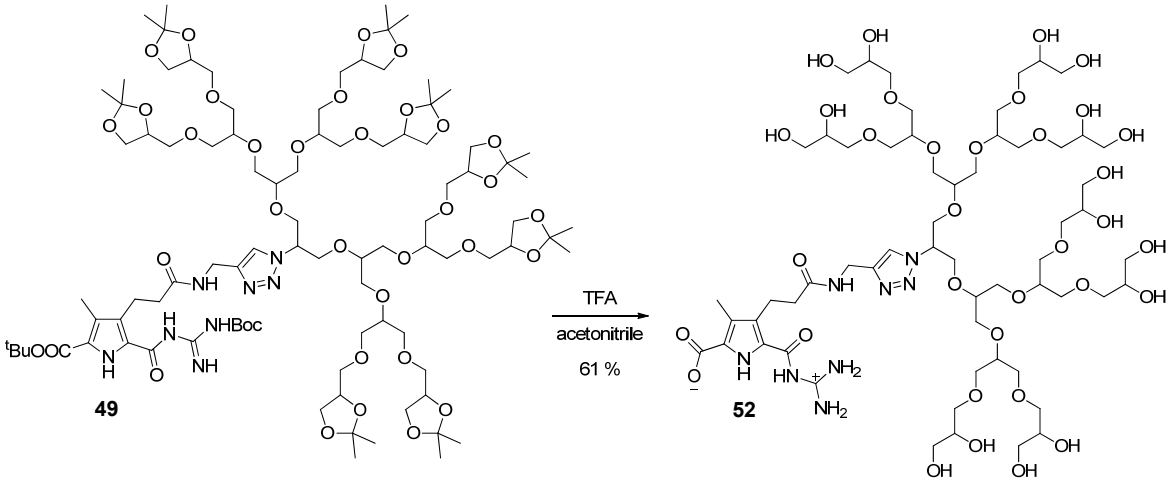

Reactant		Formula	g·mol^{-1}	eq.	mmol	ml	g·ml^{-1}	mg
^{t}BuOOC–P[^{3}Me^{4}(CH$_2$)$_2$G3]–BocG	**49**	$C_{92}H_{156}N_8O_{36}$	1950.26	1.00	0.13			250
trifluoroacetic acid		$C_2HF_3O_2$	114.02	200	25.6	1.98	1.48	2923

A solution of ^{t}BuOOC–P[^{3}Me^{4}(CH$_2$)$_2$G3]–BocG (**49**) (250 mg, 0.13 mmol, 1.00 eq.) in acetonitrile (2 ml) was treated with trifluoroacetic acid (1.98 ml, 25.6 mmol, 200 eq.). The reaction mixture was stirred at 40 °C until HPLC control indicated complete cleavage of protecting-groups. After evaporation of the solvent in vacuum the crude product was dissolved in hydrochloric acid (5 %) and freeze dried twice. The product was purified *via* reversed-phase chromatography (MPLC, RP18, 50 g, 50 µm, 25·2.5 cm, 290 nm, 35 ml·min^{-1}, gradient methanol 40 % to 50 % in 18 minutes with trifluoroacetic acid 0.05 % as an additive, retention time 7 minutes). The solvent of collected phases was evaporated in vacuum and the resulting residue was dissolved in hydrochloric acid (5 %) and freeze dried twice. The protonated product was dissolved in water and sodium hydroxide (0.1 N) was added until pH 5.8 and the solution was freeze dried. The salt contaminated zwitterion was purified *via* reversed-phase chromatography (MPLC, RP18, 50 g, 50 µm, 25·2.5 cm, 295 nm, 25 ml·min^{-1}, gradient methanol 30 % to 60 % in 15 minutes, retention time 12 minutes) to isolate $^{-}$OOC–P[^{3}Me^{4}(CH$_2$)$_2$G3(OH)$_{16}$]–G^{+} (**52**) (115 mg, 0.08 mmol, 61 % yield) as colourless high viscous resin.

product		formula	g·mol^{-1}	%	mmol	mg
$^{-}$OOC–P[^{3}Me^{4}(CH$_2$)$_2$G3(OH)$_{16}$]–G^{+}	**52**	$C_{59}H_{108}N_8O_{34}$	1473.52	61	0.08	115

^{1}H-NMR (500 MHz, $DMSO_{d6}$) δ = 2.23 (s, 3H, CH_3), 2.28, 2.97 (br.s, 2H, CH_2), 3.29–3.58 (m, 58H, CH, CH_2, OH), 3.93 (br.s, 4H, CH), 4.30 (br.s, 2H, CH), 4.55–4.59 (m, 8H, CH_2), 4.60 (d, ^{3}J = 4.86 Hz, 2H, CH_2), 4.66–4.68 (m, 6H, CH_2), 4.84 (t, ^{3}J = 5.55 Hz, 1H, CH), 7.96 (s, 1H, CH), 8.16 (br.s, 2H, NH), 8.26 (t, ^{3}J = 5.34 Hz, 1H, NH), 10.12, 12.62, 14.60 (br.s, 1H, NH); **^{13}C-NMR** (125 MHz, $DMSO_{d6}$) δ = 9.2 (CH_3), 20.9, 34.2, 35.4 (CH_2), 60.7 (CH), 63.1, 68.9, 69.2, 69.3, 69.4 (CH_2), 70.5 (CH), 70.7, 70.8, 71.6, 72.9 (CH_2), 77.8, 78.2, 78.4 (CH),118.7 (C_q), 123.0 (CH), 129.4, 134.2, 144.2 (C_q), 156.7, 161.0, 166.6, 171.8 (CN, CO); **FT-IR** (ATR) [cm^{-1}] = 3306 s, 2972 w, 2875 w, 1400 m, 1685 w, 1263 m, 1225 m, 1040 s, 925 w, 863 w; **HR-MS** (pos. ESI) m/z = calculated 1473.704–measured 1473.714 for $C_{59}H_{108}N_8O_{34} + H^+$.

6.3.3 Zwitterionic Core

6.3.3.1 Synthesis of ^{t}BuOOC–P[^{3}Me^{4}(CH$_2$)$_4$NHCbz]–BocG (57)

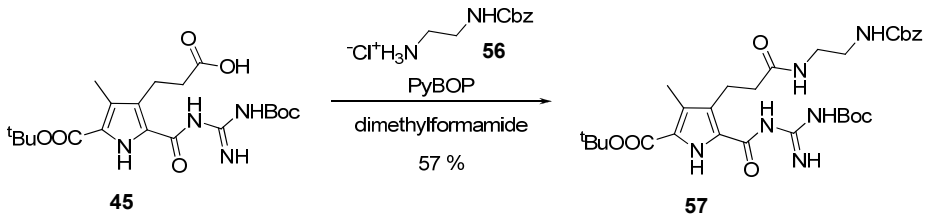

reactants		formula	g·mol^{-1}	eq.	mmol	µl	g·ml^{-1}	mg
^{t}BuOOC–P[^{3}Me^{4}(CH$_2$)$_2$COOH]–BocG	**45**	$C_{20}H_{30}N_4O_7$	438.47	1.00	1.14			500
PyBOP		$C_{18}H_{28}F_6N_6OP_2$	520.39	1.10	1.25			653
diisopropylethylamine		$C_8H_{19}N$	129.24	3.00	3.42	596	0.74	442
N-Cbz-ethylenediamine hydrochloride	**56**	$C_{10}H_{15}ClN_2O_2$	230.69	1.10	1.25			289
4-dimethylaminopyridine		$C_7H_{10}N_2$	122.17	0.100	0.114			13.9

A solution of ^{t}BuOOC–P[^{3}Me^{4}(CH$_2$)$_2$COOH]–BocG (**45**) (500 mg, 1.14 mmol, 1.00 eq.), PyBOP (653 mg, 1.25 mmol, 1.10 eq.), and diisopropylethylamine (596 µl, 3.42 mmol, 3.00 eq.) in dimethylformamide (4 ml) was treated with **56** (289 mg, 1.25 mmol, 1.10 eq.) and 4-dimethylaminopyridine (13.9 mg, 0.114 mmol, 0.100 eq.). The reaction solution was stirred at 30 °C for 2 hours and at room temperature for 16 hours. The reaction was quenched with ice water (100 ml), the precipitated solid was separated by filtration, and purified *via* normal-phase chromatography (MPLC, SiO_2, 100 g, 50 µm, 50·2.5 cm, 295 nm, 20 ml·min^{-1}, isocratic chloroform/ethyl acetate 5/5, retention time 20 minutes) to isolate ^{t}BuOOC–P[^{3}Me^{4}(CH$_2$)$_4$NHCbz]–BocG (**57**) (405 mg, 0.659 mmol, 57 % yield).

product		formula	g·mol^{-1}	mmol	%	mg
^{t}BuOOC–P[^{3}Me^{4}(CH$_2$)$_4$NHCbz]–BocG	**57**	$C_{30}H_{42}N_6O_8$	614.69	0.659	57	405

mp = 80 °C; **^{1}H-NMR** (300 MHz, DMSO$_{d6}$) δ = 1.46, 1.52 (s, 9H, CH$_3$), 2.15 (s, 3H, CH$_3$), 2.22 (t, ^{3}J = 8.04 Hz, 2H, CH$_2$), 2.92 (t, ^{3}J = 7.76 Hz, 2H, CH$_2$), 3.00–3.08 (m, 4H, CH$_2$), 4.99 (s, 2H, CH$_2$), 7.22 (t, ^{3}J = 5.07 Hz, 1H, NH), 7.24–7.35 (m, 5H, CH), 7.80, 8.48, 9.39, 10.14, 10.65 (br.s, 1H, NH); **^{13}C-NMR** (75 MHz, DMSO$_{d6}$) δ = 9.8 (CH$_3$), 20.4 (CH$_2$), 27.7, 28.0 (CH$_3$), 30.6, 36.5, 37.6 (CH$_2$), 65.2 (CH$_2$), 80.6, 82.3, 125.3 (C$_q$), 127.7, 128.3 (CH), 137.1 (C$_q$), 156.1, 157.7, 160.2, 165.4 172.2 (CN, CO); **FT-IR** (ATR) [cm^{-1}] = 1694 w, 1625 m, 1523 m, 1450 w, 1297 w, 1236 s, 1142 s, 839 w, 751 w, 694 w; **HR-MS** (pos. ESI) m/z = calculated 615.314–measured 615.319 for $C_{30}H_{42}N_6O_8$ +H^{+}.

6.3.3.2 Synthesis of ^{t}BuOOC–P[^{3}Me^{4}(CH$_2$)$_4$NH$_2$]–BocG (58)

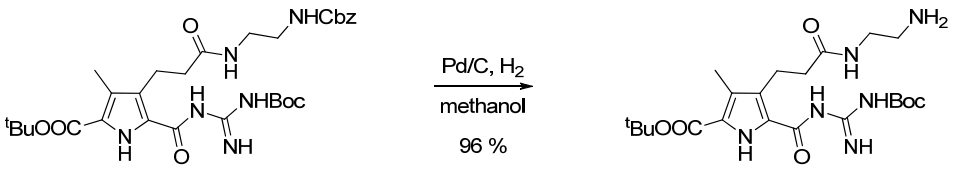

57 **58**

reactants		formula	g·mol^{-1}	eq.	µmol	mg
^{t}BuOOC–P[^{3}Me^{4}(CH$_2$)$_4$NHCbz]–BocG	**57**	$C_{30}H_{42}N_6O_8$	614.69	1.00	610	375
palladium 10 % on carbon		Pd/C	106.42	0.100	61.0	64.9

A suspension of ^{t}BuOOC–P[^{3}Me^{4}(CH$_2$)$_4$NHCbz]–BocG (**57**) (375 mg, 610 µmol, 1.00 eq.) and palladium 10 % on carbon (64.9 mg, 61.0 µmol, 0.100 eq.) in methanol (10 ml) was stirred for 2 hours in a hydrogen atmosphere until thin layer chromatography control showed complete cleavage of the Cbz-group. The catalyst was separated from the product by a syringe filter (nylon, 0.2 µm pore size) and the solvent was evaporated under reduced pressure to obtain the ^{t}BuOOC–P[^{3}Me^{4}(CH$_2$)$_4$NH$_2$]–BocG (**58**) (282 mg, 587 µmol, 96 % yield).

product		formula	g·mol^{-1}	%	µmol	mg
^{t}BuOOC–P[^{3}Me^{4}(CH$_2$)$_4$NH$_2$]–BocG	**58**	$C_{22}H_{36}N_6O_6$	480.56	96	587	282

mp = 112 °C; **^{1}H-NMR** (300 MHz, DMSO$_{d6}$) δ = 1.48, 1.53 (s, 9H, CH$_3$), 2.16 (s, 3H, CH$_3$), 2.22 (t ^{3}J = 7.67 Hz, 2H, CH$_2$), 2.56 (t ^{3}J = 6.39 Hz, 2H, CH$_2$), 2.94 (t ^{3}J = 7.74 Hz, 2H, CH$_2$), 3.01–3.07 (m, 2H, CH$_2$), 7.76, 8.50 (br.s, 1H, NH); **^{13}C-NMR** (75 MHz, DMSO$_{d6}$) δ = 9.8 (CH$_3$), 20.6 (CH$_2$), 27.7, 28.0 (CH$_3$), 36.4, 41.0, 41.7 (CH$_2$), 80.6, 81.6, 120.8, 125.3, 127.8, 128.7 (C$_q$), 154.5, 158.0, 160.2, 169.5, 172.2 (CN, CO); **FT-IR** (ATR) [cm^{-1}] = 2982 w, 2925 w, 1626 m, 1529 m, 1452 m, 1365 m, 1297 m, 1240 m, 1141 s, 838 w, 777 w; **HR-MS** (pos. ESI) m/z = calculated 481.277–measured 481.283 for $C_{22}H_{36}N_6O_6$ +H^{+}.

6.3.3.3 Synthesis of ^{t}BuOOC–P[^{3}Me^{4}(CH$_2$)$_4$PDI]–G^{+}Cl^{-} (59)

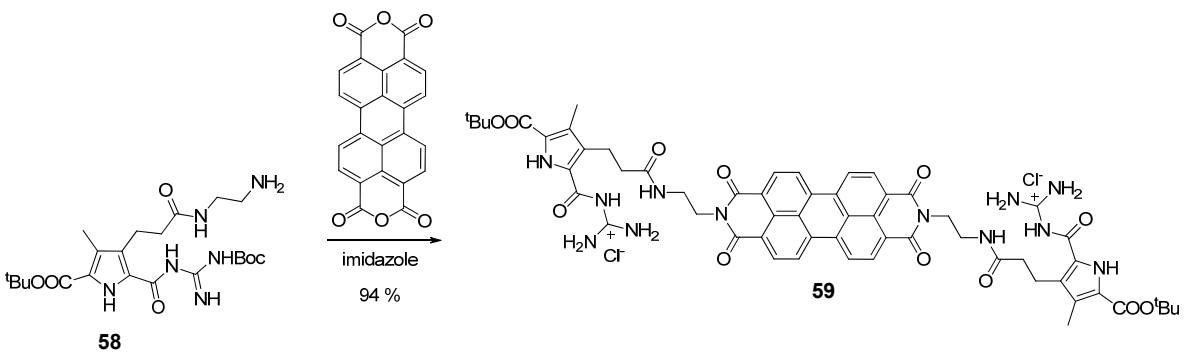

reactants		formula	g·mol^{-1}	eq.	µmol	mg
^{t}BuOOC–P[^{3}Me^{4}(CH$_2$)$_4$NH$_2$]–BocG	**58**	$C_{22}H_{36}N_6O_6$	480.56	2.20	393	189
perylene-dianhydride (PTCDA)		$C_{24}H_8O6$	392.32	1.00	178	70.0

^{t}BuOOC–P[^{3}Me^{4}(CH$_2$)$_4$NH$_2$]–BocG (**58**) (189 mg, 393 µmol, 2.20 eq.), perylene anhydride (70.0 mg, 178 µmol, 1.00 eq.) and imidazole (2 g) were heated at 130 °C under argon atmosphere for 4 hours (every 30 min the pressure was reduced to 7 mbar for time period of 5 min). The reaction melt was diluted by addition of ethanol (5 ml) and cooled to room temperature. The reaction mixture was treated with hydrochloric acid (2 N, 35 ml) and stayed without stirring for 1 hour. The formed precipitate was filtered off by a Buchner funnel, to obtain ^{t}BuOOC–P[^{3}Me^{4}(CH$_2$)$_4$PDI]–G^{+}Cl^{-} (**59**) (200 mg, 168 µmol, 94 % yield).

product		formula	g·mol^{-1}	%	µmol	mg
^{t}BuOOC–P[^{3}Me^{4}(CH$_2$)$_4$PDI]–G^{+}Cl^{-}	**59**	$C_{58}H_{62}Cl_2N_{12}O_{12}$	1190.09	94	168	200

mp = 240 °C; ^{1}**H-NMR** (500 MHz, DMSO$_{d6}$) δ = 1.51 (s, 9H, CH$_3$), 2.10–2.17 (m, 10H, 2·CH$_2$, 2·CH$_3$), 2.83 (t ^{3}J = 6.98 Hz, 4H, CH$_2$), 4.07 (br.s, 4H, CH$_2$), 7.82–8.42 (m, 8H, NH$_2$), 7.95 (t ^{3}J = 4.93 Hz, 2H, NH), 8.11–8.12, 8.33–8.34 (m, 4H, CH), 11.80, 12.40 (br.s, 2H, NH); ^{13}**C-NMR** (125 MHz, DMSO$_{d6}$) δ = 9.5 (CH$_3$), 20.2 (CH$_2$), 28.0 (CH$_3$), 35.5, 36.3 (CH$_2$), 81.4, 121.4, 122.1 (C$_q$), 123.6 (CH), 124.0, 124.7, 125.6, 127.8 (C$_q$), 130.2 (CH), 134.3 (C$_q$), 155.2, 159.7, 159.7, 162.5, 171.8 (CN, CO); **FT-IR** (ATR) [cm^{-1}] = 3058 w, 2929 w, 2760 w, 1693 m, 1654 s, 1591 s, 1578 m, 1440 w, 1400 w, 1343 m, 1279 s, 1151 s, 840 w, 809 s, 745 s; **HR-MS** (pos. ESI) m/z = calculated 1117.453–measured 1117.461 for $C_{58}H_{60}N_{12}O_{12}$ +H^{+}.

6.3.3.4 Synthesis of $^{-}$OOC–P[^{3}Me^{4}(CH$_2$)$_4$PDI]–G^{+} (55)

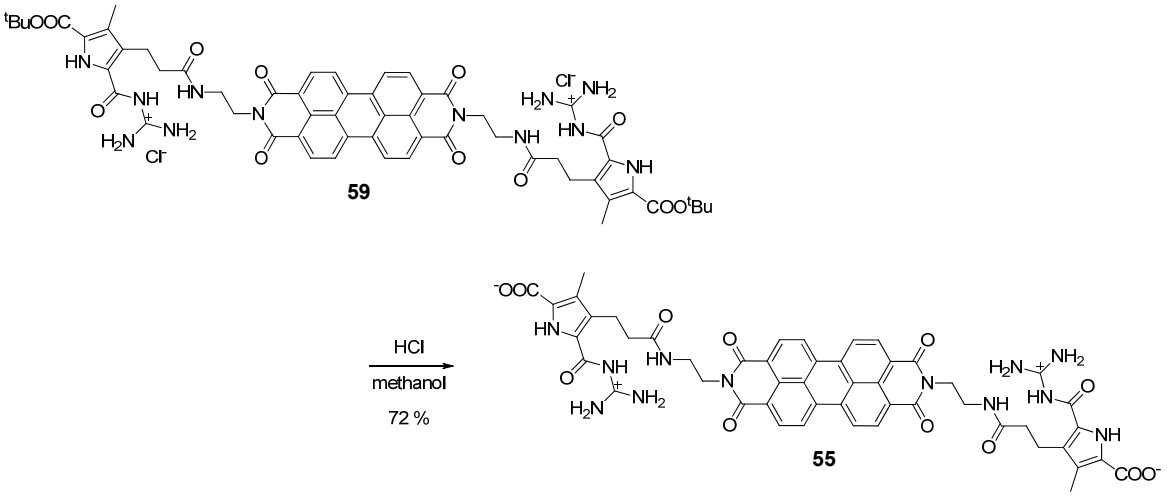

reactants		formula	g·mol^{-1}	eq.	mmol	ml	g·ml^{-1}	mg
^{t}BuOOC–P[^{3}Me^{4}(CH$_2$)$_4$PDI]–G^{+}Cl^{-}	**59**	$C_{58}H_{62}Cl_2N_{12}O_{12}$	1190.09	1.00	0.151			180
hydrochloric acid fuming 37%		ClH	36.46	647	98	3.00	1.19	3570

A solution of ^{t}BuOOC–P[^{3}Me^{4}(CH$_2$)$_4$PDI]–G^{+}Cl^{-} (**59**) (180 mg, 0.151 mmol, 1.00 eq.) in methanol (9 ml) was treated with hydrochloric acid (37 %, 3.00 ml, 98.0 mmol, 647 eq.) and stirred for 3 hours. The solvent was removed in vacuum to obtain the crude protonated product. The solid matter was dissolved in sodium hydroxide (0.1 N) and water. Hydrochloric acid (1 N) was added until pH 5.9 to precipitate a dark purple solid matter. The product was washed with water and dried in vacuum to isolate $^{-}$OOC–P[^{3}Me^{4}(CH$_2$)$_4$PDI]–G^{+} (**55**) 110 mg, 0.109 mmol, 72 % yield).

product		formula	g·mol^{-1}	%	mmol	mg
$^{-}$OOC–P[^{3}Me^{4}(CH$_2$)$_4$PDI]–G^{+}	**55**	$C_{50}H_{44}N_{12}O_{12}$	1004.96	72	0.109	110

mp >230 °C; **^{1}H-NMR**$_{protonated}$ (500 MHz, DMSO$_{d6}$, 120 °C) δ = 2.20 (s, 6H, CH$_3$), 2.27 (t, ^{3}J = 7.50 Hz, 4H, CH$_2$), 2.29 (t, ^{3}J = 7.57 Hz, 4H, CH$_2$),, 3.38 (br.s, 4H, CH$_2$), 4.18 (t, ^{3}J = 5.95 Hz, 4H, CH$_2$), 7.58 (br.s, 4H, NH$_2$), 8.05–8.16 (m, 4H, NH$_2$), 8.33 (d, ^{3}J = 7.4 Hz, 8H, 4·CH, 4·NH), 8.53 (d, ^{3}J = 7.8 Hz, 4H, CH), 11.57 (br.s, 2H, NH); **^{13}C-NMR**$_{protonated}$ (125 MHz, DMSO$_{d6}$, 120 °C) δ = 8.6 (CH$_3$), 19.6, 35.0, 36.4, 47.3 (CH$_2$), 120.9, 122.0, 122.7 (C$_q$), 123.0 (CH), 123.6, 124.8, 125.2, 127.8 (C$_q$), 129.9 (CH), 132.5, 133.1 (C$_q$), 155.4, 159.4, 160.7, 162.2, 166.8, 171.5 (CN, CO); **FT-IR** (ATR) [cm^{-1}] = 3320 w, 3160 w,

1688 w, 1647 m, 1592 m, 1438 m, 1337 s, 1271 m, 1244 m, 1177 m, 1083 w, 809 s, 745 s; **HR-MS** (neg. ESI) m/z = calculated 501.153–measured 501.156 for $C_{50}H_{44}N_{12}O_{12}$ -$2H^+$.

7. ATTACHMENT

7.1 Zusammenfassung und Ausblick

Die vorliegende Arbeit basiert auf der Idee, die Prinzipien der Supramolekularen-Chemie mit denen der Dendrimer-Chemie zu kombinieren. Zu diesem Zweck wurden verschiedene kovalente Dendrons mit einer supramolekularen Bindungsstelle entwickelt und synthetisiert. Aufgrund von nicht kovalenten Wechselwirkungen wurde erwartet, dass sich in wässriger Lösung supramolekulare Dendrimere ausbilden werden. Das auf reversiblen Wechselwirkungen basierende „self-assembly" kann es unter günstigen Umständen ermöglichen, die Bedingungen, unter denen sich Dendrimere bilden oder wieder disaggregieren, zu kontrollieren. Mit Hilfe einer Säure-Base sensitiven Bindungsstelle war es ein Ziel der vorliegenden Arbeit, diesen reversiblen Aggregationsprozess durch pH-Wert Änderungen zu steuern.

Das Synthesekonzept basiert auf der kovalenten Kombination von HAAGs Polyglycerolen erster bis dritter Generation und SCHMUCKs Guanidiniocarbonyl-Pyrrol Bindungsmotiv. Das Polyglycerol verleiht dem gebildeten Dendrimer Wasserlöslichkeit und das Guanidiniocarbonyl-Pyrrol ist eine effiziente, pH empfindliche Oxo-Anionen Bindungsstelle in Wasser (**Abbildung 7-1**).

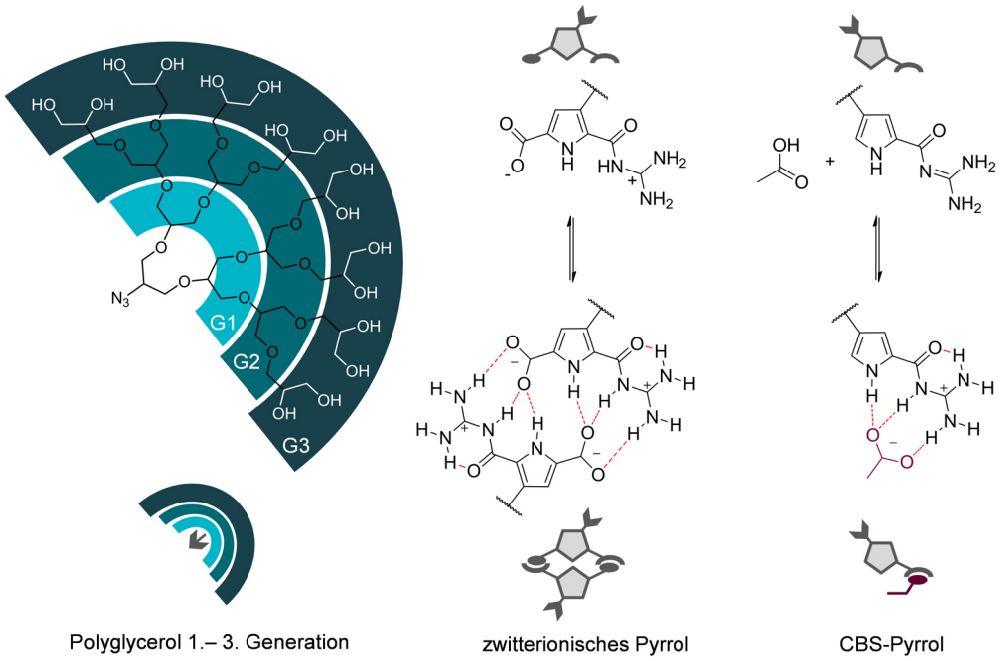

Abbildung 7-1: Die verwendeten Generationen von Polyglycerolen und das Guanidiniocarbonyl-Pyrrol Bindungsmotiv.

Die kovalente Kombination des Polyglycerols mit dem Guanidiniocarbonyl-Pyrrol führte zu verschiedenen Dendrons, welche in drei verschiedenen Methoden auf ihre Eigenschaften supramolekulare Dendrimere zu bilden untersucht wurden:

- CBS templatbasierte supramolekulare Dendrimere (CBS-T-SD),
- zwitterionisch nicht templatbasierte (ZU-SD), und
- zwitterionisch templatbasierte supramolekulare Dendrimere (ZT-SD)

Das Ziel der vorliegenden Arbeit war es, die verschiedenen Methoden für die Bildung von supramolekularen Dendrimeren zu testen und die erfolgversprechendste auf die folgenden Kriterien zu untersuchen:

- Bildung von **diskreten** supramolekularen Dendrimeren, die
- für biologische Anwendungen **stabil und löslich in Wasser** sind, und deren
- self-assembly durch pH-Änderungen **schaltbar** ist

Die verschiedenen Vorgehen wurden in **Kapitel** 4 –Results and Discussion– detailliert diskutiert und sind im Folgenden, mit der CBS templatbasierten Methode beginnend, kurz zusammengefasst.

CBS Templatbasierte Supramolekulare Dendrimere (CBS-T-SD)

Die CBS–T-SD Methode beruht auf dem Konzept supramolekulare Dendrimere durch das self-assembly von CBS-Dendrons um einen multivalenten oxo-Anionenkern aufzubauen (**Abbildung** 7-2).

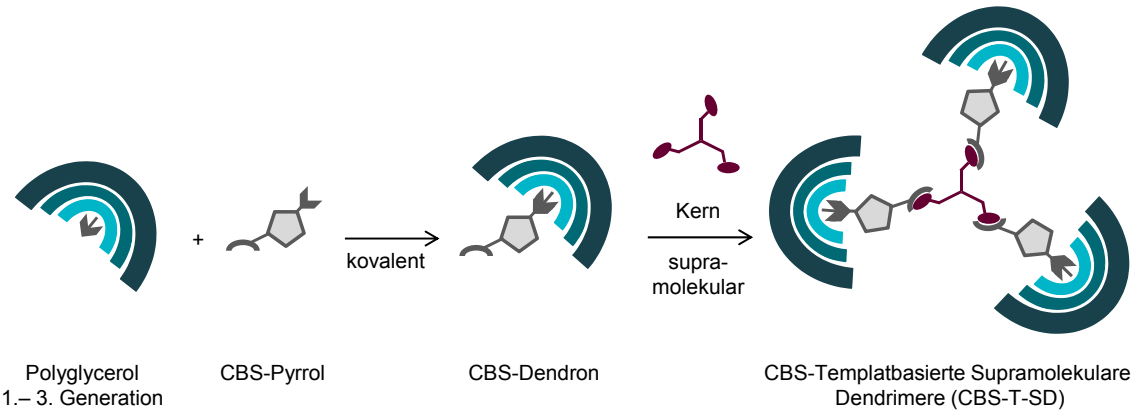

Abbildung 7-2: Schematische Darstellung der CBS-T-SD Methode.

Für das self-assembly wurden die Kernmoleküle TMA (4), EDTA (5), und NTMP (6) verwendeten. Aufgrund ungünstiger sterischer oder synthetischer Probleme einiger CBS-

Dendrons wurden verschiedene synthetische Strategien zu unterschiedlichen Polyglycerol substituierten Pyrrolen verfolgt. Am erfolgversprechendsten war das 2,4-substituierte Pyrrol 41 (**Abbildung 7-3**).

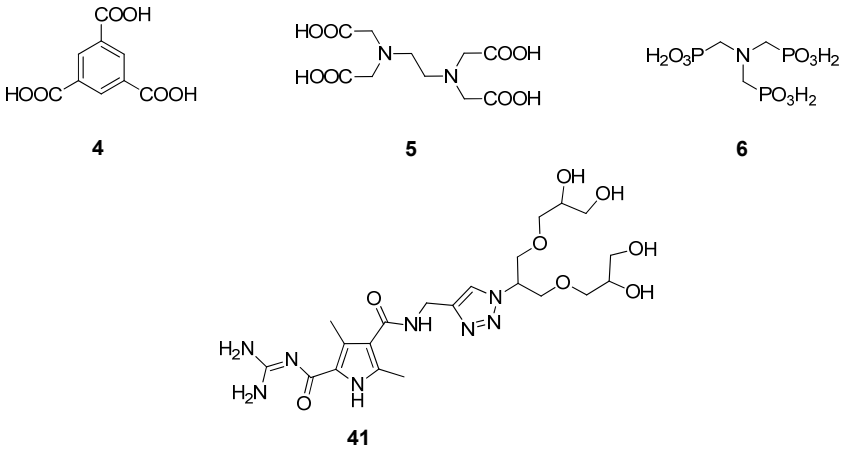

Abbildung 7-3: **Oben**: Carbonsäure und Phosphonsäure Kerne: (TMA, 4), EDTA (5), und NTMP (6).; **Unten**: Auf einem 2,4-substituierten Pyrrol basierendes CBS-Dendron erster Generation (41).

Die self-assembly Experimente zeigten, dass das Dendron 41 offensichtlich keine diskreten 3:1 beziehungsweise 4:1 Heterokomplexe mit den oxo-Anionenkernen 4–6 in Wasser ausbildet. Erste DLS-Experimente deuteten darauf hin, dass unabhängig vom Kern hauptsächlich höhere Aggregate basierend auf Dendron 41 gebildet werden. Es wurde beobachtet, dass die Größe der Aggregate durch den Protonierungsgrad des CBS-Dendrons beeinflusst wird. Das protonierte Dendron 41^+ zeigt hauptsächlich Aggregate mit einem Durchmesser im Bereich von 122–164 nm und das unprotonierte hingegen im Bereich von 255–342 nm (**Abbildung 7-4**).

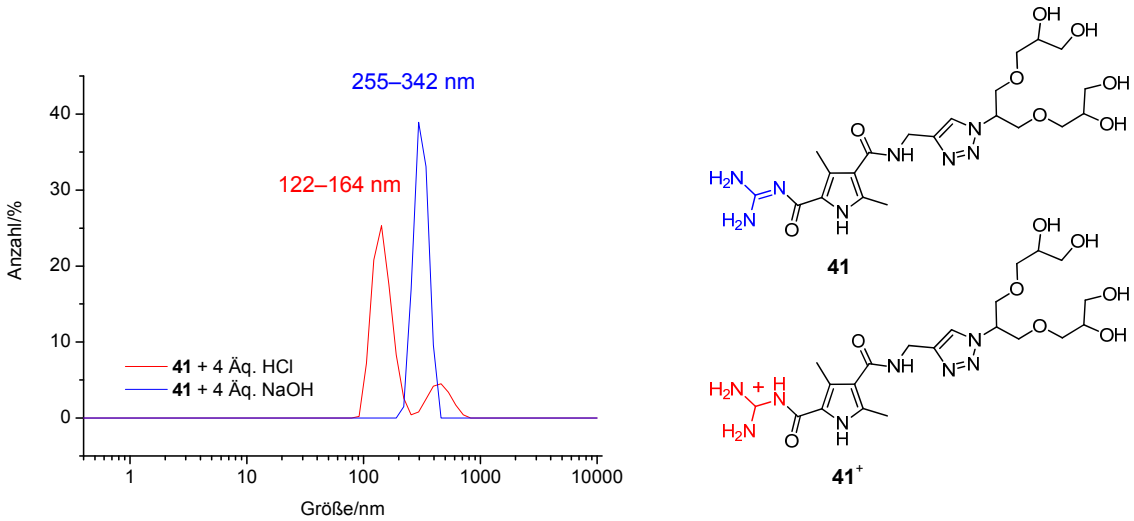

Abbildung 7-4: DLS-Experimente des CBS-Dendrons 41 (5 mM) in Wasser; **Rot**: Zugabe von 4 Äquivalenten HCl, **Blau**: Zugabe von 4 Äquivalenten NaOH.

Um die genaue Struktur der gebildeten Aggregate aufzuklären muss das CBS-Dendron 41 noch weiter mit Hilfe von AFM, DSL, cryo-EM, und SANS-Experimenten untersucht werden,. Wie erste DLS Messungen andeuten ist die Größe und Struktur möglicherweise durch pH-Wert Änderungen beeinflussbar. Da die bis dahin erhaltenen Ergebnisse für das eigentliche Ziel der Arbeit wenig erfolgsversprechend waren, wurde im Rahmen der vorliegenden Arbeit die CBS-T-SD Methode zur Darstellung von diskreten supramolekularen Dendrimeren nicht weiter verfolgt. Die Arbeit wurde weiter auf die zwitterionischen supramolekulare Dendrimere konzentriert, um die bereits genannten Ziele zu erreichen. Die hier erhalten Ergebnisse sind die am erfolgversprechendsten von allen untersuchten Systemen und werden im Folgenden kurz zusammengefasst.

Zwitterionische nicht Templatbasierte Supramolekulare Dendrimere (ZU-SD)

Zur Realisierung der in **Abbildung 7-5** dargestellten Methode musste ein selbst-komplementäres Dendron synthetisiert werden, um das supramolekulare Dendrimer, basierend auf dem homo-dimer des zwitterionischen Dendrons, zu erhalten.

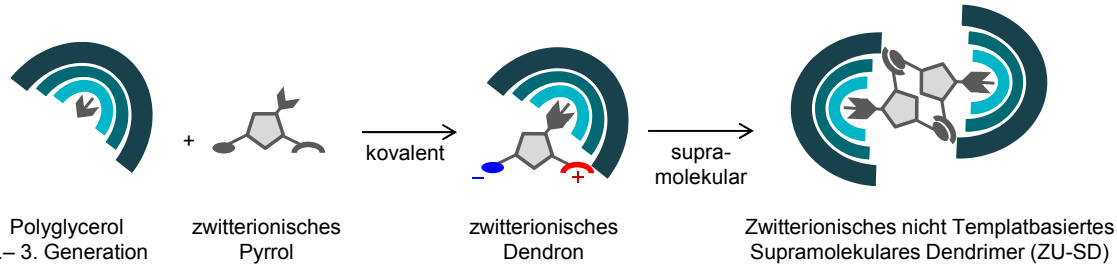

Abbildung 7-5: Schematische Darstellung der ZU-SD Methode.

Die Polyglycerole erster bis dritter Generation wurden durch eine Click Reaktion an der β-Position des Pyrrols verknüpft. Die hergestellten zwitterionischen Dendrons **50–52** sind in **Abbildung 7-6** dargestellt.

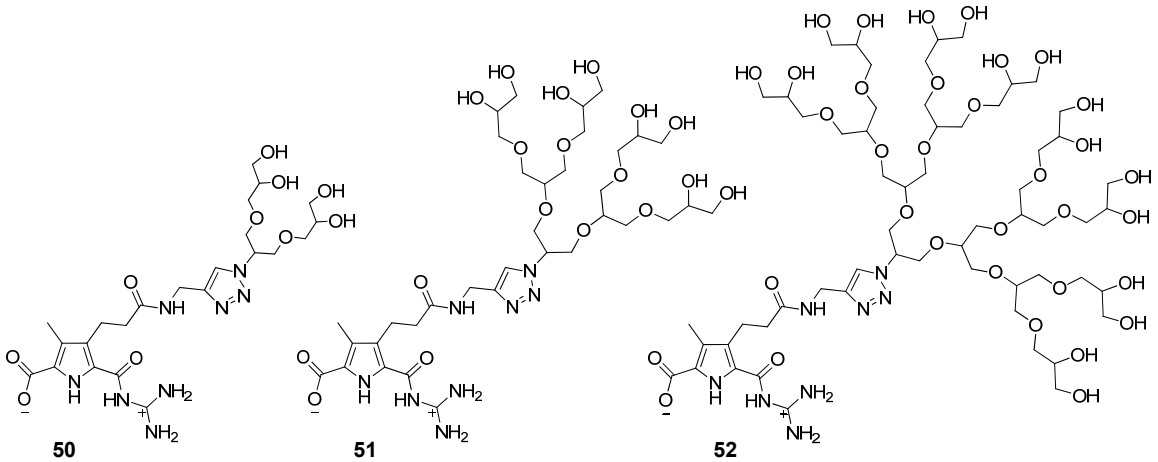

Abbildung 7-6: Zwitterionische Dendrons **50–52**

Die Kombination verschiedener analytischer Methoden, DOSY-NMR, DLS, cryo-EM, SEC und ITC zeigte, dass die zwitterionischen Dendrons eine starke Tendenz besitzen zu diskreten 1:1 Homoassoziaten im niedrigen Nanometerbereich zu dimerisieren (**Abbildung 7-7**).

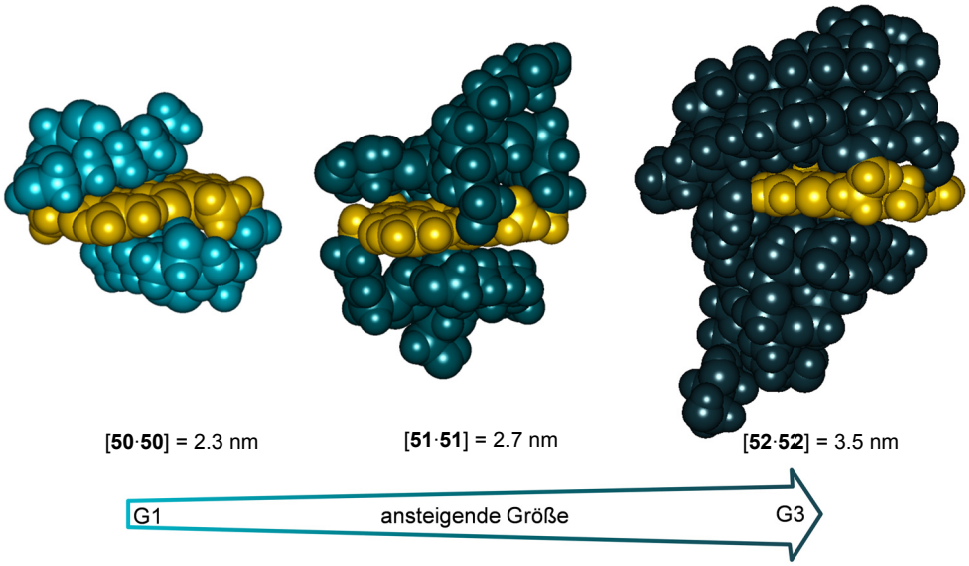

Abbildung 7-7: Von links nach rechts: Berechnete zwitterionische Struktur der Dimere [50·50]–[52·52]. Macromodel, Kraftfeld OPLS 2005 in Wasser.

pH-Abhängige DLS Messungen zeigten das erfolgreiche reversible self-assembly der zweiten (51) und dritten (52) Generation zwitterionischer Dendrons in wässriger Lösung (**Figure 5-8**).

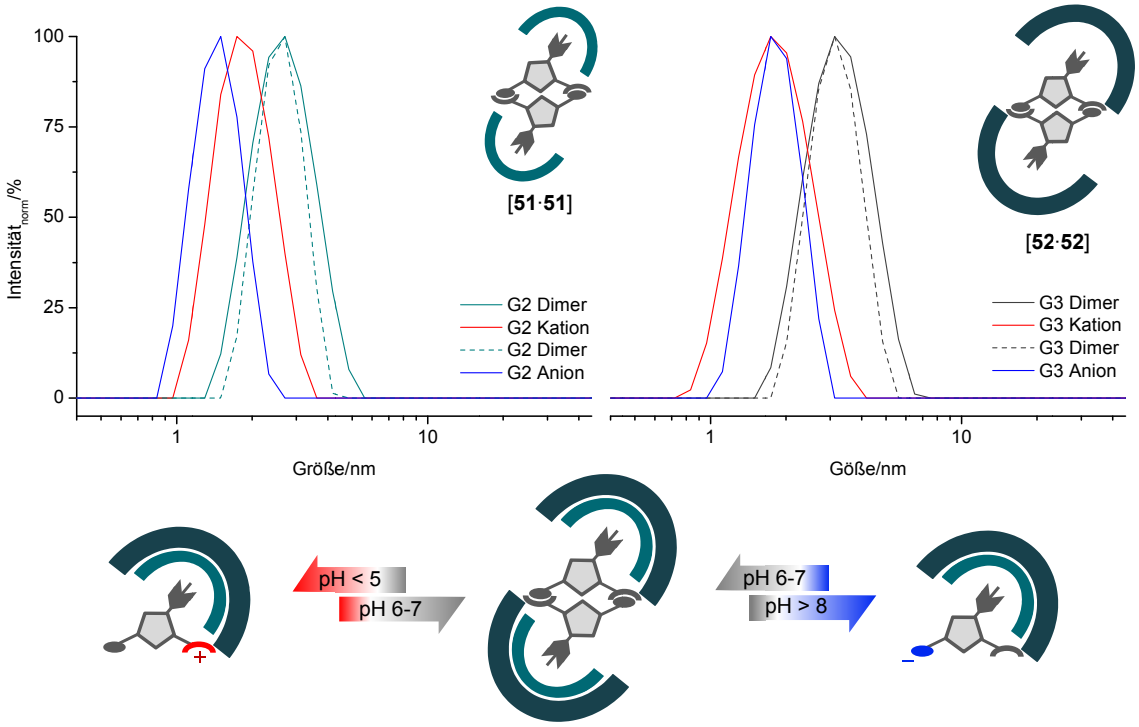

Abbildung 7-8: **Oben**: DLS-Messungen von 4.5 mM wässriger Lösung der zweiten (51) und dritten (52) Generation; **Unten**: Reversible pH-abhängige Schaltung dendritischer Dimere zu kationischen beziehungsweise anionischen Monomeren. Dimere werden nur in neutralem pH gebildet, während bei pH < 5 und pH > 8 nur die protonierten und deprotonierten Monomere vorliegen.

Dies ist das erste Beispiel eines reversiblen schaltbaren self-assembly von zwei biokompatiblen Polyglyceroldendronen zu diskreten wohldefinierten supramolekularen Dendrimeren in Wasser.[i] Die Säure-Base Eigenschaften des eingebetteten Guanidiniocarbonyl-Pyrrol Bindungsmotivs ermöglichen diese neuen reversiblen, pH schaltbaren supramolekularen Dendrimere. Diese einzigartige Eigenschaft in Kombination mit der hohen Biokompatibilität der dendritischen Polyglycerole schafft eine neue Basis für pH schaltbare Nanotransporter in Biomedizinischen Anwendungen.

Zusammenfassend lässt sich sagen, dass die hier hergestellten zwitterionischen supramolekularen Dendrimere DISKRET, STABIL und SCHALTBAR in wässriger Lösung sind. Weiterführende Arbeiten mit dem Ziel diese Dendrimere als Nanotransporter zu nutzen sollten sich zunächst auf die Weiterentwicklung des zwitterionischen Dendrons konzentrieren. Die Größe und die innere Polarität des Dimers könnten durch die folgenden Änderungen modifiziert und angepasst werden.

Die Größe des Dendrimers, eine wichtige Eigenschaft für die Einkapselung von Molekülen, kann durch die Erweiterung des Dendrons um eine zweite Polyglycerolgruppe in der β-Position des Pyrrols beeinflusst werden (**Abbildung 7-9**). Die berechnete Struktur des Dimers hat eine Größe von 4.5 nm und deutet auf ein weniger dicht gepacktes Innere des Dendrimers hin. Dies ist ebenfalls wichtiges Kriterium für die Einkapselung von Gast-Molekülen.

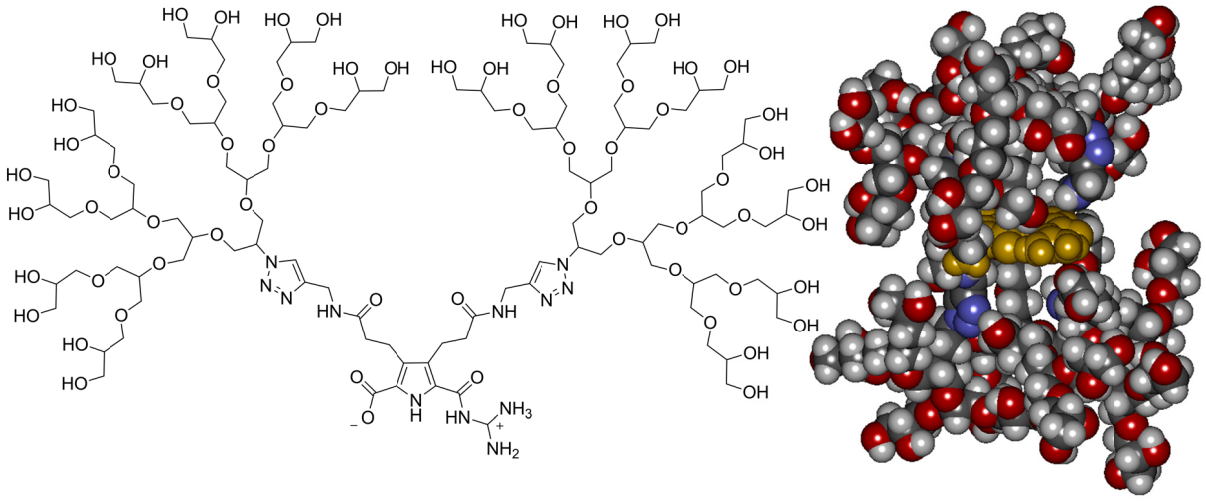

Abbildung 7-9: Vergrößerung des Dendrons durch eine zweite Polyglyceroleinheit an der β-Position des Pyrrols. **Links**: Schematisch dargestelltes Monomer; **Rechts**: Berechnetes Dimer, Größe 4.5 nm im Durchmesser.

Eine weitere Modifizierung zu einem erfolgversprechenden Nanotransporter ist die Variation der inneren Polarität. Diese könnte durch die Kombination von unpolaren Verzweigungs-

[i] Basierend auf den hydrophoben Effekt und resultierender Mizell Bildung haben die Gruppen um HIRSCH und BÖTTCHER bereits wohl definierte schaltbare Mizellen veröffentlicht.[87]

einheiten (FRÉCHET-ähnliche Dendrons) in der Nähe der Bindungsstelle mit den polaren Polyglyceroldendrons in der Peripherie geschehen (**Abbildung 7-10**).

Die berechnete Struktur des Dimers hat einen Durchmesser von 4.6 nm und deutet ebenfalls auf ein weniger dicht gepacktes Innere hin, in welchem die aromatischen Verzweigungseinheiten über und unter dem zwitterionischen Pyrroldimer organisiert sind. Zwischen dem aromatischen Bindungsmotiv und den Verzweigungseinheiten ist nach Berechnungen freier Raum, welcher für die Einkapselung von unpolaren Gast Molekülen über π-Wechselwirkung vorteilhaft sein kann.

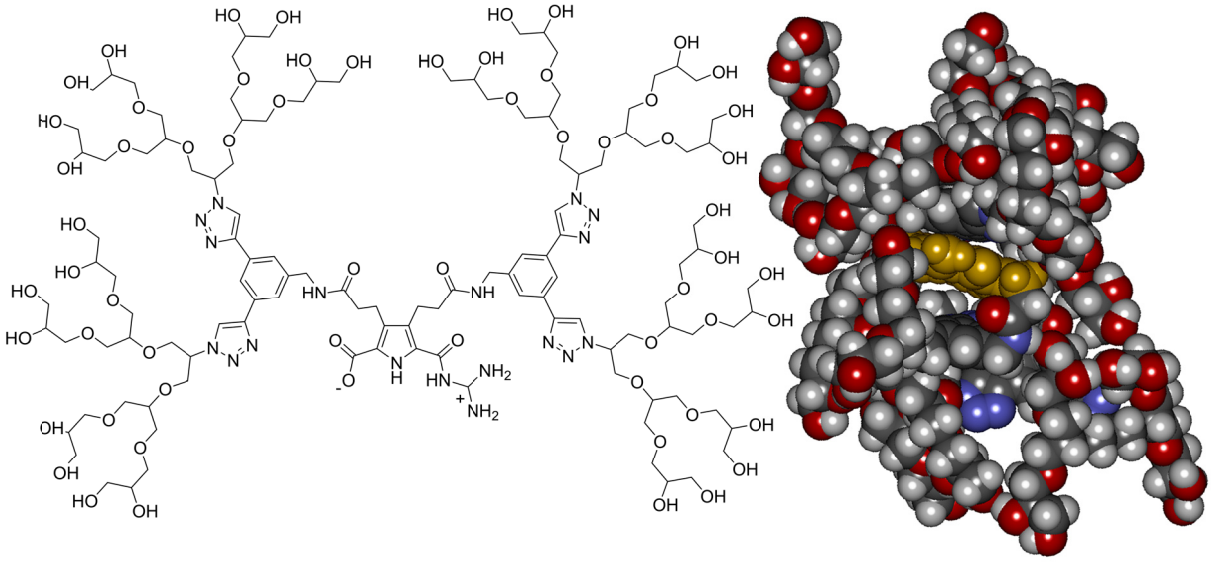

Abbildung 7-10: Veränderung der inneren Polarität mit Hilfe von aromatischen Verzweigungseinheiten zwischen der Bindungsstelle und den Polyglyceroleinheiten. **Links**: Schematisch dargestelltes Monomer; **Rechts**: Berechnetes Dimer, Größe 4.6 nm im Durchmesser.

Zusätzlich zu der ZU-SD Methode, wie oben gezeigt, wurden die zwitterionischen Dendrons **50–52** auch in einer zwitterionisch templatbasierten Methode verwendet, in der die Dendrons sich um einen zwitterionischen Kern assemblieren.

Zwitterionisch Templatbasierte Supramolekulare Dendrimere (ZT-SD)

Für die ZT-SD Methode wurde zusätzlich ein zwitterionischer Kern benötigt, um ein Heteroassoziat mit den Dendrons **50–52** zu bilden. (**Abbildung 7-11**). Für die Assemblierung von zwei Dendrons um einen zwitterionischen Kern wurde ein Perylendiimid-Derivat mit zwei zwitterionischen Pyrrolen in den Imidpositionen synthetisiert.

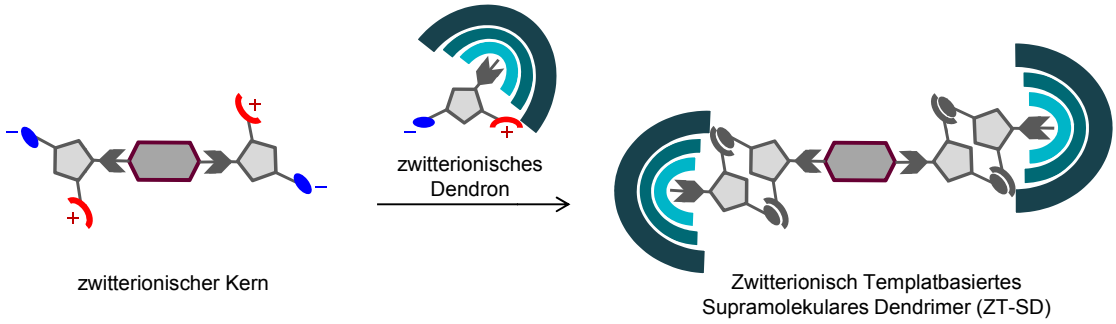

Abbildung 7-11: Schematische Darstellung der ZT-SD Methode.

Der zwitterionische Kern konnte mit Hilfe der ersten bis dritten Generation der Dendrons solubilisiert werden, wie in **Abbildung** 7-12 dargestellt.

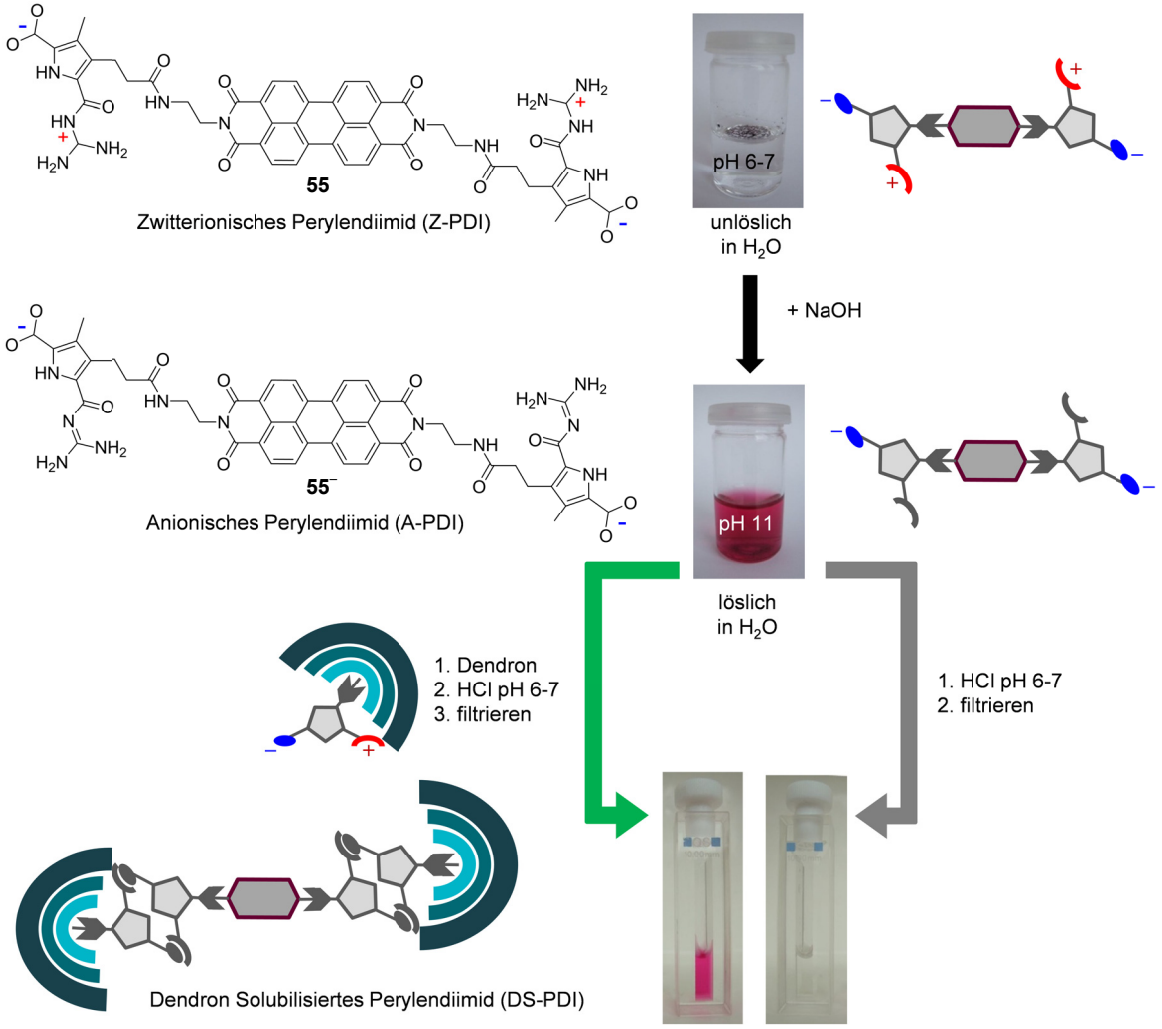

Abbildung 7-12: Löslichkeitstest des Perylendiimids **55** in Wasser; **Schwarz**: Wasser unlösliches zwitterionisches Perylendiimid **55** wurde mit 40 Äquivalenten Natriumhydroxid gelöst; **Grün**: Die wässrige Lösung von **55** wurde mit den Dendrons **50**, **51**, und **52** (je 4 Äquivalente) versetzt. Nach Einstellen des pH auf 6–7 mit Salzsäure und Filtration der 0.1 mM Lösung von **55** durch einen PTFE Spritzenfilter (0.45 µm Porengröße); **Grau**: Nach Einstellen des pH auf 6–7 mit Salzsäure und Filtration der 0.1 mM Lösung von **55** durch einen PTFE Spritzenfilter (0.45 µm Porengröße).

Die qualitative Solubilisierung des Perylenkerns **55** durch die Assemblierung mit den Dendrons **50–52** wie in **Abbildung 7-12** gezeigt wurde ebenfalls quantitativ mit Hilfe eines pH-Titrationsexperiments durchgeführt und mit Hilfe von UV/Vis Spektroskopie verfolgt. Die aufgenommenen Absorptionsspektren zeigen die Solubilisierung des monomeren Perylendiimids durch das zwitterionischen Dendron **51** (**Abbildung 7-13**).

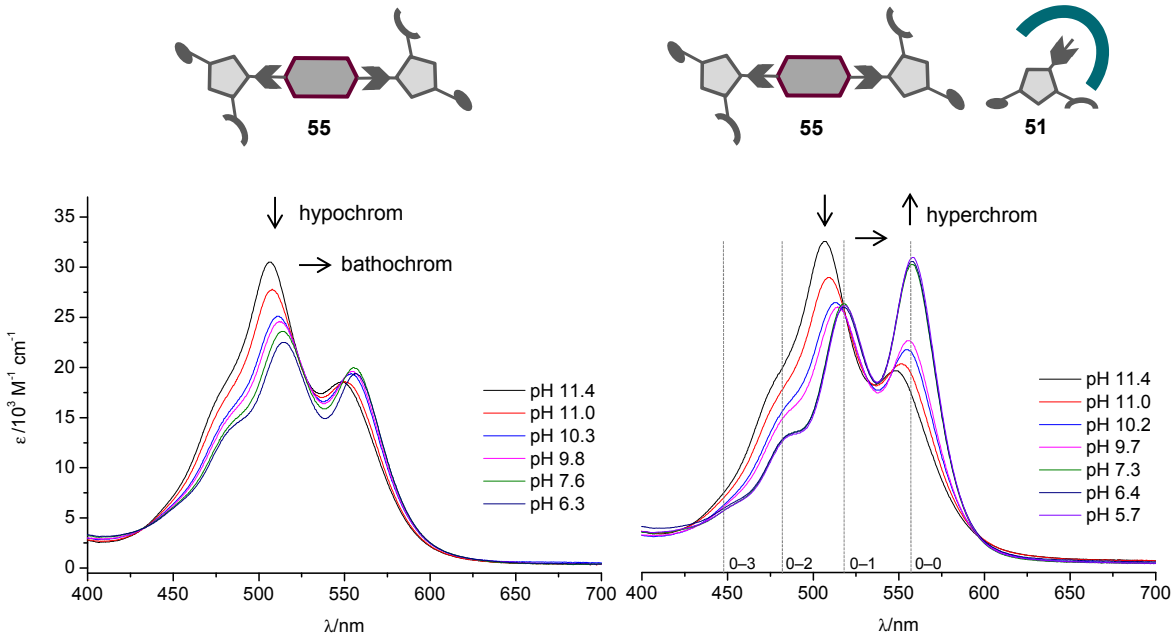

Abbildung 7-13: UV/Vis pH Titration: **Links**: Perylendiimid **55** (0.01 mM) und Natriumhydroxid (0.4 mM) –l; **Rechts**: Perylendiimid **55** (0.01 mM), Natriumhydroxid (0.4 mM), und 10 Äquivalente des Dendron **51** (0.1 mM) – Einstellen des pH mit 0.1 N HCl.

Die UV/Vis Eigenschaften von Perylendiimiden in Abhängigkeit zu den gebildeten Aggregaten sind sehr gut untersucht und somit sind die erhaltenen Spektren ein starker Beweis für die Solubilisierung von monomeren Perylendiimid **55** durch die Dendrons **50–52**.

Die beste Erklärung für die experimentellen Beobachtungen ist die Bildung eines 1:2 Heteroassoziats, in dem das Perylendiimid zwischen dem zwitterionischen Pyrroldimer eingeschlossen ist (**Abbildung 7-14**). Quantenchemisch berechnete Anregungsenergien und pH Effekte unterstreichen die Hypothese von solch einem diskreten supramolekularen Dendrimer.

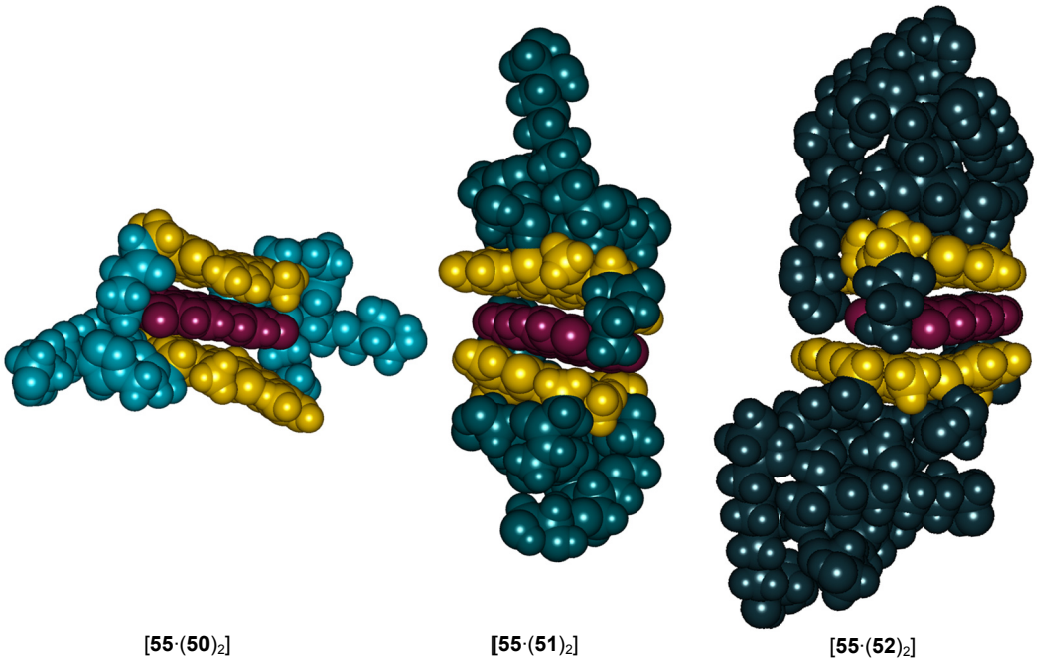

Abbildung 7-14: Molecular Modelling mit OPLS 2005 Kraftfeld in Wasser; Möglicher 1:2 Komplex des zwitterionischen Perylendiimid und der 1. bis 3. Generation zwitterionischer Dendrons.

Ein großer Nachteil dieser Systeme sind die nicht orthogonalen Bindungsmodi des zwitterionischen Kernes und der Dendrons (AA-System). Dadurch ist es schwierig wohldefinierte Systeme, wie die zwitterionischen nicht templatbasierten supramolekularen Dendrimere, zu bilden. Eine mögliches neues Konzept für eine orthogonale Bindungsstelle (AB-System) könnte auf einem weiterentwickelten Guanidiniocarbonyl-Pyrrol basieren wie in **Abbildung 7-15** dargestellt.

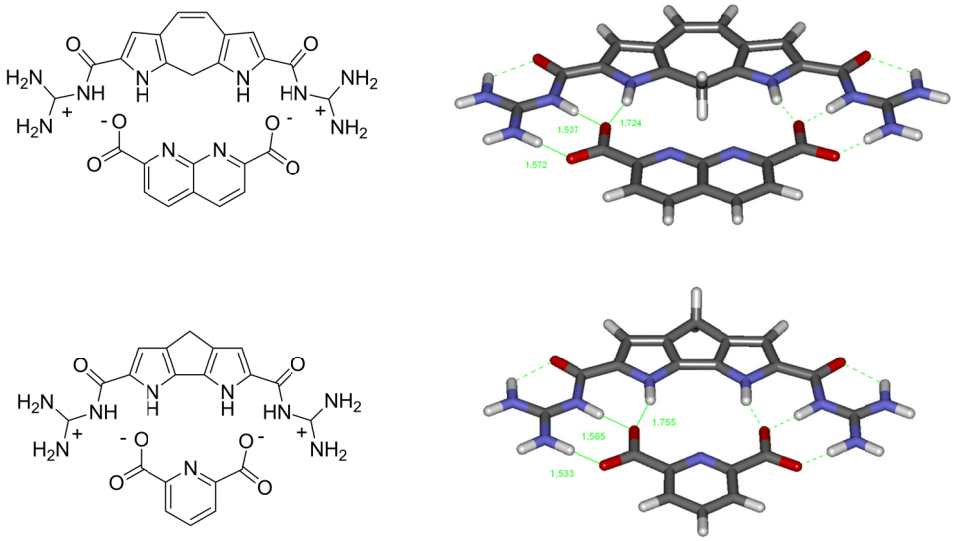

Abbildung 7-15: Mögliches neues orthogonales Bindungsmotiv basierend auf dem zwitterionischen Guanidiniocarbonyl-Pyrrol von SCHMUCK.

Das Ziel dieser Arbeit war es monodisperse supramolekulare Dendrimere zu erhalten, die in Wasser stabil und pH schaltbar sind. Dieses Ziel wurde im Falle des zwitterionischen nicht templatbasierten Konzepts, durch die Kombination der Polyglycerole von HAAG und dem zwitterionischen Guanidiniocarbonyl-Pyrrol-Carboxylat von SCHMUCK, erreicht, wie in **Kapitel 4.3.1** detailliert diskutiert. Weitere Untersuchungen dieser Aggregate, als mögliche Nanotransporter für biomedizinische Anwendungen, werden folgen und versprechen spannende Ergebnisse zu liefern.

7.2 List of Abbreviations

abbreviation	name
°	degree
°C	degree Celsius
α	polymerisation degree
δ	chemical shift
Δ	delta
ε	extinction coefficient
η	viscosity
λ	wavelength
µ	micro
A	acceptor
A-PDI	anionic perylene diimide
AFM	atomic force microscope
ATR	attenuated total reflectance
AU	absorbance units
Bn	benzyl
Boc	tert-butyloxycarbonyl
^{t}Bu	tert-butyl
ca.	circa
CBS	carboxylate binding site
CBS-T-SD	carboxylate binding site templated supramolecular dendrimer
Cbz	Benzyloxycarbonyl
$CDCl_3$	deuterated chloroform
conc.	concentrated
d	diameter
D	donor
D	diffusion coefficient
DCM	dichloromethane
DIPEA	diisopropylethylamine
DLS	dynamic light scattering
DMF	N,N-dimethylformamide
DMSO	dimethylsulfoxide

$DMSO_{d6}$	deuterated dimethylsulfoxide
DNA	deoxyribonucleic acid
DOSY	diffusion ordered spectroscopy
DS-PDI	dendron solubilised perylene diimide
eq.	equivalents
EDTA	ethylene diamine tetracarboxylic acid
e.g.	*exempli gratia*
EM	electron microscopy
ESI	electron spray ionisation
Et	ethyl
et al.	*et alii*
f	femto
f	friction
FT-IR	Fourier-transform infrared
g	gramm
G	generation
h	height
HPLC	high performance liquid chromatography
HR-MS	high resolution mass spectrometry
Hz	Hertz
i.e.	*id est*
ITC	isothermal titration calorimetry
J	Joule
k	Boltzmann constant
K	Kelvin
K	association constant
l	litre
m	milli
m	metre
M	molar
m/z	mass per charge
MALDI	matrix assisted laser desorption/ionisation
Me	methyl
min	minutes
MHz	mega Hertz

MM	molecular mechanics
mp	melting point
MPLC	medium performance liquid chromatography
n	nano
N	normal
N	Avogadro's constant
neg.	negative
NMM	N-methylmorpholine
NMR	nuclear magnetic resonance
norm	normalised
NTMP	nitrilio trimethylene phosphonic acid
p	pico
PAMAM	polyamidoamine
Pd/C	palladium on charcoal
PDI	perylene diimide
pH	pondus hydrogenii
POPAM	polypropyleneamine
pos.	positive
PPI	polypropyleneimine
ppm	parts per million
PTCDA	perylene tetracarboxylic dianhydride
PyBOP	(Benzotriazol-1-yloxy)-tripyrrolidiniophosphonium-hexafluorophosphate
r	radius
R	gas constant
RP18	reversed phase octadecyl chains
s	seconds
SANS	small angle neutron scattering
SD	supramolecular dendrimer
SEC	size exclusion chromatography
SiO_2	silicagel
T	temperature
t	time
TD-DFT	time-dependet density functional theory
TFA	trifluoroacetic acid

THF	tetrahydrofuran
TLC	thin layer chromatography
TMA	trimesic acid
UV	ultraviolet
Vis	visible
Z-PDI	zwitterionic perylene diimide
ZT-SD	zwitterionic templated supramolecular dendrimer
ZU-SD	zwitterionic untemplated supramolecular dendrimer

7.3 Physicochemical DOSY-NMR Data

7.3.1 CBS-Templated Supramolecular Dendrimers

Table 7–1: Signal dependent diffusion coefficients *D* of (**39**) (15 mM) in $DMSO_{d6}$, 500 MHz, T = 298 K.

G–P[^{3}Me^{4}G1]–Me (**39**)	D/m^2·s^{-1}	ppm
1	$1.43 \cdot 10^{-10}$	7.97 – 7.87
2	$1.41 \cdot 10^{-10}$	7.80 – 7.72
3	$1.42 \cdot 10^{-10}$	5.01 – 4.91
4	$1.41 \cdot 10^{-10}$	4.48 – 4.39
5	$1.44 \cdot 10^{-10}$	4.13 – 4.05
6	$1.41 \cdot 10^{-10}$	3.95 – 3.78
7	$1.46 \cdot 10^{-10}$	3.54 – 3.49
8	$1.45 \cdot 10^{-10}$	2.48 – 2.40
9	$1.41 \cdot 10^{-10}$	2.32 – 2.25
10	$1.44 \cdot 10^{-10}$	1.30 – 1.26
11	$1.39 \cdot 10^{-10}$	1.26 – 1.20

Table 7–2: Signal dependent diffusion coefficients *D* of **4** (15 mM) in $DMSO_{d6}$, 500 MHz, T = 298 K.

TMA **4**	D/m^2·s^{-1}	ppm
1	$2.11 \cdot 10^{-10}$	8.78 – 8.54

Table 7–3: Signal dependent diffusion coefficients *D* of **39** (15 mM) and **4** (3.75 mM) in $DMSO_{d6}$, 500 MHz, T = 298 K.

[(**39**)$_3$·**4**]	D/m^2·s^{-1}	ppm
TMA **4**	$1.49 \cdot 10^{-10}$	8.67 – 8.66
1	$1.41 \cdot 10^{-10}$	7.94 – 7.91
2	$1.33 \cdot 10^{-10}$	7.91 – 7.85
3	$1.38 \cdot 10^{-10}$	4.99 – 4.92
4	$1.38 \cdot 10^{-10}$	4.47 – 4.41
5	$1.40 \cdot 10^{-10}$	4.13 – 4.05
6	$1.39 \cdot 10^{-10}$	3.93 – 3.79
7	$1.46 \cdot 10^{-10}$	3.54 – 3.47
8	$1.41 \cdot 10^{-10}$	2.45 – 2.40
9	$1.36 \cdot 10^{-10}$	2.35 – 2.31
10	$1.42 \cdot 10^{-10}$	1.29 – 1.25
11	$1.39 \cdot 10^{-10}$	1.25 – 1.20

Table 7–4: Signal dependent diffusion coefficients *D* of **5** (3.75 mM) in $DMSO_{d6}$, 500 MHz, T = 298 K.

EDTA **5**	D/m^2·s^{-1}	ppm
1	$1.86 \cdot 10^{-10}$	3.46 – 3.45
2	$1.90 \cdot 10^{-10}$	2.79 – 2.74

Table 7–5: Signal dependent diffusion coefficients *D* of **39** (15 mM) and EDTA **5** (3.75 mM) in $DMSO_{d6}$, 500 MHz, T = 298 K.

[(**39**)$_4$·**5**]	$D/m^2 \cdot s^{-1}$	ppm
1	$1.48 \cdot 10^{-10}$	7.94 – 7.90
2	$1.44 \cdot 10^{-10}$	7.86 – 7.79
3	$1.49 \cdot 10^{-10}$	5.00 – 4.93
4	$1.46 \cdot 10^{-10}$	4.46 – 4.41
5	$1.49 \cdot 10^{-10}$	4.12 – 4.04
6	$1.47 \cdot 10^{-10}$	3.93 – 3.79
7	$1.60 \cdot 10^{-10}$	3.54 – 3.48
8	$1.56 \cdot 10^{-10}$	3.47 – 3.35
EDTA **5**	$1.59 \cdot 10^{-10}$	2.87 – 2.82
9	$1.47 \cdot 10^{-10}$	2.44 – 2.39
10	$1.44 \cdot 10^{-10}$	2.31 – 2.25
11	$1.53 \cdot 10^{-10}$	1.30 – 1.25

Table 7–6: Signal dependent diffusion coefficients *D* of **6** (3.75 mM) in $DMSO_{d6}$, 500 MHz, T = 298 K.

NTMP **6**	$D/m^2 \cdot s^{-1}$	ppm
1	$1.92 \cdot 10^{-10}$	3.21 – 3.13

Table 7–7: Signal dependent diffusion coefficients *D* of **39** (15 mM) and NTMP **6** (5 mM) in $DMSO_{d6}$, 500 MHz, T = 298 K.

[(**39**)$_3$·**6**]	$D/m^2 \cdot s^{-1}$	ppm
1	$1.28 \cdot 10^{-10}$	12.15 – 11.93
2	$1.30 \cdot 10^{-10}$	8.09 – 8.00
3	$1.27 \cdot 10^{-10}$	7.97 – 7.92
4	$1.27 \cdot 10^{-10}$	5.00 – 4.92
5	$1.26 \cdot 10^{-10}$	4.47 – 4.41
6	$1.28 \cdot 10^{-10}$	4.13 – 4.04
7	$1.25 \cdot 10^{-10}$	3.93 – 3.79
8	$1.33 \cdot 10^{-10}$	3.54 – 3.47
9	$1.22 \cdot 10^{-10}$	3.47 – 3.34
NTMP **6**	$1.30 \cdot 10^{-10}$	3.03 – 2.90
10	$1.31 \cdot 10^{-10}$	2.42 – 2.35
11	$1.21 \cdot 10^{-10}$	2.35 – 2.26
12	$1.36 \cdot 10^{-10}$	1.30 – 1.25
13	$1.21 \cdot 10^{-10}$	1.25 – 1.19

7.3.2 Zwitterionic Untemplated Supramolecular Dendrimers

Table 7–8: Signal dependent diffusion coefficients *D* of 1st generation monomeric precursor **47** (15 mM) in $DMSO_{d6}$, 500 MHz, T = 298 K.

47	$D/m^2 \cdot s^{-1}$	ppm
1	$1.45 \cdot 10^{-10}$	10.72 – 10.59
2	$1.34 \cdot 10^{-10}$	10.21 – 10.09
3	$1.35 \cdot 10^{-10}$	9.50 – 9.35
4	$1.39 \cdot 10^{-10}$	8.51 – 8.39
5	$1.38 \cdot 10^{-10}$	8.35 – 8.27
6	$1.35 \cdot 10^{-10}$	7.92 – 7.86
7	$1.39 \cdot 10^{-10}$	4.97 – 4.91
8	$1.37 \cdot 10^{-10}$	4.32 – 4.25
9	$1.38 \cdot 10^{-10}$	4.12 – 4.06
10	$1.40 \cdot 10^{-10}$	3.93 – 3.88
11	$1.31 \cdot 10^{-10}$	3.88 – 3.79
12	$1.43 \cdot 10^{-10}$	3.54 – 3.48
13	$1.37 \cdot 10^{-10}$	3.47 – 3.37
14	$1.36 \cdot 10^{-10}$	3.00 – 2.91
15	$1.43 \cdot 10^{-10}$	2.33 – 2.25
16	$1.39 \cdot 10^{-10}$	2.19 – 2.14
17	$1.41 \cdot 10^{-10}$	1.55 – 1.52
18	$1.32 \cdot 10^{-10}$	1.51 – 1.46
19	$1.42 \cdot 10^{-10}$	1.29 – 1.26
20	$1.37 \cdot 10^{-10}$	1.25 – 1.21

Table 7–9: Signal dependent diffusion coefficients *D* of 1st generation dimer {**50**·**50**} (15 mM) in $DMSO_{d6}$, 500 MHz, T = 298 K.

[**50**·**50**]	$D/m^2 \cdot s^{-1}$	ppm
1	$9.51 \cdot 10^{-11}$	12.69 – 12.61
2	$9.84 \cdot 10^{-11}$	8.26 – 8.18
3	$1.01 \cdot 10^{-10}$	8.01 – 7.95
4	$9.79 \cdot 10^{-11}$	7.92 – 7.88
5	$9.59 \cdot 10^{-11}$	4.94 – 4.87
6	$9.60 \cdot 10^{-11}$	4.67 – 4.60
7	$9.36 \cdot 10^{-11}$	4.50 – 4.44
8	$9.71 \cdot 10^{-11}$	4.32 – 4.25
9	$9.69 \cdot 10^{-11}$	3.87 – 3.75
10	$9.87 \cdot 10^{-11}$	3.55 – 3.47
11	$1.03 \cdot 10^{-10}$	3.43 – 3.36
12	$9.88 \cdot 10^{-11}$	3.28 – 3.24
13	$9.62 \cdot 10^{-11}$	2.99 – 2.95
14	$1.05 \cdot 10^{-10}$	2.32 – 2.27
15	$9.99 \cdot 10^{-11}$	2.26 – 2.23

Table 7–10: Signal dependent diffusion coefficients *D* of 1st generation monomeric precursor **48** (15 mM) in $DMSO_{d6}$, 500 MHz, T = 298 K.

48	$D/m^2 \cdot s^{-1}$	ppm
1	$1.26 \cdot 10^{-10}$	10.67 – 10.61
2	$1.19 \cdot 10^{-10}$	10.13 – 10.08
3	$1.20 \cdot 10^{-10}$	9.49 – 9.38
4	$1.22 \cdot 10^{-10}$	8.48 – 8.40
5	$1.17 \cdot 10^{-10}$	8.32 – 8.23
6	$1.18 \cdot 10^{-10}$	7.92 – 7.88
7	$1.25 \cdot 10^{-10}$	4.95 – 4.83
8	$1.24 \cdot 10^{-10}$	4.32 – 4.25
9	$1.21 \cdot 10^{-10}$	4.16 – 4.07
10	$1.17 \cdot 10^{-10}$	3.98 – 3.90
11	$1.12 \cdot 10^{-10}$	3.86 – 3.79
12	$1.22 \cdot 10^{-10}$	3.60 – 3.53
13	$1.18 \cdot 10^{-10}$	3.46 – 3.35
14	$1.15 \cdot 10^{-10}$	2.99 – 2.91
15	$1.25 \cdot 10^{-10}$	2.32 – 2.25
16	$1.20 \cdot 10^{-10}$	2.20 – 2.14
17	$1.30 \cdot 10^{-10}$	1.56 – 1.52
18	$1.15 \cdot 10^{-10}$	1.47 – 1.46
19	$1.28 \cdot 10^{-10}$	1.32 – 1.28
20	$1.11 \cdot 10^{-10}$	1.26 – 1.22

Table 7–11: Signal dependent diffusion coefficients *D* of 1st generation dimer [**51**·**51**] (15 mM) in $DMSO_{d6}$, 500 MHz, T = 298 K.

[**51**·**51**]	$D/m^2 \cdot s^{-1}$	ppm
1	$7.83 \cdot 10^{-11}$	12.70 – 12.60
2	$7.99 \cdot 10^{-11}$	8.26 – 8.17
3	$8.16 \cdot 10^{-11}$	7.98 – 7.90
4	$7.84 \cdot 10^{-11}$	4.93 – 4.81
5	$7.82 \cdot 10^{-11}$	4.66 – 4.59
6	$8.16 \cdot 10^{-11}$	4.56 – 4.53
7	$7.40 \cdot 10^{-11}$	4.51 – 4.42
8	$7.91 \cdot 10^{-11}$	4.31 – 4.26
9	$8.02 \cdot 10^{-11}$	3.97 – 3.90
10	$7.92 \cdot 10^{-11}$	3.86 – 3.78
11	$8.25 \cdot 10^{-11}$	3.59 – 3.52
12	$8.02 \cdot 10^{-11}$	3.01 – 2.95
13	$8.54 \cdot 10^{-11}$	2.32 – 2.27
14	$7.88 \cdot 10^{-11}$	2.26 – 2.21

Table 7–12: Signal dependent diffusion coefficients *D* of 1st generation monomeric precursor **49** (15 mM) in $DMSO_{d6}$, 500 MHz, T = 298 K.

49	$D/m^2 \cdot s^{-1}$	ppm
1	9.63·10–11	8.28 – 8.21
2	9.86·10–11	7.91 – 7.88
3	9.70·10–11	4.86 – 4.79
4	9.67·10–11	4.32 – 4.26
5	9.41·10–11	4.19 – 4.06
6	9.38·10–11	4.00 – 3.89
7	9.99·10–11	3.63 – 3.55
8	9.58·10–11	3.48 – 3.39
9	9.57·10–11	3.01 – 2.89
10	9.76·10–11	2.31 – 2.25
11	9.51·10–11	2.18 – 2.13
12	9.80·10–11	1.55 – 1.51
13	9.30·10–11	1.50 – 1.45
14	9.96·10–11	1.32 – 1.28
15	9.20·10–11	1.27 – 1.22

Table 7–13: Signal dependent diffusion coefficients *D* of 1st generation dimer [**52**·**52**] (15 mM) in $DMSO_{d6}$, 500 MHz, T = 298 K.

[**52**·**52**]	$D/m^2 \cdot s^{-1}$	ppm
1	$5.73 \cdot 10^{-11}$	12.76 – 12.50
2	$6.04 \cdot 10^{-11}$	8.37 – 8.20
3	$6.04 \cdot 10^{-11}$	8.06 – 7.92
4	$6.04 \cdot 10^{-11}$	4.87 – 4.79
5	$6.09 \cdot 10^{-11}$	4.70 – 4.63
6	$5.86 \cdot 10^{-11}$	4.63 – 4.59
7	$5.93 \cdot 10^{-11}$	4.57 – 4.49
8	$6.01 \cdot 10^{-11}$	4.34 – 4.26
9	$6.09 \cdot 10^{-11}$	3.98 – 3.88
10	$6.29 \cdot 10^{-11}$	3.59 – 3.53
11	$5.99 \cdot 10^{-11}$	3.52 – 3.48
12	$6.30 \cdot 10^{-11}$	3.45 – 3.38
13	$5.74 \cdot 10^{-11}$	3.33 – 3.28
14	$5.99 \cdot 10^{-11}$	3.01 – 2.94
15	$6.43 \cdot 10^{-11}$	2.32 – 2.28
16	$5.79 \cdot 10^{-11}$	2.26 – 2.21

8. BIBLIOGRAPHY

[1] Lehn J-M., "From Matter to Life: Chemistry", *Resonance J. Sci. Edu.*, **1996**, *1*, 39–53.
[2] a) **Book**: Lehn J-M., "Supramolecular Chemistry", *VCH-Weinheim*, Germany, **1995**.
b) Lehn J-M., "Perspectives in Supramolecular Chemistry–From Molecular Recognition towards Molecular Information Processing and Self-organization", *Angew. Chem. Int. Ed.*, **1990**, *29*, 1304–1319.
c) Lehn J-M., "Supramolecular Chemistry–Scope and Perspectives Molecules, Supermolecules, and Molecular Devices (Nobel Lecture)", *Angew. Chem. Int. Ed.*, **1988**, *27*, 89–112.
d) Lehn J-M., "Supramolecular Chemistry: Receptors, Catalysts, and Carriers", *Science*, **1985**, *227*, 849–856.
e) Lehn J-M., "Cryptates: Inclusion Complexes of Macrocyclic Receptor Molecules", *Pure & Appl. Chem.*, **1978**, *50*, 871–892.
[3] Schneider H-J., "Bindungsmechanismen in supramolekularen Komplexen", *Angew. Chem.*, **2009**, *121*, 3982–4036
[4] "The Nobel Prize in Chemistry 1987". Nobelprize.org. 3 Sep 2010 http://nobelprize.org/nobel_prizes/chemistry /laureates/1987/
[5] Bundesarchiv, B 145 Bild-F088117-0003 / Reineke, Engelbert / CC-BY-SA
[6] Cram D. J., "Preorganisation – from solvents to spherands", *Angew. Chem. Int. Ed.*, **1986**, *25*, 1039–1134.
[7] **Book**: Lindoy L. F., Atkinson I. M., "Self-Assembly in Supramolecular Systems", *The Royal Society of Chemistry: Cambridge*, **2000**.
[8] **Book**: Steed J. W., Turner D. R., Wallace K. J., "Core Concepts in Supramolecular Chemistry and Nanochemistry", *John Wiley & Sons: Chichester*, England, **2007**.
[9] **Book**: Steed J. W., Atwood J. L., "Supramolecular Chemistry", *John Wiley & Sons: Chichester*, England, **2000**.
[10] Stryer L., "Biochemie", *Spektrum Akademischer Verlag Heidelberg·Berlin·Oxford*, **1999**.
[11] Pedersen M., Linnanto J., Frigaard N-U., Nielsen N. C., Miller M., *Photosynth. Res.*, **2010**, *104*, 233–243.
[12] Haag R., Kratz F., "Polymere Therapeutika: Konzepte und Anwendungen", *Angew. Chem.*, **2006**, *118*, 1218–1237.
[13] Soussan E., Cassel S., Blanzat M., Rico-Lattes I., "Wirkstofftransport mit weicher Materie: Matrix- und Vesikelvektoren", *Angew. Chem.*, **2009**, *121*, 280–295.
[14] Merschky M., Schmuck C., "Synthesis and kinetic studies of a low-molecular weight organocatalyst for phosphate hydrolysis in water", *Org. Biomol. Chem.,* **2009**, *7,* 4895–4903.
[15] **Book**: Newkome G. R., Moorefield C. N., Vögtle F., "Dendritic Molecules: Concepts, Syntheses, Perspectives", *VCH Verlagsgesellschaft: Weinheim*, **1996**.
[16] **Book**: Vögtle F., Richardt G., Werner N., "Dendritische Moleküle-Konzepte, Synthesen, Eigenschaften, Anwendungen", *Teubner: Wiesbaden*, **2007**.
[17] **Book**: Boas U., Christensen J. B., Heegaard P. M. H., "Dendrimers in Medicine and Biotechnology New Molecular Tools", *The Royal Society of Chemistry: Cambridge*, **2006**.
[18] Astruc D., Boisselier E., Ornelas C., "Dendrimers Designed for Functions", *Chem. Rev.*, **2010**, *110*, 1857–1959.
[19] Bosman A. W., Janssen H. M., Meijer E. W., "About Dendrimers: Structure, Physical Properties, and Applications", *Chem. Rev.*, **1999**, *99*, 1665–1688.
[20] Tomalia D. A., Naylor A. M., Goddard W. A., "Starburst-Dendrimere: Kontrolle von Große, Gestalt, Oberflächenchemie, Topologie und Flexibilität beim Übergang von Atomen zu makroskopischer Materie", *Angew. Chem.*, **1990**, 102, 119–157.
[21] a) Flory P. J., "Molecular Size Distribution in Three Dimensional Polymers. II. Trifunctional Branching Units", *J. Am. Chem. Soc.*, **1941**, *63*, 3091–3100.
b) Flory P. J., "Molecular Size Distribution in Three Dimensional Polymers. VI. Branched Polymers Containing A-R-B_{f-1} Type Units", *J. Am. Chem. Soc.,* **1952**, *74*, 2718–2723.
[22] http://www.roempp.com "Römpp Online 3.6", *Thieme Chemistry*, **2010**.
[23] Buhleier E., Wehner W. Vögtle F., ""Cascade" and "Nonskid-Chain-like" Syntheses of a Molecular Cavity Topologies", *Synthesis*, **1978**, 155–158.

[24] a) Tomalia D. A., Baker H., Dewald J. R., Hall M., Kallos G., Martin S., Roeck J., Ryder J., Smith P., "A new Class Of Polymers", *Polym. J.*, **1985**, *17*, 117–132.
b) Tomalia D. A., Baker H., Dewald J., Hall M., Kallos G., Martin S., Roeck J., Ryder J., Smith P., "Dendritic Macromolecules: Synthesis of Starburst Dendrimers", *Macromolecules*, **1986**, *19*, 2466–2468.
[25] Newkome G. R., Yao Z-Q., Baker G. R., Gupta V. K., "Cascade Molecules: A New Approach to Micelles. A [27]-Arborol", *J. Org. Chem.*, **1985**, *50*, 2003–2004.
[26] Newkome G. R., Yao Z-Q., Baker G. R., Gupta V. K., Russo V. K., Saunders M. J., "Cascade Molecules: Synthesis and Characterization of a Benzene[9]^3-Arborol", *J. Am. Chem. Soc.*, **1986**, *108*, 850–851.
[27] Wörner C., Mülhaupt R., "Polynitrile- and Polyamine-Functional Poly(trimethylene imine) Dendrimers", *Angew. Chem. Int. Ed.*, **1993**, *32*, 1306–1308.
[28] De Brabander-van den Berg E. M. M., Meijer E. W., "Poly(propylene imine) Dendrimers: Large-Scale Synthesis by Heterogeneously Catalyzed Hydrogenations", *Angew. Chem., Int. Ed.*, **1993**, *32*, 1308–1311.
[29] a) Hawker C. J., Fréchet J. M. J., "Preparation of Polymers with Controlled Molecular Architecture. A New Convergent Approach to Dendritic Macromolecules", *J. Am. Chem. Soc.*, **1990**, *112*, 7638–7647.
b) Hawker C. J., Fréchet J. M. J., "A New Convergent Approach to Monodisperse Dendritic Macromolecules", *J. Chem. Soc., Chem. Commun.*, **1990**, 1010–1013.
c) Reimann, E., "Natürliche Stilbene. Synthese von Polyhydroxystilbenäthern durch Wittig-Reaktion", *Chem. Ber.*, **1969**, *102*, 2881–2888.
d) Kumetani T., Kana S., "Studies on the Synthesis of Heterocyclic compounds", *J. pharmac. Soc. Japan*, **1962**, *82*, 1059–1062.
[30] Wooley K. L., Hawker C. J., Fréchet J. M. J., "Hyperbranched Macromolecules via a Novel Double-Stage Convergent Growth Approach", *J. Am. Chem. Soc.* **1991**, *113*, 4252–4261.
[31] Pesak D. J., Moore J. S., Wheat T. E., "Synthesis and Characterization of Water-Soluble Dendritic Macromolecules with a Stiff, Hydrocarbon Interior", *Macromolecules*, **1997**, *30*, 6467–6482.
[32] Hummelen J. C., van Dongen J. L. J., Meijer E. W., "Electrospray Mass Spectrometry of Poly(propylene imine) Dendrimers–The Issue of Dendritic Purity or Polydispersity", *Chem. Eur.J.*, **1997**, *3*, 1489–1493.
[33] a) Kallos G. J., Tomalia D. A., Hedstrand D. M., Lewis S., Zhou J., "Molecular weight determination of a polyamidoamine Starburst polymer by electrospray ionization mass spectrometry", *Rapid Commun. Mass Spectrom.*, **1991**, *5*, 383–386.
b) Schwartz B. L., Rockwood A. L., Smith R. D., Tomalia D. A., Spindler R., "Detection of high molecular weight starburst dendrimers by electrospray ionization mass spectrometry", *Rapid Commun. Mass Spectrom.*, **1995**, *9*, 1552–1555.
c) Dvornic P. R., Tomalia D. A., "Genealogically Directed Syntheses (Polymerizations): Direct Evidence By Electrospray Mass Spectroscopy", *Macromol. Symp,*, **1995**, *98*, 403–428.
d) Tolic L. P., Anderson G. A., Smith R. D., Brothers II H. M., Spindler R., Tomalia D. A., "Electrospray ionization Fourier transform ion cyclotron resonance mass spectrometric characterization of high molecular mass Starburst™ dendrimers",.*Int. J. Mass Spectrom. Ion Proc.*, **1997**, *165/166*, 405–418.
[34] Felder T., Schalley C. A., Fakhrnabavi H., Lukin O., "A Combined ESI- and MALDI-MS(/MS) Study of Peripherally Persulfonylated Dendrimers: False Negative Results by MALDI-MS and Analysis of Defects", *Chem. Eur. J.*, **2005**, *11*, 5625–5636.
[35] Newkome G. R., Moorefield C. N., Baker G. R., Saunders M. J., Grossman S. H., "Unimolecular Micelles", *Angew. Chem. Int. Ed.*, **1991**, *30*, 1178–1180.
[36] Jansen J. F. G. A., de Brabander-van den Berg E. M. M., Meijer E. W., "Encapsulation of Guest Molecules into a Dendritic Box", *Science*, **1994**, *266*, 1226–1229.
[37] Jansen J. F. G. A., Meijer E. W., "The Dendritic Box: Shape-Selective Liberation of Encapsulated Guests", *J. Am. Chem. Soc.*, **1995**, *117*, 4417–4418.
[38] **Book:** U. Boas, J. B. Christensen, P. M. H. Heegaard, "Dendrimers in Medicine and Biotechnology", *RSC Publishing*, **2006**.
[39] Gillies E. R., Fréchet J. M. J., "Dendrimers and dendritic polymers in drug delivery", *Drug Disc. Today*, **2005**, *10*, 35–43.
[40] Crampton H. L., Simanek E. E., "Dendrimers as drug delivery vehicles: non-covalent interactions of bioactive compounds with dendrimers", *Polym. Int.*, **2007**, *56*, 489–496.

[41] a) Y. Matsumura, H. Maeda, "A New Concept for Macromolecular Therapeutics in Cancer Chemotherapy: Mechanism of Tumoritropic Accumulation of Proteins and the Antitumor Agent Smancs", *Cancer Res.* **1986**, *46*, 6387–6392.
b) Maeda H., Matsumura Y., *CRC Crit. Rev. Ther. Drug Carrier Syst.*, **1989**, *6*, 193–210.
[42] Haag R., "Supramolekulare Wirkstoff-Transportsysteme auf der Basis polymerer Kern-Schale-Architekturen", *Angew. Chem.*, **2004**, *116*, 280–284.
[43] Gingras M., Raimundo J-M., Chabre Y. M., "Cleavable Dendrimers", *Angew. Chem.*, **2007**, *46*, 1010–1017.
[44] Astruc D., Chardac, F., "Dendritic Catalysts and Dendrimers in Catalysis", *Chem. Rev.*, **2001**, *101*, 2991–3023.
[45] Kreiter R., Kleij, A. W., Gebbink R., J., M., van Koten G., "Dendritic Catalysts", *Top. Curr. Chem.*, **2001**, 217, 163–199.
[46] Scott R. W. J., Wilson O. M., Crooks R. M., "Synthesis, Characterization, and Applications of Dendrimer-Encapsulated Nanoparticles", *J. Phys. Chem.. B.*, **2005**, *109*, 692-704.
[47] Kim Y., Zimmerman S. C., "Applications of dendrimers in bio-organic chemistry", *Curr. Opin. Bio. Chem.*, **1998**, *2*, 733–742.
[48] Lee C. C., MacKay J. A., Fréchet J. M. J., Szoka F. C., "Designing Dendrimers for biological applications", *Nat. Biotech.*, **2005**, *23*, 1517–1526.
[49] Smith D. K., Diederich F., "Functional Dendrimers: Unique Biological Mimics", *Chem. Eur. J.*, **1998**, *4*, 1353–1361.
[50] Fischer M., Vögtle F., "Dendrimere vom Design zur Anwendung", *Angew. Chem.*, **1999**, *111*, 934–955.
[51] Smith D. K., Diederich F., "Supramolecular Dendrimer Chemistry: A Journey Through the Branched Architecture", *Top. Curr. Chem.*, **2000**, *210*, 183–227.
[52] Tomalia D. A., Majoros I., "Dendrimeric Supramolecular and Supramacromolecular Assemblies", *Poly. Rev.*, **2003**, *C43*, 411–477.
[53] Fréchet J. M. J., "Dendrimers and supramolecular chemistry", *PNAS*, **2002**, *99*, 4782–4787.
[54] Gittins P. J., Twyman L. J., "Dendrimers and Supramolecular Chemistry", *Supramolecular Chem.*, **2003**, *15*, 5–23.
[55] Zimmerman S. C., Lawless L. J., "Supramolecular Chemistry of Dendrimers", *Top. Curr. Chem.*, **2001**, *217*, 95–120.
[56] Smith D. K., "Dendritic supermolecules–towards controllable nanomaterials", *Chem. Commun.*, **2006**, 34–44.
[57] Smith D. K., Hirst A. R., Love C. S., Hardy J. G., Brignell S. V., Huang B., "Self-assembly using dendritic building blocks–towards controllable nanomaterials", *Prog. Polym. Sci.*, **2005**, *30*, 220–293.
[58] Rosen B. M., Wilson C. J., Wilson D. A., Peterca M., Imam M. R., Percec V., "Dendron-Mediated Self-Assembly, Disassembly, and Self-Organization of Complex Systems", *Chem. Rev.*, **2009**, *109*, 6275–6540.
[59] Zimmerman S. C., Zeng F., Reichert D. E. C., Kolotuchin S. V., "Self-Assembling Dendrimers", *Science*, **1996**, *271*, 1095–1098.
[60] Thiyagarajan P., Zeng F., Ku C. Y., Zimmerman S. C., "SANS investigation of self-assembling dendrimers in organic solvents", *J. Mater. Chem.*, **1997**, *7*, 1221–1226.
[61] Zeng F., Zimmerman S. C., Kolotuchin S. V., Reichert D. E. C., Ma Y., "Supramolecular polymer chemistry: design, synthesis, characterization, and kinetics, thermodynamics, and fidelity of formation of self-assembled dendrimers", *Tetrahedron*, **2002**, *58*, 825–843.
[62] Ma Y., Kolotuchin S. V., Zimmerman S. C., "Supramolecular Polymer Chemistry: Self-Assembling Dendrimers Using the DDA·AAD (GC-like) Hydrogen Bonding Motif", *J. Am. Chem. Soc.*, **2002**, *124*, 13757–13769.
[63] Corbin P. S., Lawless L. J., Li Z., Ma Y., Witmer M. J., Zimmerman S. C., "Discrete and polymeric self-assembled dendrimers: Hydrogen bond-mediated assembly with high stability and high fidelity", *Proc. Natl. Acad. Sci.*, **2002**, *99*, 5099–5104.
[64] Huck W. T. S., Hulst R., Timmerman P., van Veggel F. C. J. M., Reinhoudt D. N., „Nichtkovalenter Aufbau von Nanostrukturen durch Nutzen aus koordinationschemischer Methoden und von Wasserstoffbrücken-bindungen", *Angew. Chem.*, **1997**, *109*, 1046–1049.
[65] Mathias J.P., Simanek E. E., Zerkowski J. A., Seto C. T., Whitesides G. M., "Structural Preferences of Hydrogen-Bonded Networks in Organic Solution-the Cyclic $Ca_3 \cdot M_3$ "Rosette"", *J. Am. Chem. Soc.*, **1994**, *116*, 4316–4325.
[66] Freeman A. W., Vreekamp R., Fréchet J. M. J., "The self assembly of convergent dendrimers based on the melamine cyanuric acid lattice", *PMSE*, **1997**, *214*, 128

[67] Wang Y., Zeng F., Zimmerman S. C., "Dendrimers with anthyridine-based hydrogen-bonding units at their cores Synthesis, complexation and self-assembly studies", *Tet. Lett.*, **1997**, *38*, 5459–5462.
[68] Franz A., Bauer W., Hirsch A., "Complete Self-Assembly of Discrete Supramolecular Dendrimers", *Angew. Chem. Int. Ed.*, **2005**, *44*, 1564–1567.
[69] Hager K., Franz A., Hirsch A., "Self-Assembly of Chiral Depsipeptide Dendrimers", *Chem. Eur. J.*, **2006**, *12*, 2663–2679.
[70] Dirksen A., Hahn U., Schwanke F., Nieger M., Reek J. N. H., Vögtle F., De Cola L., "Multiple Recognition of Barbiturate Guests by Hamilton-Receptor-Functionalized Dendrimers", *Chem. Eur. J.*, **2004**, *10*, 2036–2047.
[71] Grimm F., Hartnagel K., Wessendorf F., Hirsch A., "Supramolecular self-assembly of dendrimers containing orthogonal binding motifs", *Chem. Commun.*, **2009**, 1331–1333.
[72] Smith D. K., "Supramolecular dendritic solubilisation of a hydrophilic dye and tuning of its optical properties", *Chem. Commun.*, **1999**, 1685–1686.
[73] Dykes G. M., Brierley L. J., Smith D. K., McGrail P. T., Seeley G.J., "Supramolecular Solubilisation of Hydrophilic Dyes by Using Individual Dendritic Branches", *Chem. Eur. J.*, **2001**, *7*, 4730–4739.
[74] Ashton P. R., Campbell P. J., Chrystal E. J. T., Glink P. T., Menzer S., Philp D., Spencer N., Stoddart J. F., Tasker P. A., Williams D. J., "Dialkylammonium-Ionen/Kronenether-Komplexe: Vorläufer einer neuen Familie „mechanisch" verknüpfter Moleküle", *Angew. Chem.*, **1995**, *107*, 1997–2001.
[75] Yamaguchi N., Hamilton L. M., Gibson H. W., "Dendritic Pseudorotaxanes", *Angew. Chem. Int. Ed.*, **1998**, *37*, 3275–3279.
[76] Gibson H. W., Yamaguchi N., Hamilton L., Jones J. W., "Cooperative Self-Assembly of Dendrimers via Pseudorotaxane Formation from a Homotritopic Guest Molecule and Complementary Monotopic Host Dendrons", *J. Am. Chem. Soc.*, **2002**, *124*, 4653–4665.
[77] Dykes G. M., Smith D. K., Seeley G. J., "Controlled Release of a Dendritically Encapsulated Template Molecule", *Angew. Chem. Int. Ed.*, **2006**, *45*, 7042–7046.
[78] Gillies E. R., Fréchet J. M. J., "Synthesis and Self-Assembly of Supramolecular Dendritic "Bow-Ties": Effect of Peripheral Functionality on Association constants", *J. Org. Chem.*, **2004**, *69*, 46–53.
[79] Baars M. W. P. L., Karlsson A. J., Sorokin V., de Waal B. F. W., Meijer E. W., "Supramolecular Modification of the Periphery of Dendrimers Resulting in Rigidity and Functionality", *Angew. Chem. Int. Ed.*, **2000**, *39*, 4362–4365.
[80] Sun H., Kaifer A. E., "Unsymmetric Dendrimers Containing a Single Ureidopyrimidine Unit: Generation-Dependent Dimerization via Hydrogen Bonding", *Org. Lett.*, **2005**, *7*, 3845–3848.
[81] Sijbesma R. P., Beijer F. H., Brunsveld L., Folmer B. J. B., Hirschberg K. J. H. K., Lange R. F. M., Lowe J. K. L., Meijer E. W., "Reversible Polymers Formed from Self Complementary Monomers Using Quadruple Hydrogen Bonding", *Science*, **1997**, *278*, 1601–1604.
[82] Beijer F. H., Sijbesma R. P., Kooijman H., Spek A. L., Meijer E. W., "Strong Dimerization of Ureidopyrimidones via Quadruple Hydrogen Bonding", *J. Am. Chem. Soc.*, **1998**, *120*, 6761–6769.
[83] Ong W., Grindstaff J., Sobransingh D., Toba R., Quintela J. M., Peinador C., Kaifer A. E., "Electrochemical and Guest Binding Properties of Frèchet- and Newkome-Type Dendrimers with a Single Viologen Unit Located at Their Apical Positions", *J. Am. Chem. Soc.*, **2005**, *127*, 3353–3361.
[84] Wong C-H., Chow H-F., Hui S-K., Sze K-H., "Generation-Independent Dimerization Behavior of Quadruple Hydrogen-Bond-Containing Oligoether Dendrons", *Org. Lett.*, **2006**, *8*, 1811–1814.
[85] Maiti P. K., Cagin T., Lin S-T., Goddard W. A., "Effect of Solvent and pH on the Structure of PAMAM Dendrimers", *Macromolecules*, **2005**, **38**, 979–991.
[86] de Greef T. F. A., Nieuwenhuizen M. M. L., Sijbesma R. P., Meijer E. W., "Competitive Intramolecular Hydrogen Bonding in Oligo(ethylene oxide) Substituted Quadruple Hydrogen Bonded Systems", *J. Org. Chem.*, **2010**, *75*, 598–610.
[87] a) Schade B., Ludwig K., Böttcher C., Hartnagel U., Hirsch A., "Supramolecular Structure of 5-nm Spherical Micelles with D3 Symmetry Assembled from Amphiphilic [3:3]-Hexakis Adducts of C_{60}", *Angew. Chem.*, **2007**, *46*, 4393–4396.
b) Kellermann M., Bauer W., Hirsch A., Schade B., Ludwig K., Böttcher C., "The First Account of a Structurally Persistent Micelle", *Angew. Chem.*, **2004**, 43, 2959–2962.
c) Burghardt S., Hirsch A., Schade B., Ludwig K., Böttcher C., "Switchable Supramolecular Organization of Structurally Defined Micelles Based on an Amphiphilic Fullerene", *Angew. Chem Int. Ed.*, **2005**, 44, 2976–2979.

[88] Frey H., Haag R., "Dendritic polyglycerol: a new versatile biocompatible material", *Rev. Molecular Biotech.*, **2002**, *90*, 257–267.
[89] Wyszogrodzka M., Haag R., "A Convergent Approach to Biocompatible Polyglycerol "Click" Dendrons for the Synthesis of Modular Core–Shell Architectures and Their Transport Behavior", *Chem. Eur. J.*, **2008**, *14*, 9202–9214.
[90] a) Huisgen R., Szeinies G., Möbius L., "1.3-Dipolare Cycloadditionen, XXXII: Kinetik der Additionen organischer Azide an CC-Mehrfachbindungen", *Chem. Ber.*, **1967**, *100*, 2494–2507.
b) Huisgen R., "Kinetics and reaction mechanisms: selected examples from the experience of forty years", *Pure & Appl. Chem.*, **1989**, *61*, 613–628.
[91] Kolb H. C., Finn M. G., Sharpless K. B., "Click Chemistry: Diverse Chemical Function from a Few Good Reactions", *Angew. Chem. Int. Ed.*, **2001**, *40*, 2004–2021.
[92] Moses J. E., Moorhouse A. D., "The growing applications of click chemistry", *Chem. Soc. Rev.*, **2007**, *36*, 1249–1262.
[93] Kainthan R. K., Janzen J., Levin E., Devine D. V., Brooks D. E., "Biocompatibility Testing of Branched and Linear Polyglycidol", *Biomacromolecules*, **2006**, *7*, 703–709.
[94] Knop, K., Hoogenboom R., Fischer D., Schubert U. S., "Anwendung von Poly(ethylenglycol) beim Wirkstoff-Transport: Vorteile, Nachteile und Alternativen", *Angew. Chem.*, **2010**, *122*, 6430–6452.
[95] Oshovsky G. V., Reinhoudt D. N., Verboom W., "Supramolecular Chemistry in Water", *Angew. Chem. Int. Ed.*, **2007**, *46*, 2366–2393.
[96] a) Rehm T., Schmuck C., "How to achieve self-assembly in polar solvents based on specific interactions? Some general guidelines", *Chem.Commun.*, **2008**, 801–813.
b) Rehm T. H., Schmuck C., "Ion-pair induced self-assembly in aqueous solvents", *Chem. Soc. Rev.*, **2010**, DOI: 10.1039/b926223g.
[97] Schmuck C., "Highly Stable Self-Association of 5-(Guanidiniocarbonyl)-1H-Pyrrole-2-Carboxylate in DMSO–The Importance of Electrostatic Interactions", *Eur. J. Org. Chem.*, **1999**, 2397–2403.
[98] a) Schmuck C., Schwegmann M., "A Molecular Flytrap for the Selective Binding of Citrate and Other Tricarboxylates in Water", *J. Am. Chem. Soc.*, **2005**, *127*, 3373–3379.
b) Schmuck C., Dudaczek J., "New guanidinium-based carboxylate receptors derived from5-amino-pyrrole-2-carboxylate: synthesis and first binding studies", *Tet. Let.*, **2005**, *46*, 7101–7105.
c) Schmuck C., "How to improve guanidinium cations for oxoanion binding in aqueous solution? The design of artificial peptide receptors", *Coo. Chem. Rev.*, **2006**, *250*, 3053–3067.
d) Schmuck C., Bickert V., "Oxoanion Binding by Flexible Guanidiniocarbonyl Pyrrole-Ammonium Bis-Cations in Water", *J. Org. Chem.*, **2007**, *72*, 6832–6839.
e) Urban C., Schmuck C., "Active Transport of Amino Acids by a Guanidiniocarbonyl–Pyrrole Receptor", *Chem. Eur. J.*, **2010**, *16*, 9502–9510.
[99] a) Schmuck C., Rehm T., Klein K., Gröhn F., "Formation of Vesicular Structures through the Self-Assembly of a Flexible Bis-Zwitterion in Dimethyl Sulfoxide", *Angew. Chem. Int. Ed.*, **2007**, *46*, 1693–1697.
b) Rehm T., Stepanenko V., Zhang X., Würthner F., Gröhn F., Klein K., Schmuck C., "A New Type of Soft Vesicle-Forming Molecule: An Amino Acid Derived Guanidiniocarbonyl Pyrrole Carboxylate Zwitterion", *Org. Lett.*, **2008**, *10*, 1469–1472.
c) Gröger G., Stepanenko V., Würthner F., Schmuck C., "Step-wise self-assembly of a small molecule with two orthogonal binding interactions leads to single stranded linear polymers in DMSO", *Chem. Commun.*, **2009**, 698–700.
[100] **Book**: Braude, E.A., Nachod F.C., "Determination of Organic Structures by Physical Methods", *Academic Press*, New York, **1955**.
[101] Griko Y. V., "Energetics of Ca^{2+}–EDTA interactions: Calorimetric study", *Biophys. Chem.*, **1999**, 117–127.
[102] Deluchat V. Bollinger J-C., Serpaud B., Caullet C., "Divalent cations speciation with three phosphonate ligands in the pH-range of natural waters", *Talanta*, **1997**, 897–907.
[103] Schmuck C., Bickert V., Merschky M., Geiger L., Rupprecht D., Dudaczek J., Wich P., Rehm R., Machon U., "A facile and efficient multi-gram synthesis of N-protected guanidinocarbonylpyrrole carboxylic acids", *Eur. J. Org. Chem.*, **2008**, 324–329.
[104] Merschky M., Schmuck C., "N-(Aminoiminomethyl)-carbamic acid, 1,1-dimethyethyl ester (Boc-guanidine)", *Electronic Encyclopedia of Reagents for Organic Synthesis*, **2009**, DOI: 10.1002/047084289X.rn01107.

[105] Cohen Y., Avram L., Frish L., "Diffusions-NMR-Spektroskopie in der Supramolekularen und Kombinatorischen Chemie: ein alter Parameter – neue Erkenntnisse", *Angew. Chem.*, **2005**, *117*, 524–560.
[106] **Book**: Schalley C. A., "Analytical Methods in Supramolecular Chemistry", *Wiley-VCH*, **2006**.
[107] Lide, D. R., "CRC Handbook of Chemistry and Physics 1995-1996", 76th Edition, *CRC Press: Boca Raton, New York, London, Tokio*, **1996**.
[108] Johnson A. W., Markham E., Price R., Shaw K. B., "The Synthesis of Tri- and Tetra-alkylpyrroles", *J. Chem. Soc.*, **1958**, 4254–4257.
[109] Jiang Y., Smith K. M., "Syntheses of some β-substituted alkyne porphyrins related to protoporphyrin-IX", *J. Chem. Soc. Perkin Trans. I*, **1996**, 1601–1606.
[110] Mironov A. F., Kozhich D. T., Vasilevsky V. I., Evstigneeva R. P., "A New, Convenient Synthesis of Pyrrolylacetylenes", *Synthesis*, **1979**, 533–535.
[111] http://www.malvern.com/common/downloads/campaign/MRK656-01.pdf, 25.07.2010, "Dynamic Light Scattering: An Introduction in 30 Minutes", *Malvern Instruments Ltd*.
[112] MacDonald S. F., "A General Route to ββ'-Substituted Pyrrole Intermediates for Porphyrin Synthesis", *J. Chem. Soc.*, **1952**, 4176–4184.
[113] Harbuck J. W., Rapoport H., "Some Observations on the Mechanism of a modified Knorr Pyrrole Condensation", *J. Org. Chem.*, **1971**, *36*, 853–855.
[114] Paine III J. B., Dolphin D., "Pyrrole chemistry. An improved synthesis of ethyl pyrrole-2-carboxylate esters from diethyl aminomalonate", *J. Org. Chem.*, **1985**, *50*, 5598–5604.
[115] Schmuck C., Rupprecht D., Urban U., Walden N., "Synthesis of Orthogonally Protected Pyrrole Tricarboxylic Acid Derivatives", *Synthesis*, **2006**, *1*, 89–96.
[116] Schmuck C., Rupprecht D., "The Synthesis of Highly Functionalized Pyrroles: A Challenge in Regioselectivity and Chemical Reactivity", *Synthesis*, **2007**, *20*, 3095–3110.
[117] Nicolaou K. C., Estrada A. A., Zak M., Lee S. H., Safina B. S., "A Mild and Selective Method for the Hydrolysis of Esters with Trimethyltin Hydroxide", *Angew. Chem. Int. Ed.*, **2005**, *44*, 1378–1382.
[118] Schmuck C., Wienand W., "Highly Stable Self-Assembly in Water: Ion Pair Driven Dimerization of a Guanidiniocarbonyl Pyrrole Carboxylate Zwitterion", *J. Am. Chem. Soc.* **2003**, *125*, 452–459.
[119] **Book**: Berger S., Braun S., "200 and More NMR Experiments", *Wiley-VCH*, **2004**.
[120] **Book**: Barth H. G., Mori S., "Size Exclusion Chromatography", *Springer Berlin*, **1999**.
[121] a) Heek T., Fasting C., Rest C., Zhang X., Würthner F., Haag R., "Highly fluorescent water-soluble polyglycerol-dendronized perylene bisimide dyes", *Chem. Comm.*, **2010**, *46*, 1884–1886.
b) Würthner F., "Perylene bisimide dyes as versatile building blocks for functional supramolecular architectures", *Chem. Comm.*, **2004**, 1564–1579.
c) Chen Z., Stepanenko V., Dehm V., Prins P., Siebbeles L. D. A., Seibt J., Marquetand P., Engel V., Würthner F., "Photoluminescence and Conductivity of Self-Assembled π–π Stacks of Perylene Bisimide Dyes", *Chem. Eur. J.*, **2007**, *13*, 436–449.
d) Chen Z., Lohr A., Saha-Möller C. R., Würthner F., "Self-assembled p-stacks of functional dyes in solution: structural and thermodynamic features", *Chem. Soc. Rev.*, **2009**, *38*, 564–584.
[122] Mizguchi J., Hino K., Tojo K., "Strikingly different electronic spectra of structurally similar perylene imide compounds", *Dyes and Pigments*, **2006**, *70*, 126–135.
[123] Seki T., Yagai S., Karatsu T., Kitamura A., "Formation of Supramolecular Polymers and Discrete Dimers of Perylene Bisimide Dyes Based on Melamine-Cyanurates Hydrogen-Bonding Interactions", *J. Org. Chem.*, **2008**, *73*, 3328–3335.
[124] Smulder M. M. J., Nieuwenhuizen M. M. L., de greef T. F. A., van der Schoot P., Schenning A. P. H. J., Meijer E. W., "How to Distinguish Isodesmic from Cooperative Supramolecular Polymerisation", *Chem. Eur. J.*, **2010**, *16*, 362–367.
[125] Langhals H., "Cyclic Carboxylic Imide Structures as Structure Elements of High Stability.Novel Developments in Perylene Dye Chemistry", *Heterocycles,* **1995**, *40*, 477-500.
[126] Langhals H., Krotz O., Polborn K., Mayer P., "A Novel Fluorescent Dye with Strong, Anisotropic Solid-State Fluorescence, Small Stokes Shift, and High Photostability", *Angew. Chem. Int. Ed.*, **2005**, *44*, 2427–2428.
[127] Heek T., Fasting C., Rest C., Zhang X., Würthner F., Haag R., "Highly fluorescent water-soluble polyglycerol-dendronized perylene bisimide dyes", *Chem. Comm.*, **2010**, *46*, 1884–1886.

[128] Ford W. E., "Photochemistry of 3,4,9,10- Perylenetetracarboxylic Dianhydride Dyes", *J. Photochem.*, **1987**, *37*, 189–204.
[129] a) Hippius C., van Stokkum I., Zangrando E., Williams R., Wykes M., Beljonne D., Würthner F., "Ground- and Excited-State Pinched Cone Equilibria in Calix[4]arenes Bearing Two Perylene Bisimide Dyes", *J. Phys. Chem. C*, **2008**, *112*,14626–14638.
b) Han J., Shaller A., Wang W., Li A., "Architecturally Diverse Nanostructured Foldamers Reveal Insightful Photoinduced Single-Molecule Dynamics", *J. Am. Chem. Soc.*, **2008**, *130*, 6974–6982.
c) Schwartz E., Palermo V., Finlayson C., Huang Y.-S., Otten M., Liscio A., Trapani S., González-Valls I., Brocorens P., Cornelissen J. M., Peneva K., Müllen Spano K., F., Yartsev A., Westenhoff S., Friend H., Beljonne D., Nolte R., Samorì P., Rowan A., ""Helter-Skelter-Like" Perylene Polyisocyanopeptides", *Chem. Eur. J.*, **2009**, *15*, 2536–2547.
d) Rehm S., Stepanenko V., Zhang X., Rehm T. H., Würthner F., "Spermine-Functionalized Perylene Bisimide Dyes–Highly Fluorescent Bola-Amphiphiles in Water", *Chem. Eur. J.*, **2010**, *16*, 3372–3382.
[130] **Book**: Bhushan B., "Handbook of Nanotechnology", *Springer*, **2007**.
[131] Wagner C., Wagenknecht H-A., "Perylene-3,4:9,10-teracarboxylic Acid Bisimide Dye as an Artificial DNA Base Surrogate", Org. Lett., **2006**, *19*, 4191–4194.
[132] Hunter C. A., "The Role of Aromatic Interactions in Molecular Recognition", *Chem. Soc. Rev.*, **1994**, *23*, 101–109.
[133] Hunter C. A., Lawson K. R., Perkins J., Urch C. J., "Aromatic Interactions", *J. Chem. Soc., Perkin Trans.2*, **2001**, 651–669.
[134] Gaussian 03, Revision E.01, M. J. Frisch, G. W. Trucks, H. B. Schlegel, G. E. Scuseria, M. A. Robb, J. R. Cheeseman, J. A. Montgomery, Jr., T. Vreven, K. N. Kudin, J. C. Burant, J. M. Millam, S. S. Iyengar, J. Tomasi, V. Barone, B. Mennucci, M. Cossi, G. Scalmani, N. Rega, G. A. Petersson, H. Nakatsuji, M. Hada, M. Ehara, K. Toyota, R. Fukuda, J. Hasegawa, M. Ishida, T. Nakajima, Y. Honda, O. Kitao, H. Nakai, M. Klene, X. Li, J. E. Knox, H. P. Hratchian, J. B. Cross, V. Bakken, C. Adamo, J. Jaramillo, R. Gomperts, R. E. Stratmann, O. Yazyev, A. J. Austin, R. Cammi, C. Pomelli, J. W. Ochterski, P. Y. Ayala, K. Morokuma, G. A. Voth, P. Salvador, J. J. Dannenberg, V. G. Zakrzewski, S. Dapprich, A. D. Daniels, M. C. Strain, O. Farkas, D. K. Malick, A. D. Rabuck, K. Raghavachari, J. B. Foresman, J. V. Ortiz, Q. Cui, A. G. Baboul, S. Clifford, J. Cioslowski, B. B. Stefanov, G. Liu, A. Liashenko, P. Piskorz, I. Komaromi, R. L. Martin, D. J. Fox, T. Keith, M. A. Al-Laham, C. Y. Peng, A. Nanayakkara, M. Challacombe, P. M. W. Gill, B. Johnson, W. Chen, M. W. Wong, C. Gonzalez, and J. A. Pople, *Gaussian, Inc., Wallingford CT*, **2004**.
[135] Leonard J., Lygo B., Procter G., "Praxis der Organischen Chemie", *Wiley-VCH*, **1996**.
[136] Meyer V. R., "Praxis der Hochleistungs-Flüssigchromatographie", *Wiley-VCH,* **2009**.
[137] Hesse M., Meier H., Zeeh B., "Spektroskopische Methoden in der organischen Chemie", *Thieme Stuttgart*, **2005**.
[138] a) Helmchen G., Glatz B., "Ein apparativ einfaches System und Säulen höchster Trennleistung zur präparativen Mitteldruck-Flüssigkeitschromatographie", Universität Stuttgart **1978,** Anhang I der Habilitationsarbeit von Prof. Dr. G. Helmchen.
b) Ade E., Helmchen G., Heiligenmann G., "Syntheses of the stereoisomer of 17,21-Dimethylheptatriacontane – Sex Recognition Pheromen of the Tsetse Fly", *Tet. Let.*, **1980**, 21, 1137-1140.
[139] Preparation was done by Monika Wydzogrodzka, working group Prof. Dr. Rainer. Haag